Università Iuav di Venezia
School of Doctorate Studies
Doctoral Programme in Architecture, City and Design
Track: Innovation for Building and Cultural Heritage

"MASONRY ARCH BRIDGES IN VENICE: EXPERIMENTAL AND NUMERICAL PROCEDURES FOR STRUCTURAL IDENTIFICATION"

DISSERTATION

Anna Manzato

Advisor: Prof. Antonella Cecchi

Co-Advisor: Dr. Giosuè Boscato

Prof. Sebastiano Trevisani

Venezia, 2019

Abstract

Keywords: *Conservation, Masonry arch bridge, Structural identification, Material characterization, Numerical procedures*

Masonry arch bridges are an important part of architectural historical heritage. Their presence is a characteristic feature of the Italian and European landscape. A large number of research and studies about. This theme have been produced in literature during time. Regarding Venetian bridges, except for the most famous architectures. Data are lacking given by research results are lacking.

A procedure for structural identification and for the evaluation of the material mechanical characteristics for historical masonry bridges is here presented with the aim of their conservation and restoration. The procedure, based on experimental measurements and numerical analyses, requires, at first, the measurements of the bridge's fundamental frequencies, then, through the calibration of bridge FE Model, allows the estimation of the average materials characteristics. In particular, for the frequency acquisition data, the procedure proposes the use of a compact digital tromograph, a highly sophisticated measuring device, equipped with accelerometric and velocimetric transducers, that allows fast and low cost vibration measurements. Successive analyses, by means of fast Fourier transform, permit to estimate the fundamental frequency of the structure. For one study case the validity of the results obtained is confirmed by making a comparison with a measurement campaign performed using accelerometers as instruments.

The proposed research consists of an initial overview of the evolution and development of masonry arch bridges (Section 2), following focus on Venetian bridge (Section 3). Then, mechanical properties, structural behaviour and collapse mechanism of masonry arch bridge are examined (Section 4). In this research attention has been paid to analyse the fundamental frequencies and comparing the frequencies with numerical and analytical models. An Operational Modal Analysis has been performed to different case studies (section 5). The thesis provides state of the art regarding the methods of analysis and the techniques of structural modelling of masonry arch bridges, outlining the different approaches, the fields and the limits of applicability (Section 6). In this research the structural identification of four masonry arch bridges located in Venice has been carried out. The structural identification and materials characterization have been performed and have been described in all the different phases (Section 7). The procedure for the structural identification by means of frequency measurements and numerical models calibration, proposed in section 7, has been applied to 4 study cases realized with similar geometrical and material characteristics but different material of the parapet (Section 8). Lastly, some conclusions about the procedure are given, highlighting the accuracy and limits (Section 9).

Acknowledgements

Firstly, I would like to express my sincere gratitude to my advisor Prof. Antonella Cecchi, who expertly guided me through my academic education with motivation and Knowledge.

I extend my gratitude to Dr.Giosuè Boscato and Prof. Sebastiano Trevisani, for mentoring, technical support and encouragements.

I would also like to thanks for helping me on my course:

- Labsco (*Laboratorio di Scienza delle costruzioni dell'Università IUAV Di Venezia*)
- Circe (*Laboratorio di Cartografia e Gis dell'Università IUAV Di Venezia*)
- Prof. Daniele Baraldi and Phd Claudia Britto De Carvalho (*Università IUAV Di Venezia*) for their valuable guidance
- My Phd collage Martina Belmone and Eleonora Spoldi

My deep gratitude goes to my family and friends for their continued support and love.

Table of Contents

Abstract.....iii

List of Figures.....xi

List of Tables.....xxiii

Section

1 Introduction 1

1.1 Thesis layout..... 2

2 State of the Art 5

2.1 The evolution of bridges during history..... 6

2.2 The development of bridge types 8

2.3 Historical and typological evolution of masonry arch bridges..... 9

2.4 Masonry bridges..... 9

2.5 Evolution and development of masonry bridges 10

2.5.1 Roman bridges..... 11

2.5.2 Medioeval bridges 15

2.5.3 The bridges of the Modern Age..... 18

2.5.4 From the XVIII century to the end of masonry bridges 21

2.6 Morphology of masonry arch bridges..... 23

3 Venetian bridges..... 33

3.1 From wood bridges to stone bridges 33

3.2 The bridges construction..... 34

3.3 Arch bridges 35

3.3.1 The arch shape..... 37

3.3.2 Basements and Foundations 39

3.3.3 The exterior structure..... 40

3.3.4 The walking level 41

3.3.5 The evolution of parapets 42

3.4 The realization of gas and water pipelines 43

4 Structural behaviour of masonry arch bridges 47

4.1 Scientific studies on masonry..... 47

4.2 Characteristics and problems of masonry 48

4.3 Properties of masonry 49
4.3.1 Compressive strength of masonry. 51
4.3.2 Tensile strength of masonry 55
4.3.3 Behaviour under complex stress states 56
4.3.4 Compressive strength of masonry in current rules 58
4.3.5 Flexural strength of masonry in current design rules 59
4.3.6 Shear strength of masonry in current rules 60
4.3.7 Venetian masonry characterization 61
4.4 Structural behaviour 62
4.5 The safety theorem 68
4.6 Collapse mechanisms 69
5 Experimental Analysis, instruments and software 73
5.1 Operational Modal Analysis 73
5.2 Frequencies measurements instruments 74
5.2.1 Moho Tromino settings and description 74
5.2.2 Software and analysis of Tromino data 76
5.2.3 Accelerometers settings and description 78
5.2.4 Software and analysis of accelerometers data 78
6 Numerical modelling 81
6.1 Modelling of masonry 81
6.2 Scale-levels of masonry analysis 82
6.3 Masonry analysis 85
6.3.1 Linear Analysis 86
6.3.2 Non-linear analyses 86
6.3.3 Limit analyses 87
6.4 Masonry modelling 88
6.4.1 Analytical models made with beam elements 88
6.4.2 Finite Element method (FEM) 90
6.4.3 Discrete Element method (DEM) 92
7 Structural Identification 95
7.1 Geometrical Survey 96
7.2 Experimental measurements 99
7.3 Modelling procedure 100

7.4 Analytic Method 101
7.5 Modal and Static analysis 102
7.6 Model calibration, Structural identification and Material characterization 103
8 Case Studies 105
8.1 "De L'Arzere" bridge 105
8.1.1 History and description 105
8.1.2 Geometric survey 106
8.1.3 Experimental measurements 107
8.1.4 Results analysis 116
8.1.5 2-D and 3-D F.E. Model description 117
8.1.6 Structural and material identification 130
8.2 Foscarini bridge 131
8.2.1 History and description 131
8.2.2 Geometric Survey 132
8.2.3 Experimental measurements 132
8.2.4 Results analysis 133
8.2.5 2-D and 3-D F.E. Models description 136
8.2.6 Structural and material identification 150
8.3 S. Lorenzo bridge 151
8.3.1 History and description 151
8.3.2 Geometrical survey 152
8.3.3 Experimental measurements 152
8.3.4 Results analysis 153
8.3.5 2-D and 3-D F.E. Models description 156
8.3.6 Structural and material identification 170
8.4 Guglie bridge 170
8.4.1 History and description 171
8.4.2 Geometric survey 172
8.4.3 Experimental measurements 172
8.4.4 Results analysis 173
8.4.5 2-D and 3-D F.E. Model 176
8.4.6 Structural and material identification 189
9 Conclusion 191

References 193

List of Figures:

Fig. 2.1 Salgina Tower bridge, Schurders, Svizzera 7
Fig. 2.2 Golden Gate bridge in S.Francisco, California 7
Fig. 2.3 Narni bridge, Italy. Fig. 2.4 Plauen bridge, Germany 7
Fig. 2.5 Firth of Forth bridge, Edinburgh, Scotland. 8
Fig. 2.6 S. Martino bridge, Valle d'Aosta, Italy. 11
Fig. 2.7 Alcàntara bridge,Spain. 12
Fig. 2.8 Pont du Gard, Vers Pont du Gard, Francia. 12
Fig. 2.9 Aqueduct of Ferreras, Tarragona, Spain. 13
Fig. 2.10 Aqueduct of Segovia, Spain. 13
Fig. 2.11 Milvio bridge, Rome, Italy. 13
Fig. 2.12 Sestio bridge, Rome, Italy. 13
Fig. 2.13 Andùjar bridge, Andalusia, Spain. 14
Fig. 2.14 Mèrida bridge, Extremadura,Spain. 14
Fig. 2.15 Augusto bridge, Rimini, Italy. 14
Fig. 2.16: The Flaviano Bridge, Saint-Chamas, France. 14
Fig. 2.17 Bibey bridge, Galicia, Spain. 15
Fig. 2.18 Espalion bridge, France. 15
Fig. 2.19 Entraygues bridge, Aveyron , France. 15
Fig. 2.20 Ponte Vecchio bridge, Florence, Italy. 16
Fig. 2.21 Bridge of Scaligeri, Verona, Italy. 16
Fig. 2.22 Vell de Manresa bridge, Barcelona, Spain. 16
Fig. 2.23 Maddalena bridge, Mozzano, Italy. 16
Fig. 2.24 Orthez bridge, France. 17
Fig. 2.25 Monnow bridge, Monmouth, England. 17
Fig. 2.26 Julien bridge, Bonnieux, France. 17
Fig. 2.27 Mostar bridge, Bosnia. 18
Fig. 2.28 Ponte Amidonniers, Tolosa, Spain. 19
Fig. 2.29 Rialto bridge, Venice, Italy. 19
Fig. 2.30 S. Trinità bridge, Florence, Italy. 19
Fig. 2.31 Aqueduct of Pegoes, Tomar, Portugal. 20
Fig. 2.32 Aqueduct delle Aguas Livres, Lisbon, Portugal. 20

Fig. 2.33 Neuf bridge, Paris,France. 20
Fig. 2.34 Royal bridge, Paris,France. 20
Fig. 2.35 Gabriel bridge, Blois, France. 21
Fig. 2.36 Concordia bridge, Paris, France. 22
Fig. 2.37 Nemours bridge, Paris, France. 22
Fig. 2.38 Telford's bridge, Gloucester, England. 23
Fig. 2.39 Sejournè, Pont des Amidonnier, Touluse, France 23
Fig. 2.40 Sejournè, Fontpederuse railway viaduct, France. 23
Fig. 2.41 Example of centering: above cantilever centering, below supported centering, (Torre, 2003). 25
Fig. 2.42 The main element of a masonry arch bridge (Proske and van Gelder, 2009) 26
Fig. 2.43 Different pattern in skewed arch barrel (McKibbins et al.,2006). 27
Fig. 2.44 Rise to span ratio 27
Fig. 2.45 The main element of a masonry arch (Heyman, 1982) 28
Fig. 2.46 Typical configuration of modern masonry arch bridge (Torre, 2003). 28
Fig. 2.47 Typical configuration of an arch barrel (Torre, 2003). 29
Fig. 2.48 Different typologies of spandrel and backfill (Torre,2003). 30
Fig. 2.49 Typical configuration of pier (Torre, 2003). 31
Fig. 2.50 Typical configuration of abutments (Torre, 2003). 32
Fig. 3.1: Detail of "Miracle of the cross" painted by Carpaccio V.(1496). An ancient drawbridge made of wood. (Resini, 2011). 33
Fig. 3.2: "Della Paglia" bridge made of stone. 34
Fig. 3.3: "Dei Ragusei" bridge made of cast iron. 35
Fig. 3.4: : "De l'Accademia" bridge made of wood 35
Fig. 3.5: "Rialto" bridge. The vault is made by Istria stone 36
Fig. 3.6: "De L'Arzere" bridge. The vault is made of bricks 36
Fig. 3.7: "Prefetto" bridge. The vault is made by reinforced concrete 36
Fig. 3.8: "S.Rocco" bridge characterized by Hump (donkey-back) vault shape 37
Fig. 3.9: "Lombardo" bridge characterized by lowered vault shape 37
Fig. 3.10: "Squero" bridge characterized by barrel vault shape 38
Fig. 3.11: "De la Ceraria" bridge, located in Rio Novo, characterized by policentric vault shape, designed by Miozzi in 1932. 38
Fig. 3.12: Gaettini., Mazzoni ., design for a bridge near S. Marcuola. Detail of support pillars and support poles. 40

Fig. 3.13: Drawing of Marzoni for the reconstruction of S. Polo bridge. 41
Fig. 3.14: Different decorative typologies of outer arch (archivolt) of the vault 41
Fig. 3.15: Drawing by Arch. Zuanne Pastori, “S. Lorenzo” bridge, 1738. 42
Fig. 3.16: Railings made of wrought iron supported by pillars in Istria stone of “De L’Arzere” bridge. 42
Fig. 3.17: “Guglie” bridge. Railings made of Istria stone parapets..... 43
Fig. 3.18: “Frari” bridge. Railings made of Istria stone parapets 43
Fig. 3.19: “Molin” bridge watercolour drawing on the second half of XIX century. Gas pipelines location 44
Fig. 3.20: Particular of the lateral structure realized in “De le Scuole” bridge 45
Fig. 3.21: Particular of the lateral parapets in Istria where the pipes are located in “Scalzi” bridge 45
Fig. 4.1 Stressed inside unites and mortar 53
Fig. 4.2 Strength domain of masonry subjected to bi-axial compression – tensile stresses . 54
Fig. 4.3 Typical stress-strain curve for masonry (Hendry et al. 2004)..... 55
Fig. 4.4: Different mechanism of cracking due to horizontal tensile (Bakes, 1985) 56
Fig. 4.5 Mechanisms of cracking due to tensile – compression tests (Page, 1981) 58
Fig. 4.6: Plane of failure schemes. 60
Fig. 4.7 Part of a masonry arch (Heyman 1982)..... 63
Fig. 4.8 Funicolar polygon (Heyman, 1982)..... 64
Fig. 4.9 Line of thrust and moment in the centre line of three pin arch (Heyman, 1982) 64
Fig. 4.10 Middle third rule, distribution of stresses (Heyman, 1982). 65
Fig. 4.11 Real arch and middle-third rule (Heyman, 1982) 66
Fig. 4.12Bending Moment normal force diagram with yield surface in a rigid unilateral masonry (Heyman, 1982) 67
Fig. 4.13 Formation of hinges mechanism in masonry arch (Heyman, 1982)..... 68
Fig. 4.14 Geometrical factor of safety (Heyman, 1982) 69
Fig. 4.15 Opening of springing. 70
Fig. 4.16 Closing of springing. 70
Fig. 4.17 Asymmetric mechanism with fixed springing. 70
Fig. 4.18 Symmetric mechanism with fixed springing 71
Fig. 4.19 Positive and negative work 71

Fig. 5.1: Instruments location. 74

Fig. 5.2: Moho Tromino Instrument. 75

Fig. 5.3: Window of analysis parameters. 76

Fig. 5.4:Example from Tromino manual: traces selection for modal analysis of the structures. The reference site is emphasized by a red arrow. The other sites are emphasized by blue arrows. In this analysis the value of the smoothing is 1%. 77

Fig. 5.5: Example from Tromino manual of spectral relationship between homologous components. 77

Fig. 5.6: PCB Piezoeletronics type 393 C. 78

Fig. 6.1: Evolution of beam models, taken from Proske and Van Gelder, 2009. 89

Fig. 7.1: Perspective drawing of “Guglie” bridge. 106

Fig. 7.2:”De L’Arzere bridge” Points cloud 107

Fig. 7.3: Laser scanner Faro Focus 3-D S120. 107

Fig. 7.4: “S. Lorenzo” bridge, showing the positioning of black and white checkerboard targets to be used later in the phase of scan elaboration. 108

Fig. 7.5: Ortophotos of “De L’Arzere bridge obtained from the points cloud. 108

Fig. 7.6: 3-D geometrical model realized in AutoCAD software. 109

Fig. 7.7: Example of 3-D Model obtained by the acquired from the survey using Straus Software. 109

Fig. 7.8: Instruments location. 110

Fig. 7.9: Two hinges arch with backfill considered. 111

Fig. 8.85: Frequencies of Longitudinal-x direction. 156

Fig. 8.86: 2-D Model 1 “S. Lorenzo” bridge. 157

Fig. 8.87: 2- D Model 1 Diagram showing boundary condition. 157

Fig. 8.88: 2-D Model 2 “S. Lorenzo” bridge. 158

Fig. 8.89: 2- D Model 2 Diagram showing boundary condition. 158

Fig. 8.90: 2-D Model 3 “S. Lorenzo” bridge. 158

Fig. 8.91: 2- D Model 3 Diagram showing boundary condition. 159

Fig. 8.92: 3-D Model of “S. Lorenzo” bridge 160

Fig. 8.93: Static Analysis. 2-D Model realized with hinges in correspondence of the foundations. 161

Fig. 8.94: Model 1 static analysis of “S. Lorenzo” bridge. 161

Fig. 8.95: Model 2 static analysis of “S. Lorenzo” bridge. 162

Fig. 8.96: Model 3 static analysis of “S. Lorenzo” bridge. 162

Fig. 8.972: 2-D Model 1 natural frequency analysis: First modal shape. 163
Fig. 8.98: 2-D Model 1 natural frequency analysis: Second modal shape. 163
Fig. 8.99:2 -D Model 1 natural frequency analysis: Third modal shape. 164
Fig. 8.100: 2-D Model 1 natural frequency analysis: Fourth modal shape. 164
Fig. 8.101: 2-D Model 2 natural frequency analysis: First modal shape. 165
Fig. 8.102: 2-D Model 2 natural frequency analysis: Second modal shape. 165
Fig. 8.103: 2-D Model 2 natural frequency analysis: Third modal shape. 165
Fig. 8.104: 2-D Model 2 natural frequency analysis: Fourth modal shape. 166
Fig. 8.105: 2-D Model 3 natural frequency analysis: First modal shape. 166
Fig. 8.106: 2-D Model 3 natural frequency analysis: Second modal shape. 167
Fig. 8.107: 2-D Model 3 natural frequency analysis: Third modal shape. 167
Fig. 8.108: 2-D Model 3 natural frequency analysis: Fourth modal shape. 167
Fig. 8.109: 3-D Model natural frequency analysis: First modal shape. 168
Fig. 8.110: 3-D Model natural frequency analysis: Second modal shape. 169
Fig. 8.111: 3-D Model natural frequency analysis: Third modal shape. 169
Fig. 8.112: 3-D Model natural frequency analysis: Fourth modal shape. 169
Fig. 8.113: Photo of “Guglie” bridge. 171
Fig. 8.114: Particular of Venice’s map by Jacopo de Barberi,1500 171
Fig. 8.115: Particular of sheld 171
Fig. 8.116: Particular of one mask 171
Fig. 8.117: Detail of project drawing 172
Fig. 8.118: Detail of the parapet and a section 172
Fig. 8.119: Instrument location. 173
Fig. 8.120: Frequencies of Vertical-y direction. 174
Fig. 8.121: Frequencies of Transversal-z direction. 175
Fig. 8.122: Frequencies of Longitudinal-x direction. 176
Fig. 8.123: 2-D Model 1 for “ delle Guglie” bridge. 177
Fig. 8.124: 2- D Model 1 Diagram showing boundary conditions. 177
Fig. 8.125: 2-D Model 2 for “ delle Guglie” bridge. 178
Fig. 8.126: 2- D Model 2 Diagram showing boundary conditions. 178
Fig. 8.127: 2-D Model 3 for “ delle Guglie” bridge. 178
Fig. 8.128: 2- D Model 3 Diagram showing boundary conditions. 179
Fig. 8.129: 3-D Model of “delle Guglie” bridge. 180

Fig. 8.130: Static Analysis. 2-D Model realized with hinges in correspondence of the foundations. 181
Fig. 8.131: Model 1 static analysis of “delle Guglie” bridge. 182
Fig. 8.132: Model 2 static analysis of “delle Guglie” bridge. 182
Fig. 8.133: Model 3 static analysis of “delle Guglie” bridge. 182
Fig. 8.134: 2-D Model 1 natural frequency analysis: First modal shape. 183
Fig. 8.135: 2-D Model 1 natural frequency analysis: Second modal shape. 184
Fig. 8.136: 2-D Model 1 natural frequency analysis: Third modal shape. 184
Fig. 8.137: 2-D Model 1 natural frequency analysis: Fourth modal shape. 184
Fig. 8.138: 2-D Model 2 natural frequency analysis: First modal shape. 185
Fig. 8.139: 2-D Model 2 natural frequency analysis: Second modal shape. 185
Fig. 8.140: 2-D Model 2 natural frequency analysis: Third modal shape. 185
Fig. 8.141: 2-D Model 2 natural frequency analysis: Fourth modal shape. 186
Fig. 8.142: 2-D Model 3 natural frequency analysis: First modal shape. 186
Fig. 8.143: 2-D Model 3 natural frequency analysis: Second modal shape. 187
Fig. 8.144: 2-D Model 3 natural frequency analysis: Third modal shape. 187
Fig. 8.145: : 2-D Model 3 natural frequencies analyses: Fourth modal shape. 187
Fig. 8.146: 3-D Model natural frequency analysis: First modal shape. 188
Fig. 8.147: 3-D Model natural frequency analysis: Second modal shape. 189
Fig. 8.148: 3-D Model natural frequency analysis: Third modal shape. 189
Fig. 8.149: 3-D Model natural frequency analysis: Fifth modal shape. 189
Fig. 8.1: “De L’Arzere” bridge 115
Fig. 8.2: De L’Arzere bridge 116
Fig. 8.3: “De L’Arzere bridge” Points cloud. 116
Fig. 8.4: Orthophotos obtained by point cloud 117
Fig. 8.5: Tromino instrument locations. 118
Fig. 8.6: Ratio of vertical frequencies. 118
Fig. 8.7: Ratio of longitudinal frequencies. 118
Fig. 8.8: Ratio of transversal frequencies. 119
Fig. 8.9: Location and name of accelerometer sensors. 120
Fig. 8.10:Position and direction of the two acquisitions run. 120
Fig. 8.11: Example of some recordings that had the best signal-to-noise ratio (S/N). 121
Fig. 8.12: Example of some recordings that had the best signal-to-noise ratio (S/N). 121

Fig. 8.13: Location of accelerometers sensors. 122
Fig. 8.14: Stabilization diagram. 123
Fig. 8.15: Modal shapes, frequencies and damping ratio of the bridge. 124
Fig. 8.16: 2-D Model 1 “De L’Arzere” bridge 126
Fig. 8.17: 2- D Model 1 scheme of boundary condition. 126
Fig. 8.18: 2-D Model 2 “De L’Arzere” bridge 127
Fig. 8.19: 2- D Model 2 scheme of boundary condition. 127
Fig. 8.20: 2-D Model 3 “De L’Arzere” bridge. 127
Fig. 8.21: 2- D Model 3 scheme of boundary condition. 127
Fig. 8.22: 3-D Model “De L’Arzere” bridge. 128
Fig. 8.23: Static Analysis. 2-D Model realized with hinges in correspondence of the foundations. 129
Fig. 8.24: Model 1-De L’Arzere bridge static analysis 130
Fig. 8.25: Model 2-De L’Arzere bridge static analysis 130
Fig. 8.26: Model 3-De L’Arzere bridge static analysis 130
Fig. 8.27: 2-D Model 1 natural frequencies analyses: First modal shape. 132
Fig. 8.28: 2-D Model 1 natural frequencies analyses: Second modal shape. 132
Fig. 8.29: 2-D Model 1 natural frequencies analyses: Third modal shape. 132
Fig. 8.30: 2-D Model 1 natural frequencies analyses: Fourth modal shape. 132
Fig. 8.31: 2-D Model 2 natural frequencies analyses: First modal shape. 133
Fig. 8.32: 2-D Model 2 natural frequencies analyses: Second modal shape. 133
Fig. 8.33: 2-D Model 2 natural frequencies analyses: Third modal shape. 134
Fig. 8.34: 2-D Model 2 natural frequencies analyses: Fourth modal shape. 134
Fig. 8.35: 2-D Model 3 natural frequencies analyses: First modal shape. 134
Fig. 8.36: 2-D Model 3 natural frequencies analyses: Second modal shape. 135
Fig. 8.37: 2-D Model 3 natural frequencies analyses: Third modal shape. 135
Fig. 8.38: 2-D Model 3 natural frequencies analyses: Fourth modal shape. 135
Fig. 8.39: 3-D Model natural frequencies analyses: First modal shape. 137
Fig. 8.40: 3-D Model natural frequencies analyses: Second modal shape. 138
Fig. 8.41: 3-D Model natural frequencies analyses: Third modal shape. 138
Fig. 8.42:. 3-D Model 3 natural frequencies analyses: Fourth modal shape. 138
Fig. 8.43: “Foscarini” bridge. 139
Fig. 8.44: “Foscarini” bridge. 140

Fig. 8.45: “Foscarini bridge” Points cloud. 140
Fig. 8.46: Orthophotos obtained by point cloud. 141
Fig. 8.47: Instruments location. 141
Fig. 8.48: Ratio of vertical frequencies. 142
Fig. 8.49: Ratio of transversal frequencies. 142
Fig. 8.50: Ratio of longitudinal frequencies. 142
Fig. 8.51: 2-D Model of 1 “Foscarini” bridge. 143
Fig. 8.52: 2- D Model 1 scheme of boundary condition. 144
Fig. 8.53: 2-D Model of 2 “Foscarini” bridge. 144
Fig. 8.54: 2- D Model 2 scheme of boundary condition. 144
Fig. 8.55: 2-D Model of 2 “Foscarini” bridge. 145
Fig. 8.56: 2- D Model 3 scheme of boundary condition. 145
Fig. 8.57: 3-D Model “Foscarini” bridge 146
Fig. 8.58: Static Analysis. 2-D Model realized with hinges in correspondence of the foundations. 147
Fig. 8.59: Model 1 static analysis of “Foscarini” bridge. 147
Fig. 8.60: Model 2 static analysis of “Foscarini” bridge 148
Fig. 8.61: Model 3 static analysis of “Foscarini” bridge 148
Fig. 8.62: 2-D Model 1 natural frequencies analyses: First modal shape. 149
Fig. 8.63: 2-D Model 1 natural frequencies analyses: Second modal shape. 149
Fig. 8.64: 2-D Model 1 natural frequencies analyses: Third modal shape. 150
Fig. 8.65: : 2-D Model 1 natural frequencies analyses: Fourth modal shape. 150
Fig. 8.66: 2-D Model 2 natural frequencies analyses: First modal shape. 151
Fig. 8.67: 2-D Model 2 natural frequencies analyses: Second modal shape. 151
Fig. 8.68: 2-D Model 2 natural frequencies analyses: Third modal shape. 151
Fig. 8.69: 2-D Model 2 natural frequencies analyses: Fourth modal shape. 151
Fig. 8.70: 2-D Model 2 natural frequencies analyses: First modal shape. 152
Fig. 8.71: 2-D Model 2 natural frequencies analyses: Second modal shape. 152
Fig. 8.72: 2-D Model 2 natural frequencies analyses: Third modal shape. 153
Fig. 8.73: 2-D Model 2 natural frequencies analyses: Fourth modal shape. 153
Fig. 8.74: 3-D Model natural frequencies analyses: First modal shape. 154
Fig. 8.75: 3-D Model natural frequencies analyses: Second modal shape. 154
Fig. 8.76: 3-D Model natural frequencies analyses: Third modal shape. 155

Fig. 8.77: 3-D Model natural frequencies analyses: Fourth modal shape. 155
Fig. 8.78: “S. Lorenzo” bridge 156
Fig. 8.79: “Miracolo della croce” by Jacopo De Barberi. 156
Fig. 8.80: “S. Lorenzo bridge”: the points cloud. 157
Fig. 8.81: Orthophotos obtained by points cloud. 157
Fig. 8.82: Instruments location. 158
Fig. 8.83: Ratio of vertical frequencies. 158
Fig. 8.84: Ratio of transversal frequencies. 158
Fig. 8.85: Ratio of longitudinal frequencies. 159
Fig. 8.86: Ratio of vertical frequencies. 159
Fig. 8.87: Ratio of transversal frequencies. 159
Fig. 8.88: Ratio of longitudinal frequencies. 160
Fig. 8.89: 2-D Model 1 of “S. Lorenzo” bridge. 161
Fig. 8.90: 2- D Model 1 scheme of boundary condition. 161
Fig. 8.91: 2-D Model of 2 “S. Lorenzo” bridge. 161
Fig. 8.92: 2- D Model 2 scheme of boundary condition. 162
Fig. 8.93: 2-D Model of 3 “S. Lorenzo” bridge. 162
Fig. 8.94: 2- D Model 3 scheme of boundary condition. 162
Fig. 8.95: 3-D Model of “S. Lorenzo” bridge 163
Fig. 8.96: Static Analysis. 2-D Model realized with hinges in correspondence of the foundations. 164
Fig. 8.97: Model 1 static analysis of “S. Lorenzo” bridge. 165
Fig. 8.98: Model 2 static analysis of “S. Lorenzo” bridge. 165
Fig. 8.99: Model 3 static analysis of “S. Lorenzo” bridge. 165
Fig. 8.1002: 2-D Model 1 natural frequencies analyses: First modal shape. 166
Fig. 8.101: 2-D Model 1 natural frequencies analyses: Second modal shape. 167
Fig. 8.102:2 -D Model 1 natural frequencies analyses: Third modal shape. 167
Fig. 8.103: 2-D Model 1 natural frequencies analyses: Fourth modal shape 167
Fig. 8.104: 2-D Model 2 natural frequencies analyses: First modal shape. 168
Fig. 8.105: 2-D Model 2 natural frequencies analyses: Second modal shape. 168
Fig. 8.106: 2-D Model 2 natural frequencies analyses: Third modal shape. 169
Fig. 8.107: 2-D Model 2 natural frequencies analyses: Fourth modal shape. 169
Fig. 8.108: 2-D Model 3 natural frequencies analyses: First modal shape. 169

Fig. 8.109: 2-D Model 3 natural frequencies analyses: Second modal shape. 170
Fig. 8.110: 2-D Model 3 natural frequencies analyses: Third modal shape. 170
Fig. 8.111: 2-D Model 3 natural frequencies analyses: Fourth modal shape. 170
Fig. 8.112: 3-D Model natural frequencies analyses: First modal shape. 172
Fig. 8.113: 3-D Model natural frequencies analyses: Second modal shape. 172
Fig. 8.114: 3-D Model natural frequencies analyses: Third modal shape. 172
Fig. 8.115: 3-D Model natural frequencies analyses: Fourth modal shape. 173
Fig. 8.116: Photo of “Guglie” bridge. 174
Fig. 8.117: Particular of Venice’s map by Jacopo de Barberi,1500 174
Fig. 8.118: Particular of sheld 174
Fig. 8.119: Particular of one mask 174
Fig. 8.120: Particular of project drawing 175
Fig. 8.121: Particular of the parapet and a section 175
Fig. 8.122: Instrument location. 176
Fig. 8.123: Ratio of vertical frequencies. 176
Fig. 8.124: Ratio of transversal frequencies. 177
Fig. 8.125: Ratio of horizontal frequencies. 177
Fig. 8.126: 2-D Model 1 for “ delle Guglie” bridge. 178
Fig. 8.127: 2- D Model 1 scheme of boundary condition. 178
Fig. 8.128: 2-D Model 2 for “ delle Guglie” bridge. 178
Fig. 8.129: 2- D Model 2 scheme of boundary condition. 179
Fig. 8.130: 2-D Model 3 for “ delle Guglie” bridge. 179
Fig. 8.131: 2- D Model 3 scheme of boundary condition. 179
Fig. 8.132: 3-D Model of “delle Guglie” bridge. 180
Fig. 8.133: Static Analysis. 2-D Model realized with hinges in correspondence of the foundations. 181
Fig. 8.134: Model 1 static analysis of “delle Guglie” bridge. 182
Fig. 8.135: Model 2 static analysis of “delle Guglie” bridge. 182
Fig. 8.136: Model 3 static analysis static analysis of “delle Guglie” bridge. 183
Fig. 8.137: 2-D Model 1 natural frequencies analyses: First modal shape. 184
Fig. 8.138: 2-D Model 1 natural frequencies analyses: Second modal shape. 184
Fig. 8.139: 2-D Model 1 natural frequencies analyses: Third modal shape. 185
Fig. 8.140: 2-D Model 1 natural frequencies analyses: Fourth modal shape. 185

Fig. 8.141: 2-D Model 2 natural frequencies analyses: First modal shape. 186
Fig. 8.142: 2-D Model 2 natural frequencies analyses: Second modal shape..... 186
Fig. 8.143: 2-D Model 2 natural frequencies analyses: Third modal shape. 186
Fig. 8.144: 2-D Model 2 natural frequencies analyses: Fourth modal shape..... 186
Fig. 8.145: 2-D Model 3 natural frequencies analyses: First modal shape. 187
Fig. 8.146: 2-D Model 3 natural frequencies analyses: Second modal shape..... 187
Fig. 8.147: 2-D Model 3 natural frequencies analyses: Third modal shape. 188
Fig. 8.148: : 2-D Model 3 natural frequencies analyses: fourth modal shape. 188
Fig. 8.149: 3-D Model natural frequencies analyses: First modal shape. 189
Fig. 8.150: 3-D Model natural frequencies analyses: Second modal shape..... 189
Fig. 8.151: 3-D Model natural frequencies analyses: Third modal shape. 190
Fig. 8.152: 3-D Model natural frequencies analyses: Fifth modal shape. 190

List of Tables:

Tab. 4.1: Laboratory compressive tests on Venetian masonries. 61

Tab. 4.2: In situ double flat jack tests..... 61

Tab. 6.1: Methods of analysis and levels of assessments – COST-345 (2004). 81

Tab. 6.2: Safety factors for different computation strategies according to Lourenço, 2002. 92

Tab. 8.1: Comparison bettween the results obtained by RUN1 and RUN 2 measurements.116

Tab. 8.2: Mean values of dynamic parameters. 116

Tab. 8.3: Experimental measurements frequency values and Mass participation direction.116

Tab. 8.4: Percentage error value between the data obtained by the two different monitoring methodologies..... 117

Tab. 8.5: Assumed material properties for 2-D F.E. models. 118

Tab. 8.6: Adopted material Properties of 3-D models. 120

Tab. 8.7: Results of natural frequency analysis of 2-D Model 1..... 123

Tab. 8.8: Results of Natural frequency analysis of 2-D Model 2. 125

Tab. 8.9: Results of natural frequency analysis of 2-D Model 3..... 126

Tab. 8.10: Results of Natural frequency analysis of 3-D Model 128

Tab. 8.11: Dynamic parameters and difference between Tromino experimental data and 2-D / 3-D models. 130

Tab. 8.12: Experimental measurements frequency values and Mass participation direction.136

Tab. 8.13: Assumed material properties for 2-D F.E. models. 137

Tab. 8.14: Assumed material Properties of 3-D models. 139

Tab. 8.15: Results of natural frequency analysis of 2-D Model 1. 143

Tab. 8.16: Results of Natural frequency analysis of 2-D Model 2 144

Tab. 8.17: Results of natural frequency analysis of 2-D Model 3. 146

Tab. 8.18: Results of natural frequencies analysis of 3-D Model..... 148

Tab. 8.19: Dynamic parameters and difference between Tromino experimental data and 2-D / 3-D models. 150

Tab. 8.20. Experimental measurements values and Mass participation direction. 156

Tab. 8.21: Assumed material properties of 2-D F.E. models..... 157

Tab. 8.22: Mechanical properties of materials for 3-D model. 159

Tab. 8.23 Results of natural frequency analysis of 2-D Model 1..... 163

Tab. 8.24: Results of Natural frequency analysis of 2-D Model 2 164

Tab. 8.25: Results of natural frequency analysis of 2-D Model 3. 166
Tab. 8.26: Results of natural frequency analysis of 3-D Model. 168
Tab. 8.27: Dynamic parameters and difference between Tromino experimental data and 2-D / 3-D models.. 170
Tab. 8.28: Experimental measurements values and Mass participation direction. 176
Tab. 8.29: Properties of 2-D models materials. 177
Tab. 8.30: Material properties of materials for 3-D model. 179
Tab. 8.31: Results of natural frequency analysis of 2-D Model 1. 183
Tab. 8.32: Results of natural frequency analysis of 2-D Model 2 185
Tab. 8.33: Results of natural frequency analysis of 2-D Model 3 186
Tab. 8.34: Results of natural frequency analysis of 3-D Model. 188
Tab. 8.35: Dynamic parameters and difference between Tromino experimental data and 2-D / 3-D models. 190

1 Introduction

Venice is a singular city in many aspects, among these the most important ones are that it is developed on the water and its characteristic construction methods is unique all over the word. For these reasons it is our duty to take into account the preservation of its architecture and to keep it in operation. Regarding Venetian bridges few of them have been investigated except the most famous ones, like the “Rialto” bridge and the Venice “Trans-Lagoon” rail bridge. Four case-studies have been selected located in this city. The choice of the study cases is due to similar geometrical and material characteristics. In this research, a procedure for the evaluation of structural identification and material characterization is proposed for historic masonry bridges. The procedure, based on experimental and numerical analyses requires, at first, the measurements of the bridge fundamental frequencies, then, through the calibration of FE models, allows the estimation of the average elastic modulus. In particular, for the frequency acquisition data, the procedure proposes the use of a compact digital tromograph, which allows fast and low cost vibration measurements (Mucciarelli, M. 2010; Iliceto & Boaga, 2006 ; Teza et al, 2015). The data obtained using tromograph for the reference study case, that is the L’Arzere bridge, are compared and validated utilizing also accelerometers positioned in the same measurements location. For the numerical modelling, the procedure suggests an initial 2-D Model examination in order to have a fast analysis and to obtain an average range of value to attribute to the material properties and constraints of the bridge. Successively, utilizing the value obtained with 2-D Model analysis, it is possible to perform a more complex 3-D Model that gives more and exhaustive information about the structural condition and the damage of the bridge, and also a series of more detailed considerations.

1.1 Thesis layout

Section 2 – State of the Art

The evolution during the history and the morphology of masonry arch bridges are described in this section. A brief history of the evolution of this bridges typology and their constitutive features is provided. A description of masonry arch bridges still in service is given, in order to outline the dimension of the problem of their conservation. Then structural elements and behaviour of a masonry arch bridge are described.

Section 3 – The Venetian bridges

In this section Venetian bridges are described starting from their first construction examples. A description is given of the different types and the evolution of their particular arch shapes and their structural elements.

Section 4 – Structural behaviour of masonry arch bridges

A description of properties and problems of masonry is given, starting from an overview of the developed scientific studies. The structural behaviour and the safety theorem are described, furthermore an illustration and a description of the different collapse mechanisms is provided.

Section 5 – Experimental analysis, instrument and software

The Operational Modal Analysis (O.M.A) is described in this section. It is a non-destructive technique that aims at identifying the modal properties of a structure. The procedure is based on vibration data collected when the structure is under its operating conditions, without initial, or artificial, excitation. The instrument that has been utilized in this research is a Tromograph and the data obtained is confirmed utilizing accelerometers for the measurement performed in the case study of “De L’Arzere” bridge.

Section 6 – Numerical modelling

The thesis provides, in this section, a state of the art literature review on the methods of analysis and the techniques of structural modelling of masonry arch bridges, outlining the different approaches, the fields and the limits of applicability.

Section 7 – Structural identification

In this research the structural identification of four masonry arch bridges located in Venice has been carried on. In this section are described the way in which the structural identification and materials characterization have been performed describing all the different phases which are: Geometrical survey, experimental measurements, modelling procedure, Analytic method, Modal and Static Analysis finally Models calibration and Structural identification.

Section 8 – Case study

The procedure for the structural identification by means of frequency measurements and numerical models calibration, proposed in section 7, has been applied to 4 study case, which are realized with similar geometrical and material characteristics but different material of the parapet.

Section 9 – Conclusion

In the last section general observations are given on the procedure utilized, and the way in which it was applied to the case studies is outlined. The method used is fast and not expensive. It allows to perform a simple and rapid modelling to obtain primary consideration and information that characterized the structures, which are the object of analysis. Lastly, further development are suggested.

2 State of the Art

Introduction

A significant part of the heritage of road and railway works of Italy is represented by masonry bridges for the number of realizations, for the quality of their environmental integration and for the efficiency of their technical performances. They are considered superior for any technical aspect of operation compared to bridges made of reinforced concrete and to metallic ones. The vulnerability of the piers on the riverbed that hinder the flowing of the water represents the weak points of masonry bridges because in this type of bridges the piers are made thicker and closer together.

Masonry bridges have a life duration of many centuries, as shown by many roman and medieval bridges still in operation. As a matter of fact, that several roman and medieval bridges are still in operation with very high permanent weight. By reference to metal and reinforced concrete materials, masonry bridges have limited maintenance costs. They also have and a very high permanent self- weight. This feature, together with the mechanical characteristics of the structure, represents a very high resistance and rigidity of the construction with respect to mobile loads. This is the most important aspect of masonry bridges, as a consequence the passing of loads does not produce considerable deformations and vibrations. This allows bridges that are even centuries old and which are today, following to subsequent modifications, subjected to higher weights than the loads for which they were planned.

In the early decades of the XX century, when metal bridges and reinforced concrete bridges were in common use, there was a return of interest in the study of masonry bridges which, despite the higher construction cost, were the best in terms of performance. During these years Giuseppe Campanella published his treatise "Ponti in muratura" (Milan, 1928) to recognize the quality of its performance and the need to keep it in operation when possible, respecting the building. Camillo Guidi in "Scienza delle Costruzioni" (Turin, 1928) recognizes the validity of these structures, certainly not with the prospect of starting to build masonry bridges again. asonry bridges belong to the cultural heritage of the Country: as architectural works and evidence of theoretical knowledge and constructive abilities that are the basis of the current Structural Engineering.

The issue of bridges of historical interest belonging to Italy’s cultural heritage and the consequent need for their protection and conservation was the subject of studies by Luciano Re "Architettura e conservazione dei ponti piemontesi" (Turin, 1996) and "I ponti piemontesi. Progetti e cantieri "(Torino, 1999). As a consequence of these studies historical masonry bridges have been guaranteed to belong to the cultural heritage and projects for their conservation have been developed (Torre, 2003).

The history of masonry arch bridges is very long and interesting: the Romans have built wonderful bridges, after the downfall of the Roman Empire their construction declined, to

resume again during the Middle Ages, with a constant increase, from the Renaissance to the XVIII century. French and English engineers produced a great technological development, and in the XIX century masonry arch bridges reached their maximum evolution level. In the following period masonry structures were replaced by steel and concrete structures. This led to forgetting masonry structures and, in particular, the study of stone arch bridges. As a consequence the technological knowledge developed during their long history has been lost.

However, their study was considered again in the decades following World War II. The evaluation of their safety and bearing capacity has been of fundamental importance, due to the high number of masonry arch bridges belonging to Italy's road and rail network.

2.1 The evolution of bridges during history

The birth and development of bridges are important events in the evolution of civilisation. Bridges play a key role in the relationships between people and social groups, they are a core element of the civil development and the road network of an area. Their spreading testifies the wealth in trade and communication and technological progress; it is also an indicator of the economical and social boundary condition of an area and of an era. It is assumed that early bridges, although primordial and consisting of a single trunk placed to cross a stream, have been built very early in history.

The evolution of bridges is linked to the progress of materials, the structural behaviour and the construction development that characterized them.

During history different kind of structures and materials have been used for bridges construction and all of them have followed their development and their structural typologies. It is very difficult to define a sequential history of bridges but big spans are indicators of progress and development, even if for each material and type of structure specific features exist and an independent development is observed. It is not possible to compare an arch bridge made of concrete with a suspension bridge, because they cannot be studied using the same parameters. The importance of Salgina Tobel bridge (Fig. 2.1), an arch made of reinforced concrete with 90 meters of span, is the same of Golden Gate bridge(Fig. 2.1), a suspended one realized with 1280 meters of span. They have been built at the same time, the first one was competed in 1930 and the second one in 1937.

Fig. 2.1 Salgina Tower bridge, Schurders, Svizzera

Fig. 2.2 Golden Gate bridge in S.Francisco, California

The first bridges were made of wood but, nowadays, just a few of them still exist. This kind of bridges were considered less important than those made of stone. Until the middle of XIX century, when metal bridges started to be taken into account, most structures were made of wood. A great part of them have been built as a temporary solution waiting for the building of stone bridges.

Stone arch bridges provided a new level of opportunity for excellence, which is a characteristic element of Italian and European landscape. Masonry arch bridge was born as a durable solution when *"(men) began to worry about the immortality of their name ..."* considering that the bridges made of stone were *"...more lasting and give greater glory to their makers*" (Palladio, 1570).

Masonry bridges have been predominant since the Roman period and until XIX century; the construction technique that was used, the vault with ashlars, remained almost unchanged. In the XIX century, although metal bridges were already widespread, stone bridges were built in the West until the beginning of the XX century and in China they continued to be built even after the second half of the century. Unlike wooden bridges, several stone bridges still remain and most of them are still in service.

Spans of considerable dimensions have been built with arches made of stone. The Romans built Narni bridge (Fig. 2.3) realized with an arch of 32 meters span over the Nera river. During the middle ages the bridge of Trezzo was built sull'Adda, with a special rise of 72 meters. The biggest bridge made of stone in Europe was Plauen bridge (Fig. 2.4) built in 1903 on Syria Valley in Germany. This bridge had a span of 90 meters while the bridge realized with the bigger arch made of stone is Fong-Hun, it has been built in China over Ou Zhao-Ho river and has a 120 meters of span.

Fig. 2.3 Narni bridge, Italy.

Fig. 2.4 Plauen bridge, Germany

The construction of metallic bridges began at the end of XVIII century and had a large development during the XIX century, which was defined the century of metal bridge. During this period bridges made of stone stopped being built. The typologies of metallic bridges that are used nowadays, except cable-stayed bridges, which appeared in the middle of XX century, had already been used during the XIX century by making use of truss beams.

2.2 The development of bridge types

In this paragraph attention is given to the different types of structures, whose evolution, and materials, has followed a different development for each type. The first bridges made of wood were realized as girder bridges built as beams or supported deck. This solution continued to be applied over time. Truss beams, initially realized in wood, were the following step; those, from the XIX century, have been realized by a combination of cast iron and wood and later only made of metallic materials. Cantilever bridges spread during the second half of XIX century and reached the bigger spans in the word. The largest span bridge was the Firth of Forth, see Fig. 2.5, that has 521 meters of span (Tyrell, 1911). From XIX century girder bridges made of reinforced concrete started to spread and later pre-stressed reinforced concrete. Nowadays, truss beams are less frequently adopted while girder bridges made of steel and concrete are still used. Most of bridges which are built today are made of prestressed reinforced concrete did the same.

Fig. 2.5 Firth of Forth bridge, Edinburgh, Scotland.

Until the end of XVIII century, the only know durable material was stone and therefore the main construction technique for bridges were structures constituted by arches with stone ashlars. All bridges realized with stone were arch bridges. Even the first iron bridges had an arch shape probably due to the influence imparted by stone bridges.

2.3 Historical and typological evolution of masonry arch bridges

Four basic materials have been used for the construction of bridges: wood, stone, cast-iron and concrete. Bricks made of fired clay as well as metal likes aluminium are used less frequently; in particular aluminium is used in particular cases for the construction of bridges and in some of their structural elements. Nowadays composite materials are also being used, they are created utilizing fibres of very resistant materials connected with a mould made of resin, those materials are very strong. Materials have a fundamental importance on the development of the structure configuration and also on the configuration of bridges. History can be divided in two big periods: the period of masonry bridge and the period of iron and concrete.

In the first period two materials were used: stone and wood. Bricks have also been used, but bridges built in this material can be considered a subgroup of stone ones. The brick is an element of small dimension that allows the realization of arch with ashlars overlapping, therefore the morphology of masonry bridges is not so different from the morphology of bridges realized with stone blocks.

2.4 Masonry bridges

Stone is the material that was used for the building of the first bridges in Italy in pre-Roman times up to the XVIII century, this material is the only one utilizable for durable work during the time.

Nowadays, the arch bridge made of stone are no longer realized in Europe because they are too expensive. Most of the built bridges are still standing and in operation supporting condition of load heavier than design condition.

In many cities of European countries, as a consequence of the stone bridges high carrying capacity, heavy traffic has been deviated from the new bridge or iron bridge, realized during the second half of XIX century, to the ancient bridge or stone bridge. This case happened in the city of Salamanca for the iron bridge “Enrique Esteban” that is not able to support the weight of trucks and so the traffic has been deviated to the Roman bridge (Navarro and Balboa, 1994). The same situation has happened in the city of Saragoza, the traffic has been carried from the iron bridge “Pilar” over the Ebro river, to the bridge made of stone (Troyano1985). The high capacity of stone bridge is not due only to the quality of construction but in particular on the capacity of stone arch to carry out the bridge structural function.

Arches are the most suitable form for resistance to loads through a compression mechanism. Stone ashlar arches admits directrices that can move far enough from trust line, it is possible to produce hinges in the joints between the ashlars and containing the

thrust line into the arch thickness. This characteristic concurrently with the role of the fill and spandrel walls, that increases the useful thickness, allows large tolerance in the geometry of the arches. The arch, thanks to its shape, is a structure that supports the vertical loads through a resistance mechanism in which the predominant stress is that of compression. Arch is the structure more suitable for materials that do not have tensile strength and thus it is perfect for masonry. For this reason all the bridges made of masonry are based on the static principle of the arch.

The attitude of stone bridges to support loads significantly higher than the design ones, is not only due to the good operation of the arch, but also to the relationship of own weight and load that is very large due to their considerable weight. In the case of stone bridges, the resistant capacity was not the reason for which it was necessary to replace them but problems due to size or geometry. The durability of the stone bridge material and its ability to support current traffic loads make these bridges the best-preserved category of engineering works and the reason why so many stone bridges still exist.

The vault in the stone bridges remains practically unchanged by the Romans until the XVIII century, that happened only for this constructive system. Generally the vaults of the bridges are cylindrical, with the joints between the ashlars alternating to connect the elements over the entire width of the bridge, only the big ashlars of Pont du Gard (Fig. 2.8) and other roman bridge realized with the same technique of this aqueduct were realized without joints alternating. The vault is divided into independent arches, probably hooked together. There are some variations on the cylindrical vault, for example the ribbed vault.

The construction of stone bridge is quite simple, only the foundations have some problems due to the water flow rate and the flood of the river and not to the structure. The arch bridge is the best structural system for bridge construction, until the arrival of iron, utilizing durable materials as stone and brick.

Many bridges are made with bricks , some of them are attributed to the Romans. Most of the aqueducts for water supply system of the city of Rome have been realized with this material.

2.5 Evolution and development of masonry bridges

The Romans invented and developed arched bridges with stone ashlars. It is not correct to say that the bridges built during the Middle Ages are superior to those of Rome but not even inferior. During the Renaissance, the polycentric elliptical arches and lowered circular arches, that had already been used by the Romans, began to be used more frequently. No major changes occurred in stone bridges until the XVIII century, when the French engineer Jean Rodolphe Perronet reduced significantly the size of the piles and increased the lowering of the arches.

At the end of the XVIII century, the discovery of cast iron as a building material generated a radical transformation in bridges contributing to their spectacular development in the XIX century. The advent of cast iron did not prevent the continued construction of stone bridges until the end of XX century, but the bridges designed by Paul Sèjournè represented the “swan song” of the era of the stone bridge and son marked its conclusion. Today the stone is used only to restore historic bridges or as a decorative covering element.

The application of arches and vaults for bridging space is very old, probably several thousand of years old. Short span barrel vaults were already built about 5000 years ago in Mesopotamia, also Sumerian and Egyptian probably knew about vault. There are many different theories on how this type of structure has been invented. The Ancient Greeks knew arch structure; however they did not use it, their architecture was based uniquely on horizontal and vertical structural elements. A step in the development arch was during the time of the Etruscans, who are considered as the inventor of the wedge stone arch. The second step was done during the Roman period. The Romans on one hand improved the quality of the placement of the stones on the other they invented the mortar. Moreover they introduced pentagonal-shaped stones to link arch and spandrel walls, obtaining the improvement from wide vaults, built by the Etruscans, to wide-spanned arch bridges (Proske and Van Gelder, 2009)

2.5.1 Roman bridges

Roman arches are mainly round arches; the lowered arch is used only in special cases. The bow lowering is the ratio between rise and span of the arch. The rise is the difference in height between the crown and the springing. In the case of round arches, the value of the bow lowering is 1/2, in the pointed arch this ratio is greater while in the lower it is smaller. The still existing Roman bridge with the longest span is the San Martino Bridge, located in Val d’Aosta, in the north of Italy, which has a span of 35.5 meters (Fig. 2.6).

Fig. 2.6 S. Martino bridge, Valle d’Aosta, Italy.

Roman arch is characterised by geometric perfection: all the voussoirs have the same dimension both in elevation, from springing to keystone, and in arch width, and generally

the geometry of the arch precisely reproduces a circumference. Examples of this perfection are the bridges over the Tevere river in Rome, the Alcàntara Bridge over the Tago River (Fig. 2.7), and many others spread out in the territories civilised by the Romans.

Fig. 2.7 Alcàntara bridge,Spain.

The most famous Roman bridges were part of the great aqueducts that supplied the cities with water overcoming the wide valleys they met on their way. To build aqueducts and bridges with a great height was very complex, in particular the realisation of high piers. The Romans solved this problem by superposing a bridge above the a bridge above the other, in order to create two or three levels of arches which have the function of stiffening and bracing. The Pont du Gard (Fig. 2.8), aqueduct of the Roman city of Nîmes in the south of France, built in the 15 BC, still amazes for its majesty and the gracefulness of its arches. This aqueduct has a height of 47.5 meters and a length of 230 meters. The two overlapping bridges have arches whose span is 25 meters, large span for stone bridges. Finally they completed the aqueduct with an upper bridge consisting of arches with a span which is equal to 1/3 of those of the lower arches, and a height of 7.4 meters.

Fig. 2.8 Pont du Gard, Vers Pont du Gard, Francia.

The Ferreras and Terragonae aqueducts realized for the water supply of the cities of Tarraco and Segovia are constructions of the same type realized with two overlapping bridges.

Fig. 2.9 Aqueduct of Ferreras, Tarragona, Spain.

Fig. 2.10 Aqueduct of Segovia, Spain.

The Alcàntara bridge presents the same problems that have already been described for the aqueducts because the piers have a maximum height of 47 meters. In this case the solution was found giving to the piers a dimension big enough in order to avoid the use of bracings at different height. This bridge is particular for dimension and composition, it has a big span and the distance between the piers of the larger arch is 28.8 meters. The height of the piers is equal to that of the aqueducts which, as we have seen, had various levels of wind bracing. The Alcàntara bridge is probably the best expression of the degree of perfection achieved by Roman engineers.

Many bridges were built in the city of Rome and it is surroundings, many of them on the river Tevere (Fig. 2.11 and Fig. 2.12). The first were built during the Republican period. Among these, the oldest is the Emilio bridge built in 179 BC; it is currently known as the "broken bridge" because only one arch, with a decoration from a later period, is left.

Fig. 2.11 Milvio bridge, Rome, Italy.

Fig. 2.12 Sestio bridge, Rome, Italy.

The bridges built by the Romans, from their origin to the end of the Empire, had a great evolution thanks to the experience developed in the construction of bridges. The ratio between pier width and span of the arch has been strongly reduced respect of the initial value that was equal to the unit, this means that the pier had the same value of the arch span. The bridge of Andujar, on the river Guadalquivir (Fig. 2.13), has preserved this ratio. In Alcantara bridge, built with piers height 47 meters, the ratio has the value of 1/3,38.

The large size of the piers realized on the first Roman bridges were the cause of the adoption of the little lightening arch open in the fill and spandrel wall. These performed different functions such as: increasing the flow capacity of the bridge, decreasing the thrust

of the water on the spandrel walls during floods and creating an element that lightens the large mass built by the whole of the piers and the thickness of the arch.

Fig. 2.13 Andùjar bridge, Andalusia, Spain.

Fig. 2.14 Mèrida bridge, Extremadura,Spain.

Later, the piers started to be thinner and the little arches disappeared becoming blind arches.

Fig. 2.15 Augusto bridge, Rimini, Italy.

The Romans never built defence towers in their bridges; those found in some of them were added in the Middle Ages. Triumphal arches, usually in the centre, were instead built in some bridges as in Alcàntara (Fig. 2.7), sometimes at the ends like in the Flavian bridge on the Toulombre River, in France.

Fig. 2.16: The Flaviano Bridge, Saint-Chamas, France.

2.5.2 Medioeval bridges

The perfection reached by the Roman bridges was not overcome in the Middle Ages and not even in the modern age; this does not mean though that they are of inferior quality. In the Middle Ages the dominant architectural styles were the Romanesque and the Gothic, which are characterized by the complete knowledge of the use of the vault. The bridges built in this period are thinner than the Roman ones. The slenderness of the arches increases considerably by decreasing the ratio between the thickness of the ashlars and the arch span. In Roman bridges the slenderness varies from 1/8 to 1/18 in the Bibey bridge (Fig. 2.17), the average value is 1 / 12.5.

Fig. 2.17 Bibey bridge, Galicia, Spain.

During the Middle Ages arches of all types were built: round arches, pointed arches and lowered arches. The pointed arches of Gothic bridges are typical in this period. In many countries, Gothic bridges have been preserved with pointed arches and buttress that reach the crowning, such as the Espalion bridge and the Entraygues bridge, both located in France.

Fig. 2.18 Espalion bridge, France.

Fig. 2.19 Entraygues bridge, Aveyron , France.

The arches of the Avignon bridge on the river Rhône are lowered and have spans of 34 meters as well as Ponte Vecchio arches on the river Arno in Florence, built in the fourteenth century, with a maximum span of 30 meters and a lowering of 1/7 (Fig. 2.32). It is one of the best-known medieval bridges and the constructions houses on it have been maintained.

Fig. 2.20 Ponte Vecchio bridge, Florence, Italy.

Spans of medieval bridges are generally greater than those of Roman bridges, as the Scaliger Bridge over the Adige River in Verona (Fig. 2.21), which has a lowered arch of 48.7 meters and is one of the largest medieval bridges. A faithful reproduction of this bridge, built during in the XIV century and destroyed during the Second World War was rebuilt in 1945. This bridge was built in the XIV century and then destroyed during the Second World War, it was rebuilt with a faithful reproduction of the original one.

Fig. 2.21 Bridge of Scaligeri, Verona, Italy.

Medieval bridges had an evolution similar to that of Roman bridges. In the bridges built during the XI and XII centuries the little lightening safe arches of Roman derivation are often found; in the following centuries they were used less, although there are some gothic bridges built in the XI and XII century that had lightening arch.

Fig. 2.22 Vell de Manresa bridge, Barcelona, Spain. Fig. 2.23 Maddalena bridge, Mozzano, Italy.

It was previously described that the Romans often built triumphal arches in the centre or at the ends of some bridges. Instead in medieval bridges, defence and watch towers were have been built, and positioned in the centre or at the ends of the bridge. Usually, the towers had a door that could be closed to prevent passage (Fig. 2.24 and Fig.2.25). The towers were used for military defence and to collect the toll that had to be paid by everyone crossing the bridge because, in the Middle Ages, most of them were privately owned. There are not many bridges that maintain the towers, in the XVIII and XIX centuries most of them disappeared to rid the roadways from any obstacle and improve their traffic capacity.

Fig. 2.24 Orthez bridge, France.

Fig. 2.25 Monnow bridge, Monmouth, England.

In the late Middle Ages and at the beginning of the Modern Age many bridges had constructions above them which made it difficult to be crossed. Nowadays very few bridges still preserve these buildings for the same reason why towers disappeared. The most famous bridge that still preserves these buildings is the Ponte Vecchio on the river Arno in Florence (Fig. 2.20), built in 1345, which has buildings along the entire length of its spandrel walls; pedestrian traffic passes within the deck.

One of the main features of the medieval bridges is the hump (donkey-back) profile, that is composed by two ramps whose vertex is located above the main arch. As we have seen, this shape derives from the size of the rise required by the arch to develop its shape, in the round arches this corresponds to half the span. For this reason it was necessary to rise above the banks of the river in order to develop the vaults; the problem has been solved in this way in all ages.

Fig. 2.26 Julien bridge, Bonnieux, France.

A problem that caused the ruin of many stone bridges is the overturning of the spandrels due to the thrust of the fill. The Romans, as mentioned in the previous paragraph, used lightening arches on the spandrels, also to reduce their thrust. Later this system was used until the present day.

Fig. 2.27 Mostar bridge, Bosnia.

2.5.3 The bridges of the Modern Age

In the Renaissance there was a return to classical scheme, in particular the Roman one. Piers' and arches' dimensions became again the same of roman bridges. Leon Battista Alberti defined some rules for the design of bridges, on the base of the Roman Bridge of Augusto (Fig. 2.15) in Rimini, Italy (Alberti, 1483):

- the slenderness of the arch should be between 1/10 and 1/15 of the arch span
- the slenderness of the piers between 1/4 and 1/6 of the arch span

The slenderness of the arches was closer to that adopted by the Romans than to the Medieval one, but the piers dimension were closer to the values of the Middle Ages. In the Modern Age, the bridges span are generally inferior to those of medieval bridges. This return to the Roman models does not mean a relegation, but rather it is conversely the opposite, because many elements confirm a progress.

During the Renaissance, bridges with decreasing span arches, from the centre to the extremities, are frequent. "Donkey back" profiles developed from this solution. This composition has still been used after the Renaissance until the late XX century, however, more and more bridges have a horizontal profile.

Fig. 2.28 Ponte Amidonniers, Tolosa, Spain.

The Rialto Bridge on the Grand Canal in Venice (Fig. 2.29) is one of the most famous bridges of the XVI century , built by Antonio Da Ponte at the end of the century. The arch span is 27.5 meters and the rise is 7.30 meters with a ratio of 1/4 and very pronounced hump. This shape is a characteristic of Venice bridge because the banks are almost at water level and bridges must be raised to allow navigation. The Rialto Bridge has galleries for shops on both sides and the arcades are with steps and follow the slopes of the bridge. Its composition, the accuracy of its forms, and the richness of the materials have made it one of the most famous monuments of Venice.

Fig. 2.29 Rialto bridge, Venice, Italy.

The “S. Trinità” Bridge in Florence on the Arno River, built by architect Bartolomeo Ammanati is another bridge belonging to the XVI century and which confirms an evolution compared to medieval bridges. It consists of three polycentric arches that are slightly acute on the crown and very lowered (Fig. 2.42).

Fig. 2.30 S. Trinità bridge, Florence, Italy.

The Mostar bridge over the Nereva river in Bosnia (Fig. 2.27) was built in the XVI century for the will of the Ottoman Empire by the architect of the Sultan Hajrudin, but it was destroyed in 1993 during the war. It has been recently rebuilt in its original shape.

In this period a new era of development of hydraulic works has developed in the West and this gave a further boost to the construction of the aqueduct bridges.

Fig. 2.31 Aqueduct of Pegoes, Tomar, Portugal.

Fig. 2.32 Aqueduct delle Aguas Livres, Lisbon, Portugal.

In the XVII and XVIII centuries in most European countries a strong development of the communication routes began, which required the construction of many bridges. The French technique was the reference model as it was the most advanced. The round arch continued to be used but the elliptical arch and, to a lesser extent, the lowered arch became increasingly common. The lowering of the arches became ever greater until it reached the Perronet bridges of the second half of the XVIII century.

The oldest bridges of Paris on the Seine River date back to the early XVII century: the oldest among those that have survived is the Neuf bridge (Fig. 2.23), which was completed in 1607. This bridge was repaired and partially rebuilt more than once because it was damaged mainly due to defective foundations. In the middle of the XIX century all the arches of the shorter stretch were repaired and the profile was rectified, almost completely eliminating the hump. Six of the seven arches were reconstructed, transforming them into elliptical, although with minimal lowering (Gaillard, 1982). Also the Pont Marie and the Pont Royal (Fig. 2.34), both on the Seine, were built in those years.

Fig. 2.33 Neuf bridge, Paris,France.

Fig. 2.34 Royal bridge, Paris,France.

2.5.4 From the XVIII century to the end of masonry bridges

In this century the figures of the architect and engineer, who until then performed the same tasks, began to be separated. The Pont Gabriel in Blois on the Loire, a magnificent bridge, can be considered the debut of the era of engineers (Fig. 2.35)

Fig. 2.35 Gabriel bridge, Blois, France.

In the second half of the 18th century, the French engineer of Swiss origins, Jean Rodolphe Perronet, introduced a series of innovations in stone bridges that contributed to an authentic revolution. He was the founder of the "Ecole des Ponts et Chaussées" in 1747, the first Engineering school in the world and can be considered the first modern engineer. He designed and built numerous bridges in which he introduced significant innovations (Mesqui, 1986).

The main innovation provided by him were:

- Reduction of the Piers/Span ratio from 1/5 to 1/10, taking advantage of the compensation of the thrust of two adjacent arches;
- Increasing of the lowering of the arch, with Rise/Span ratio up to 1/15, by using of mono-centric shallow arches instead of poly-centric or elliptical;
- Introduction of a clear discontinuity between the arch directrix and the vertical facing; in some bridges, the arches are connected to the piers through the corne de vache;
- Invention of a system that allows the removal of all the centering formwork simultaneously;
- Invention of the pier-abutment, although he never used it.

Unfortunately only two bridges of Perronet have endured: Concordia in Paris and Nemours (Fig. 2.36 and Fig. 2.37), both are intact and in operation.

Fig. 2.36 Concordia bridge, Paris, France.

Fig. 2.37 Nemours bridge, Paris, France.

The nineteenth century was the period of greatest development of bridges, but at the same time it was also the period where masonry bridges became to became obsolete. A new structural material, cast iron (then steel) and concrete, started spreading and at the beginning of the twentieth century masonry ceased to be deployed. Despite the progressive abandoning, between the '800 and the early '900 several very interesting masonry bridges were built. The lesson of the French school spread across Europe. Thanks to the contribution of the theory of structures, masonry arches with considerable span were realised.

The biggest contribution was provided by the great English engineers of the nineteenth century, who developed the first steel bridges but mastered also the technique of masonry and wood, such as John Rennie and Thomas Telford. The '800 was also the century of the railway, which had a significant impact on the bridges. In those years large railway viaducts in masonry have been realised, on the base of the Roman aqueducts, but introducing important innovations. In particular the height and slenderness of piers has been considerably increased. The last great engineer and builder of masonry arch bridges was Séjourné, also author of a very famous treatise (Séjourné, 1913). With the treatise provided by Rondelet (Rondelet, 1831) are the fundamental references for the knowledge of the stone bridges.

Fig. 2.38 Telford's bridge, Gloucester, England.

Fig. 2.39 Sejournè, Pont des Amidonnier, Touluse, France. France.

Fig. 2.40 Sejournè, Fontpederuse railway viaduct,

In the 900s masonry material was abandoned in favour of the new structural material, and masonry arches ceased to be constructed. Nevertheless, thousands of masonry arch bridges are still in service. Exhaustive information of the history of masonry arch bridges can be found in (Troyano, 2006).

2.6 Morphology of masonry arch bridges

In a period of about 100 years, roughly from 1830 to 1930, modern masonry arch bridges were built. Common structural solutions and some structural and constructive characteristics, that vary on the basis of construction time and geographical area and the calculation method adopted by the designer, are present in this type of bridge. Many common aspects may be outlined.

The construction of stone bridges is fairly simple, the construction technique used is the vault made by ashlars, which mainly remained unchanged by the Romans until the '800: in the construction, the stone elements have a very much smaller dimension compared to the span to overcome. The voussoir arch is the perfect structure for this type of material: therefore, as long as bridge have been built up in masonry, the technique had not substantial changes.

The construction of masonry arch bridge is realised through temporary framework, called centering, usually made of wood (Fig. 2.41). Centering may be supported by the ground or may be attached to the piers or abutments and span as cantilever beams. The techniques of construction and centering have been subjected to several technological innovations during the history. Briefly, temporary frameworks are realised and placed to overcome the span, between piers and or abutments. Centering is shaped on the base of the arch profile, usually their initial shape is defined in order to accommodate further movements due to the weight of the arch before its completion. The voussoirs are placed on the extrados of the centering, starting from the springing and arriving to the crown. The construction of the arch ends with the placing of the keystone. Once the arch has been realised the centering is removed. The removal is performed eliminating provisional supports placed under the centering, usually wooden wedges which are destroyed when the arch is done, or through other systems, such as sand bags which are punched in order to be emptied. An innovative method was developed by Perronet, who invented a system to remove at the same time all the centering placed under adjacent spans.

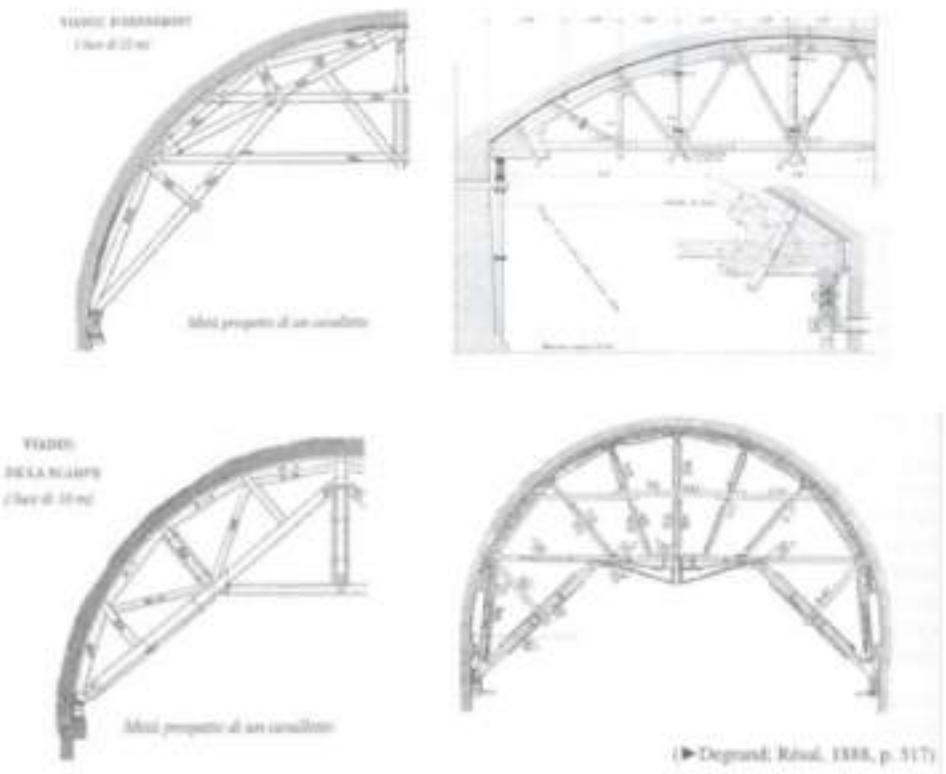

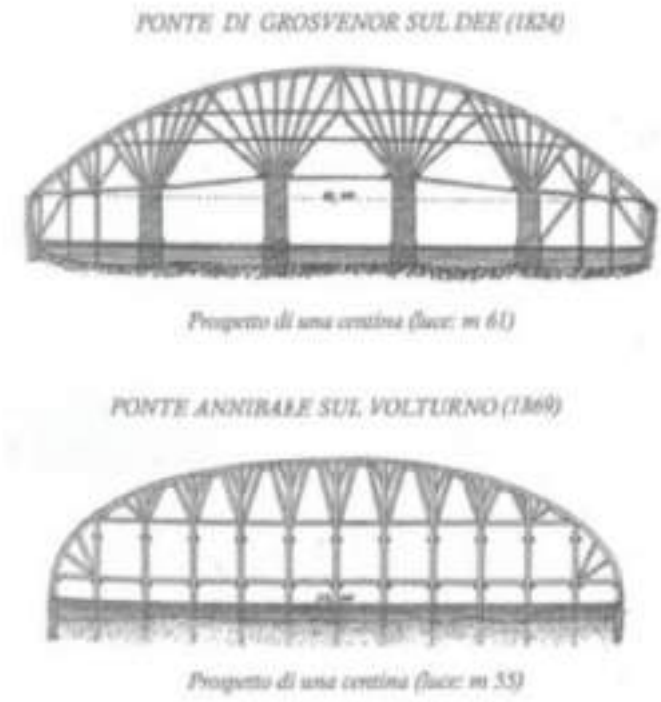

Fig. 2.41 Example of centering: above cantilever centering, below supported centering, (Torre, 2003).

The geometry of bridges depends on which obstacle had to be overcome. In general, the orography of the valley determines the main typologies of masonry arch bridges:

- Wide and deep valleys are crossed by viaducts, multi-span bridges on high piers. Viaducts were built by Romans for their aqueducts, then the typology spread with the railway, indeed aqueduct are particularly suitable to overcome height difference with low slope and/or wide curvature radius, as required by railway network.
- Wide and shallow valleys are crossed by multi-span bridges on low piers. This are the proper bridges, typical in case of rivers.
- Minor valleys and small rivers are usually crossed by single-span bridges.

The main elements of a stone bridge are (McKibbins et al., 2006):

- The arch, which is the main structural element, which allows clearing the obstacle and carrying the deck.
- The support structures of the arches:
  - Abutment, a body, usually of masonry, which provides the resistance to the vertical forces and to the thrust of the arch;
  - Pier, an intermediate support between adjoining bridge spans;
  - Pier-abutment, a mix between a pier and an abutment, that is a wider pier that, thanks to its dimensions, allows avoiding the global collapse of the bridge due to the collapse of a span with the consequent a-symmetric thrust. For the same reason, it can be very useful in the construction of bridge.

- The area overlying the arch barrel under the road surface (or equivalent), occupied by the spandrel walls, fill material or voids, and occasionally hidden elements such as internal spandrel walls. It consists of two main elements:
    - Backfilling (also called backing or filling), the material, usually Low-quality fill, used to give support behind a structure. For a masonry arch bridge, backfill material is placed in the spandrels between the arch barrel and the road surface and retained laterally by the spandrel walls and/or wingwalls. It normally consists of granular material gravel or building debris, which may have been excavated for the foundations, it consists of construction waste.
    - Spandrel walls, masonry walls that are placed on the edge of the arch barrel and that limits the extent of, and retains, the backfill. Sometimes “internal” spandrel walls may be present at other locations on the arch.

Beside the external structure of the bridge there are its foundation, typically made by wooden piles, inserted in the ground, and massive stones. They are the part of the bridge that is not visible, so any information on the consistency of the foundation works shall be deducted from the historical bibliography on construction techniques.

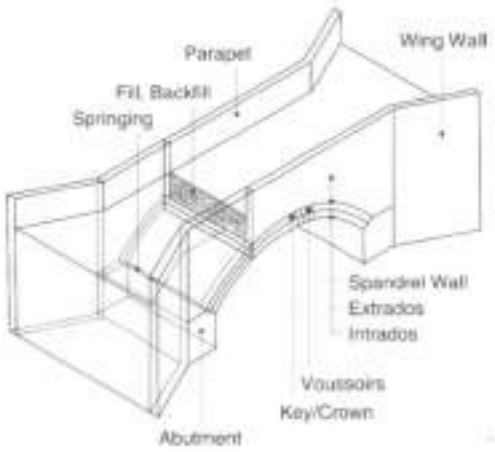

Fig. 2.42 The main element of a masonry arch bridge (Proske and van Gelder, 2009)

The arch is the main structural element of a masonry bridge. The arch is a curved structural member capable of supporting vertical loads across an opening and transferring these loads to piers (Fig. 2.49) or abutments (

Fig. 2.50). The arch barrel is the load-bearing part of the arch. It is generally made with barrel vaults, having a cylindrical intrados and a straight plant. Instead skewed arches are used when the road axis passes through the river or valley along a path that is not perpendicular to the axis of the valley. Skewed arch barrel may be realised with different construction patterns (Melbourne and Hodgson, 1995).

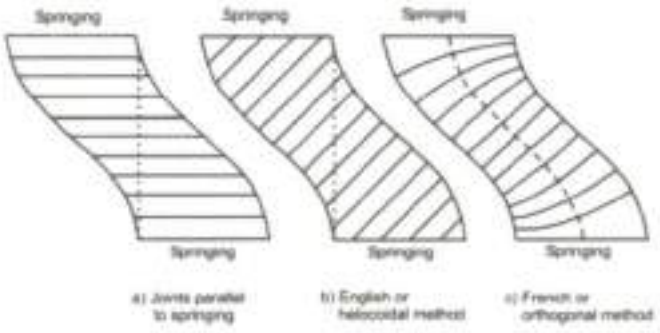

Fig. 2.43 Different pattern in skewed arch barrel (McKibbins et al.,2006).

The intrados of the arch may be define by a circular directrix, by an elliptical directrix or may be poly-centric. The shape of the arch is determined by the ratio between rise and span R/S:

- R/S = 1/2, round arch;
- R/S < 1/2, shallow arch;
- R/S > 1/2, pointed arch.

Fig. 2.44 Rise to span ratio

The principal parts of a masonry arch are (Mckibbins et al., 2006):

- The springing: plane from which an arch springs, such as the junction between the vertical face of the abutment and the arch barrel.
- The haunch, the lower section of the arch barrel towards the springing.
- The keystone or crown: the highest and last-placed stones in an arch. In the arch barrel of a bridge there are a series of keystones at the crown, across its width, which are often left projecting on side elevations.
- The extrados: in an arch or vault is the top surface of the arch barrel, the outer (convex) curve of an arch.
- The intrados: in an arch or vault is the inner surface of the arch barrel ie the inner (concave) curve of the barrel.

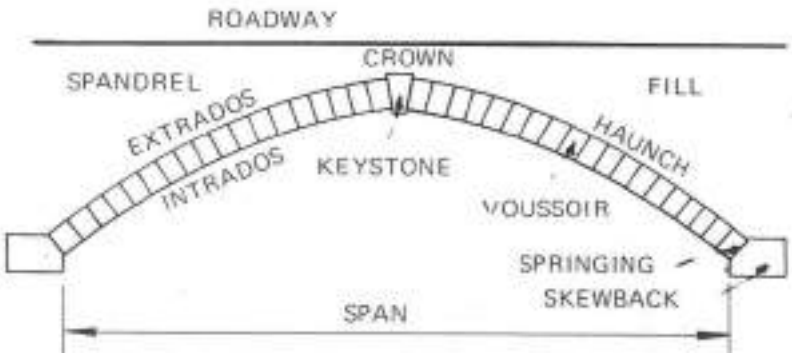

Fig. 2.45 The main element of a masonry arch (Heyman, 1982)

The material used for almost all the structural element is the masonry, made with stones, bricks or both the material. Piers, arches and spandrel walls are generally made with high quality masonry. Backfilling is made with incoherent filler, sand, stones and bricks. Backfilling often consists of two layers, separated by the waterproof system, usually realised with a concrete saddle. The lower backfill plays also a structural role in order to allocate the loads distribution and to improve stability conditions, while the upper one simply fill the space between spandrel to reach the surface road. The typical configuration of modern masonry arch bridge and an exhaustive description of its elements and material has been provided in (Torre, 2003), here some of the illustrations given by this masonry arch dictionary are reported. Illustrations regards typical configuration of masonry arch bridges built in the XIX century in Italy, in particular in the Piemonte region.

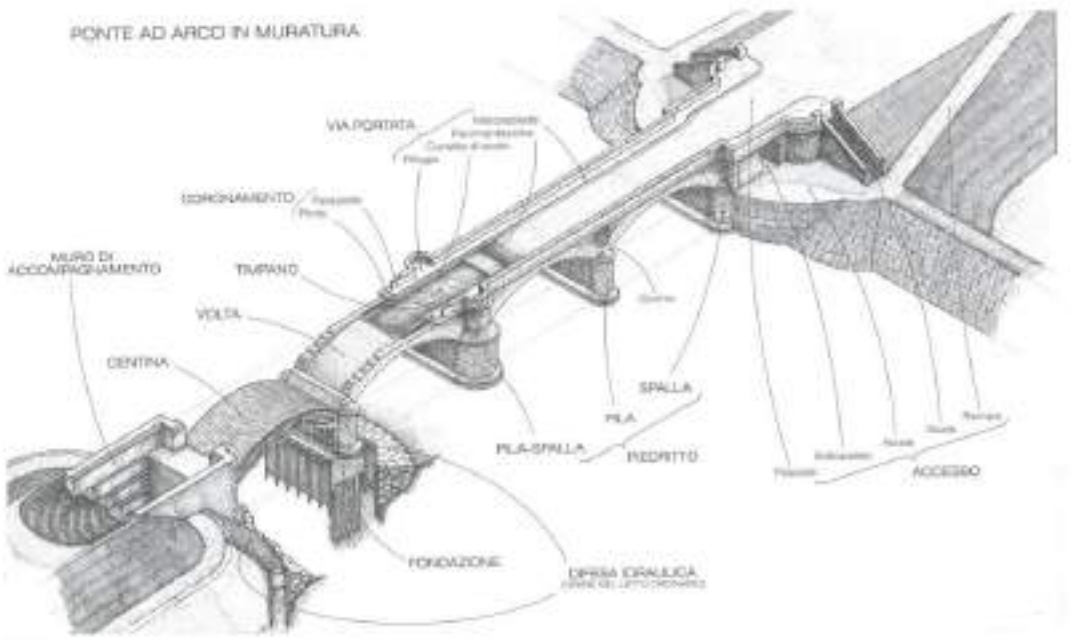

Fig. 2.46 Typical configuration of modern masonry arch bridge (Torre, 2003).

In the figure reported above is possible to notice:

- The different typologies of supports (piedritto): piers (pila), abutments (spalla) and pier-abutment (pila-spalla);
- Arch barrel (volta) both in construction and completed;
- Centering (centina);
- Spandrel (timpano) and backfill and the road surface; • Foundations and protective systems of hydraulic defence;
- Foundations (fondazioni) and protective systems of hydraulic defence;

In the following illustration elements are described more in detail.

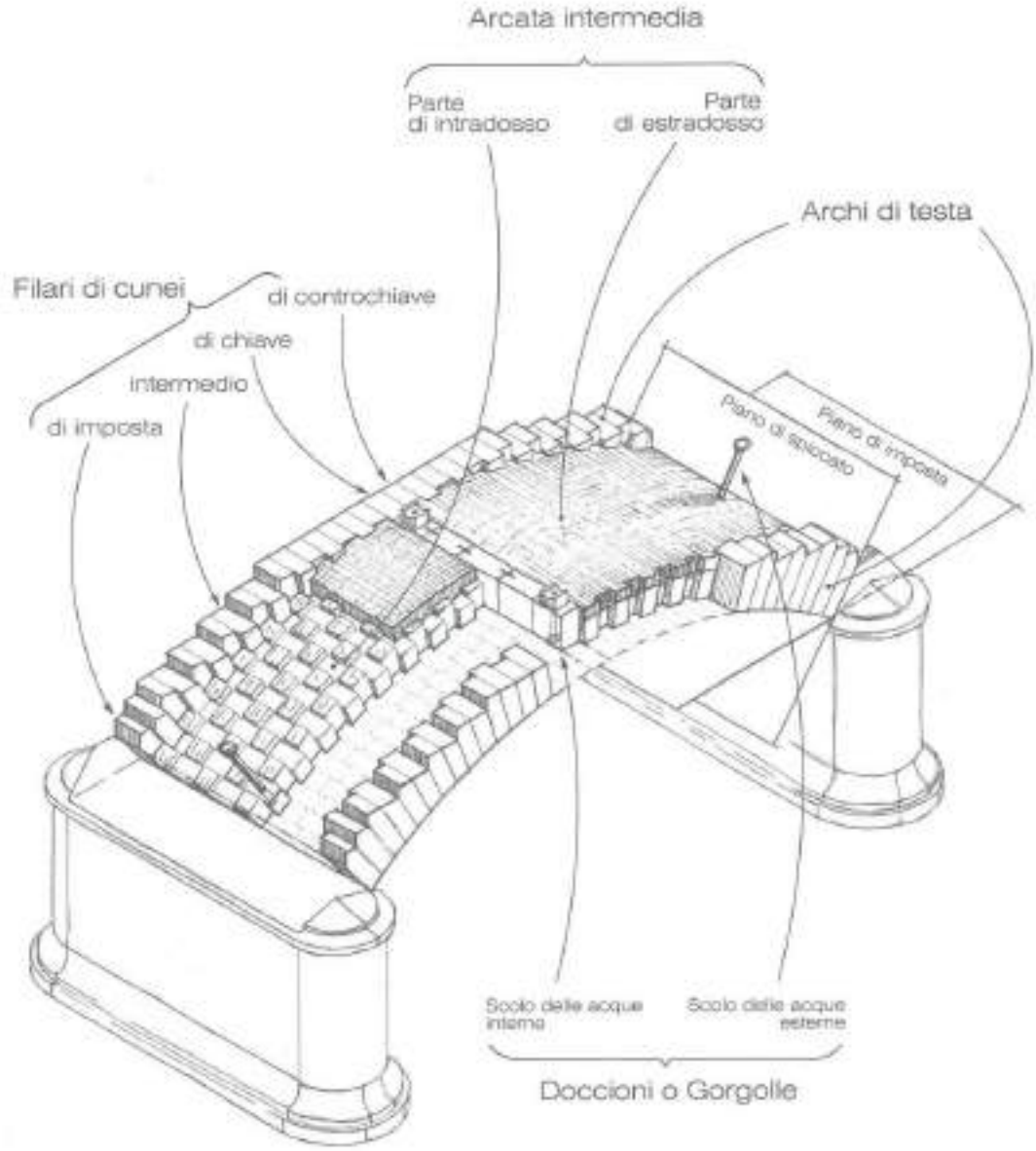

Fig. 2.47 Typical configuration of an arch barrel (Torre, 2003).

In the Fig. 2.47 is possible to notice:

- The front arches and the barrel, with the difference between the intrados, made of blocks, and the extrados.
- The different typologies of voussoirs (cunei)

Fig. 2.48 Different typologies of spandrel and backfill (Torre,2003).

In Fig. 2.48 the elements of a typical spandrel are represented: spandrel walls, upper and lower backfilling and the waterproof system. In the figure is represented an enlightened spandrel, made by transversal or longitudinal lightening arches is shown. In Fig. 2.49 Typical configuration of pier (Torre, 2003).

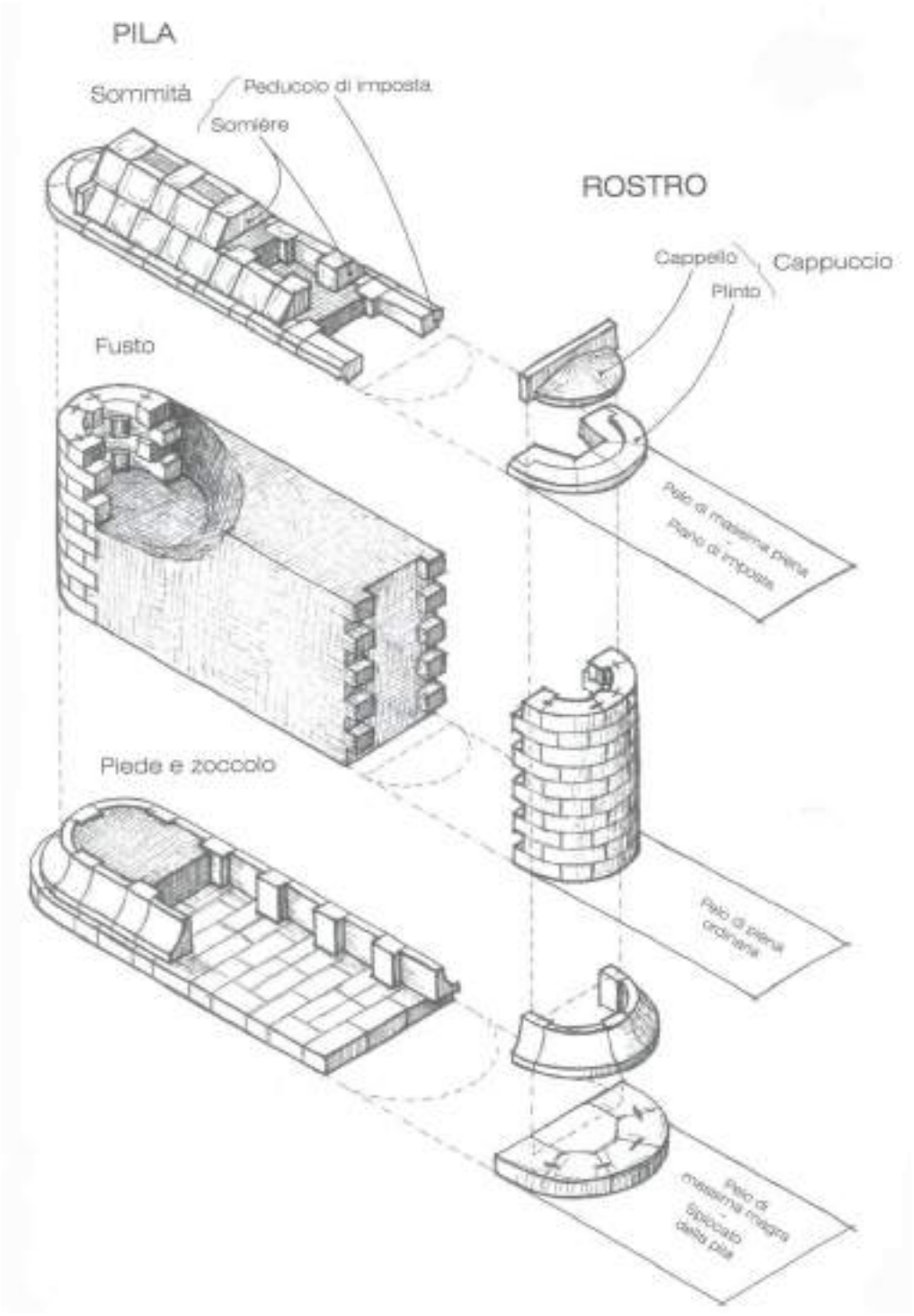

Fig. 2.49 Typical configuration of pier (Torre, 2003).

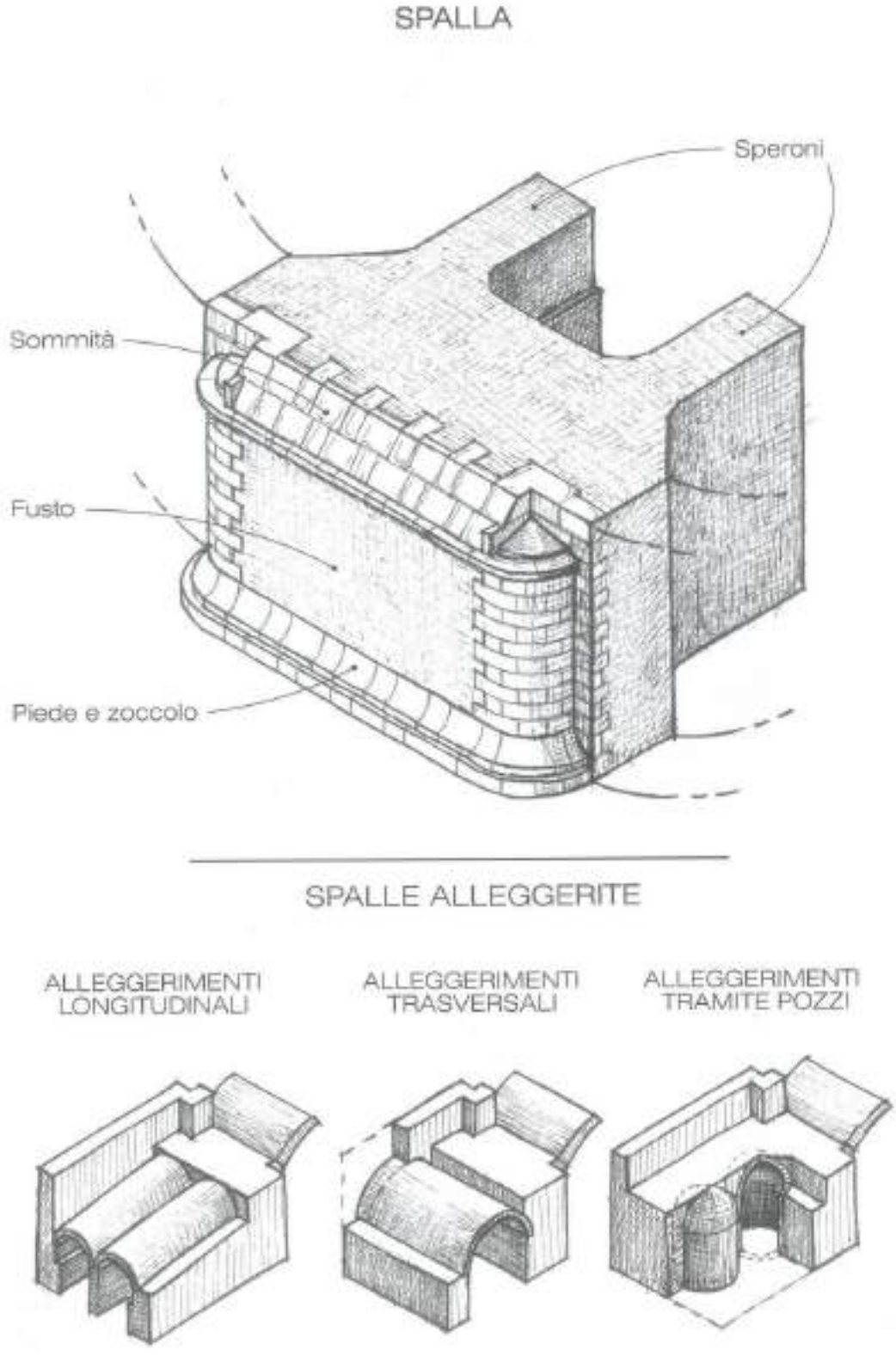

Fig. 2.50 Typical configuration of abutments (Torre, 2003).

3 Venetian bridges

In ancient time the city of Venice appeared as a set of many small islands which emerged from the lagoon water; these constituted small autonomous community nuclei. Residences were built with the main entrance pointing to the water and as close as possible to the margin of the island.

Connections between the islands were made by boats utilizing the canals which were the only way to communicate for social and work reasons.

The existing complex network of streets (named in Venice “Calle”) had a secondary importance making a comparison to the network of water and its development was not created according to the evolution of the other islands’ streets. In this way the walk network of the different islands are not aligned to each other.

The first pedestrian path started to be defined with the progress of urban development and, as a consequence, the possibility of moving from one island to the others had become an increasing issue. For this reason a sort of bridge had been constructed utilizing moving planks made of wood; in this way navigation was not hindered.

3.1 From wood bridges to stone bridges

During the IX century, the first wooden bridges were built, the largest number were drawbridges to allow easy navigation on the canals as is possible to see in Jacopo de Barbari’s map realized at the end of XIII century (Fig. 3.1).

Fig. 3.1: Detail of “Miracle of the cross” painted by Carpaccio V.(1496). An ancient drawbridge made of wood. (Resini, 2011).

Wood is an excellent material for construction but when it is immersed into water it presents a dangerous problem. It produces considerable damage in correspondence of the

part of the structure submerged by water during high tide and exposed to the air during the hours of low tide. This characteristic was a significant source of problems for Venetian habitants, who had to face frequent landslide of the banks as a consequence of eroded wooden slings.

The need to build more solid banks began early to be a priority. The part of submerged structures was protected utilizing stone blocks. Blocks were positioned on a solid base of wooden poles, which were totally immersed in the mud of the channel bed and were not in contact with air and water. In this way the foundations of Venice can be preserved for the eternity.

The choice of Istria stones is due to the fact that this type of material was extracted from the quarry of the Istria peninsula that is located on the other side of the Gulf of Venice and consequently supply was easy. Furthermore, this material was particularly suitable for the marine environment due to its characteristics.

After the reconstruction of banks and foundations with Istrian stone, even bridges began to be reconstructed using the same material. In this way the problem of the continuous repairs to which they were subjected was solved.

3.2 The bridges construction

Nowadays, in Venice there are about 450 bridges, realized with several design shapes, arch shapes and materials. Regarding construction features is possible to distinguish three principal categories of material for their construction:

- Stone bridges

Fig. 3.2: “Della Paglia” bridge made of stone.

- Iron bridges

Fig. 3.3: “Dei Ragusei” bridge made of cast iron.

- Wooden bridges

Fig. 3.4: : “De l’Accademia” bridge made of wood

A large amount of mixed bridges had been built in the city. Stone and iron bridges are considered permanent structures, while wooden ones are classified as temporary, despite the fact no one considered their substitution as issue during the past.

3.3 Arch bridges

The arch vault is the principal structure of a bridge made of stone. It may be realized with different materials as a consequence of the importance of the construction.

- Istria stone vault: ashlars are modelled as appropriate and jointed together or separated by thin sheets of lead in successive realizations. In the most important bridges, the vault made with masonry are completely covered by Istria stone.

Fig. 3.5: “Rialto” bridge. The vault is made by Istria stone

- Brick vault: the bricks are jointed with mortar made with double or triple course. In the simplest bridges, intrados, which is the part of the vault that can be seen passing under the bridge is made only with bricks or covered by a layer of plaster that, in a short time, is deteriorated by humidity.

Fig. 3.6: “De L’Arzere” bridge. The vault is made of bricks

- Reinforced concrete vault : This type of vault became widespread during the first half of XX century and it was used for all the bridges constructed in Rio Novo.

Fig. 3.7: “Prefetto” bridge. The vault is made by reinforced concrete

3.3.1 The arch shape

The vault of an arch may be realized with 4 different shapes:

- Hump (Donkey-back) vault : The oldest bridges, if they cross very narrow canal, have this shape. It has the advantage of offering a good height over the water at the centre of the bridge, allowing an easier passage of the boats. However, this solution requires rather steep steps.

Fig. 3.8: "S.Rocco" bridge characterized by Hump (donkey-back) vault shape

- Lowered vault: Is the most widespread shape. The curvature radius of the arch is bigger than the middle measure of the channel width. The structure is more flatten and pedestrians have a more comfortable passage. This shape is adopted for the channels that exceed 6 meters in width. Two meters' height from medium sea level to the crown of the intrados is maintained and in this way the passage of boats is guaranteed.

Fig. 3.9: "Lombardo" bridge characterized by lowered vault shape

- Barrel vault: The arch has the exact shape of a semi circumference with a rise corresponding to the half of the span. This shape is adapted to channels whose width does not exceed 4 or 5 meters.

Fig. 3.10: “Squero” bridge characterized by barrel vault shape

- Polycentric vault: This type of shape is defined by a traced curve that connects part of arches made by different radii and centres. This type of arch shape does not belong to the Venetian tradition. It became widespread during XIX century with the bridges designed by Salvadori and was also adopted by Miozzi in the first half of XX century for new bridges constructions in Rio Novo. The advantage of this solution is that the passage for boats under the bridge is easier not only in the centre but also on the sides. However, this innovation in the method of building infrastructures provided designers with executive issues, and, at times, undesired end results. Thrust drop is an insidious problem due to material withdrawal. This phenomenon causes undesired and considerable bending stress. The innovative “compensatory systematic lesion” method, is an excellent solution to remove the effects caused during the deformation phase. This technique was created by Miozzi. The construction system was described by its designer as the “compensatory systematic lesion” method, and consisted in the creation of three kinematic joints, which were open when the voussoirs were laid and gradually closed as the formwork was removed. This resulted in a structure that was isostatic during the deformation phase as weight was transferred from the falsework to the actual arch, without causing any bending stresses during these phases. (Lora and Poretti, 2014)

Fig. 3.11: “De la Ceraria” bridge, located in Rio Novo, characterized by policentric vault shape, designed by Miozzi in 1932.

3.3.2 Basements and Foundations

Bridge are supported by two bases called “abutments” or “ancient pillars”, these are located on each bank of the crossed channel. A girder structure transfers the weight directly on the basements, differently an arch structure downloads a vertical weight and a horizontal thrust. The abutments of a bridge must be sized in order to withstand such considerable forces. If these considerable forces are not properly counterbalanced they tend to distance the two bases from each other, causing the consequent collapse of the entire structure.

The support structures, in order to resist to these forces, can be of two types:

- “Fondamenta” are located inside the vertical walls belonging to the walkway plane. The section of the channel maintains the same dimension and there is no shrinkage of the channel section.
- Completely or partially to the walkway plane: this is the most widespread type of structure, where the two arch supporting pillars protrude about one meter or more from each bank.

In addition to these main solutions there exist a lot of other solutions, which have been used on a case by case basis.

All bridge abutments are placed on a base obtained by reinforcing the ground soil with poles made of larch wood. Their dimensions are 20 cm in diameter and 2 meters long; they are fixed on previously dredged canal bed.

The bed is positioned 2,50 meters under the level of normal excavation, that corresponds at the middle point of Venetian canals. In this way air contact is prevented, and no degradation occurs. Among the poles large flakes of Istria stone are inserted and the whole is covered with crossed tables of larch drowned in a special mortar called “Malta grassa di sabbion”.

The basement is built over the bed, it is constructed by using squared blocks of Istria stone in the lower part, while all the structure is coated using the same material. Istria stone is the only material that is able to resist to the action of brackish water.

Fig. 3.12: Gaettini., Mazzoni ., design for a bridge near S. Marcuola. Detail of support pillars and support poles.

The sdtructure of the foundations is constituent by the following elements:

- “I Corsarolli”: Blocks made of Istria stone placed in the outer part of the pier with the aim of protecting the structure located behind, which is made of bumt (“cotto”) bricks;
- “Le cadene o Catene”: Blocks made of stone inserted horizontally with special joints between the bricks to better tie together the different parts of the structure;
- “I cantonali”: elements made of stone which form the edges of the basement’s parallelepiped;
- “Il regolon e il Fasson”: Specially modelled blocks made of stone, which are located at the top of the pillar, on which the arch is set.

3.3.3 The exterior structure

The walking area consists of a more or less complex set of steps interrupted by a central flat surface. The lateral flanks are contained by a pair of small walls called Tympani or embankments; these link the arch with the line of walking plane. Between those two elements there is a frame called “Ghiera” o “Armilla”, it is made of stone ashlars jointed by “Cadene” as it is explained in section 3.3.2, usually decorated. The aim of those elements is that of hiding any sliding of Istria stones which may be caused by differential settlement.

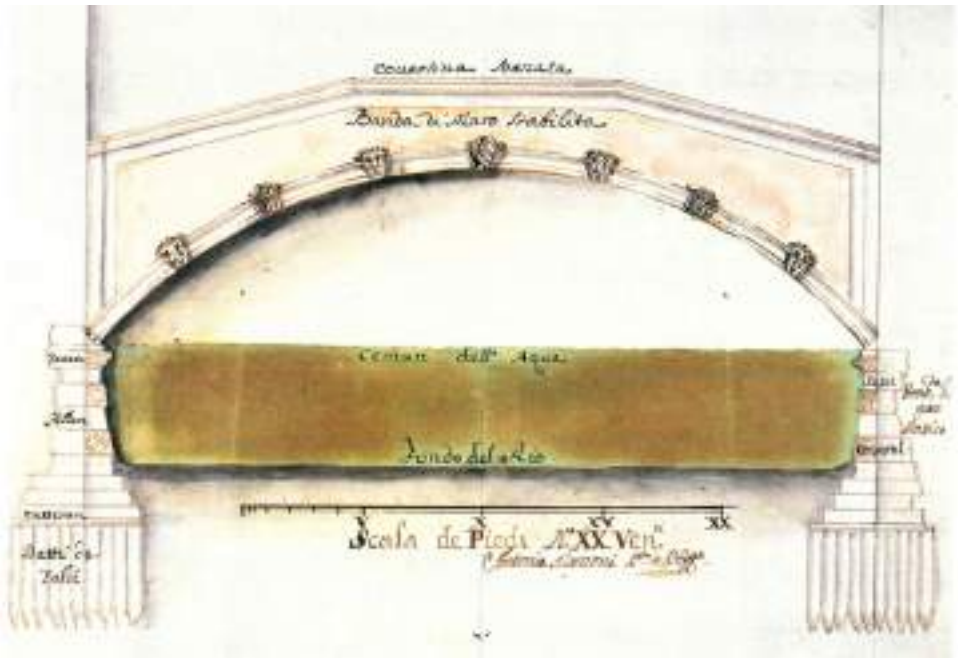

Fig. 3.13: Drawing of Marzoni for the reconstruction of S. Polo bridge.

Fig. 3.14: Different decorative typologies of outer arch (archivolt) of the vault

3.3.4 The walking level

Since ancient times, the steps of bridges were constructed with very long and sloping steps because Venetian inhabitants used horses to move along the streets. There is evidence of this also in all ancient painting of Venice, where the bridges are represented without lateral bands and the step flooring were made by bricks or stones.

During the centuries, a radical modification of the steps of the bridges has been carried out and they were been reconstructed in a less steep and more homogeneous manner, with rise of 17-18 cm and treads of 45-50 cm.

At the centre of the bridge there is, as it was already explained, a central flat surface. Other smaller flat surfaces are called “Pattesini” and are used in the bridges to interrupt the series of steps.

In the past, the step floor and the flat surface were made by either terracotta or trachyte, in the last century these materials were replaced by bitumen. There have been numerous

drawbacks to the use of this material during particularly hot summers. During the last years, bitumen has been replaced by slabs by Euganean trachyte .

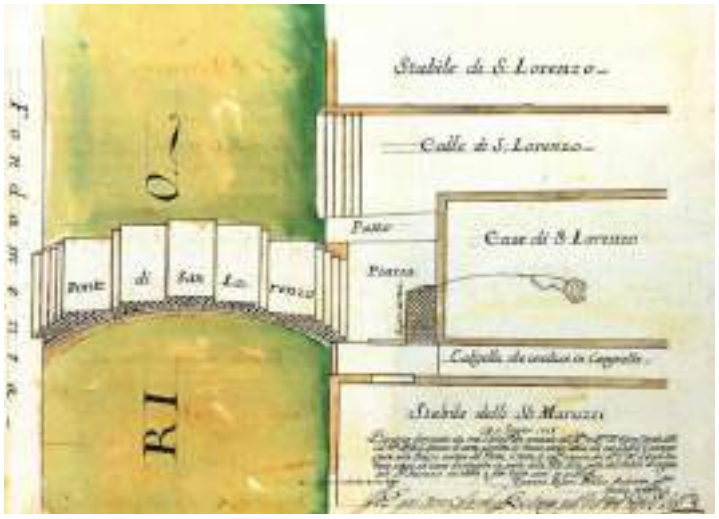

Fig. 3.15: Drawing by Arch. Zuanne Pastori, "S. Lorenzo" bridge, 1738.

3.3.5 The evolution of parapets

As is well known, in ancient times all Venetian bridges were devoid of parapets, which were all built in later times.

Steps and side bands were substituted during Austrian domination. The little brick walls added during the last years of the Serenissima Republic were all replaced with elegant railings made of wrought iron supported by pillars in stone or by columns in cast iron.


Fig. 3.16: Railings made of wrought iron supported by pillars in Istria stone of "De L'Arzere" bridge.

The most important bridges had elegant lateral sides in marble; this type of parapet was generally defined as a balustrade.

Fig. 3.17: “Guglie” bridge. Railings made of Istria stone parapets

Fig. 3.18: “Frari” bridge. Railings made of Istria stone parapets

3.4 The realization of gas and water pipelines

The introduction of gas and water pipelines carried out during the second half of the XIX century have radically changed the way of living of Venetian citizens and modified the structure of Venice bridges. This radical modification started in 1839 with the arrival of gas, and was followed by potable water in 1867.

With the diffusion of these new distribution networks it was inevitable that bridge structures would also be used as a support for the various pipelines that had to cross the channels.

Many obstacles had to be dealt with the construction of gas and water pipelines, since the crossing of many canals created many difficulties for the designer of the time (Barizza, 1984).

Initially, interventions to fragile structures like bridges were considered too complicated and architects preferred to resort to underpass systems of the canals using specially designed siphon pipes. These were located into a dug-out trench, positioned about 50 cm

beneath the bed of the canal. In this way the structures of bridge sub- foundations could not be damaged. This system had not given positive results for the difficulty of construction and for the high cost of siphons maintenance. For this reason, siphons were gradually abandoned and, in the last century, replaced by pipes placed along the bridges.

The use of bridges also for supporting pipes and cables of the underground network required radical intervention to adapt and in numerous cases to completely transform ancient stone structures to. In general, all pipes and cables were located in a space created between the arch extrados and the overlying walking surface.

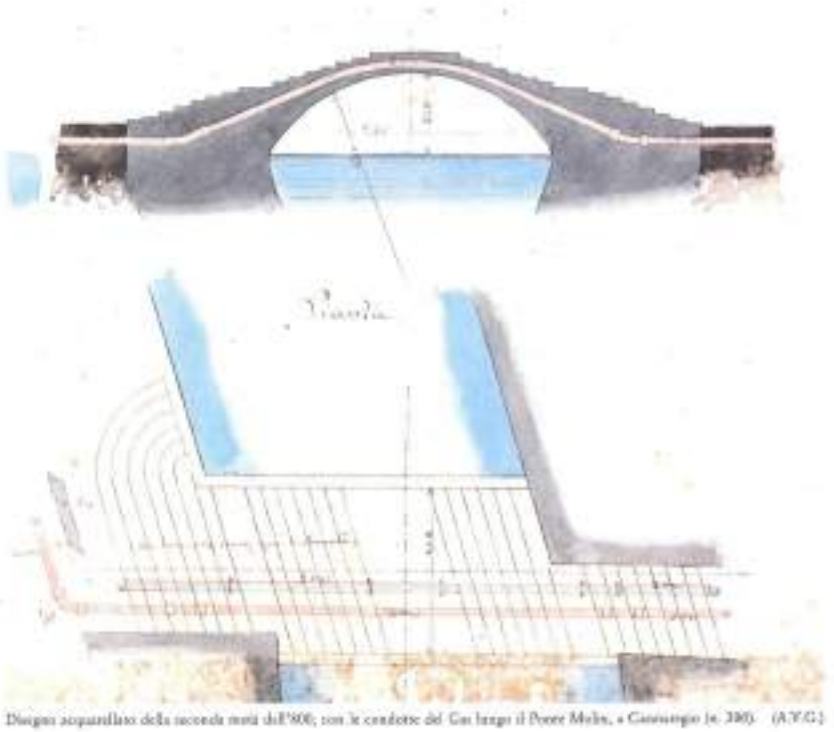

Fig. 3.19: “Molin” bridge watercolour drawing on the second half of XIX century. Gas pipelines location

In some particular cases, the unusual construction technique adopted for the construction of the bridge or the excessive diameter of the pipe to be laid did not allow traditional positioning. As a consequence, designers were compelled to devise very ingenious solutions. Among many other, it is worth mentioning two cases: “De Le Scuole” bridge and “Degli Scalzi” bridge.

“De Le Scuole” bridge is located on Giudecca island and was created as a single block made of concrete, in which there is no place to position pipelines. Then a new lateral structure was added and all pipelines and cables were positioned inside it.

Fig. 3.20: Particular of the lateral structure realized in “De le Scuole” bridge

The “Scalzi” bridge, designed by Miozzi in the first half of the XX century and inaugurated on October 28, 1934, seems to be a very thin construction. The designer wanted this bridge to be so thin that it could not even be imagined with the traditional Engineering techniques in use at that time.

The elegant structure has a very slender arch shape, which was realized with ashlars made of full thickness Istrian stone, simply leaning on each other, without the interposition of any connection system; their thickness is 1.30 meters in correspondence of the set bow and 0.8 meters on the keystone. The insertion of pipelines and cables inside the extrados was impossible to take into consideration with such a reduced thickness.

The solution found by the designer consisted in building the two lateral parapets in Istria stone with a hollow handrails of suitable dimensions in order to contain all pipes. This design choice is extremely simple and therefore even more ingenious.

Fig. 3.21: Particular of the lateral parapets in Istria where the pipes are located in “Scalzi” bridge

4 Structural behaviour of masonry arch bridges

4.1 Scientific studies on masonry

Masonry is among the oldest structural materials, particularly widespread in the Mediterranean area and used for centuries by different cultures. The technical-scientific literature on its mechanical properties, structural behaviour and constructive techniques is very wide.

Hereafter a brief overview is presented, since the beginning of the Strength of Material Science, on the trends that involved masonry studies in the last two centuries.

In the beginning of the 19th century, Rondelet (1802), Young (1807) and Navier (1838) published important treatises on structural theories. These publications represented the theoretical knowledge of the époque and defined the principles of the Science of Material and Strength of Materials. Contemporary to the development of building treatises, experimental tests were conducted on building materials

Gauthey (1809), Rennie (1818) and Vicat (1833) studied compressive tests on bricks. These analyses were made by testing bricks used for the construction of masonry arch bridges in order to define their structural characteristics.

In 1845, San Bertolo presented a more exhaustive study on masonry. In publication, the previous studies carried out on brick masonry by Gauthey and Rennie, and the studies conducted by Coulomb (1756) on stone masonry are reported. San Bertolo introduced a sort of reference value for the compressive strength to be considered for designing new structures. These values were: 40 kg/cm^2 for clay bricks and 602 kg/cm^2 for stones.

Curioni (1864-1884) published an encyclopaedic work divided into six volumes and appendices that can be considered as a collection of XIX century engineering knowledge. The treatise develops a more complete analysis, elaborating also reference values for the compressive strength, for the realization of new structural design made with different types of masonry and other buildings materials (reinforced concrete, cast iron) reproduced in tables with average values. Other examples of studies regarding compressive strength of masonry specimens, presented under the form of tables with average values, can be found in Gabba (1876) and Collignon (1869).

Manuals, like Baukunde des Architekten (1884) and following publications by Colombo (1877), Breymann (1903), Donghi (1905) and Masciari Genoese (1915) characterized the beginning of the XX century.

The attention placed on the masonry at the beginning of the XX century was significantly decreasing due to the wide use of new building materials like reinforced concrete, cast iron and steel.

Despite new materials, many authors dealt with structural behaviour of masonry arches. Pippard and Ashby (1936), Pippard (1948) and Heyman (1969) approached the stability of arch bridges. In particular, Heyman was the first to extend in a clear and explicit way both the kinematic and static theorems of limit analysis to masonry arches, according to which the structure is safe if a thrust line which lies inside the arch depth can be determined and is in equilibrium with the external loads.

4.2 Characteristics and problems of masonry

Masonry is a heterogeneous composite materials, it is anisotropic and exhibits with a non-linear behaviour. It is the result of the union of blocks and mortar, which are arranged more or less regularly, put together to compose a structural element that is not continuous.

The kind and quality of material components, the way it has been built, the dimension of blocks, the thickness and position of joints, the pattern which blocks laid inside wall, and generally the geometry, influence the behaviour of the material itself.

Masonry is the main constituent material of a masonry arch bridge. The differences between historical masonries and contemporary masonries are very important for the analysis and understanding of the structural behaviour.

In the case of historical masonry, it is very difficult to define the mechanical characteristics of the structure, which depend on the whole history of the structure and on the accumulated damage during the centuries. The mechanical properties strongly depend on the state of conservation. Each case has to be analyzed in order to recognize its specific features and the best method to evaluate them. Recently built masonries structures are designed to comply with contemporary standards and with standardisation; in this way it is possible to know how they are built and the qualities of the used materials. This means that they are designed responding to prescribed current requirements.

Looking at historical masonries is not possible to identify standard characteristics, due to some randomness in texture elements, such as the materials involved, the pattern which blocks form and their connections. All these issues influence will determine the mechanical behaviour of historical masonry structure.

If experimental tests, which are essential to establish mechanical properties of existing masonries are not undertaken, values must be taken from historical literature.

In order to evaluate the mechanical properties of historical masonry, some relevant aspects need to be considered. A very important aspect influencing the mechanical behaviour of historical masonry is the pattern in which the blocks have been connected together to create the wall, usually called bond. Correct typology of bond has linear, plane and regular horizontal joints, staggered vertical joints and present transversal connections. Other

aspects contributing to the rightness of bond are the regularity in dimension of blocks and thickness of mortar joints. When masonry is built fulfilling the so called “regola d’arte” (Giuffrè, 1991) it shows a monolithic behaviour. If masonry is realized in this way its structural behaviour presents better performances and its mechanical properties increase.

Instead masonry realized in an incorrect way, with a wrong bond, produces worse performances, its mechanical properties decrease and a non-monolithic behaviour may appear, with choking into separate portions and layers. The decrease of performances increases with the number of defects.

Important historical masonry buildings are usually made fulfilling the “state of the art”.
Referring to masonry arch bridges, masonry is generally built in the correct way. The structural elements constituting the masonry arch bridge, namely arches, piers and spandrel walls are made of good quality masonry, made of bricks or squared blocks of stones, while filling in spandrel and hollow piers is made with incoherent material, stone, sand and bricks. Regarding its structural role, filling could be considered as an isotropic material with brittle breaking. Instead there are different approaches to characterize the mechanical behaviour of masonry.

Actually there are some typical common recurring aspects that needs to be outlined in order to study masonry. The main mechanical characteristics of masonry are:

- Low and uncertain resistance to tensile stress;
- Quite good compressive strength;
- Shear strength depending on compression, on the base of Coulomb’s law on friction law;
- Load/displacement curve is linear elastic only for very low load levels, and turns to a non-linear behaviour for loads which are just larger than the former.

4.3 Properties of masonry

The properties of masonry strongly depends on the properties of its individual constituents. Components of masonry are identified by three main entities: the blocks, the mortar and the joint interfaces with their own mechanical properties. The joint interfaces are an abstraction to represent the interaction between blocks and mortar layers.

Compressive strength is the propriety that has been most investigated for every element, while in the literature there are not many contributions on the tensile and the shear strength. Compression tests of mortar and blocks that have been done to evaluate the compressive strength of masonry are related to the ultimate strength of the material. These tests are performed also for designing new buildings and defining the ultimate strength of the material. They do not provide much information about the linear and non-linear range of response.

The different deformability of mortar and blocks has great importance in relation to the collapse mechanism of a wall due to compression (Hilsdorf,1969). The greater deformability of mortar with respect to blocks is limited by friction that produces an effect of confinement of mortar. This phenomenon, yields two effects: first it generates a state of three-axial compression on the mortar joints, second it produces bi-axial tensile stresses (which are orthogonal to the load direction). The three-axial compression state of mortar increase its compressive strength (McNary and Abrams, 1985). However, the compressive strength of blocks is larger, with respect to mortar, while their deformability is lower.

Blocks show an elastic-brittle behaviour; while mortar has a tensile strength considerably lower than that of blocks, breaking occur in the elastic-plastic phase and its behaviour under shear and compression actions is non-linear, with large inelastic deformations (Page, 1981 and Page,1983).

Very low tensile strength of mortar and brittle behaviour of blocks are proven by tests regarding the behaviour of blocks and mortar under shear and tensile actions. Rather than qualities of material, the low tensile and shear strength of masonry depend on the interface (Van Der Pluijm, 1992). The weakest point of masonry is the joint interface, in where non-linear behaviour is more evident. Values of tensile and shear strength of the interface are very low. Breaking due to shear stresses is one of main causes of collapse of buildings, particularly under seismic or cyclic actions (Atkinson et al., 1989). Shear tests under different level of compression show a linear relation between compression stress and shear strength (Van Der Pluijm, 1993).

Friction does not depend on the material while the cohesion of the interface is related to the quality of mortar. For this reason there are few different models that represent interfaces with Mohr-Coulomb's law. Tests on constituent materials of masonry, which have been previously cited, are usually performed in laboratory on specimens made of today's masonries. Instead only few experimental campaigns of tests about compressive, tensile and shear strength have been carried out on historic masonries (Binda et al., 1995).

The definition of mechanical properties and suitable models for each case are difficult to establish due to the randomness that characterizes historical masonries; therefore theoretical models may be not able to describe correctly the real behaviour. It is possible to refer to analytical models the mechanical characteristic of a "general" masonry, related to its component and to its behaviour. Compressive, tensile and shear strengths of masonry are described, mainly referring to the studies carried out by (Tassios, 1977 and Di Pasquale, 1977). It is important to specify that object of the study is the ordinary masonry, i.e. without any kind of reinforcement and built with a correct bond in absence of constructive mistakes or damages.

Establishing a relation between the aspects of historical masonry and an analysis based on mathematical considerations is part of this study. Parameters useful to describe the features and the behaviour of historical masonries can be found using theoretical models.

Current design rules in the European Union (EU), the United States of America (USA) and Italy provide clues about the mechanical properties of masonry structures. The European Committee For Standardization provides *Eurocode 6* (EC 6) as a directive designing of masonry structures, while the Italian technical standards reference for masonry properties is given by *Aggiornamento delle Nuove Norme Tecniche per le Costruzioni* (NTC 2018). In USA, standards are entitled the *Building Code Requirements for Masonry Structures* (ACI 530/ASCE 5/TMS 402) and the *Specification for Masonry Structures* (ACI 530.1/ASCE 6/TMS 602) These standards for the structural design of masonry elements have been declared in accordance with the American Concrete Institute (ACI), American Society of Civil Engineers (ASCE) and The Masonry Society (TMS).

4.3.1 Compressive strength of masonry.

The main factors that influence the strength behaviour of masonry are:

- strength and geometry of the blocks;
- strength of mortar;
- strain of blocks and mortar;
- thickness of mortar joints;
- hygroscopicity of the blocks;
- type of bond and constructive system.

It is difficult to establish a "standard" strength because the compressive masonry strength f_{wc} depends on the kind and quality of material used and on their configuration.

Actually there are several empirical relations for the compressive strength of masonry f_{wc} that combine it with the compressive strength of blocks f_{bc} and mortar f_{mc}. In literature several empiric relations can be found, which have been determined by experiments:

- For good quality material:

$$f_{wc} = \sqrt{f_{bc}};\ f_{wc} = \sqrt[3]{f_{mc}};\ f_{wc} = \sqrt[4]{f_{mc}} \quad \text{(Hendry,1981)}$$

$$f_{wc} = f_{bc}/6 + \sqrt{(f_{bc} \cdot f_{mc}}/4 \ - f_{mc}/20 \quad \text{(Tassios, 1983)}$$

$$\text{if } f_{bc} < f_{mc}: \quad f_{wc} = (1 - 0.8 \cdot \sqrt[3]{\alpha}) \cdot f_{bc}$$

$$\text{if } f_{bc} > f_{mc:} \quad f_{wc} = (1 - 0.8 \cdot \sqrt[3]{\alpha} \cdot [f_{mc} + 0.4(f_{bc} - f_{mc})]$$

where α is the thickness of joints (Tassios, 1988)

- For middle quality material:

$$f_{wc} = 0.7\sqrt{f_{bc}} \cdot \sqrt[3]{f_{mc}} \quad \text{(Brocker; 1961)}$$

- For low quality material:

$$f_{wc} = (\,2/3\;f_{bc} - f_0) + \delta f_{mc} \quad \text{(Tassios, 1988)}$$

where f_0 and δ are coefficients depending on the blocks material

The parameters that influence the cubic compressive strength of masonry can be divided in two groups. The first group consists of those parameters that affect the real mechanics of collapse: the kind and the quality of blocks and mortar, the thickness of joints and the adherence. The second group includes the parameters which influence the distribution of stresses inside blocks, hence the static behaviour: the geometry of blocks, the kind of support and the way they are realised. It is important to underline that the compressive strength of masonry is always lower than the compressive strength of blocks. On the contrary, if reference is made to the case of masonry made using steel connectors, used for the linkage between blocks, then the strength value of masonry is larger than that of blocks. In any observed case it is possible to notice that under compressive stress a masonry panel cracks parallel to the principal direction of load. This is a consequence of the appearance of tensile stresses which are orthogonal to the direction of compression. The reason of a collapse obtained through vertical cracking is due to the different characteristics of the strains of its components (Hilsdorf, 1969). The adherence that constrains the relative displacements do not allow the respective movements of materials: bricks are under bi-axial tensile stresses and mortar under three-axial compression stresses. On the base of these considerations some researchers - Hilsdorf, Hendry, Tassios - developed theoretical elastic models to evaluate the relation between stress and strain and the compression strength of masonry.

To better understand the mechanics of collapse under a state of compressive stress, it is convenient to consider a little cube made by bricks and mortar under a uni-axial compression stress σ_z. The hypothesis of this model implies an elastic behaviour of material, presuming both mortar and bricks to be homogeneous and isotropic. The consequent lateral stresses due to the compression in direction z are: tensile stress in direction x and y for bricks, σ_{bx} and σ_{by}, and compressive stress acting along x- and y-direction for mortar, σ_{mx} and σ_{mx}, due to the friction between mortar and bricks faces:

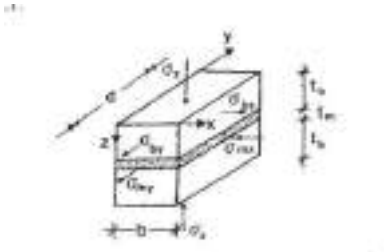

Fig. 4.1 Stressed inside unites and mortar

By enforcing and the equilibrium of stresses and the compatibility of strain it is possible to obtain the tensile stress of bricks $\sigma_b = \sigma_{bx} = \sigma_{by}$. As a consequence of Hooke's law, strains of bricks along x and y, ε_{bx} and ε_{by} , are:

$$\varepsilon_{bx} = 1/E_b \cdot [\sigma_{bx} + v_b(\sigma_{z-}\sigma_{by})]$$

$$\varepsilon_{by} = 1/E_b \cdot [\sigma_{by} + v_b(\sigma_{z-}\sigma_{bx})]$$

The strains of mortar along x and y, ε_{mx} and ε_{my}:

$$\varepsilon_{mx} = 1/E_m \cdot [-\sigma_{mx} + v_m(\sigma_{z-}\sigma_{my})]$$

$$\varepsilon_{my} = 1/E_m \cdot [-\sigma_{my} + v_m(\sigma_{z-}\sigma_{mx})]$$

In which E is Young's modulus and *v* Poisson's ratio. The compatibility implies that strains of bricks and mortar are equal:

$$\varepsilon_{bx} = \varepsilon_{mx} \quad \text{and} \quad \varepsilon_{by} = \varepsilon_{my}$$

$$1/E_b \cdot [\sigma_{bx} + v_b(\sigma_z - \sigma_{by})] = 1/E_m \cdot [-\sigma_{mx} + v_m + (\sigma_z + \sigma_{my})]$$

$$1/E_b \cdot [\sigma_{by} + v_b(\sigma_z - \sigma_{bx})] = 1/E_m \cdot [-\sigma_{my} + v_m + (\sigma_z + \sigma_{mx})]$$

The resultant of compression forces of mortar has to be equal to the resultant of tensile forces of blocks in order to have the equilibrium, in both directions x and y. Where according to Fig. 4.1 :

$$\sigma_{bx} \cdot d \cdot t_b = \sigma_{mx} \cdot d \cdot t_m \qquad \sigma_{bx} = \alpha \cdot \sigma_{mx}$$

$$\sigma_{by} \cdot d \cdot t_b = \sigma_{my} \cdot d \cdot t_m \qquad \sigma_{by} = \alpha \cdot \sigma_{my}$$

$$\alpha = t_m/t_b < 1$$

Defining β as the ratio between Young's modulus of blocks and mortar, multiplying all terms by E_b and making use Hooke's law, it follows:

$$\sigma_{bx} + v_b\sigma_z - v_b\sigma_{by} = \beta[(-\sigma_{bx}/\alpha + v_m(\sigma_z + \sigma_{by}/\alpha)]$$

$$\sigma_{by} + v_b\sigma_z - v_b\sigma_{bx} = \beta[(-\sigma_{by}/\alpha + v_m(\sigma_z + \sigma_{bx}/\alpha)]$$

Then the tensile stress in bricks due to vertical compression is:

$$\sigma_{bx} = \sigma_{by} = [\alpha(v_m - \beta v_b)/(1 + \alpha\beta - v_m - \alpha\beta v_b)]\sigma_z$$

Where $\beta = E_m/E_b$<1 that is a homogenization coefficient.

A decrease of the value of compression stress σ_z is due to the presence of the tensile stresses σ_{bx} and σ_{by} and implies that bring to failure, $\sigma_{zu.}$ The tensile strength of a block is related to the compression strength of the block itself: $f_{bt} = \lambda f_{bc}$.

If a linear relation between tensile and compression strength is assumed, then failure under compression will occur when:

$$\sigma_{zu}/f_{bc} + \sigma_t/\lambda f_{bc} = 1$$

The compressive strength of masonry f_{wb} is equal to σ_{zu}, therefore:

$$f_{wc}/f_{bc} = 1:\{1 + [\alpha(v_m - \beta v_b)/\lambda(1 + \alpha\beta - v_m - \alpha\beta v_b)]\}$$

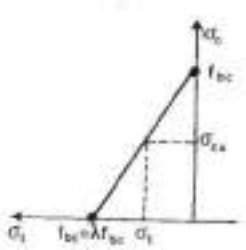

Fig. 4.2 Strength domain of masonry subjected to bi-axial compression – tensile stresses

Assuming this relation, as shown in Fig. 4.2, the influence of the thickness of joints on the compression strength is evident, in fact the strength decreases as the mortar joint thickness increases. This model allows also to point out the relationship between masonry strength and the resistance of its components. Applying the same relation but adopting different values for bricks and mortars, the compressive strength of masonry varies: f_{wc} raises up when also f_{bc} raises (Hendry, 1981). The velocity of increase depends on the quality of mortar: if the quality of mortar is good, the strength of masonry increases rapidly, otherwise slowly, referring to the proportionality. At the same time the increase of f_{wc} is not linear respect to the increase of f_{mc}: to double f_{wc} it needs to increase fivefold f_{mc}.

Masonry is usually considered as a linearly elastic material; on the other hand tests indicate that the stress-strain relationship is approximately parabolic. This assumption is considered reliable for the calculation of normal deformation because under service conditions masonry is generally loaded only up to a fraction of its ultimate load. The deformation behaviour of masonry, the relation σ - ε between stresses and strains can be expressed as:

$$\sigma/f_{wu} = 2(\varepsilon/\varepsilon_u) - (\varepsilon/\varepsilon_u)^2$$

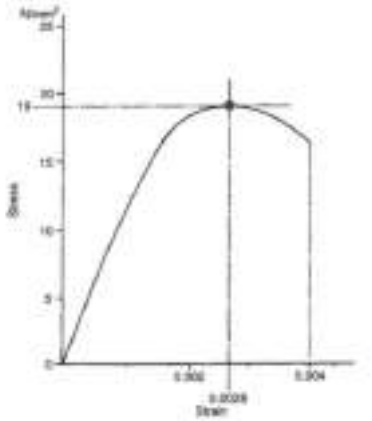

Fig. 4.3 Typical stress-strain curve for masonry (Hendry et al. 2004)

The diagram in Fig. 4.3 shows the relation between stresses and strains and it is based on tests (Hendry et al., 2004): ε_0 is the maximum strain of a specimen under compression loads, with a value between 0.25 % and 0.35 %; f_{wu} is the ultimate compressive strength; E_{w0} is Young's modulus for the initial portion while E_{wu} is that at maximum compression.

This relation describes correctly the initial rising phase of the diagram while is not completely reliable regarding the second phase. The analysis of the deformation behaviour of masonry is extremely laborious and suffers from uncertainty, especially when trying to determine the value of elastic modulus E. The elastic modulus is considered equal to the tangent to the curve σ - ε only for values of f_w less than 0.4 f_{wu}. Without direct experimental measurements it is possible to refer to empirical relations (Schubert,P., and Wesche, K., 1984, Hendry, 1981).

Values provided belong to those ranges:

- Young's modulus of blocks: E_{b}= (300 ÷ 400) f_{bc}
- Young's modulus of mortar: E_{m} = 900 f_{mc}
- Young's modulus of masonry: E_{w} = (500 ÷ 1000) f_{wc}
- Poisson's ratio: ν = 0.1 ÷ 0.2

4.3.2 Tensile strength of masonry

The direction of a crack depends on stress direction. When tension is applied along a vertical direction, breaking affects mortar, yielding a detachment between blocks and mortar, hence the cracks are horizontal. For this reason the vertical tensile strength of masonry f_{wt} can by expressed as a percentage value of the tensile strength of mortar f_{mt}:

$$f_{wt} = \xi f_{mt}$$

Where ξ is a coefficient depending on the compactness of mortar and by its conservation state. Usually it has a value close to 2/3.

In the horizontal direction the tensile strength of masonry depends on the resistance opposed by joint to the sliding between mortar and to the tensile strength of blocks. As a consequence there are two cracking mechanisms: in the first case the cracks occur only in the joints because they depend only on mortar strength, while in the second one cracks take place also in the blocks and depend on blocks strength.

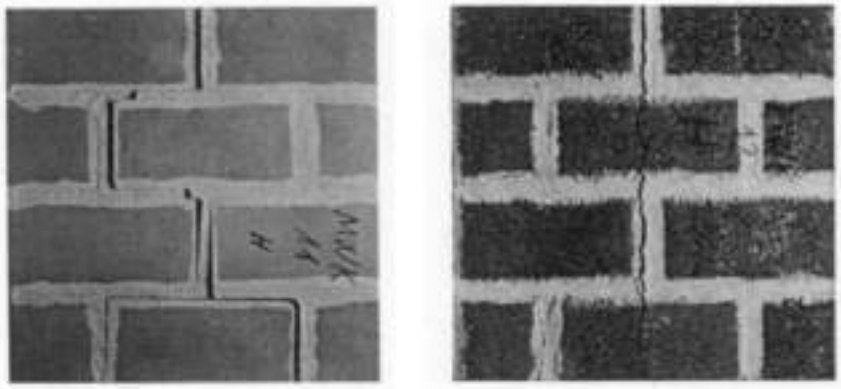

Fig. 4.4: Different mechanism of cracking due to horizontal tensile (Bakes, 1985)

Masonry has very low and uncertain tensile strength. It is impossible to calculate the tensile strength of masonry respect to the variation of the angle of the main tensile stress; also it is necessary to take into consideration even the role of the lateral compression stress. The consequence is that masonry has to be considered as a material without tensile strength. Moreover it is not possible to evaluate its shear strength based on its tensile strength.

4.3.3 Behaviour under complex stress states

All combinations of stress and strain which can involve all three spatial dimensions give complex stress states.

However, the results obtained from experimental tests denote that the anisotropic behaviour of masonry can be reduced to an orthotropic behaviour. For this reason, bi-axial tests are very interesting in order to understand the global behaviour of masonry. In fact, tests highlight several aspects of the response of masonry for actions normal to the planes of the mortar joints, but they also allow understanding the shear response. Considering the behaviour of masonry under tensile stress, usually the biaxial tests have been carried out to investigate the behaviour of masonry in relation to the variation of the angle of horizontal mortar joints with reference to the principal stresses of compression-tension. In this field the works by Page represent the main reference (Page, 1981 and Page, 1983). As it is represented in Fig. 4.5, three types of bi-axial tests have been carried out: tensile-tensile,

tensile-compression, compression-compression. The results allow defining strength domains of resistance related to generic stress states in the plane.

In the case of tensile – tensile tests the strength domain is strongly dependent on the angle which horizontal mortar joints form with the direction of principal stresses. Same relevance of this aspect is highlighted by tests in the case of tensile – compression stresses. Several cracking mechanisms can occur, involving both horizontal and vertical mortar joints, depending on the inclination of the joints. It is interesting to point out that when the angle of inclination is equal to 0, so that the tensile stress acts horizontally while compression acts vertically, there is an increment of the tensile strength of masonry, due to the effect of vertical compression that does not allow any sliding and/or opening of joints. Instead in the case of compression – compression tests the behaviour of masonry is not so strictly dependent on the inclination of joints. Considering the strains due to bi-axial stresses, it is interesting to point out that in case of compression – compression tests the response of masonry is strongly Non linear, while in the case of tensile – compression tests breaking occurs in the linear elastic field. Moreover during the linear phase the behaviour of masonry could be considered isotropic, while in the non-linear phase it is anisotropic, due to the weakness of mortar compared to blocks (Page, 1983; Dhanasekar et al., 1985).

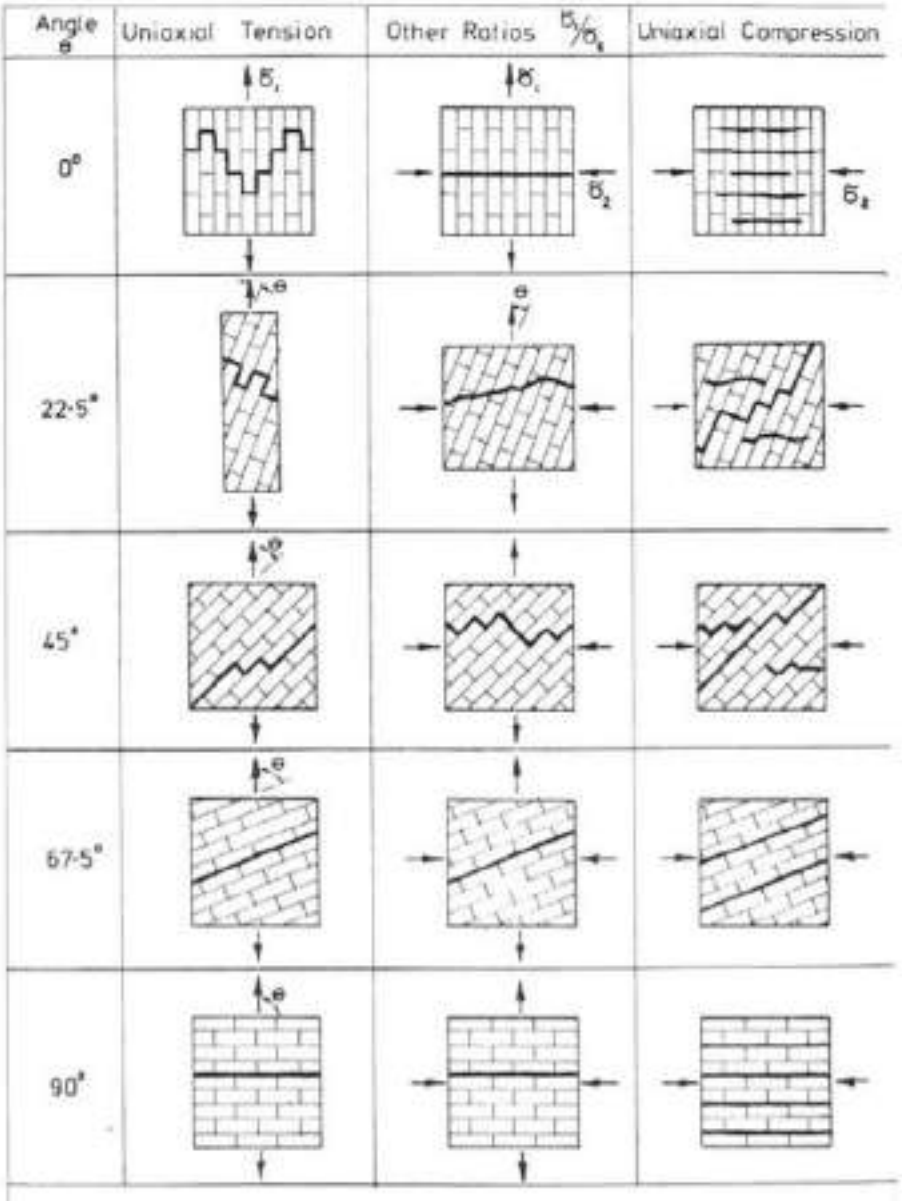

Fig. 4.5 Mechanisms of cracking due to tensile – compression tests (Page, 1981)

4.3.4 Compressive strength of masonry in current rules

Compressive strength of masonry is now addressed, as it is defined by EC 6 (Section 3.6) and NTC 2018 (Section 4.5.3).

The EC 6 prescribe that f_k (characteristic compressive strength) and f_{vk0} (characteristic initial shear strength under zero compressive stress) shall be determined from results of tests on masonry specimens, while, the short term secant modulus of elasticity, E shall be determined by tests in accordance with EN 1052-1. In the absence of them, E, may be

assumed to be equal to $K_E * f_k$ (with K_E =1000, recommended value by EC 6). The shear modulus, *G*, may be taken as 40% of the elastic modulus, *E*.

From the characteristic strength f_k it is possible to define the design compressive strength f_d, reducing it by a partial factor Υ_M due to the material. This reduction factor is defined as a function of the performance classes and strength of the used elements, according to:

$$f_{\mathrm{d}} = f_{\mathrm{k}}/\Upsilon_{\mathrm{M}}$$

The EC 6 (Section 2.4.3) gives numerical values to be attributed to factor Υ_M. By the way it provides also the National Annex (Annex A) where it delegates to all countries the task of defining the national parameters to be used for design. Parameters to be adopted in Italian design rules are defined by NTC 2008, Table 4.5.II.

As it is explained in the EC 6, the characteristic compressive strength of masonry f_k shall be determined from results of tests on masonry specimens, in accordance to EN 1052-1. The results of the tests can be expressed in terms of equation:

$$f_k = K f_\beta^\alpha f_m^b$$

where:

- f_k is the characteristic compressive strength of the masonry, in N/mm^2;
- K = 0.60 f_m;
- α= 0.65, β = 0.25;
- f_b is the normalized average compressive strength of the block, in the direction of the applied action effect, in N/mm^2;
- f_m is the compressive strength of the mortar, in N/mm^2

4.3.5 Flexural strength of masonry in current design rules

The EC6 proposes to consider the following situations in relation to out-of plane bending:

a) flexural strength having a plane of failure parallel to the bed joints (f_{xk1});

b) flexural strength having a plane of failure perpendicular to the bedjoints (f_{xk2});

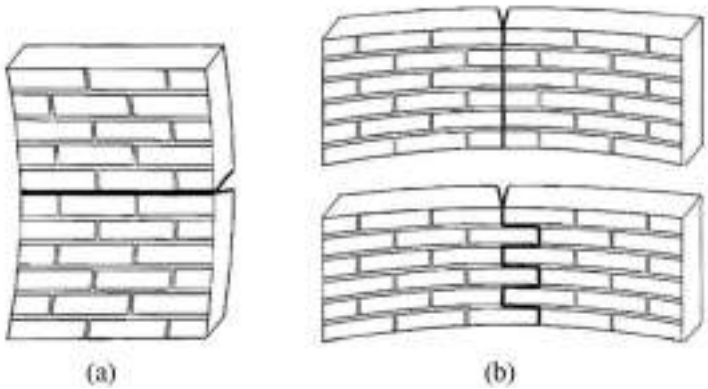

Fig. 4.6: Plane of failure schemes.

EC 6 defines that characteristic flexural strength of masonry may be determined by tests on masonry specimens in accordance to EN 1052-2, or it can be established from an evaluation of test data based on the flexural strengths of masonry obtained from appropriate combinations of blocks and mortar. Values of f_{xk1} and f_{xk2} to be used in a particular country may be found in its National Annex or taken from the tables in EC 6, Section 3.6.3.

4.3.6 Shear strength of masonry in current rules

EC 6 suggests that the characteristic shear strength of masonry, f_{vk}, should be determined from the results of tests on masonry samples, in accordance to 1052-3 or EN 1052-4, or obtained from a database.

The characteristic shear strength of masonry, f_{vk}, using general purpose mortar, or thin layer mortar in beds of thickness from 0,5 mm to 3,0 mm, or lightweight mortar so as to be considered as filled, may be obtained from the equation:

$$f_{vk=}f_{vk0} + 0.4\sigma_d$$

where:

- f_{vk0} is the characteristic initial shear strength, under zero compressive stress;
- σ_d is the design compressive stress acting on a direction perpendicular to the shear in the structural element under consideration, using the appropriate load combination based on the average vertical stress over the compressed part of the wall that is providing shear resistance.

4.3.7 Venetian masonry characterization

Since it was not allowed to remove any samples from the buildings which are the object of this study, the laboratory analyses proposed in the last paragraph were performed with the use of solid clay bricks and special mortar (CP/5), which are able to simulate the behaviour of historic mortars.

However, in the past few decades several researches focused their attention on the characterization of Venetian masonry through destructive tests both in situ and in laboratory. For example, in the researchers presented by Zago and Riva (1981, 1982), a series of experimental tests conducted on 130 clay bricks is proposed. The sample have been taken from the original buildings (ecclesiastical, residential or infrastructures); moreover several masonry specimens obtained directly from the buildings or built with original bricks and new mortar with low structural characteristics have been tested. More recent experimental research carried out on Venetian historical buildings, aimed to check the structural behaviour of a masonry building under fire action (Russo et al, 2008), or to evaluate the state of stress of historical bell towers (Lionello et al, 2005).

Since the aforementioned research were carried on with different purposes, the specimen dimension is variable, as well as material components and analysis techniques, hence it is not possible to perform any direct comparison with data obtained in laboratory. In order to provide an overview on the mechanical characteristics of Venetian masonries, Tab. 4.1 and Tab. 4.2, which provide a summary of the aforvementioned research.

Researches	Location	Specimen Dimension	Specimen Age	***E*** (GPa)
Zago & Riva, 1982	Cà Grande, Tron palace, Zambelli-Pema palace, Badoer palace	l:50-52 b:26-40 h:34-53	XIII XIV XV XVI XIX	Mortar layers < 10mm 1.4 - 2.3 - 2.8 Mortar layers > 13mm 1.2 - 1.6
Russo et al, 2008	Molino Stucky	l:13-26 b:12-13 h:21-23	XIX	Fire-damaged 0.8 undamaged 1.1

Tab. 4.1: Laboratory compressive tests on Venetian masonries.

Researches	Location	Specimen Age	***E*** (GPa)		
Russo et al, 2008	Molino Stucky	XIX		undamaged 2.7	
Lionello et al, 2005	S. Stefano bell tower	XV XVI	External core 4.0	2.8	Inner core 2.8

Tab. 4.2: In situ double flat jack tests.

4.4 Structural behaviour

Technologically, masonry bridges are structures of the past. The last constructions of this type of bridges were done during the first 20-30 years of the XX century; later attention for this type of structure disappeared and it was substituted by the design and the construction of the new structures made with new materials, like steel or reinforced concrete. From that time the attention for structures made of masonry declined.

The main element of the historic masonry bridge is the masonry arch, which define its architectural and Engineering features and characterizes its structure and form. The structural behaviour of the whole bridge is strongly dependent on the features of the masonry arch, which provide the main contribution to the load-bearing capacity, although not the only one. For this reason, the comprehension of its behaviour is fundamental for studying and understanding the masonry arch bridges.

Masonry arches are structure made of wedge -shaped blocks - stones or bricks – called voussoirs, placed one next to the others, with or without mortar joints, in order to precisely create an arch ring. In large-span, arch voussoirs are usually stones cut with high precision and assembled without mortar, or just with a minimum of it meanwhile in a small -span arches may be realised using stones roughly cut or bricks assembled with mortar joints. These constructions technique the masonry arches were born in ancient times and they were perfected during the Roman Empire. They were utilized from Renaissance to the XIX century. In a small -span arches may be realised using stones roughly cut or bricks assembled with mortar joints.

Before proceeding to the arch construction, a timber temporary false-work, called centering, is built. This structure is removed once the arch has been completed with the placement of the keystone. Once the arch has been completed and the centering removed, in order to create an horizontal extrados, some filling is placed on the arch to make it suitable to carry a road. In order to stabilise the arch ring, part of the filling is often placed on abutments before the removal of centering. Filling could be made with different materials and is retained by spandrel walls, built on the arch rings on the two faces of the bridge. According to the dimension of the road, a series of parallel masonry walls are built. The symmetry of the arch and its capacity to bear with loads is given by backfill and spandrels. Even if they are not real structural elements, they have nevertheless a stabilising effect on the arch and its self-weight.

The masonry of the barrel, which commonly does not have the same height of the external arches, is often realized differently to the external surface: either the voussoirs, which are not visible, might be cut with less precision, or barrel may be made of bricks while the external arches are made by stones. A constant radial thickness is not always found, the parallel arch rings that compose the barrel may be independent but very often the arch voussoirs have different axial lengths in order to interlock each other and create a continuous prismatic arch barrel.

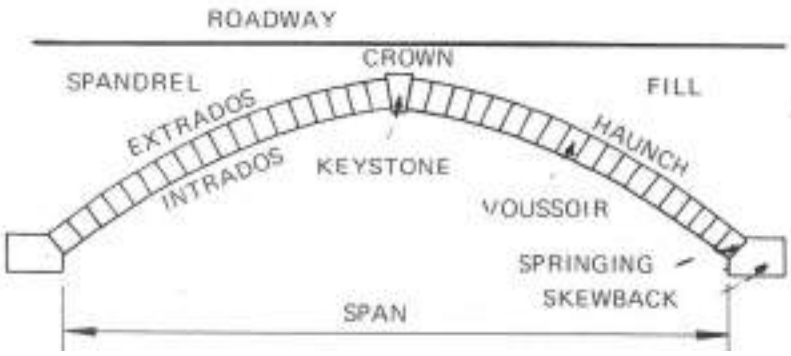

Fig. 4.7 Part of a masonry arch (Heyman 1982)

The arch is a structure that transmits the applied loads applied and the self-weight to the abutments or to the piers through compression. Understanding the mechanical behaviour of masonry arches is a target which has been reached only in the last century even if investigations began since the middle age. For centuries its behaviour was assessed without any theoretical consideration but only on the base of experience and practice. From Renaissance and until the XVIII century, with the birth of the theory of structures where the approach became more theoretical, authors used to deal with masonry arches providing geometrical and empirical rules for their design and assessment. The study of masonry arch can be considered as the first step in the development of this new subject.

In the XX century masonry arch started to be taken into consideration again as useful element in the theory of structures, applying the modern principles to this ancient structure. A complete overview of the history of arch analysis and the evolution of the structural theories has been provided by Kurrer (Kurrer, 2008).

Between the many authors who dealt with this issue, Heyman is the one who better discusses the application of ultimate load theory for masonry structures and voussoirs arches (Heyman, 1966 and 1982). In its “Stone skeleton”, 1966, and later in “The masonry arch”, 1982, which can be considered as a milestone, he gives a complete and exhaustive dissertation about the behaviour of masonry arch. Heyman’s contributions are so fundamental that it is difficult to imagine today’s state of the art without his work (Kurrer, 2008).

The funicular polygon is the simplest tool for the analysis of arches. By using this method it is possible to define the resultant, its direction and the application point of a system of plane applied vectors (Fig. 4.8). This method may be used to determine a possible thrust line and to find the equilibrium. The values of the horizontal reactions have to be known or assumed. A preliminary static analysis has to be done in order to ensure that the system is in equilibrium. By the way the funicular polygon provide the line of thrust in an arch subjected to a given load; however it is the thickness of the voussoirs above and below the thrust line that ensures the stability of the arch (Heyman, 1982).

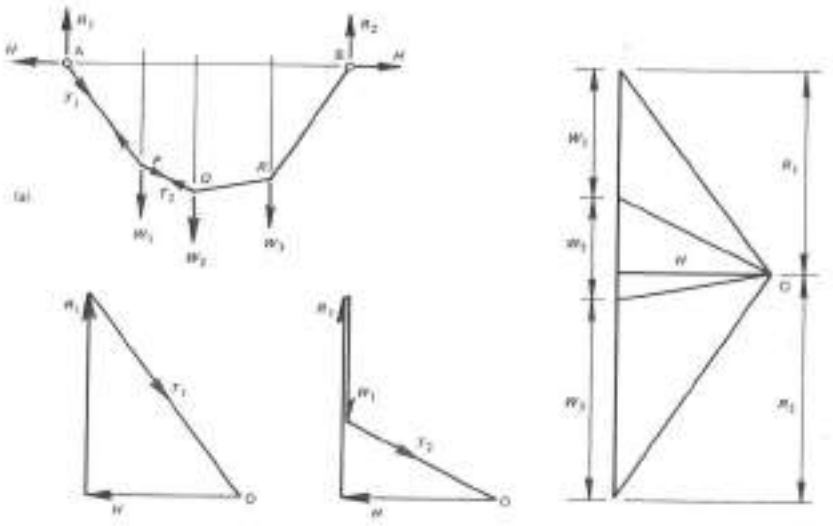

Fig. 4.8 Funicolar polygon (Heyman, 1982)

Considering the centre line of a three-pins arch loaded by a series of vertical forces, the bending moment cannot be transmitted by frictionless hinges, and the funicular polygon, corresponding to the thrust line, has to pass through them. At the same time, the thrust line does not coincide with the centre line of the arch except at the three hinges. In fact, considering a section of the arch obtained through a cut of the arch rib at a distance x from the hinge, in order to preserve its equilibrium, it is necessary to introduce a bending moment M, in addition to horizontal and vertical forces. By simple statics, the bending moment in the arch ring is equal to the horizontal component H multiplied by the distance between the thrust line and the centre line of the arch, as it is shown in the Fig. 4.9. The thrust line moves in position according to the loads applied.

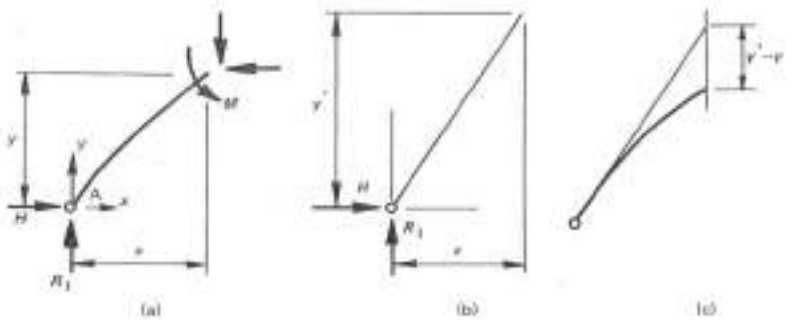

Fig. 4.9 Line of thrust and moment in the centre line of three pin arch (Heyman, 1982)

In a voussoir arch having the same centre line of the previous arch, in order to maintain equilibrium, it is necessary to apply the thrust along the funicular polygon. In any cross section of the arch there are a normal and a tangential component. The value of the

tangential component is small enough so that it is possible to assume that sliding between voussoirs is not allowed (Heyman, 1982). The normal thrust and point of application is important to describe the behaviour of the arch. The distribution of stresses varies according to the position of the thrust line with reference to the centre of mass of cross-section (Fig. 4.10). In the case where thrust is applied voussoirs are equally compressed by a uniform distribution of stresses. When the thrust moves from the centre of the section to its edge the stress distribution changes. When the load is applied between the centre of mass and one-third of the cross-section the stress distribution becomes linear with the maximum value at the edge closer to the load and the minimum at the opposite edge. The limit value is achieved when the load is applied at one third to the centre of mass of the cross-section, then in this case the value of stress at the opposite edge is equal to zero. Moving the load off the centre, part of the section is no more compressed and would transmits a tensile stress. However it is assumed that the arch, and in general masonry, is not able to transmit tensile stresses, through joints whether or not they are filled with mortar, since, even in this latter case assembled with or without mortar joints, even if mortar is present its tensile strength is very low and uncertain. The distribution of stresses is linear, but where tensile stress acts the voussoirs tend to separate. Indeed only when thrust line lies in the “core” of the cross-section, the stress-state in the voussoirs is a compressive one. In an arch, which usually has a rectangular cross-section, this core coincides with the middle third. The respect of the so-called “middle third rule” has been considered until the 60s of the XX century as a fundamental criterion that an arch has to satisfy. The following Fig. 4.10 shows the previously described stress distributions.

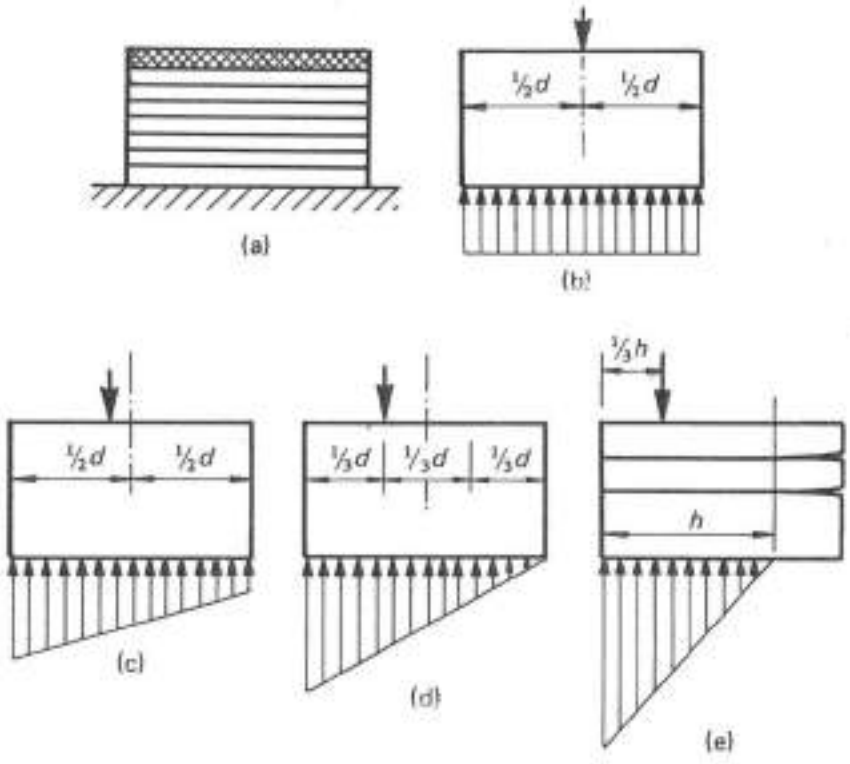

Fig. 4.10 Middle third rule, distribution of stresses (Heyman, 1982).

The middle third criterion requires that the thrust line lies in a thinner imaginary arch ring having a depth of one-third of the real arch. In reality, linear elastic behaviour does not occur. It is possible to find different thrust lines which are in equilibrium under the effect of the same given loads and such that their positions are arbitrary. In one way, it is possible to say that fulfilling the middle third criterion guarantees that the real arch has a geometrical safety with respect to the thinner arch.

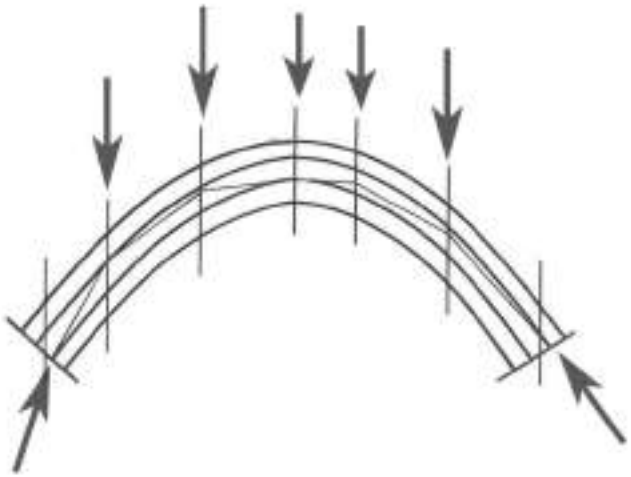

Fig. 4.11 Real arch and middle-third rule (Heyman, 1982)

Ultimate load theory was developed initially for steel structures, but can be applied to masonry structures provided that masonry material complies with certain conditions. Drucker was the first author who suggested the use of ultimate load analysis for studying the equilibrium of masonry arch; he was followed by others authors, such as Kooharian, Onat and Prager, which described the material conditions the voussoirs have to satisfy so that ultimate load theory can be rigorously applied and the corresponding yield surfaces drawn (Drucker, 1953; Kooharian, 1953; Onat and Prager, 1953; Prager, 1959). As it was previously said, here we refer mainly to Heyman's works (Heyman, 1966, 1982 and 1995).

Masonry material has to satisfy three conditions in order to satisfy the ultimate load theory:

- The compression strength of masonry is infinite;
- The tensile strength of masonry is zero;
- Adjacent masonry elements cannot slide on one another;

These conditions have been already discussed in the previous part of the section, concerning the modelling of masonry as Not Resisting Tension (NRT) material. If these conditions are satisfied, the resultant stress is acting perpendicularly to any cross-section

and is a compression force N. A hinge occurs when the force N is applied to the edge of the cross-section. This leads to a yield surface bounded by two straight lines. The bending moment M is the product of the normal force N by its eccentricity e: M = N×e; the eccentricity must be lower than the half depth of the arch. For values of M and N that are included in the yield surface the force N acts inside the section and therefore the thrust line lies inside the arch profile: the masonry arch is stable. For values of M and N that lie on the lines defining the yield surface the force N acts on the edge of the section and a hinge is produced. In case the values of M and N that are not inside the yield surface then the force N is lies outside the arch: the masonry arch is not stable.

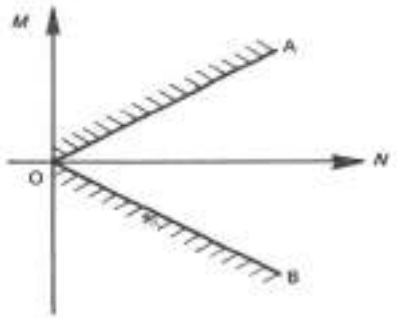

Fig. 4.12Bending Moment normal force diagram with yield surface in a rigid unilateral masonry (Heyman, 1982)

According to the utimate load theory, the precise knowledge of the position of the thrust line is not relevant. The abutments are not rigid and they are subjected to small movements due to the arch which presses against them. The thrust of the arch produces a spreading of the abutments so the span of the arch increases. In reality the arch pushes against abutments that are not rigid: they are subjected to small movements and for large values of thrust, they may yield. In order to contrast this the arch adapts itself changing its geometry: cracks occur to allow the necessary movements. A crack forms in the intrados at the crown and two cracks occur at the extrados at the abutments. The arch becomes a three-hinge arch, a statically determinate structure, the three hinges determine the position of the thrust line. Movements may be asymmetrical, abutments movement could be both horizontal and vertical, and only one abutment may yield. For every possible movement there is a different crack pattern: the arch replies to the changes in the boundary conditions by opening and closing cracks.

Thanks to NRT material properties, cracks are not dangerous because they are a consequence of the ability of the masonry arch to adapt to changes in the boundary conditions. The thrust line, which must pass through the developed hinges, is defined by the distribution of cracks. When the cracks pattern changes, the position of the thrust line changes too. In reality it is not possible to know or predict the crack pattern and it is impossible to know the exact position or location of the thrust line. Two extreme positions of the thrust line are possible, corresponding to the maximum or the minimum horizontal thrust. It has been assumed that compression strength is infinite, thus the collapse of the

arch occurs as a consequence of the development of a kinematic failure mechanism. When the thrust line touches the edge of the arch a hinge forms and rotation is allowed. The three-hinged arch is a statically determinate structure, but the development of one or more hinges makes it a kinematically admissible hinged mechanism that may produce the collapse of the arch requiring material crushing as represented in Fig. 4.13.

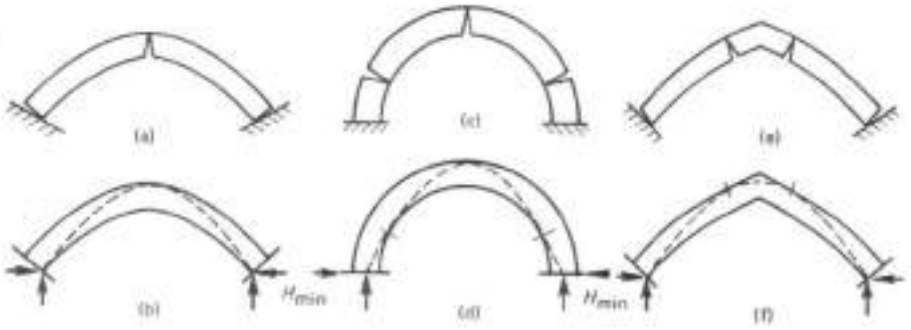

Fig. 4.13 Formation of hinges mechanism in masonry arch (Heyman, 1982)

4.5 The safety theorem

One way to understand if the arch is able to resist to loads, both external and self weight, is to draw a thrust line for the complete arch lying within the profile of the arch. Finding an equilibrium condition which does not violate the hinge condition is sufficient for the arch to be considered safe. This condition is statically admissible and corresponds to a lower bound of the ultimate load. Instead an upper bound of the ultimate load is given by a kinematic maximum load resulting from an admissible kinematic mechanism, quantifiable through the principle of virtual displacements: this condition is kinematically admissible. In case of masonry arch, any thrust line drawn for a given load satisfies the equilibrium conditions.

Masonry has to resist to compression stresses so material conditions need to be respected as well. The stress resultants have to act inside the voussoirs in each cross section. In this case the thrust line lies completely inside the arch profile and the arch is stable and will not collapse under the given loads. The safety theorem does not give any information about the boundary conditions: in response to the support movements, cracks occur in the arch. When the boundary conditions change the arch finds a new equilibrium. It means that the thrust line changes its position but is always lying inside the arch profile.

The aim of the safety theorem is that it is not necessary to find the “actual” line of thrust: when one of them is found, which satisfies equilibrium and is internal to the arch profile, then the arch is shown to be safe. Arches will not collapse under these loads if a suitable

thrust line is found. The safety of the load-bearing structure can be assessed without the necessity of making assumptions about its actual state.

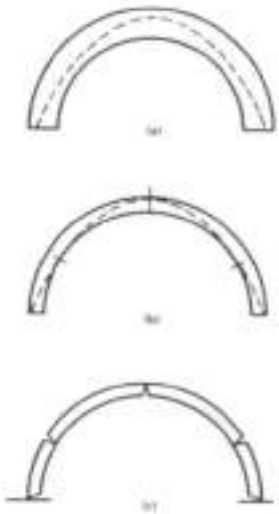

Fig. 4.14 Geometrical factor of safety (Heyman, 1982)

The safety of masonry arches can be evaluated by the ultimate load theorems, providing an upper and a lower bound. A safety factor is found by comparing the geometry of the real arch with the geometry of an arch which has the minimum necessary thickness to carry the given loads. If the thrust line completely lies inside its profile, the arch is safe. The arch having the minimum necessary thickness can be found reducing the thickness of the real arch until it is possible to find only one single line of thrust lying within it. The geometrical factor of safety is given by comparing the thickness of the two arches. Heyman recommends a value of 2, meaning that the thickness of the real arch is the double of that of the minimum arch, for the most unfavourable loading case (Kurrer, 2008; Heyman, 1982).

4.6 Collapse mechanisms

Thereafter the principal mechanisms of collapse are described. Possible kinematic mechanisms are illustrated by figures with a brief description.

Fig. 4.15 Opening of springing.

The rotation and/or translation of the piers or abutments creates the kinematic mechanism of collapse with opening of springing and the formation of three hinges: one at the key in the extrados, the other two at intrados of the haunches (Fig. 4.15).

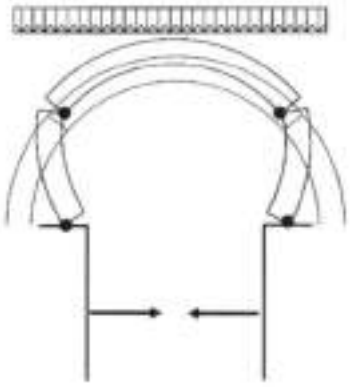

Fig. 4.16 Closing of springing.

It is shown in Fig. 4.15 and previously described, also the kinematic mechanism of collapse with closing of springing is due to a rotation and/or a translation of the piers or abutments, or a part of them. Differently from the previous case four hinges are formed: two at the extrados of the springing plus two at the intrados of the haunches (Fig. 4.16).

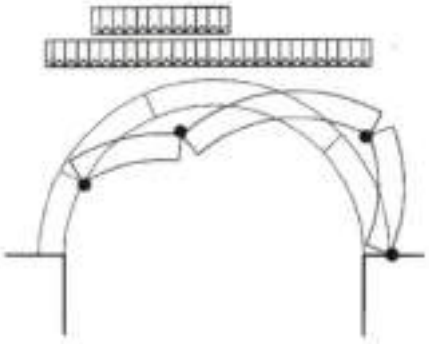

Fig. 4.17 Asymmetric mechanism with fixed springing.

In the case of an-symmetric kinematic mechanism with fixed springing four hinges are formed as it is shown in Fig. 4.17. The hinges are developed alternatively at the intrados and at the extrados. Usually, the last hinge in the less loaded side of the arch occurs at the extrados of the springing. The other hinge at the extrados of the arch takes place in the most loaded side of the arch and develops along, or near to, the line of action of a possibility concentrated load.

Fig. 4.18 Symmetric mechanism with fixed springing

In Fig. 4.18, the symmetric kinematic mechanism with fixed springing due to a uniform load is presented. It creates the five symmetrical hinges, alternatively developed at the extrados of the springing, at the intrados of the haunches and at the extrados at the crown.

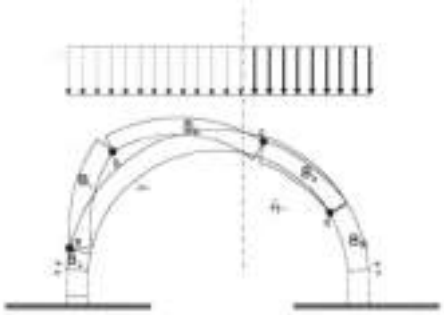

Fig. 4.19 Positive and negative work

Considering the loading acting on an arch, it is possible to identify two different types of work: a positive work, where the load activates a possible mechanism, and a negative work, where the load resists to the mechanism activated by the positive one. As the Fig. 4.19 above described, the right, drawn by the solid line, does a “positive” work. The left part, drawn by a dashed line, does a “negative” work.

However, the arch may collapse with a different mechanism of collapse under the same load. The arch is safe and can carry on the applied load if and only if, for all possible kinematic mechanisms eligible, the absolute value of the total negative work is greater than the positive one.

5 Experimental Analysis, instruments and software

5.1 Operational Modal Analysis

Laboratory analyses and the information given by the literature are particularly significant since they provide experimental results which are relevant to the material used for the construction. However, the seismic behaviour of masonry structures depends not only on material properties but also on the axial stresses that arise from the static vertical loads combined with the dynamic loading (Salvatore et al., 2003). The knowledge of dynamic properties, together with site seismicity and stratigraphy, should be the starting point for an accurate estimation of the seismic safety of these structures (Ferraioli et al., 2011). Hence, a reliable evaluation of the dynamic properties of a structure is particularly important for the analysis of its dynamic behaviour.

In this research, for the analysis of structural behaviour and materials characterization of masonry bridges, attention has been paid on the analysis of the fundamental frequencies. In order to analyse the fundamental frequencies of the study cases, and compare these with numerical and analytical models, an Operational Modal Analysis (OMA) has been carried out. OMA is a non-destructive technique that aims at identifying the modal properties of a structure. The procedure is based on vibration data collected when the structure is under its operating conditions, without initial, or artificial, excitation. The modal properties of a structure, usually, include the natural frequencies, damping ratios and mode shapes. In an ambient vibration test, the chosen structure can be under a variety of excitation sources, i.e., weak ground motions due to both natural and anthropogenic sources.

In this research, Operation modal analysis has been performed on four case studies of masonry bridges in Venice:

- “De L’Arzere” bridge
- “Foscarini” bridge
- “Guglie” bridge
- “S. Lorenzo” bridge

The choice of these bridges is due to the possibility of comparison between the four different case studies mentioned above and is motivated by similar characteristics, like the same arch shape, similar dimension of the span and construction materials. The only difference is the material of the parapet.

5.2 Frequencies measurements instruments

Assuming that stochastic noise is constant during a measurement session, digital tromographs have been used to perform a low-cost OMA (Operation Modal Analysis). For the case study of “De L’Arzere” bridge, a measurement campaign has been conducted also with accelerometers in order to validate the dynamic identification carried out with tromograph. The accelerometer measures the signal as acceleration and the tromograph records the signal as velocity.

The location of the accelerometers is coincident with that used for tromograph measurements.

Fig. 5.1: Instruments location.

A different type of tromographic acquisition has been conducted for the experimental measurement campaign of the other bridges. The differences consist in the location of the instruments, the number of acquisitions and in the typologies of acquisition made, either synchronized or non-synchronized.

5.2.1 Moho Tromino settings and description

Moho Tromino is usually used as a measurement device of soil frequency resonance and it analyzes the micro tremor that derives from the ambient seismic noise.

Micro tremors are characterized by very small oscillations with respect to earthquake movements. The frequencies object of the micro tremor studies are between 0,1 and 20 Hz. Ambient seismic noise would be considered different: wind, sea waves or ocean waves but also anthropic noise such as machinery, vehicles, etc, that are easy to recognize, because they are characterized by high frequencies.

- The noise is called “micro seism” when the frequencies are less than 0,5 Hz and the noise sources are natural (oceanic noise and big entity meteorological conditions)
- The wind and the local meteorological conditions are characterized by frequencies of ≈ 1 Hz
- The noise is defined “micro tremor” when the frequencies are higher than 1 Hz and the noise source are human activity or seismic noise (Bard, 2008)

Methods for the acquisition of micro tremors are called passive methods when they are based on the measurement and analysis of soil vibrations induced by non-quantifiable sources.

For this research two digital, compact tromographs, Moho Tromino (Fig. 5.2), were used to perform non-synchronized and synchronized vibration measurements. This instrument is equipped with three vibration sensors placed orthogonally one to another; each includes an electrodynamic transducer (velocimeter) and a capacitive transducer (accelerometer). The (f_s) sampling frequency, can be set up to 128 Hz, 256 Hz, 512 Hz or 1024 Hz. The weight of the instrument is 1.1 kg and, although the mass of each sensor is very low (10 grams), the performance of the instrument, whose resonance frequency is 4.5 Hz, is acceptable in the typical frequency range of interest, i.e., from 0.1 Hz to several hundred Hz (Micromed, 2010). As a consequence the tromograph, for the evaluation of high frequencies range, can be utilized also for Engineering applications and not only for stratigraphic use.

Fig. 5.2: Moho Tromino Instrument.

Starting from the acquisition of the signal in time domain, the dynamic identification was done by analysing the dynamic parameters obtained for frequencies’ domain utilizing Fourier transform FFT (Fast Fourier Transform).

The value of sampling frequency utilized is 512 Hz for all measurements that have been performed; it is the correct value for an optimal definition, considering the typologies of measurement campaign.

The time length of any acquisition is 16 minutes. It is important that the signal is statically averaged. This time adopted is the better compromise between the stability of the signal and the management of the data.

5.2.2 Software and analysis of Tromino data

The Moho Tromino data analysis was performed, in all cases, using frequency domain decomposition (FDD) implemented in the Grilla® software package.

This software is articulated into three moduli developed for the vibrations analysis, it is used for stratigraphic studies and for calculating the principal modal shape and frequencies of a structure (Micromed, 2013).

The window size utilized is 20 sec; this value is adopted depending on the registration duration time. Usually for time registration greater than 10 minutes, the window size is 20-30 seconds. The value of smoothing adopted is 5%; for the structures a correct range is considered from 1% to 5% (Fig. 5.3).

Fig. 5.3: Window of analysis parameters.

All recorded traces were cleaned manually from the transient noise.

It is necessary to filter registration data from the antrophic and ground noises in order to understand the vibration values of the structures and this is possible only using Standard Spectral Ratio (SSR) operation. In this way it is possible to isolate only the characteristic of the structure. This can be achieved by selecting the acquired analyzed tracks and using as a reference site the measurement made externally or in correspondence to the foundations of the structure, that is the site respect to which other traces have to be compared (Fig. 5.4).

Fig. 5.4:Example from Tromino manual: traces selection for modal analysis of the structures. The reference site is emphasized by a red arrow. The other sites are emphasized by blue arrows. In this analysis the value of the smoothing is 1%.

In the Grilla window, named Amplitude Spectral Ratio, namely the one which appears when this analysis is executed, it is possible to understand the values and the direction of the structure vibration movements of homologous components.

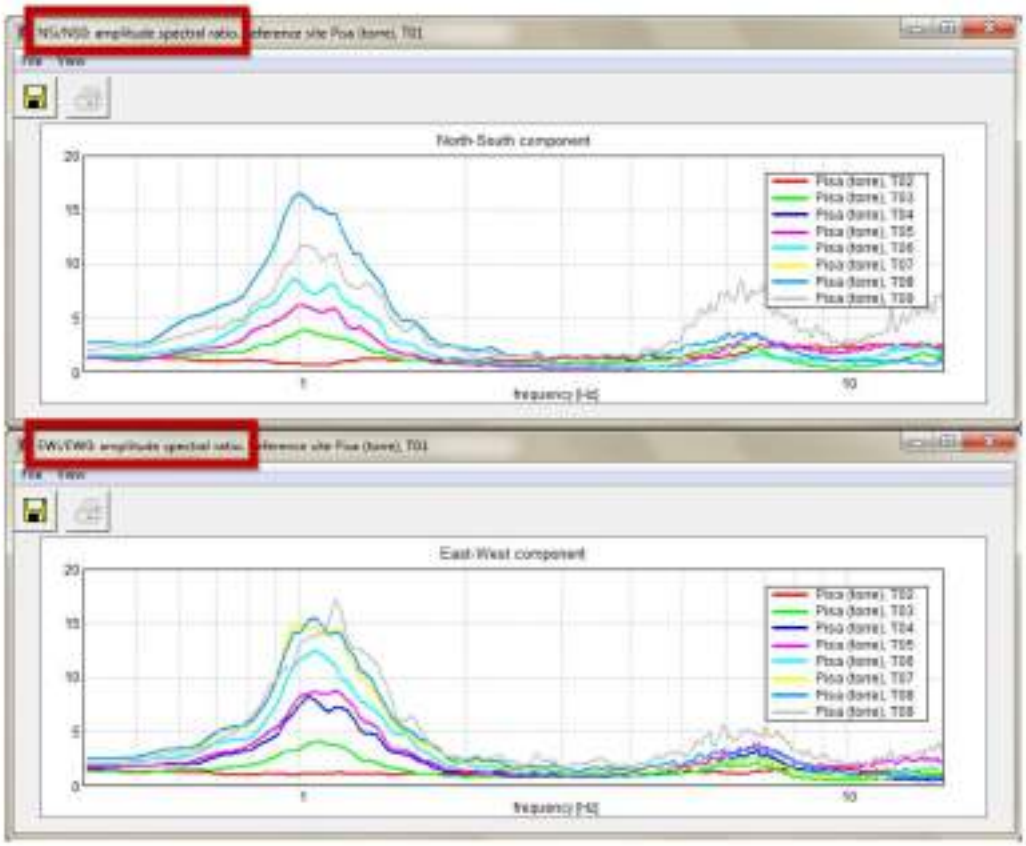

Fig. 5.5: Example from Tromino manual of spectral relationship between homologous components.

Two different types of tromographic acquisition have been conducted for the experimental measurement campaign. The differences consist in the location of the instruments, the

number of acquisitions and in the typologies of acquisition which have been made, synchronized or non-synchronized.

5.2.3 Accelerometers settings and description

The experimental vibration modes are determined by analyzing the global response of structure to ambient vibration due to wind, traffic and other unknown excitation input.

The measurements were taken while the structures were excited by ambient vibrations by using uniaxial piezoelectric accelerometers, PCB Piezoeletronics type 393 C

Fig. 5.6: PCB Piezoeletronics type 393 C.

For ambient vibration measurements with unknown input the implementation of the frequency-domain Linear Least Squares estimators is proposed. The method is based on the application of a fast-stabilizing frequency domain parameter estimation through the Least Squares Complex Frequency (LSCF) estimator (Guillaume et al., 2003).

In detail, for each recording, the cross-power spectrum function was determined in the domain of frequency, with reference to a number of measurement points. A modes extraction method based on the series of data that represent the only system's response was applied on the sole input of the ambient vibration (El-Kafafy et al, 2012). The main vibration modes were thus identified by the best match with the compared cross-spectrum functions previously yielded from the time histories of each channel. Stabilization diagrams are obtained for some of the signals made available by dynamic monitoring. The identification procedure entails a series of pre-processing operations on the signals (mean removal, de-trending, filtering).

5.2.4 Software and analysis of accelerometers data

From the history of each channel the structural response data were extracted. The ratio, expressed in decibel, is acceptable if the ratio between Signal and Noise is S/N > 10 dB, while it needs filtering if 6<S/N<10 dB.

For each recording, the crosspower spectrum function is determined in the domain of frequency, with reference to a number of measurement points, in order to determine the vibration modes and the respective modal parameters as frequency, damping and deformed shape.

A modes extraction method based on the series of data that represent the only system's response is applied on the sole input of the ambient vibration (Ewins et al., 2000).

As is well known, the ratio between the system's response and the stress that excites it is given by matrix H expressed by the following equation:

$$[H(\omega)] = \sum_{i=1}^{n} \frac{(v_i)(l_i^T)}{j\omega - \lambda_i} + \frac{(v_i)(l_i^H)}{j\omega - \lambda_i} \qquad \text{Eq.(5.1)}$$

where n is the number of modes, j is Jacobean matrix and H denote the complex conjugate and the transposed complex conjugate respectively; $(v_i) \in$ C is the vector of modal shape; $(l_i^T) \in$ C is the vector of the factors of modal participation; λ_i are the poles of the system, related to the natural frequencies (ω, i.e. eigenvalues) and damping values (ζ) by means of the following relationship:

$$\lambda_i \lambda_i^* = \zeta_i \omega_i \pm j\sqrt{1 - \zeta_i^2} - \omega_i \qquad \text{Eq.(5.2)}$$

Within the representation of the dynamic system by means of the $H(\omega)$ matrix, the response of the system itself to a dynamic stress is represented in the domain of frequencies by the well known matrix $S_{YY} \in$ Cmxm , that means the output spectrum:

$$[S_{YY}(j\omega)] = [H(\omega)][S_{uu}(\omega)][H(\omega)]^H \qquad \text{Eq.(5.3)}$$

where $S_{uu} \in$ Ckxj is the matrix that represents the stress the system is subjected to (input spectrum). While performing operational modal analysis, only the S_{YY} matrix is known; beside assuming that the input spectrum is of unknown entity, the central term of Eq.(5.3)is actually constant and is thus independent from the frequency:

$$[S_{YY}(j\omega)] = [H(\omega)][S_{uu}][H(\omega)]^H \qquad \text{Eq. (5.4)}$$

Eq. (5.4) and Eq.(5.1) allow for analytical definition of the relationship between the system's response spectrum which is (known, since it was yielded by measured quantities) and its modal parameters.

$$[S_{YY}(j\omega)] = \sum_{i=1}^{n} \frac{(v_i)(g_i)}{j\omega - \lambda_i} + \frac{(v_i^*)(g_i^*)}{j\omega - \lambda_i^*} + \frac{(l_i^T)(v_i)}{-j\omega - \lambda_i} + \frac{(g_i^*)(v_i^*)}{-j\omega - \lambda_i} \qquad \text{Eq.(5.5)}$$

Eq.(5.5), (g_i) is defined, since the input data include the only response of the system, that is the operational factor of reference, (l_i^T).Value (g_i) is a function of both the modal parameters of the system and the constant input spectrum.

The main vibration modes were thus identified by the best match with the compared cross-spectrum functions previously yielded from the time histories of each channel.

The stabilization diagram is considered the most common tool to select the physical poles. In this diagram the resonance frequency and the respective damping ratio of the identified poles is visualized for different model orders.

The modal shapes have been extracted from the experimental measurements of the acceleration and consequently a 3-D geometric schematic model is constructed with the commercial software LMS Test.Lab: Siemens PLM Software. (http://www.lmsintl.com).

6 Numerical modelling

One of the most important research topics in the field of civil and conservation Engineering is the identification of properly defined static and dynamic modelling to understand the structural behaviour of masonry historical buildings. There are many reasons that may motivate the modelling of an historical building. The definition of objectives, the recognition of problems and the identification of the structures are the essential requirements for the modelling of masonry. To evaluate the safety of masonry structures, several analysis methods may be adopted. In each method of analysis there are different specificities, related to the purpose of the methodology, that chiefly depend on the type of action with respect to which it is necessary to which evaluate the safety of the structure.

The safety and the load-bearing capacity evaluation of masonry arch bridges have been studied by many authors. In order to perform structural analysis it is necessary to develop an appropriate numerical model. The structural behaviour of a masonry arch bridge has been analyzed using different models; the choice between them depends on the respective questions and the provided resources. The report prepared for the EU Commission during the COST-345 in 2004 gives a list of analyses methods recommended for different levels of assessment.

Description level	Models
1	Empirical or two-dimensional-model, linear elastic arch frame
2	Two or three -dimensional, linear elastic or elastic-plastic, allowing for cracking
3	Two or three dimensional, linear or non-linear, elastic or plastic, Allowing for soil-structure interaction, cracking, site-specific loading and material properties
4	FEM analysis of specific details of the structure being assessed not considered in the previous levels
5	Reliability analysis based on probabilistic models

Tab. 6.1: Methods of analysis and levels of assessments – COST-345 (2004).

6.1 Modelling of masonry

The strategy of masonry modelling has to take into account important aspects:

The dimension of the analyzed object has a variable size, ranging from a group of buildings to an architectural detail, going through the building or parts of it. Moreover, at the material level, masonry can be modelled with different levels of detail: from a micro-scale, where the constituent elements of masonry are taken into account; to a macro-scale, where the object of modelling is a whole portion of structure.

The structural scheme represents the synthesis of geometric and mechanical structure and has an important role in masonry modelling.

In order to understand the mechanical behaviour of the structure it is necessary to formulate a number of assumptions and to define a constitutive law that allows to describe the material behaviour.

Several types of analysis may be performed by implementing different types of models: linear, non-linear, or limit analysis; static or dynamic.

The difficulty of modelling masonry structures depends on three fundamental problems:

- The composite nature of masonry, made up of a complex system of blocks and joints, assembled with several possibilities of bond and realised with different constructive techniques and materials.
- The size of heterogeneity, with respect to the size of masonry structure, which strongly influences the scale of the model.
- Several geometric complexities typical of masonry constructions, and the relative difficulties on its structural modelling, which impose the adoption of 2-D and 3-D approaches.

In the study of masonry structures the use of a local model to describe parts of the structure, or global models, representing the structure in its whole, is a hard topic. In fact the preparation of a global model is time consuming and, because of the resulting large dimension of the model, when analyzing the results some important aspects could be left out of sight. From one point of view, modelling some structural parts and details instead of modelling large and complex structures is preferable. More generally, a global model is worth the cost because it is able to implicitly catch the interactions between the different parts of the building, but usually it is too complex to use, from the conceptual and operative points of view, in the case of a historical construction. From another point of view, local models tend sometimes to over-simplify the analysis through rough hypotheses; nevertheless they have the advantage of using intuitive structural schemes, which allow an easy interpretation of the results.

6.2 Scale-levels of masonry analysis

In literature, many models and tools of analysis have been developed. They may be distinguished by the scale of the problem analyzed, by constructive features, by the type of masonry, by the acting forces. It is possible to divide the different approaches to masonry modelling according to the scale:

- The micro-scale: masonry constituent elements are modelled separately; this type of modelling is used for structures of small dimension or made by huge blocks.
- The meso-scale: masonry is considered as an equivalent continuum material and constitutive equations are formulated through homogenisation. These models

usually are implemented in finite element procedures and are used for complex masonry structures.

- The macro-scale: it is used for constructions where a characteristic behaviour may be primarily recognised, modelled through structural elements of larger dimensions, called macro-elements. This approach is adopted in codes devised for the seismic analysis of buildings.

In the following, a short overview of the literature dealing with model scale is given.

At micro-scale, masonry is modelled as a discrete system of elements: blocks, joints and interfaces. Many contributions have focused on micro-polar modelling of periodic masonry (Masiani et al., 1995; Sulem and Mühlhaus, 1997; Stefanou et al., 2008) based on an idealisation of masonry as an assemblage of rigid blocks interacting through linear elastic interfaces and represented as a Lagrangian system. Casolo proposed a Cosserat homogenisation based on a heuristic evaluation of the mean local rotation of the brick units (Casolo, 2006) to overcome the limits deriving from the assumption of rigid blocks. The Cosserat homogenisation technique has been proposed first for continuously deformable heterogeneous media (Forest and Sab, 1998) and then has been extended to periodic masonry (Bacigalupo and Gambarotta, 2011) and by Addessi, whose recent contribution includes elastic damage constitutive equations at the micro-scale (Addessi et al., 2010). In Bacigalupo and Gambarotta (Bacigalupo and Gambarotta, 2011) an evaluation of the reliability of Cosserat homogenisation has been obtained analysing a boundary shear layer problem concerning masonry walls.

At the micro-scale, the equilibrium limit analysis is the base of the main approaches developed in the literature. In general, the non-linearity of the material is concentrated in joints while blocks are supposed to be rigid and infinitely resistant (Livesley, 1978; Gilbert and Melbourne, 1994; Baggio and Trovalusci, 2000; Ferris and TinLoi, 2001; Orduna and Lourenço, 2005). Other approaches are based on the distinct element method (Cundall, 1976). They require a dynamic incremental analysis, performed through the explicit integration of the equations of motion (Azevedo et al., 2000; De Felice and Giannini, 2001; Lemos, 2007).

At the meso-scale, masonry is modelled as an equivalent continuum. The constitutive model may be defined either through a phenomenological approach by smeared cracking or by a Not Resisting Tension (NRT) model (Lourenço et al., 1998; Pietruszczak and Ushaksaraei, 2003), through homogenisation or by direct identification techniques. Advanced homogenisation techniques have been developed in order to define in-plane (Anthoine, 1995; Lourenço and Rots, 1997; Cecchi and Sab, 2002a) and out of-plane (Cecchi and Sab, 2002b; Cecchi et al., 2005) elastic properties of the material and its failure domain (Corigliano and Maier, 1995; De Buhan and De Felice, 1997; Sutcliffe et al., 2001; Sab, 2003; Milani et al., 2006; Cecchi et al., 2007; Cecchi and Milani, 2008). These techniques present the advantage of knowing, at the meso-scale, the main characteristics of masonry at micro-scale. However currently their complexity does not allow for the formulation of an evolutive non-linear constitutive law. An interesting approach to face this problem is the

Transformation Field Analysis (TFA) method, recently applied to masonry by Sacco (Sacco, 2009).

Further methods are based on multi-scale approaches, where the microstructural behaviour of masonry (micro-scale) is related to the continuum (meso-scale) through a micromechanical analysis (Gambarotta and Lagomarsino, 1997; Luciano and Sacco, 1997; Pegon and Anthoine, 1997; Massart et al., 2004; Calderini and Lagomarsino, 2008). All the cited constitutive models have been developed by describing masonry as a Cauchy continuum, for which two main drawbacks may be pointed out: it does not allow to keep into account the absolute size of the microstructure, and to describe scale effects; the macroscopic fields of the Representative Volume Element RVE are supposed to be non-uniform. In order to overcome such drawbacks, various authors have proposed models based on generalised continua. Particular attention has been paid to the Cosserat continuum, where an internal scale parameter is considered (Masiani et al., 1995; Trovalusci and Masiani, 2003; Casolo, 2006; Basile et al., 2007).

In the case of meso-scale, and also in the case of the micro-scale, the modelling techniques developed in literature mainly refer to regular periodic masonries. Indeed, in the common practice, in order to analyse non-periodic and irregular masonries, phenomenological Not Resisting Tension (NRT) or smeared cracking constitutive models have been adopted frequently. In the field of masonry types, the work carried out by Cluni and Gusella (Cluni and Gusella, 2004), is interesting, since it is oriented to define the elastic properties of the material. Starting from studies on homogenisation techniques for non-periodic solids, Cecchi and Sab have studied the elastic homogenisation of non-periodic regular masonries through a perturbative approach (Cecchi and Sab, 2009).

At the macro-scale there are two important modelling approaches: the structural element modelling and the equilibrium limit analysis of "macro-blocks". Both these techniques have been developed for the analysis of buildings subjected to horizontal forces, in particular to seismic forces. The structural element modelling approach is to evaluate the overall response of masonry structures made up of walls with regular openings, describing the in-plane behaviour of single structural elements. The technique is based on the identification of macroscopic structural elements (portions of structure such as "piers" or "spandrels"), defined from a geometrical and kinematic point of view through finite elements (either shell or frame) and described from a static point of view, by taking into account their internal forces. A first class of models is based on the use of one-dimensional elements, such as "variable geometry" struts (Calderoni et al., 2007; Braga and Dolce, 1982) or shear-deformable beams (Tomazevic, 1978; Tomazevic and Weiss, 1990; Braga and Liberatore, 1990).

Other models consider the walls as "equivalent frames", where deformable elements - piers and spandrels - connect rigid nodes – i.e. parts of the wall which are not usually subjected to damage. Masonry panels, where the non-linear response is concentrated, may be described both through detailed models or through more simplified ones, like non-linear beams (D'Asdia and Viskovic, 1994; Magenes and Della Fontana, 1998; Brencich and

Lagomarsino, 1998; Magenes et al., 2000). By concentrating damage locations, sliding and rotations in predefined sections of the structural elements, these models allow performing non-linear incremental collapse analyses of entire buildings. The modelling of the whole structure is obtained by assembling masonry walls, idealised as 2-D frames, and horizontal floors, which are not necessarily assumed to be rigid. It is worth noting that the above described macro-scale approaches are oriented to evaluate the overall response of masonry constructions by considering the response of structural elements to in-plane only forces. This is justified because in complex masonry structures, the lack of connections between their parts may induce partial collapses due to out-of-plane actions.

A further macro-scale modelling approach is present in the literature: the equilibrium limit analysis of macro-blocks. It may be useful to evaluate the response of masonry structures, which can be reasonably assumed to be monolithic. This latest approach can be successfully adopted for large-scale models (Abruzzese et al., 1992; D'Ayala and Speranza, 2003; Casapulla and D'Ayala, 2006; Curti et al., 2006).

In this thesis the modelling of the masonry has been carried out by elaborating 2-D and 3-D models at the meso-scale.

6.3 Masonry analysis

On masonry structures it is possible to carry out numerous analysis types. They can be divided into three groups:

- Linear analysis: The starting assumption is that materials have an elastic behaviour obeying to Hooke's law. There are two different kinds of linear analyses, which are linear static and modal analysis.
- Non-linear analysis: This analysis studies the complete behaviour of the structure: elastic range, cracking and post elastic regimes, until collapse occurs. Adopting this approach, it is possible to carry out both non-linear static and non-linear dynamic analyses.
- Limit analysis: The aim of this analysis is to identify a load multiplier which provokes the collapse. This analysis refers to two different theorems: the static theorem and the kinematic theorem.

6.3.1 Linear Analysis

Linear analyses are the simplest type: they assume an elastic behaviour of materials, obeying Hooke's law. Indeed it is necessary to know the elastic properties of masonry and the values of maximum allowable stresses. Analyses of this kind allows obtaining the deformed shape and the stress distribution in the structure. In order to take into account the possibility of cracking of masonry and the consequent redistribution of stresses, it is possible to assume a reduction of stiffness in correspondence to cracked portions. Linear analyses are useful to understand the behaviour of masonry structure under service loads, when the material still shows an elastic behaviour, but they are not able to provide the collapse limits. It is convenient to use this type of analysis to study the whole structure in order to identify its global behaviour and to find out the portions where tension stresses may produce cracking. There are two different kinds of linear analyses:

• Linear static, where a system of forces is applied to the building, assuming a linear relationship between loads and the corresponding displacements. Applied forces are usually acting in the vertical direction, like self-weight and other dead loads, but is also possible to apply horizontal static forces.

• Modal analysis, to evaluate the natural frequencies of vibration of the structure. Modal analysis, associated with the design response spectrum, can be performed on two-and three-dimensional structures, in order to evaluate the stresses values within the elements.

6.3.2 Non-linear analyses

Non-linear analyses allow studying the complete behaviour of the structure: elastic range, cracking and post elastic ranges, until the collapse. There are two different types of non-linear behaviour: mechanical, due to the non-linearity of the material; geometrical, due to the fact that points where loads are applied change with the increase of actions. Non-linear analyses are very useful to investigate structures affected by damages, in order to identify the loss of stiffness. To carry out this type of analyses it is necessary to know both elastic and inelastic properties and the strength of materials. Non-linear analyses can provide as results the stress and strain distribution and the spreading of damage spreading of until collapse of the structure is reached. Non-linear analyses may be performed in spread or dynamic field:

• **Static non-linear analyses**, known as "pushover" analysis, apply to the structures vertical and horizontal loads, monotonously increasing them until collapse occurs. The method can be used both to evaluate the bearing capacity of existing buildings and to perform seismic analysis; it is provided by regulations. The analysis is frequently performed on two-dimensional portions of building, which have been extrapolated from the whole structure.

• **Dynamic non linear analyses**, known as “time history”, allows to carry out a dynamic analysis in the time domain in order to evaluate strains and stresses due to actions which vary with time, such as seismic forces. This type of analysis is suitable for both linear and non-linear range and allows simulating the complete behaviour of the structure during the full duration of an earthquake. However, because of its complexity it is not frequently used in practice.

Safety assessment at the ultimate limit state, in this case of nonlinear analyses, consists in the comparing the capacity of ultimate displacement of the structure and the demand of such displacement.

6.3.3 Limit analyses

Limit analyses have the aim to determine the collapse load, identifying a load multiplier that produces the collapse. Limit analysis refers to two different theorems (Drucker et al., 1952):

• The static theorem (lower bound): assumes that the plastic collapse multiplier load is the largest of the entire multipliers corresponding to statically admissible set (i.e. stress distribution in equilibrium with the external forces, which fulfill the plastic conditions in any point of the structure).

• The kinematic theorem (upper bound): where the plastic collapse multiplier load is the smallest of the entire multipliers corresponding to the admissible set (i.e. a kinematic mechanism, related to the distribution of plastic hinges, which fulfill the kinematic condition).

Therefore there are two possible methods of limit analyses:

• The static method, which assumes a statically admissible distribution of stresses in order to find the maximum multiplier of load;

• The kinematic method, which assumes a kinematically admissible distribution of displacements, in order to define collapse mechanisms depending on geometrical parameters; it is aimed at finding the minimum multiplier that activate a valid mechanism.

According to the uniqueness theorem, a multiplier that is both statically and kinematically admissible coincides necessarily with the collapse multiplier. Limit analyses are very helpful in the study of masonry buildings, because it is difficult to establish the real values of stress, while it is possible to study their structural behaviour through the identification of possible collapse mechanisms. As it has been previously said, the masonry constitutive model is of fragile type, with a higher value of strength in compression than in tension. Therefore this type of analysis is applied to NRT models and macro blocks models.

6.4 Masonry modelling

In the present Section, some considerations about the different approaches to structural modelling on masonry arch bridge are given, highlighting the main advantages and limitation of the different methods of analysis. The correct understanding of how masonry arch bridges behave is of fundamental importance. The factors which influence performance and behaviour should be identified. The global behaviour of a masonry arch bridge is related to the influence of each single element, both structural (like piers and arch) and non-structural (namely backfill and spandrel). Therefore the adopted model should be able to take into account all the relevant elements of a masonry arch bridge.

In masonry structures the difference between structural and non-structural elements is not so evident, hence models which consider them as a continuum, such as F.E. Models, seems to be more appropriate to represent the real structure of a bridge. However a problem could be the characterisation of the mechanical properties of masonry material: homogenisation procedures are suggested to overcome this lack of knowledge.

Discrete Element Models (DEM) is characterized by the definition of the elements (block) modelled as a rigid bodies and the contact between themselves. The DE Model has been carried out adopting a micromodelling strategy based on discrete crack, blocks are modelled as independent bodies and mortar joints as elastoplastic Mohr- Coulomb interfaces (Baraldi et al., 2019) It may be a very powerful method for the study of masonry arch bridges, especially if combined with FEM. However, their practical application is still difficult. Limit analysis is a consistent method for the assessment of the safety of the bridge, but does not provide much information about the service behaviour of the bridge. Considering the availability of different effective methods a combined use of them is suggested, on the base of the specific needs. In this view multi-scale analysis seems to be best suited to establish a procedure of analysis.

6.4.1 Analytical models made with beam elements

Since the development of analytical models, beam elements have been introduced. Initially beam models had to be very simple in order to allow hand computation. For this reason initially beam models were used only on static determined structures typically: two hinges arch, three hinges arches and fixed arch (Fig. 6.1) and did not considered the structure as a whole, loosing several important aspects of the bridge behaviour. Nowadays, thanks to the possibilities given by automatic computing, using these types of models is made possible: as a consequence to consider many effects of arch bridge load behaviour, with very precise results can be taken into account. Presently many beam models also consider the presence of backfill, elastic foundation, and roadway structures (Voigtländer, 1971; Model, 1977; Gocht, 1978). However, considering the different contributions given by each structural

element to the global behaviour of masonry arch bridge, the development of beam models encountered several difficulties and in many cases such models are strongly criticized (Proske and Van Gelder, 2009).

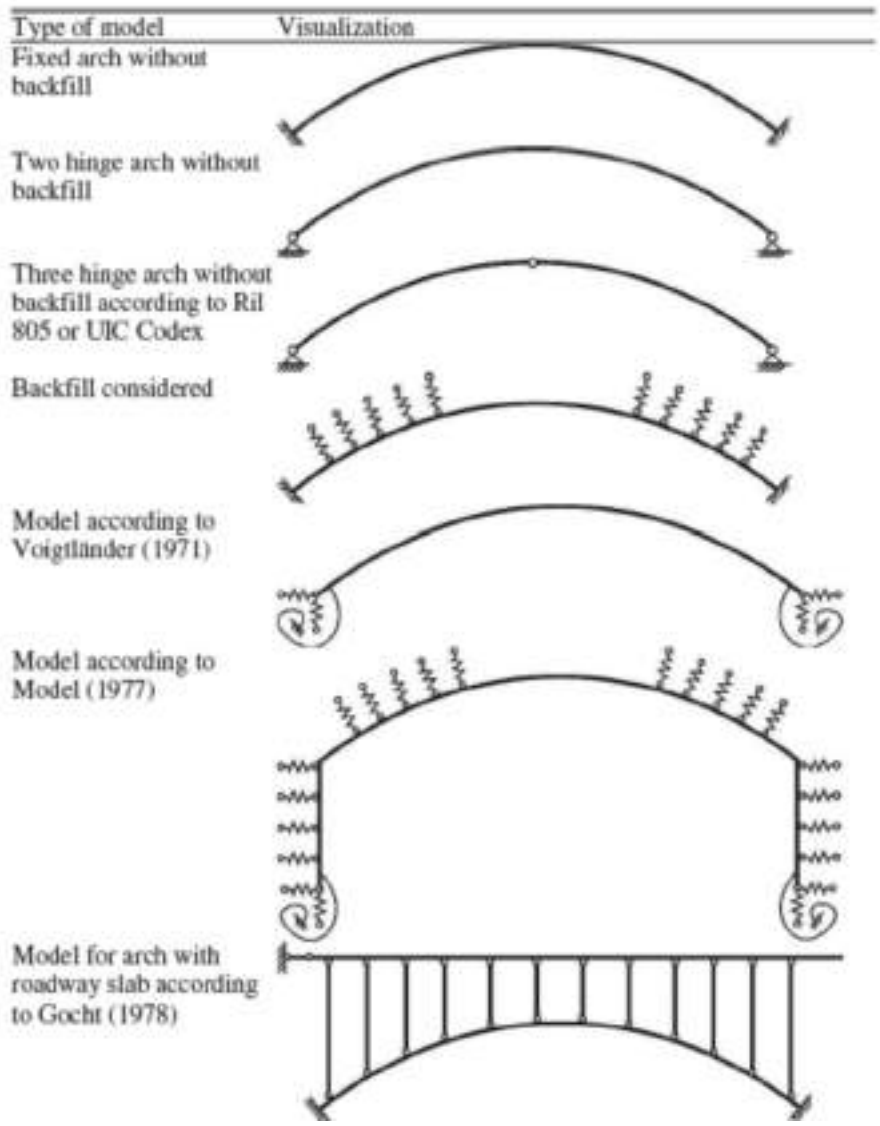

Fig. 6.1: Evolution of beam models, taken from Proske and Van Gelder, 2009.

Recently beam models of the arch have been realised in order to allow the development of hinges, on the base of plasticity theory for masonry (Heyman, 1966). Hinges represent the areas where crack opening may occur in a similar way to what happens in limit analysis. These types of models allow either to define the equilibrium state inside the arch or to find the kinematic chains of blocks and relative kinematism. For this reason, beam models may belong to the category of models which are useful for the previously described limit analysis. There exist, however, several non-linear beam models which are more complex and may provide further information. A comprehensive review of beam models for the arch has been provided by Gilbert (Gilbert, 2007).New software codes, such as RING (Limit State

Ltd, 2008) and Archie-M (Harvey, 2008) which are specific for the analysis mixed of masonry arch bridges, make use of these non-linear beam elements.

Compound beam models are a particular category of beam models. Early studies on this topic have been carried on recently and are effective in describing the behaviour of beam made of two different parts, such as steel-concrete or wood-concrete structures (Hannawald, 2006). Recently their application has been proposed for masonry arch bridges. The cross section of the beam is not only the arch itself but is increased further to take into account part on the extrados, to represent the effect of backfill. The properties of the two materials may be characterised by different Young's moduli. A partial load is transmitted to the backfill, the position of the thrust line varies according to the properties of the cross-section and produces a more reliable solution with reference to a standard beam model. A relevant aspect is the distinction between solid or sliding joints inside the compound cross sections: when relative sliding is prevented the joint is considered as a solid one, while in case sliding is allowed, the contribution of the backfill to the load-bearing capacity decreases. The occurrence of sliding is more likely to happen than a solid joint, depending on the constructive features of the extrados and the backfill, with particular reference to the type of bond. The properties of the compound beam cross section are defined easily on the base of geometry and stiffness of the original cross-section, providing a factor that is used to define the properties of the materials. However, in the case of arch bridges, the thickness of the backfill changes considerably along of the arch and this factor has to be taken into account.

6.4.2 Finite Element method (FEM)

The finite Element Method (FEM) is a widely used method in numerical structural analysis. FEM is usually adopted to realize complex simulations of the structural behaviour and it is a powerful tool to study stresses and strain in structures. It can describe the structural response of a structure in great detail but with high computational costs. The method can be used to perform static and dynamic analyses on one- two or three-dimensional models, depending on the type of element chosen and the adopted constitutive law.

When applied to masonry structures, it may be used to analyse localised portions or specific elements and supplemented by other techniques, it may help in the structural assessment. Finite element models of masonry and concrete arch bridges have become popular since the 80's, where the first finite element analyses of arch bridges have been carried out (Crisfield, 1985; Towler, 1985). By using FEM models, it is possible to assess the safety of a bridge with reference to several conditions, from traffic loads to seismic actions. Analyses can be performed both in the elastic regime and in the non-linear range. Analysis performed in the elastic range is very useful in order to represent the behaviour of an historical bridge under service loads or to evaluate the safety margin with respect to the original design. It can provide a detailed distribution of strains and stresses but it is not

suitable to describe comprehensively the ultimate strength of the bridge. On the other hand the use of non-linear constitutive laws (Pegon and Anthoine, 1997; Gambarotta and Lagomarsino, 1997; Alpa and Monetto, 1994) may not be easy because of the high number of parameters results difficult to analyze, in particular in case of three-dimensional models of the whole bridge. Even if very powerful, due to computational costs, to the correct definition of parameters and to the difficulties in the evaluating the results, this type of models did not have a wide diffusion. However they have been used in case of monumental structures, which require a deeper analysis (Podestà, 2001), or by some authors to study the seismic behaviour of masonry arch bridges (Karaesmen et al., 1996; Oliveira et al., 1995). It is important to select both the elements to be used and the scale of model, from the entire bridge to specific parts of it. As in the case of the other masonry structures, geometry can be idealised in different ways, namely, by considering the structure to be made of one-dimensional elements, two-dimensional elements, shell elements or three-dimensional elements. At a first sight, it would seem reasonable to use three-dimensional elements. However, three-dimensional models are usually very expensive from the computational point of view with respect to the time that is necessary to set up the model, perform the actual computation and analyse the results. The results of models incorporating shell elements are reasonably difficult to check due to the variation of stresses along the thickness of the elements. In addition, a large thickness of the structural elements might yield a poor approximation of the actual state of stress. Increasing the details and size of the model might result in a large amount of information that may blur other important aspects. For this reason in literature it is possible to find more simple FEM models that reduce the bridge to a dimensional model (Crisfield, 1984 and 1985; Bridle and Highes, 1990; Choo et al., 1991; Molins and Roca, 1998a) or in more detailed two-dimensional models (Loo and Yang, 1991; Falconer, 1994; Boothby et al., 1998; Lourenço and Rots, 2000) and three-dimensional (Rosson et al., 1998). Codes usually advised to make use of simple one-dimensional models also for complex structures (Molins and Roca, 1998b) and two-dimensional models for simple structures. However, thanks to the increase of the computing capacity and to the efforts paid by many authors in the last years, nowadays an increasing number of professional finite element programs include modules for realistic material description of masonry which are often used for the simulation of arch bridges. An interesting example to be cited is the model proposed by Ford that has been implemented within Straus7, the same program which has been used in the case study (Ford et al., 2003). Further information will be provided in section 7.

Lourenço provided a summary of different computation strategies (Lourenço, 2002), including Discrete Element Method, which will be described in the next paragraph. He suggested that, in the analysis of masonry historical structures, it is better to use two-dimensional models than three-dimensional models, to avoid using shell elements in regions which are important for the global behaviour of the structure and to model structural parts and details instead of modelling complete and large structures. An important aspect regarding F.E. Modelling of a masonry arch bridge is that very complicated simulation techniques are characterised by a high level of uncertainty due to

an increasing number of input variables. Defining a numerical safety factor for the different computation strategies, its value increases with their complexity, reflecting the increasing of uncertainty (Lourenço, 2002).

Approach/analysis type	Safety factor
Allowable stress (f_{ta} = 0.2 MPa)	0.31
Kinematic limit analysis	1.8
Geometric safety factor	1.2
Physical nonlinear and no tensile strength	1.8
Physical and geometrical nonlinear and no tensile strength	1.7
Physical nonlinear and tensile strength of 0.2 MPa	2.5
Physical and geometrical nonlinear and tensile strength of 0.2 MPa	2.5

Tab. 6.2: Safety factors for different computation strategies according to Lourenço, 2002.

FEM modelling gives very reliable results; at the same time the richness of details could make the results not so clear. Considering the computational costs, complex FEM models are not always suitable to perform analyses of masonry arch bridges. However, simple FEM models are able to provide easily the distribution of stresses and strain.

6.4.3 Discrete Element method (DEM)

The most widely used method in computational solid mechanics is the Finite Element Method. In recent decades a set of computational methods have been developed to deal with particulates, jointed rock, granular flows and problems where the so-called emergent properties of a system are a result of interaction between a large numbers of individual solid particles. The most widely used method for a large class of these problems is the Discrete Element Method. When large cracks occur, FEM might exhibit convergence problems, therefore the advantage of assuming homogenous material properties over certain space regions cannot hold anymore: the application of DEM is a valid alternative. DEM provides a consistent procedure to study masonry structures thanks to the possibility of creating models made of separated blocks. In particular, these models can properly represent the behaviour of historical masonry constructions, which could be considered as made of dry stone blocks exhibiting a periodic pattern. Discrete models to investigate masonry behaviour are proposed under the hypothesis of rigid blocks connected by mortar interfaces. These assumptions are justified from the observation that, in the case of historical masonry, mortar is much more deformable than blocks and its thickness is often negligible when compared to block dimensions. Hence the blocks are modelled like rigid bodies connected through Mohr-Coulomb interfaces. In other words, masonry is seen as a

molecular skeleton in which the interactions between the molecules (rigid blocks) are represented by forces and moments, which depend on their relative displacements and rotations (Lourenço and Rots, 1993; Lofti and Bensons Shing, 1994; Markov, 1999). This assumption seems particularly valid in the case of masonry arch bridges where the arch is made by stone. In general DEM application may be very useful to the study of masonry arch bridges (Maunder, 1993; Lemos, 1995; Owen et al., 1998; Roberti and Calvetti, 1998; Thavalingam et al., 2001; Brookes and Collings, 2003; Bićanić et al., 2003; Jackson, 2004; Schlegel 2004; Rouxinol et al., 2007). Although DEM is a very general and consistent method, the problem for practical application is still an extensive computation time and a great multitude of different material parameters that are often unknown or difficult to measure on the real structure. Its application may be very useful for the study of a single arch, while in case of complex structures it could be too complicated to use; moreover it does not provide a synthetic model. Furthermore, DEM could show cracks and mechanisms of collapse, but they can be deeply mesh influenced: to avoid this problem. A very refined mesh is needed, increasing the computational costs. However, in case of stone arches this problem is not relevant, on the contrary the stone ashlars of the arch may be perfectly modelled through DEM.

In the early 1990s the two methods FEM and DEM were combined and the resulting method was defined the combined FEM-DEM (Munjiza, 2004). It is in essence a discrete element method with individual elements meshed into finite elements. Finite elements permit to model elastic deformation, while discrete element algorithms allow to model interaction, fracture and fragmentation processes. The combination of DEM and FEM allows studying both linear and nonlinear masonry behaviour. Nowadays, there is a big development of new methods for the study of masonry structures based on combinations of DEM and FEM.

7 Structural Identification

In this research the structural identification of four masonry arch bridges located in Venice has been carried on. The selected case studies are:

- “De L’Arzere” bridge
- “Foscarini” bridge
- “Guglie” bridge
- “S. Lorenzo” bridge

The choice is motivated, as already explained in section 5.1, by similar construction characteristics.

For each case study the procedure adopted is:

- Geometrical survey: This was obtained obtained starting from archive research for the case study of “Guglie” bridge as evidenced in figure Fig. 7.1. For the others cases studies, historical research did not given any geometrical information and a metric survey has been performed with laser scanner technique as explained in section 7.1.The geometrical model was realized using AutoCAD software and the F.E. Model Analysis was performed by using the computer code Straus software, as it is possible to see in Fig. 7.6: 3-D geometrical model realized in AutoCAD software Fig. 7.6 and Fig. 7.7 for the case study of “De L’Arzere” bridge.
- Experimental measurements: two different types of experimental measurement campaign were carried out as it has been explained in section 5, by using 5 recording points for the reference Case study of De L’Arzere bridge using Tromino and accelerometers instruments in order to validate the obtained data. For the other bridges the measurement procedure was simplified and it is possible to see the Tromino location recording points, as they are shown in Fig. 7.8
- Modelling procedure: 1-D, 2-D and 3-D models were considered by using the information obtained by geometrical survey. 1-D F.E. Model has been carried out in order to calculate the vertical maximum displacement in the middle cross-section. 2-D F.E. Models, under plain strain assumption, were adopted to simulate different boundary conditions and to obtain model results which are comparable to the experimental values. As a consequence of the observations and the results obtained by 1-D and 2-D F.E. Models, a full 3-D F.E. Model, for any studied bridge, has been created.
- Analytical Method: This method has been used to check the 1-D F.E. model results against the maximum vertical displacement in the middle cross-section provided by the analytical solution corresponding to Eq.(7.1).

- Modal and Static analyses: modal analyses for any 2-D Models have been performed. Starting from experimentally measured data, as a preliminary investigation, the values of mechanical materials characteristics of the bridge were identified. Static analysis, only under service self-weight, has been carried out in order to evaluate structural deformation.
- Calibration of the model and Structural identification: the models realized for the study cases have been calibrated with the results obtained with the experimental measurement. Structural identification and mechanical characteristics of the materials have been identified.

7.1 Geometrical Survey

Starting from the historical geometrical survey given by archival research, for the case study of “Guglie” bridge, 2-D and 3-D models were realized.

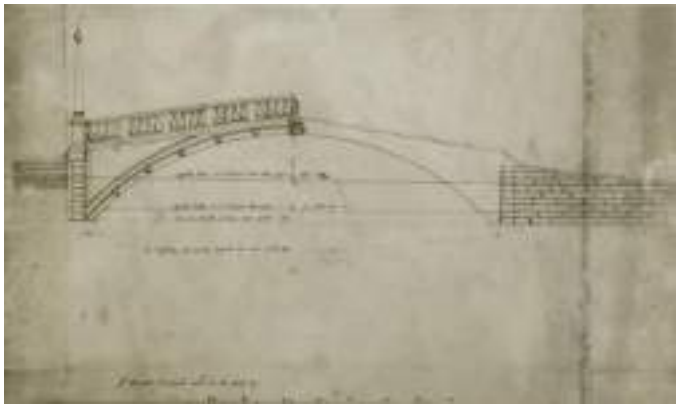

Fig. 7.1: Perspective drawing of “Guglie” bridge.

For the other case studies the archival and bibliographic research has produced scarce documentation and a geometrical survey has been carried out with 3-D laser scanning technique.

Although, there are several available techniques to generate three-dimensional survey information; the motivations of choosing this technique is a consequence of the difficulty to take geometric information for the particular environment of Venice and for the presence of water (Balletti, et al., 2014).

Laser scanning allows fast digitisation and an easy visualisation of a measured object directly in a 3-D environment: this tool allows to acquire the coordinates and also RGB radiometric values, generating a very dense point cloud. During data acquisition we used a phase-based laser scanner CAM2 Faro Focus 3-D S120: it is characterised by acquisition times as high as 976000 points per second with a high level of precision (±2 mm in a range of distance from 0.6 to 120 m). The scans have been carried out with angular increments of 0.035° in order to have a point every 6 mm at a distance of 10 meters. Moreover, the

number of scans depends on different factors, such as the object's dimension and the presence of obstacles which shadow areas.

Fig. 7.2:"De L'Arzere bridge" Points cloud

The chosen procedure can be divided in two phases:

- acquisition phase
- processing phase

Acquisition phase:

The positioning of specific signals: we placed black and white checkerboard targets useful for the subsequence phase of scan elaboration. Their position has been planned based on the assumption that two scans should have at least 3 targets in common.

Fig. 7.3: Laser scanner Faro Focus 3-D S120.

The laser scanner measures two angular directions and their slope distance, and at the end of this phase, it returns 3-D coordinates of all points; for this reason, it is an iso-determined system.

Both the intensity and the radiometric value are recorder by this laser scanner. The first value is the return signal intensity whereas the RGB value is given by an integrated sensor that acquires colours images at the end of the metric acquisition.

Processing phase:

The high number of scans and the proximity to the analysed object allows to obtain a very dense cloud: one of the main problems is precisely the difficulty to work with such a high number of datapoints.

For recording (i.e. matching together) the different scan views, the FARO Scene software has been used: this program easily recognises some specific signals, such as the black and white checkerboard targets which were used for this purpose.

The scans were registered by applying the “cloud on cloud” procedure, identifying for each scan some homologous points represented by black and white checkerboard targets. At the end of the procedure, we obtained an average residual error of ± 0,004 m.

Fig. 7.4: “S. Lorenzo” bridge, showing the positioning of black and white checkerboard targets to be used later in the phase of scan elaboration.

The scan views were then imported in Pointools software in order to obtain some orthophotos from the points cloud (Fig. 7.5). These are images in orthogonal projection and, for this reason, directly measurable and useful for the graphic redrawing of the surveyed data. The orthophotos have been generated with a pixel dimension of 0.005 m

Fig. 7.5: Orthophotos of “De L’Arzere bridge obtained from the points cloud.

Orthophotos were then imported into AutoCAD software in order to redraw 2-D geometrical drawings directly by using the data acquired during the survey and to generate the 2-D and 3-D models also useful also for the structural analysis; in fact, at the end of the survey process, the models were imported into Straus software for further elaboration.

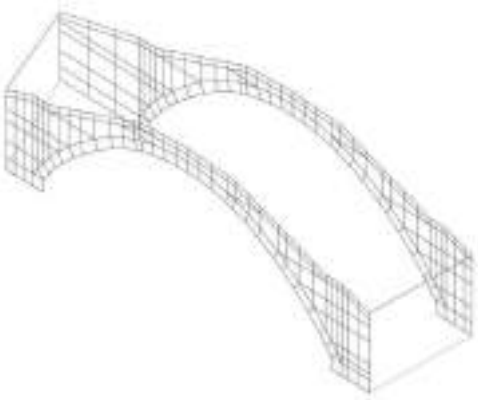

Fig. 7.6: 3-D geometrical model realized in AutoCAD software.

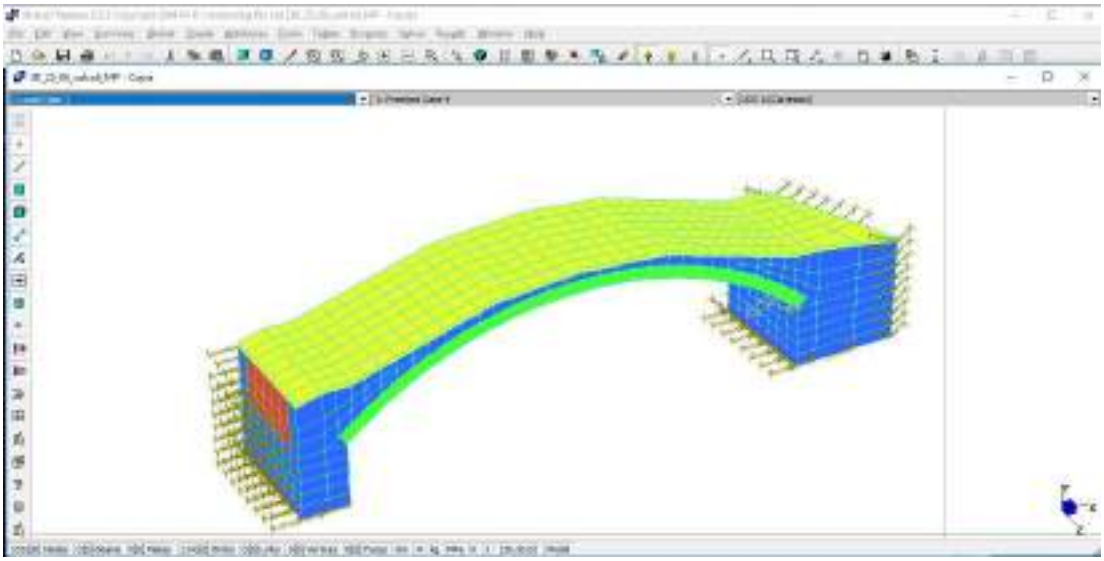

Fig. 7.7: Example of 3-D Model obtained by the survey using Straus Software.

7.2 Experimental measurements

For the study case of “De L’Arzere” bridge, tromographic acquisitions were carried out with two non-synchronized instruments setting, as explained in section 5.2.2 and located as shown in Fig.5.1. The same measurement location, as mentioned in section 5.2.4, have been used for accelerometers, in order to validate the results obtained with the tromographic measurement campaign, see section 5.2.1. The modal properties of this structure, namely, the natural frequencies and mode shapes, have been identified and the comparison of the results obtained from the two different measurement campaign confirm

that the Moho Tromino is an alternate and valid instrument to realize cheaper and faster analysis.

The experimental measurements using Moho Tromino that were made on the other bridges “Foscarini”, “Guglie” and “S. Lorenzo” has taken into account as a reference the result obtained by the Operational Modal Analysis O.M.A. made in “De L’Arzere” bridge. This was possible because, as already explained, all bridges that were studied have the same characteristics; as a consequence, the measurements campaigns have carried on faster. Only tromographic acquisitions were done and conducted with two instruments, adopting the same settings of “De L’Arzere” bridge measurements, considering four instrument locations and two sections of data registration:

- two along the bridge named S and CL1: located on the abutment and, laterally, on the crown of the bridge respectively as marked by blue points in Fig. 7.8
- two on the crown named CL2 and CC2: located in the middle and laterally of the crown (in correspondence of the CL1 instrument position) as marked by red points in Fig. 7.8.

Each tromographic acquisition is recorded at a frequency of 512 Hz for a duration of 16 minutes.

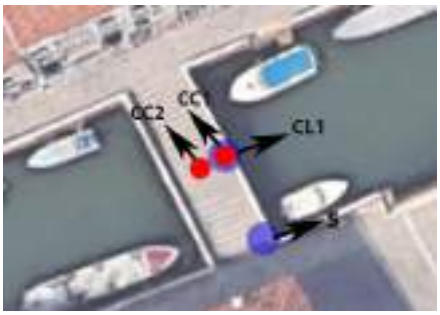

Fig. 7.8: Instruments location.

7.3 Modelling procedure

Starting from the information given by geometrical survey, 1-D, 2-D and 3-D models were developed.

Three 2-D F.E. Models, under plain strain assumption, were constructed in order to simulate different boundary conditions and to obtain a model comparable with the experimental result values.

Static analysis, only under service self-weight, has been carried out in order to evaluate the structural deformation.

- **2-D Model 1**: In the foundations the nodes are fixed along the direction and in correspondence of the abutments the nodes are only fixed in the horizontal direction.

- **2-D Model 2**: In correspondence with the abutments none of the degrees of freedom are constrained, whereas at the foundations level the nodes are fixed along both vertical and horizontal directions.
- **2-D Model 3**: In the foundations the nodes are fixed in both vertical and horizontal directions, whereas in correspondence of the abutments the nodes are only elastically constrained by means of springs.

As a consequence of the observations and the results obtained by 1-D and 2-D F.E. Models, a full 3-D F.E. Model, for any studied bridge, has been created paying particular attention to the way the nodes are restrained, to the value of stiffness of the elastic springs and to the mechanical characteristics of materials. Modal and Static analyses have been performed also for 3-D models.

- **3-D Model**: In the foundations the nodes are fixed in the vertical direction, whereas in horizontal and transversal direction are only elastically constrained by means of springs. In correspondence of the abutments the nodes are only constrained by elastic springs in both transversal and horizontal directions.

7.4 Analytic Method

This procedure was performed in order to compare the results obtained by numerical models with some closed-form solutions.

A hinge has been placed in correspondence of the foundations and numerical and analytical result for the maximum displacement in the middle cross-section obtained by a static analysis (D_y), have been compared. For the analytical solution the following equation was utilized:

$$D_y = \frac{pl^2}{8EF} \cdot \frac{2 + \frac{25}{128} \cdot \frac{l^2}{f^2}}{1 + \frac{15}{8} \cdot \frac{i^2}{f^2}} \qquad \text{Eq.(7.1)}$$

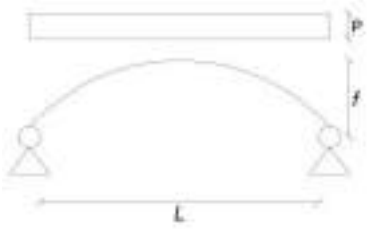

Fig. 7.9: Two hinges arch with backfill considered.

D_y = maximum displacement in the middle section obtained by closed form solution

E= Elastic modulus

F= Section Area

f= Rise of the arch

p= Loads

l= Span of the arch

i= Radius of Inertia

The percentage error ($\Delta dN_M/A_{\mathrm{M}}$) derived from the comparison between the values obtained was been calculated utilizing the following equation:

$$\Delta dN_M/\mathrm{A_M} = \frac{\mathrm{D_y}NM - \mathrm{D_y}AM}{\mathrm{D_y}AM} \cdot 100 \qquad \text{Eq. (7.2)}$$

$\mathrm{D_y}NM$ = maximum displacement in the middle section in Numerical Model

$\mathrm{D_y}AM$= maximum displacement in the middle section obtained by Analytical method

7.5 Modal and Static analysis

As explained in Section 7.3, Modal analysis for all analysed bridges was performed by adopting different constraints. The analysis was performed under service self-weight and with the weight of the parapet, which was considered to be massless, since its mass had no structural effect. The First four (4) vibration modes, for each bridge, were evaluated.

A static analysis was carried out for all study cases and the maximum displacement in the middle section was evaluated for the three different models. The percentage difference of the maximum displacement in the middle section was found for all case studies making a comparison between Model 1 and Model 2 ($\Delta dM_2/\mathrm{M_1}$) and between Model 1 and Model 3 ($\Delta dM_3/\mathrm{M_1}$) utilizing Eq. (7.3) and Eq. (7.4).

$$\Delta dM_2/\mathrm{M_1} = \frac{\mathrm{D_{yM2}} - \mathrm{D_{yM1}}}{\mathrm{D_{YM1}}} \cdot 100 \qquad \text{Eq. (7.3)}$$

$\Delta dM_2/\mathrm{M}_1$= percentage difference of the maximum displacement in the middle section between Model 2 and Model 1

$\mathrm{D}_{\mathrm{yM2}}$= maximum displacement in the middle section Model 2

$\mathrm{D}_{\mathrm{yM1}}$= maximum displacement in the middle section Model 1

$$\Delta dM_3/\mathrm{M}_1 = \frac{\mathrm{D}_{\mathrm{yM\,3}} - \mathrm{D}_{\mathrm{yM1}}}{\mathrm{D}_{\mathrm{YM1}}} \cdot 100 \qquad \text{Eq. (7.4)}$$

$\Delta dM_3/\mathrm{M}_1$= percentage difference of the maximum displacement in the middle section between Model 1 and Model 2

$\mathrm{D}_{\mathrm{yM3}}$= maximum displacement in the middle section Model 3

7.6 Model calibration, Structural identification and Material characterization

The models realized for the case studies were calibrated with the results obtained by experimental measurements.

The data derived from the measurement performed with the Tromino are values of velocity for increasing frequency in the vertical, transversal and horizontal directions.

Mode of 2-D Models were calibrated only if the measurement attributed to a frequency value had no component in the transversal direction since 2-D models can only exhibit in-plane vibration modes.

The transversal data obtained with experimental measurements have been utilized for the calibration of 3-D model since these models may exhibit both in-plane and out-of-plane vibration modes.

In this way structural identification was carried out and the mechanical characteristics of materials were identified without the use of invasive tests and without damaging the structure.

8 Case Studies

As explained in section 5.1 in this research four study cases were studied. The adopted cases are relevant to bridges which were built with similar geometrical and material characteristics but different parapet materials.

The bridges are:

- “De L’Arzere” bridge
- “Foscarini” bridge
- “Guglie” bridge
- “S. Lorenzo” bridge

8.1 “De L’Arzere” bridge

“De L’Arzere” bridge is located in the “Sestiere di Dorsoduro” in “Fondamenta delle Procuratie” and it crosses the canal of “S.Maria Maggiore”. It is made of masonry and Istria stone (compact lithographic limestone of the Tithonian age from Istria peninsula). The parapets were made of cast iron supported by little columns made of Istria stone.

Fig. 8.1: “De L’Arzere” bridge

8.1.1 History and description

At the beginning of VII century this bridge was made of wood and it was a gangway. From a document dated April 1792 and addressed to the Senate, it was underlined that it was necessary to build a new bridge.

Fig. 8.2: De L'Arzere bridge

The structure which exists nowadays preserves the principal historical characteristics. During the years some restorations were carried out and in XIX century the iron-made parapets were added.

8.1.2 Geometric survey

A geometrical survey carried out with laser scanner technique as explained in section 7.1.

Seven scans (POD files) were obtained; the number of cloud points was 153419991.

Fig. 8.3: "De L'Arzere bridge" Point cloud.

Fig. 8.4: Orthophotos obtained by point cloud

From the data imported by the points cloud in AutoCad, it was possible to know all the geometrical dimensions of the bridge. The span of the De L'Arzere bridge is 13,67 m and the thickness in correspondence to the keystone and the crown is 0,68 m. The measure of the rise is 2,45 m.

8.1.3 Experimental measurements

As explain in Chapter 7, the experimental measurement campaign was performed using two different types of instruments: Tromino and accelerometers, in order to make a comparison and validate the obtained results. The case study of "De L'Arzere" bridge was used as a reference for the other measurement campaigns.

8.1.3.1 Tromino measurements campaign

For the study case of "De L'Arzere" bridge two instrument were used for non-synchronized measurements, each measurement has been done at f_s = 512 Hz, for 16 minutes; the N_S and E_W horizontal components are recorded along the longitudinal and transversal axes of the bridge respectively. 5 measurements were taken laterally on the right side and other 5 laterally on the left side of the bridge. In this way it was possible to identify the mode shapes, natural frequencies and damping ratios of the whole structure.

The first measurements, one on the left site and one on the right see (Fig. 8.5), were always performed on the abutment, the second on the middle of the upstairs, the third laterally in the middle of the crown, the fourth and the fifth in correspondence of the same position of the first and second measurements but located on downstairs. Two other acquisitions done in order to evaluate soil vibration. This complete survey was performed in 1 hour and 36 minutes.

Fig. 8.5: Tromino instrument locations.

The signal process of acquired data was performed as was already explained in section 5.2.1.

The results obtained by the measurements carried on the left side (b measures) and on the right side (a measures) are shown in Fig. 8.5.

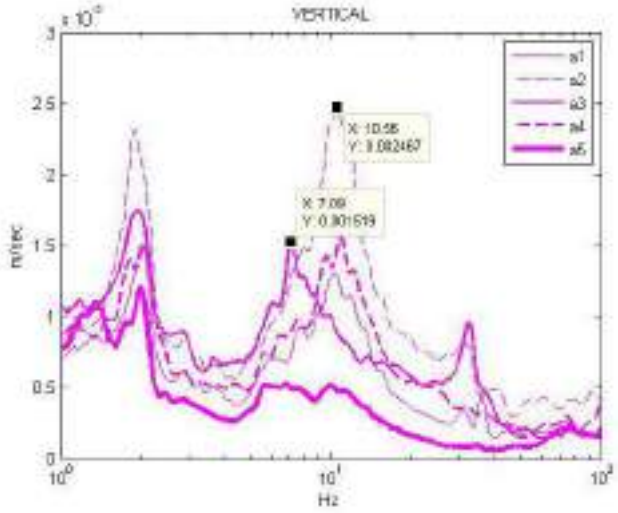

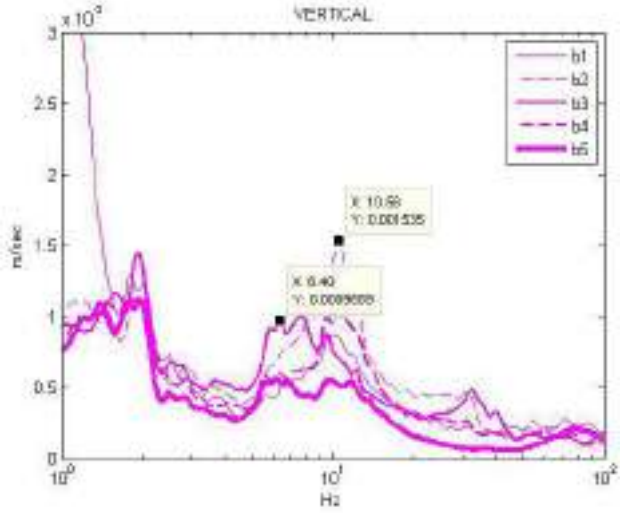

Fig. 8.6: Frequencies of Vertical-y direction.

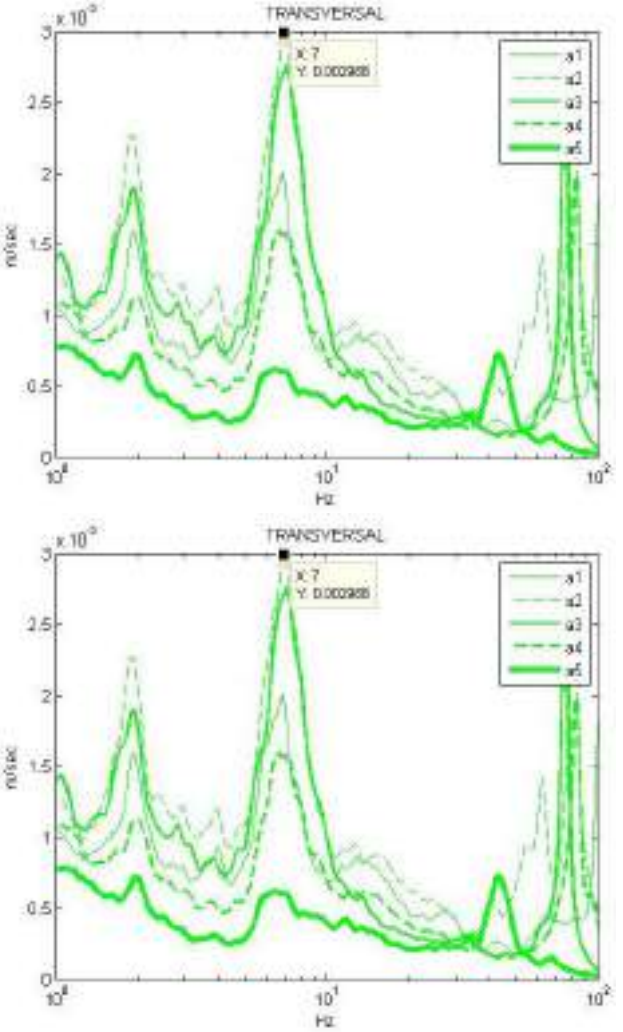

Fig. 8.7: Frequencies of Transversal-z direction.

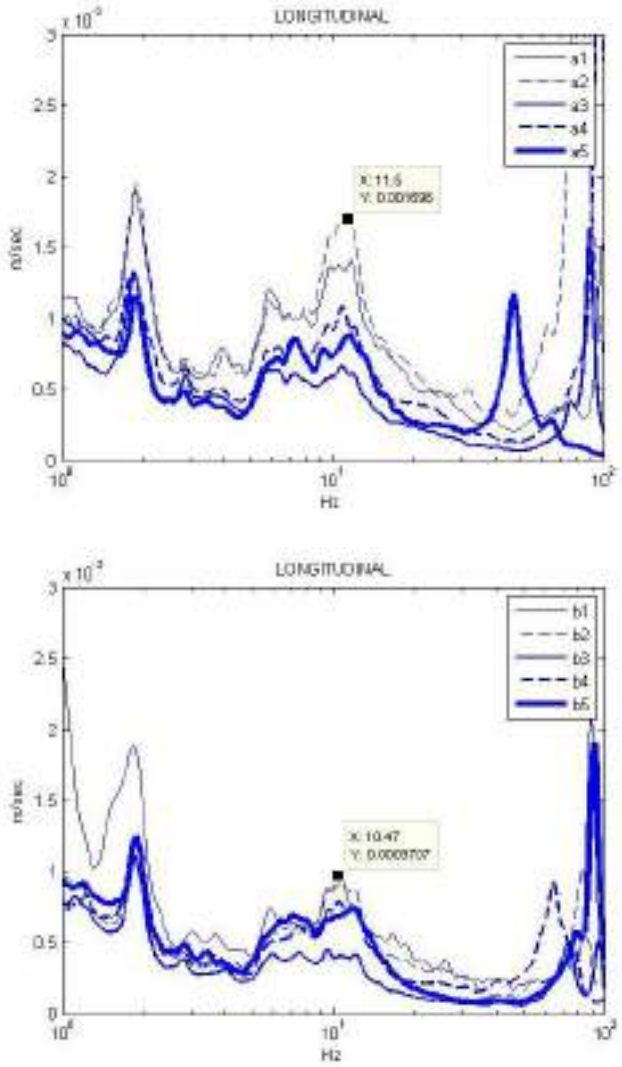

Fig. 8.8: Frequencies of Longitudinal-x direction.

As it is evident, the data obtained by Tromino measurement campaign and elaborated with Grilla software underline, utilizing an average value between the two different acquisitions, a first peak at 6.9 Hz and the modal shape is principally developed in transversal direction with a smaller component in vertical direction. The second peak is at 10.6 Hz and has a vertical direction, the third mode recorded is at 11Hz and it is developed in longitudinal direction.

- 6.9 Hz: First peak in transversal-z direction
- 10.6 Hz: Second peak in vertical-y direction
- 11 Hz: Third peak in longitudinal-x direction

The measurements exclude a 2 Hz peak value, which is associated to the human walk noise (Bachmann, 1992 a and 1992 b).

8.1.3.2 Accelerometers measurements campaign

As already explained another campaign of measurements was done, by making use of accelerometers in order to validate the results obtained by the campaign made with the Tromino instrument, see Fig. 8.13.

The experimental setup was designed to investigate the global dynamic behaviour of the structure. The test setup conducted by 2 runs of acquisition though 8 uniaxial piezoelectric accelerometers (PCB Piezotronics type 393C) with a nominal sensitivity of about 1 V/g, and a measurement range of ±2.5 g peak; the frequency range (±5%) is 0.025 to 800 Hz while the broadband resolution (1 to 10000 Hz) is 0.0001 g rms (root mean square). The data acquisition system is the HBM MX840A amplifiers with 28 channels, a resolution of 24 bit and a maximum frequency range of 19.2 KHz. The accelerometers were placed on the deck of the bridge, see Fig.5.1. and are marked by red point and labelled by P1, P2, P3, P4, P6, P7, P8, P9, P10 in Fig. 8.9.

Fig. 8.9: Location and name of accelerometer sensors.

To obtain reliable outcomes a dynamic monitoring program has been planned, with 12 measuring points and 2 runs of acquisition, that are described here below (Fig. 8.10).

The first run involves the sensor position from point 1 to point 5 while Run 2 includes the sensor position from point 6 to point 10 and point 3 as a reference. All measuring points acquire the signal in vertical direction represented by axis z. Only the P3 measuring point registers the signal not only in vertical direction but also in horizontal and transversal direction represented respectively by axes y and x.

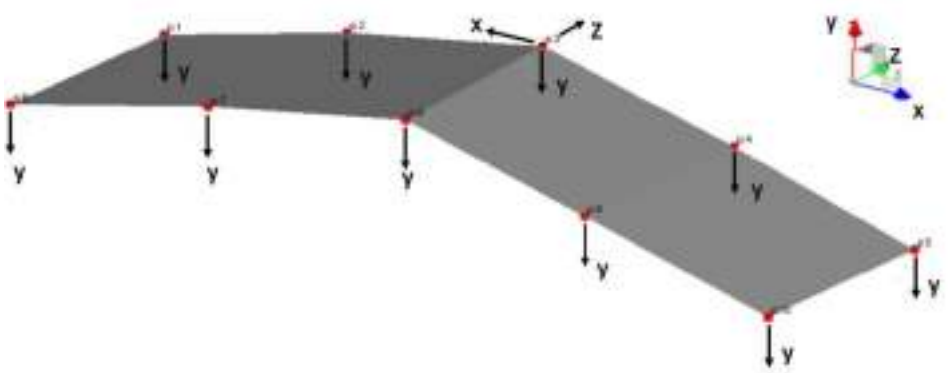

Fig. 8.10:Position and direction of the two acquisitions run.

The signal process of acquired was performed as already explained in section 5.2.4.

The acquisition of the signals was conducted in similar environmental conditions, with a temperature of about 10º C and 40% of humidity. 12 accelerometric directions subdivided in two schemes of acquisition RUN 1 and RUN 2 were correlated by a scaling process through the check points R3 (in x, y, and z directions) assumed as fixed references. From the time history of each channel, that covered an acquisition time of about 30 minutes, the structural response data has been extracted with reference to each of the 2 runs and shows, as an example, some recordings that had the best signal-to-noise ratio (S/N) (UNI 9916, 2004). The ratio, expressed in decibel, is acceptable if S/N > 10 dB, while it needs filtering if 6<S/N<10 dB. The robust reliability of signals is demonstrated by the acquisition with the lowest S/N, that is equal to 12.3-DB.

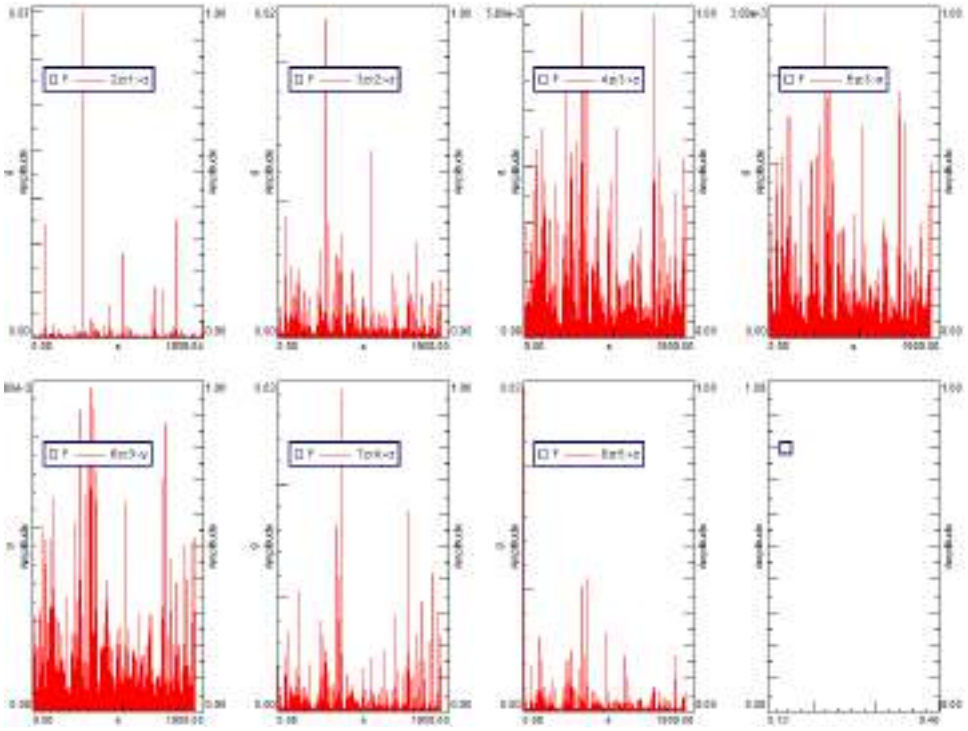

Fig. 8.11: Example of some recordings that had the best signal-to-noise ratio (S/N).

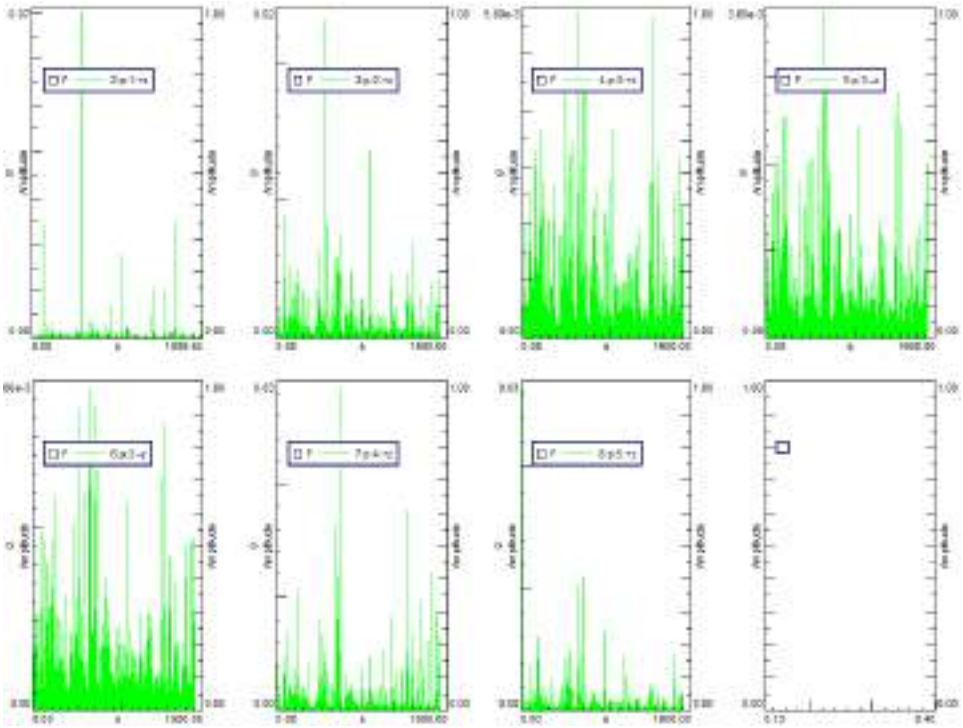

Fig. 8.12: Example of some recordings that had the best signal-to-noise ratio (S/N).

The maximum values of acceleration, expressed as a fraction of gravity acceleration g, throughout the stages of acquisition reaches +0.07g for run 1 and for run 2. Each acceleration-time graph makes reference to a single channel and to the respective monitored direction.

The main vibration modes were thus identified by the best match with the compared cross-spectrum functions previously yielded from the time histories of each channel (Fig. 8.11 and Fig. 8.12).

The mode shapes and respective parameters, as frequency (Hz) and damping ratio (ζ), are indicated in Fig. 8.15.

It can be noted that the first bending vibration mode of the structure happens at 6.4 Hz for run 1 registration and to 6.8 Hz for run 2 registration. The second bending mode corresponds to 12.3 Hz for run 1 registration and to 10.8 Hz for run 2 registration. The third mode shape, that involve the structure, occurs at a frequency of 32.4 Hz for run 1 registration and at a frequency of 36.6 Hz for run 2. It corresponds to a torque vibration mode. In all these cases an average value has been considered, as illustrated in Tab. 8.2.

The difference in values obtained by run 1 and run 2 is due to the asymmetrically shaped bridge that is not at a right angles with the canal as already explained in Section 8.4.2. The bridge presents a different stiffness from one side is compared with the other. The test setup was conducted with two runs of acquisition with a point as a reference positioned on the decks of the bridge (Fig. 8.10).

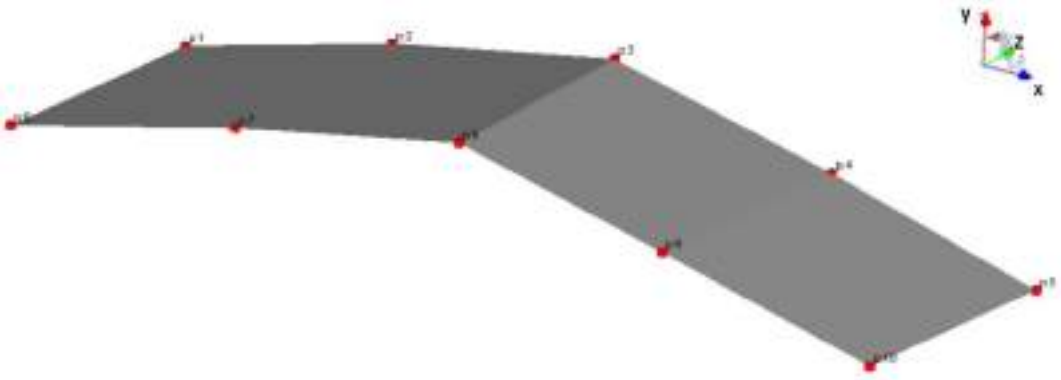

Fig. 8.13: Location of accelerometers sensors.

In the stabilization diagram (Fig. 8.14) resonance frequencies and the respective damping ratios of the identified poles are visualized for different model orders.

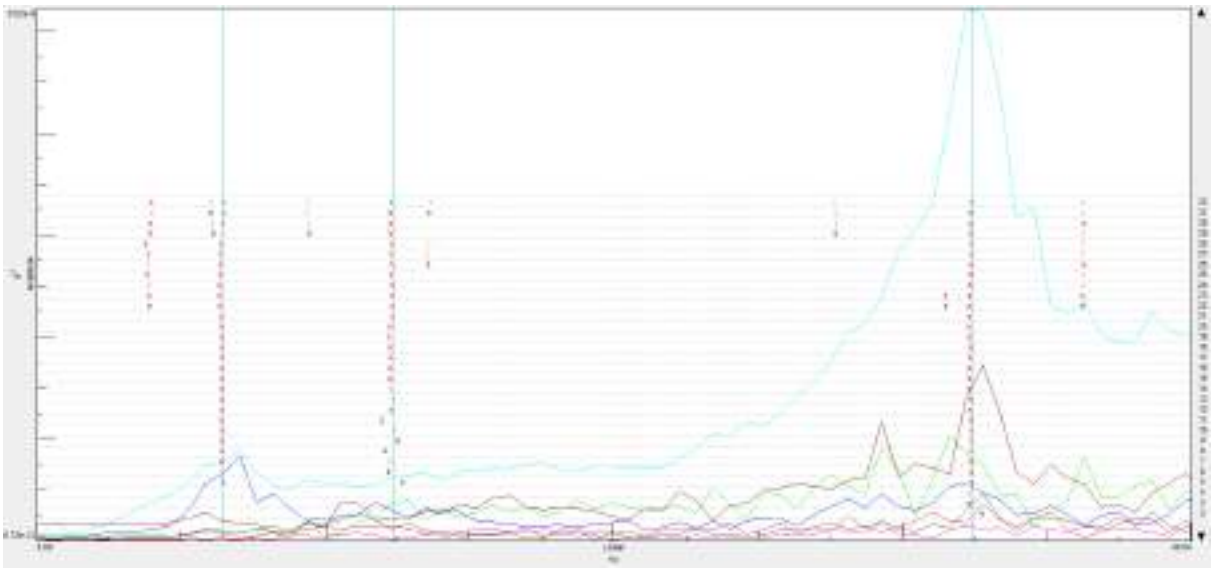

Fig. 8.14: Stabilization diagram.

The modal shapes were extracted from the experimental measurements and 3-D geometric schematic model, as was already explained, and it was constructed by making use of LMS Test. Lab: Siemens PLM Software.

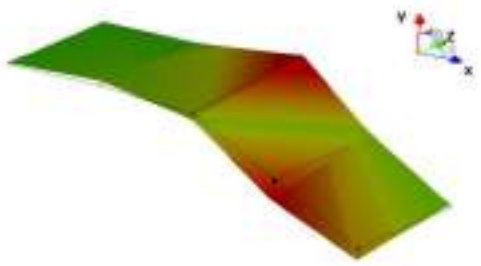

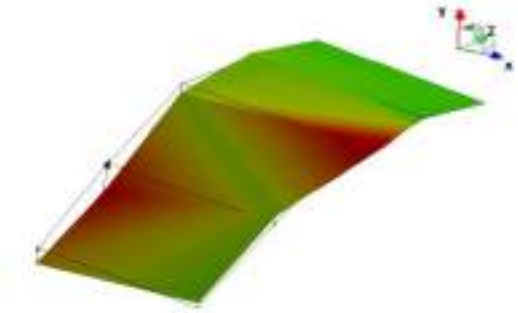

1° mode: Frequency 6.6 Hz, damping ratio 8.9%

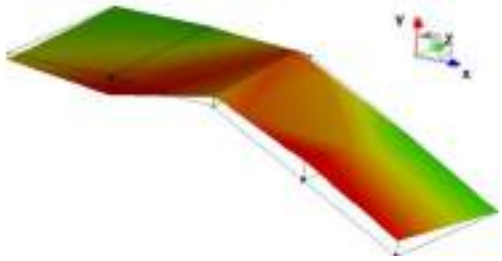

2° mode: Frequency 11.6 Hz, damping ratio 3.6%

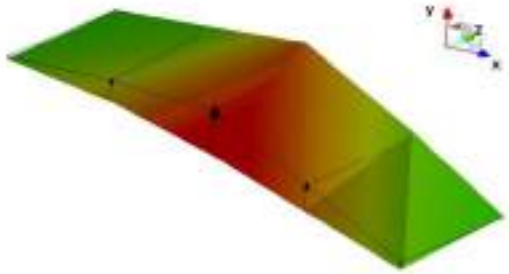

3° mode: Frequency 34.5 Hz, damping ratio 2.7%

Fig. 8.15: Modal shapes, frequencies and damping ratio of the bridge.

The reliability of the adopted procedure was checked with a Least-Square assessment of the scale factor between two vectors and with the corresponding coefficient of correlation, obtained by comparing the matrix of each mode to itself, applying the well known Modal Assurance Criterion (MAC), (Ewins, 2000).

The outcomes point out the good correlation among the modes obtained from the different schemes of acquisition (see Tab. 8.1), and the reliability of the adopted procedure of dynamic identification. The modal shape analysed through the MAC should be at least 90% (Ewins, 2000); in detail the values in excess of 90% should be attained for well-correlated modes while the values of less than 10% for uncorrelated modes.

RUN1	RUN2	Frequency		Frequency Difference (Hz)	Damping		Damping Difference (%)	MAC (%)
		RUN1 (Hz)	RUN2 (Hz)		RUN1 (%)	RUN2 (%)		
Mode 1	Mode 1	6.4	6.8	0.4	12.6	5.2	7.5	97.2
Mode 2	Mode 2	12.3	10.8	1.5	4.2	3.1	1.1	99.3
Mode 3	Mode 3	32.4	36.6	4.20	4.2	1.1	3.1	99.2

Tab. 8.1: Comparison between the results obtained by RUN1 and RUN 2 measurements.

Tromino	**Frequency**	**Damping**
1° mode	6.6 Hz	8.9%
2° mode	11.55 Hz	3.6%
3° mode	34.5 Hz	2.7%

Tab. 8.2: Mean values of dynamic parameters.

8.1.4 Results analysis

Tromino Measurements	**Mode shape direction**	**Accelerometers Measurements**	**Mode shape direction**
6.9 Hz	Transversal motion	6.6	Transversal motion
10.6 Hz	Vertical motion	11.55 Hz	Vertical motion
10.6 Hz	Longitudinal motion	34.5 Hz	Torsional motion

Tab. 8.3: Experimental measurements frequency values and Mass participation direction.

Tomino measurements campaign:

- 6.9 Hz: First peak in the transversal-z direction.
- 10.6 Hz: Second peak in the vertical-y direction.
- 11 Hz: Third peak in the longitudinal-x direction.

Accelerometers measurement campaign:

- 6.6 Hz: First peak in transversal-z direction.
- 11.55 Hz: Second peak in the vertical-y direction.
- 34.5 Hz: Third peak that represents a torsional mode.

The differences in the results are due to the different acquisitions during the accelerometer campaign because the transversal and longitudinal directions have not been considered in all measurements points. The results confirm that the Tromino can be considered a valid

alterative to the instruments usually employed for the operational modal analysis, see Tab. 8.4.

Mode	Tromino	Accelerometers	Difference
1°	6.9 Hz	6.6 Hz	4.3%
2°	10.6 Hz	11.5 Hz	8.5%

Tab. 8.4: Percentage error value between the data obtained by the two different monitoring methodologies.

As explained in Section 8.1.3.1, the first frequency acquired by Tromino experimental measurements has a peak value of 6.9 Hz and corresponds to a vibration mode in transversal direction. Section 8.1.3.2 shows the result of 6.6 Hz performed utilizing an accelerometer instrument. The values obtained by the different measurement campaign are in accordance, with a difference percentage equal to 4.3% .

Making a comparison between Tromino and accelerometers delete a second peak in the vertical direction is evident, at 10.6 Hz and 11.5 Hz respectively therefore values are sufficiently in agreement with each other with a difference percentage equal to 8.5%.

The third mode that has been recorded using the accelerometer is a torsional mode at 34.5 Hz because transversal motions have not been acquired while the third mode acquired using Tromino has a value of 11 Hz and it is in transversal direction. This is a consequence of the fact that, as already explained in section 8.1.3.2, all measuring points acquire the signal in vertical direction represented by axis z. Only the P3 measuring point registers the signal not only in vertical direction but also in horizontal and transversal direction represented respectively by axes y and x (Fig. 8.10). Therefore is not possible to correlate all measurements points in the transversal direction and for this reason there is only one reference peak to take into consideration.

8.1.5 2-D and 3-D F.E. Model description

Here by a 2-D discretization for F.E. models is proposed, the transversal cross-section of the bridge presenting constant mechanical characteristic. They models were constructed by using 350 3-node elements. Hence, 2-D, 3 nodes plane elements, under plane strain assumption, were analysed considered.

The 2-D reference system is characterized by axes x and y, namely:

- x axis: Horizontal direction on the plane and longitudinal motion of participating mass.
- y axis: Vertical direction on the plane and vertical motion of participating mass

The material constituents of the bridge are: masonry, fill that is realized by scrap material and the pavement realized with Istria and Basalt stone. The mechanical characteristics that

are density (***γ***), Poisson's ratio (***v***) and Young's modulus (***E***) of the material adopted are reported in Tab. 8.5.

Materials	**Model properties**		
	E (MPa)	***v***	***γ*** (Kg/m^3)
Masonry	2300	0.2	2000
Fill	1000	0.2	2000
Pavement	2500	0.2	1800

Tab. 8.5: Assumed material properties for 2-D F.E. models.

2-D Model 1:

The node constraints applied to Model 1 are mentioned in section 7 as evidence in Fig. 8.16

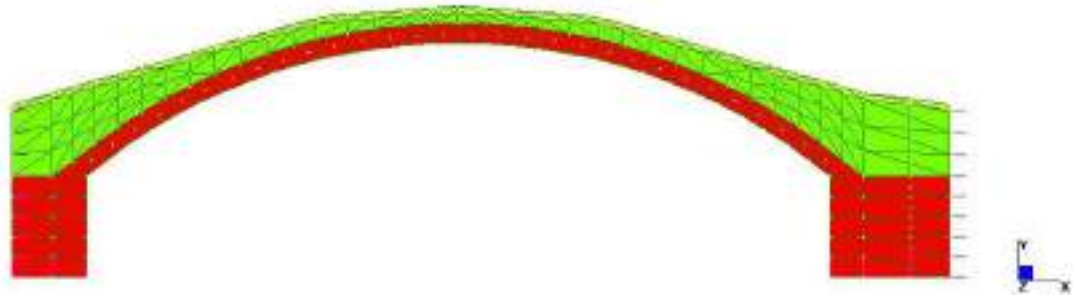

Fig. 8.16: 2-D Model 1 "De L'Arzere" bridge

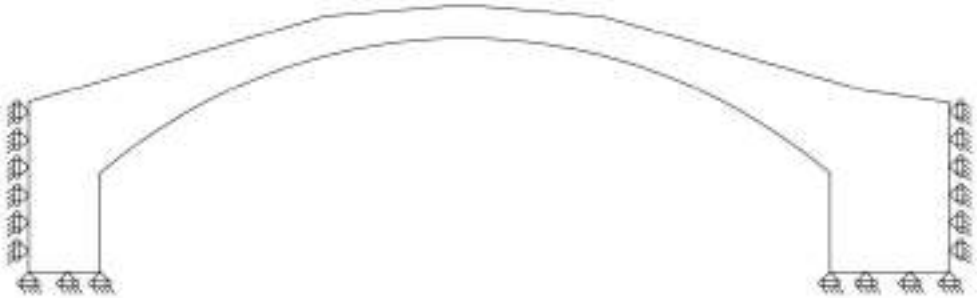

Fig. 8.17: 2- D Model 1 Diagram showing boundary conditions.

2-D Model 2:

The node constraints applied to the Model 2 are mentioned in Chapter 7 as evidence in Fig. 8.18

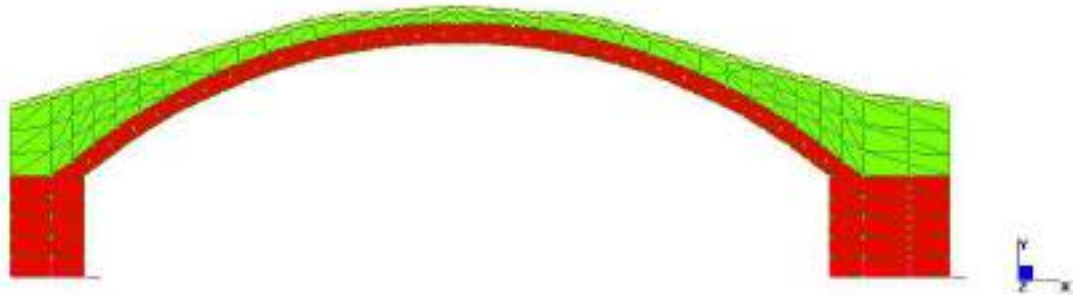

Fig. 8.18: 2-D Model 2 “De L’Arzere” bridge

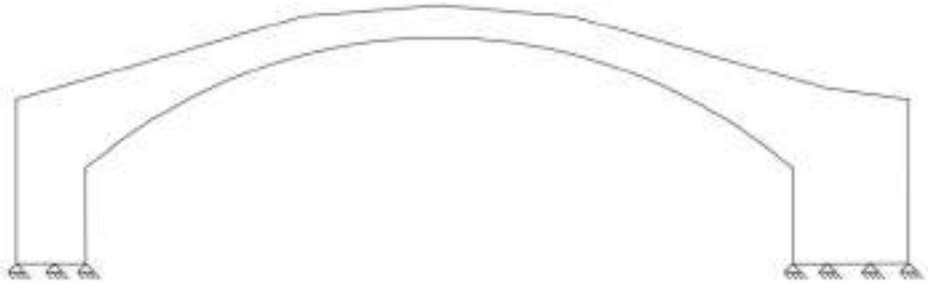

Fig. 8.19: 2- D Model 2 Diagram showing boundary conditions.

2-D Model 3:

The node constraints applied to the Model 3 are mentioned in section 7 as evidence in Fig. 8.20. The springs have a high stiffness value of $1{,}2 \cdot 10^{7}$N/m in the horizontal direction.

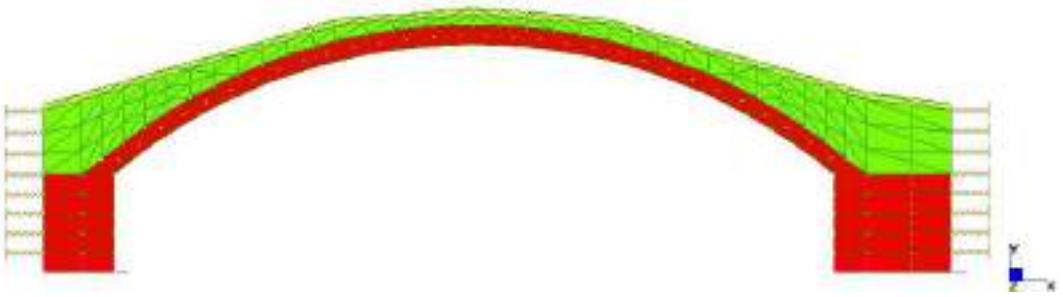

Fig. 8.20: 2-D Model 3 “De L’Arzere” bridge.

Fig. 8.21: 2- D Model 3 Diagram showing boundary conditions.

3-D Model:

A 3-D F.E. model was constructed by using with 1125 8-nodes elements and 112 6-nodes elements. In the foundation the spring stiffness value is $5.8 \cdot 10^7$ N/m and the springs are positioned in the vertical transversal and the horizontal direction. In correspondence of the abutments the spring stiffness value is $1 \cdot 10^8$N/m in the horizontal and the transversal direction.

The 3-D reference system is characterized by the x, y, and z axes which represent:

- x axis: Horizontal direction on 3-D reference system and longitudinal motion of participating mass.
- y axis: Vertical direction on 3-D reference system and vertical motion of participating mass.
- z axis: Out of plane direction and transversal motion of participating mass.

For 3-D model also the Istria stone has been considered as a different material, see Tab. 8.6.

Materials	**Model properties**		
	E (MPa)	***v***	***γ*** (Kg/m^3)
Masonry	2300	0.2	2000
Fill	1000	0.2	2000
Pavement	2500	0.2	1800
Istria stone	10000	0.2	2100

Tab. 8.6**:** Adopted material Properties of 3-D models.

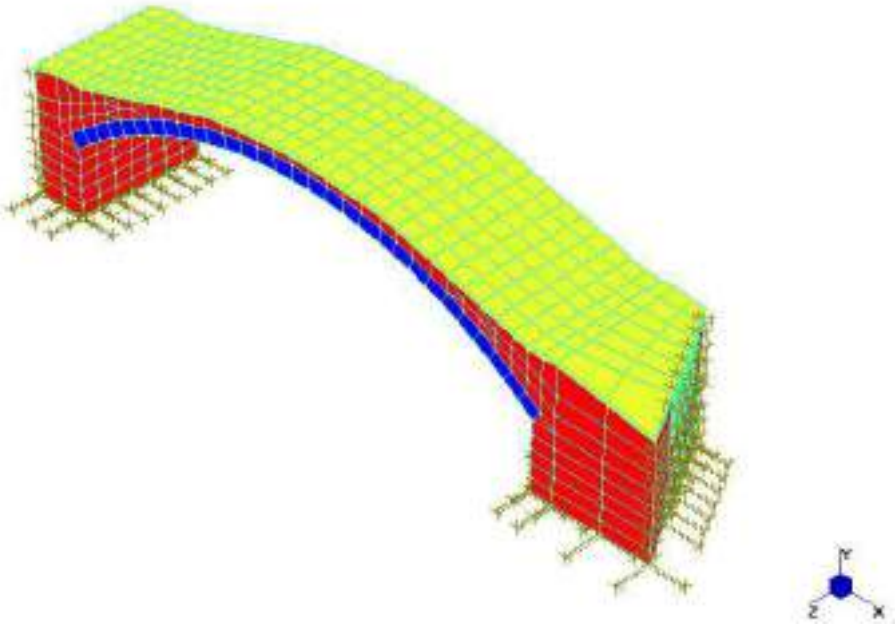

Fig. 8.22: 3-D Model “De L’Arzere” bridge.

8.1.5.1 2-D Analytical solution

As already explained in Section 7.4, the 2-D numerical model was validated against an exact solution, by making use of Eq. (7.4) and making a comparison between the results obtained in terms of the maximum displacement of the middle cross-section.

$$AD_y = \frac{pl^2}{8EF} \cdot \frac{2 + \frac{25}{128} \cdot \frac{l^2}{f^2}}{1 + \frac{15}{8} \cdot \frac{i^2}{f^2}}$$

$$AD_y = \ 0.0038\text{m}$$

AD_y= Analytical displacement in the middle section in the vertical direction

E= 3000 MPa

F= 0.37 m^2

f=2.45 m

p = 22.928 kN/m^2

l = 13.67 m

i =0.106 m^2

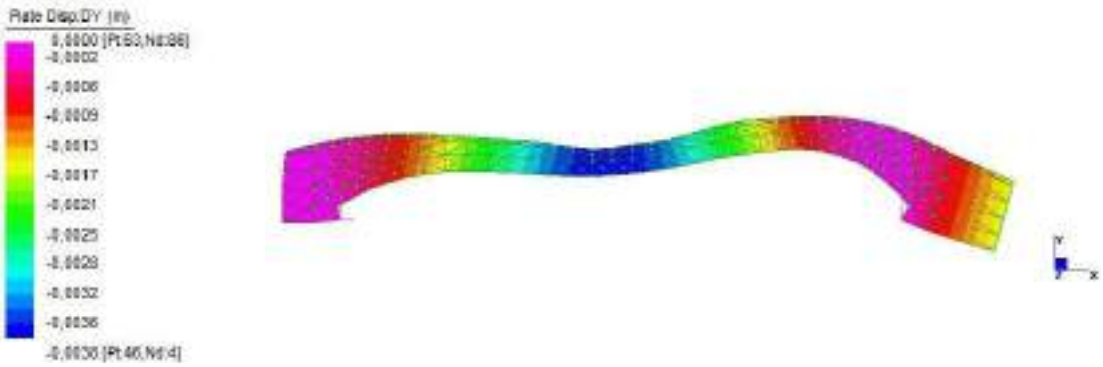

Fig. 8.23: Static Analysis. 2-D Model realized with hinges in correspondence of the foundations.

$$MD_y = 0.0038m$$

MD_y= Model displacement in the middle section in vertical direction

The maximum vertical displacement produced by the analytical solution is in accordance with the numerical output, giving a value close to 0,0038 m.

8.1.5.2 2-D Static analysis

In the case of Model 1 the maximum displacement in the middle cross-section is 0,0026 m

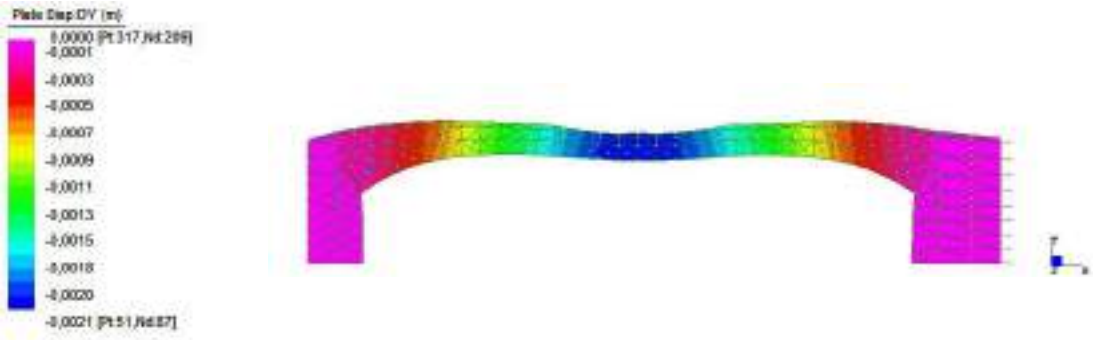

Fig. 8.24: Model 1-De L'Arzere bridge static analysis

In the case of Model 2 the maximum displacement in the middle cross-section is 0,0030 m

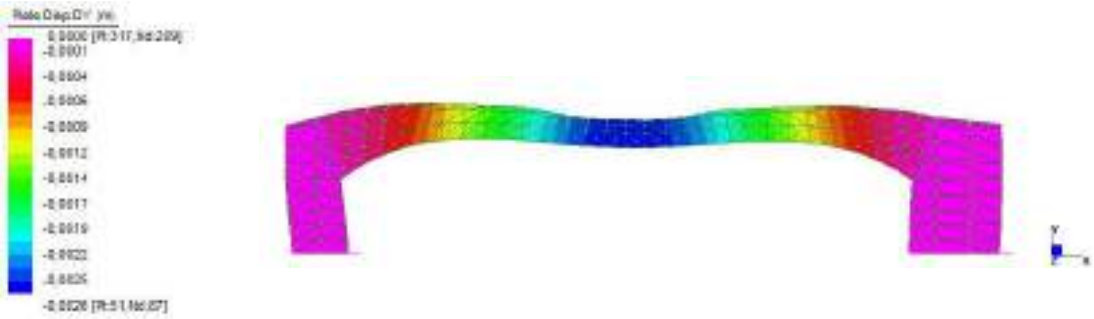

Fig. 8.25: Model 2-De L'Arzere bridge static analysis

In the case of Model 3 the maximum displacement in the middle cross-section is 0,0027 m.

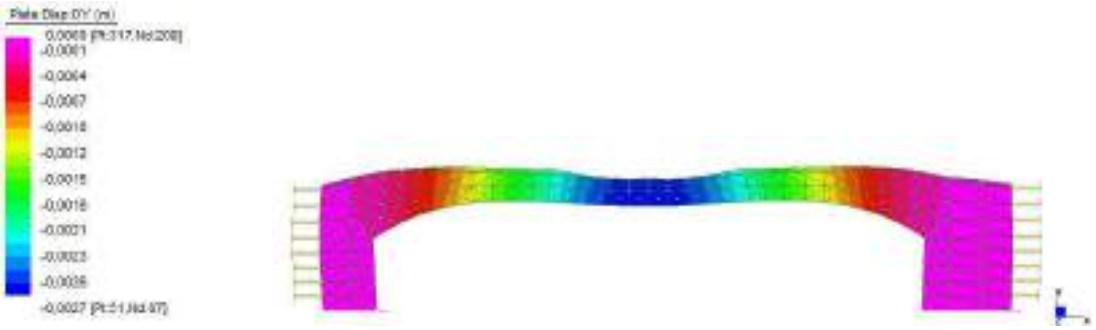

Fig. 8.26: Model 3-De L'Arzere bridge static analysis

The percentage difference in displacement between Model 1 and Model 2, see Eq. (7.3) and between Model 1 and Model 3, Eq. (7.4) have been evaluated, as follows:

$$\Delta diff M_2/\mathrm{M}_1 = \frac{0{,}0030\mathrm{m} - 0{,}0026\mathrm{m}}{0{,}0026\mathrm{m}} \cdot 100 = 15\%$$

$$\Delta diff M_3/\mathrm{M}_1 = \frac{0{,}0027\mathrm{m} - 0{,}0026\mathrm{m}}{0{,}0026\mathrm{m}} \cdot 100 = 3\%$$

The obtained results underline that the constraints adopted in Model 3 produce a solution closer to that provided by model 1.

8.1.5.3 -D Modal analysis

A Modal analysis, as explained in Chapter 7, was carried out. The corresponding results are hereby presented and commented upon. In Tab. 8.7 MP-X, MP-Y, MP-Z represent the Mass Participant in the x, the y and the z- axes directions.

Model 1:

Mode	Frequency	Modal mass	MP-X	MP-Y	MP-Z
	Hz	Kg	%	%	%
1	9.439E+00	9.282E+03	0.025	34.102	0.000
2	1.067E+01	1.669E+04	12.597	0.063	0.000
3	1.900E+01	1.699E+04	0.072	14.763	0.000
4	2.653E+01	1.896E+04	43.347	0.006	0.000
Total Mass Participation			56.041	48.934	0.000

Tab. 8.7: Results of natural frequency analysis of 2-D Model 1.

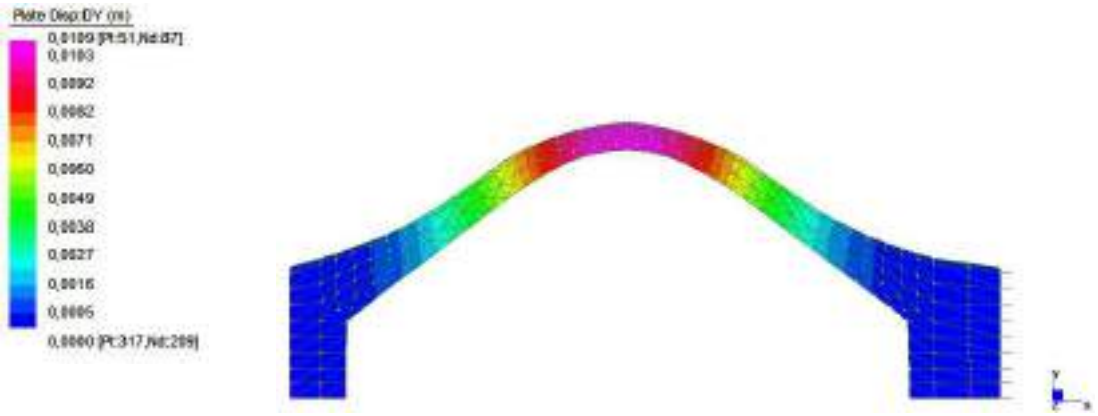

Fig. 8.27: 2-D Model 1 natural frequency analysis: First modal shape.

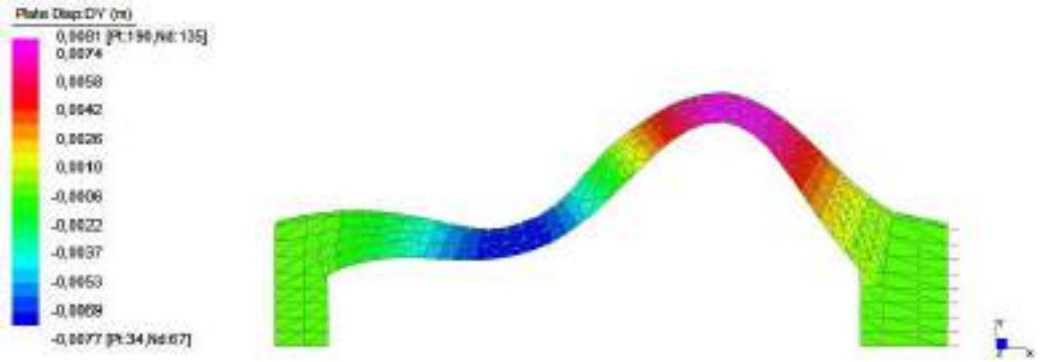

Fig. 8.28: 2-D Model 1 natural frequency analysis: Second modal shape.

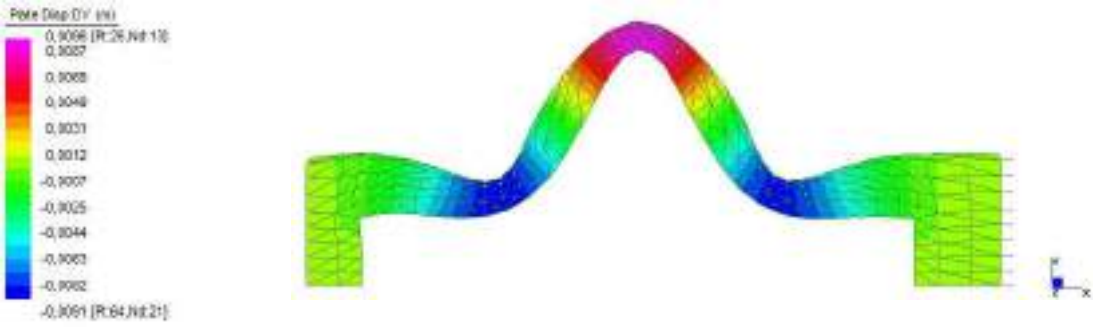

Fig. 8.29: 2-D Model 1 natural frequency analysis: Third modal shape.

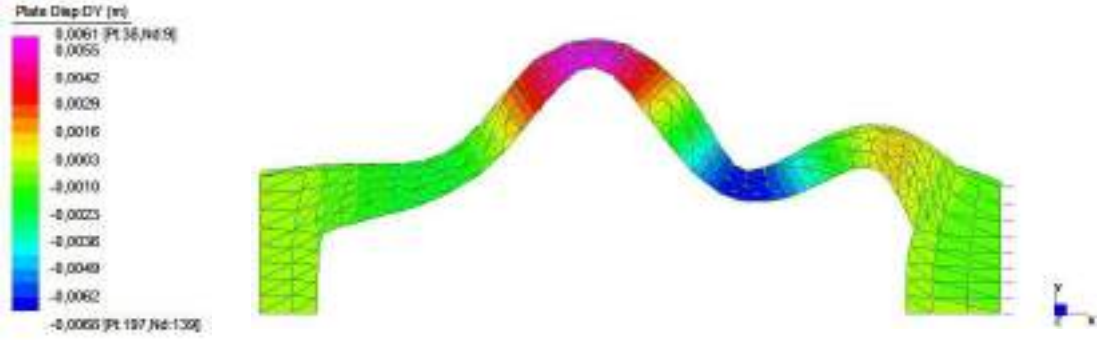

Fig. 8.30: 2-D Model 1 natural f frequency analysis: Fourth modal shape.

Model 2:

Mode	Frequency	Modal mass	MP-X	MP-Y	MP-Z
	Hz	Kg	%	%	%
1	7.655E+00	1.846E+04	33.284	3.987	0.000
2	8.677E+00	9.454E+03	4.784	24.928	0.000
3	1.624E+01	1.717E+04	1.039	18.864	0.000
4	1.766E+01	1.853E+04	37.773	0.739	0.000
Total Mass Participation			76.818	49.486	0.000

Tab. 8.8: Results of Natural frequency analysis of 2-D Model 2.

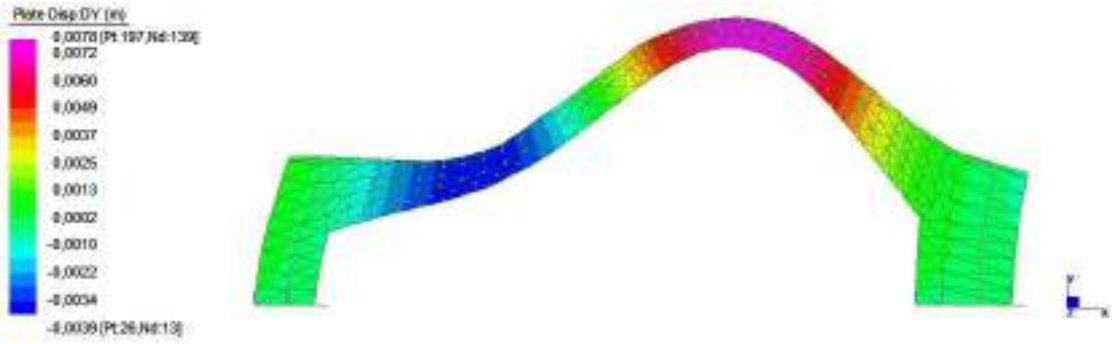

Fig. 8.31: 2-D Model 2 natural frequency analysis: First modal shape.

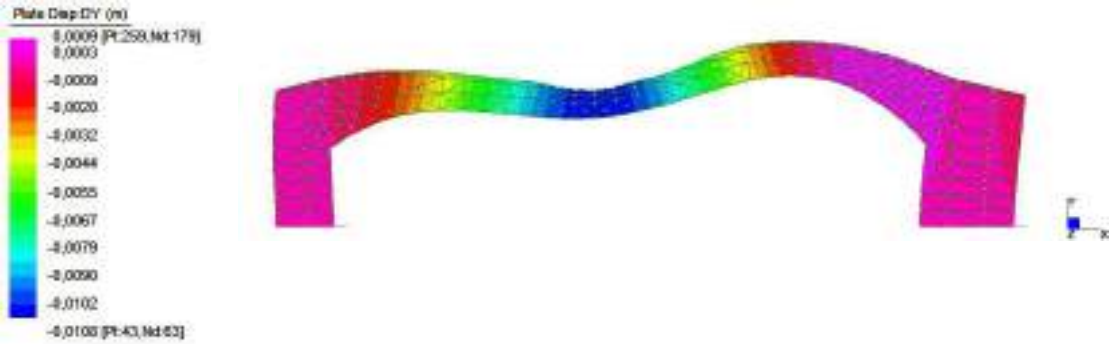

Fig. 8.32: 2-D Model 2 natural frequency analysis: Second modal shape.

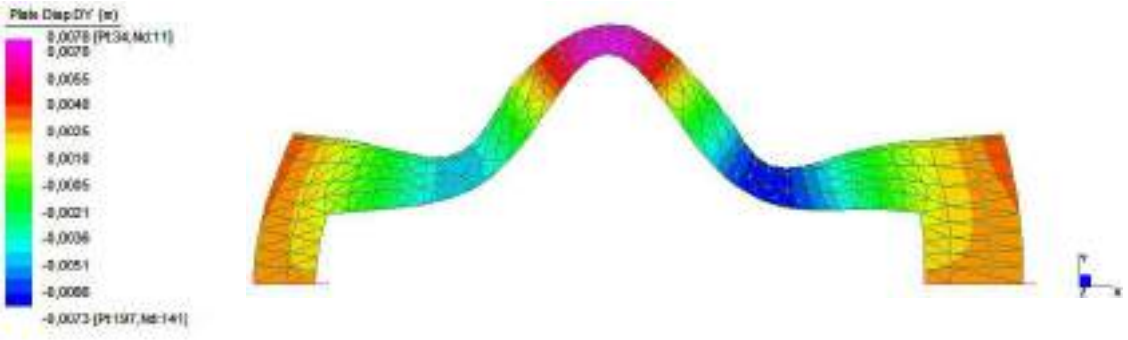

Fig. 8.33: 2-D Model 2 natural frequency analysis: Third modal shape.

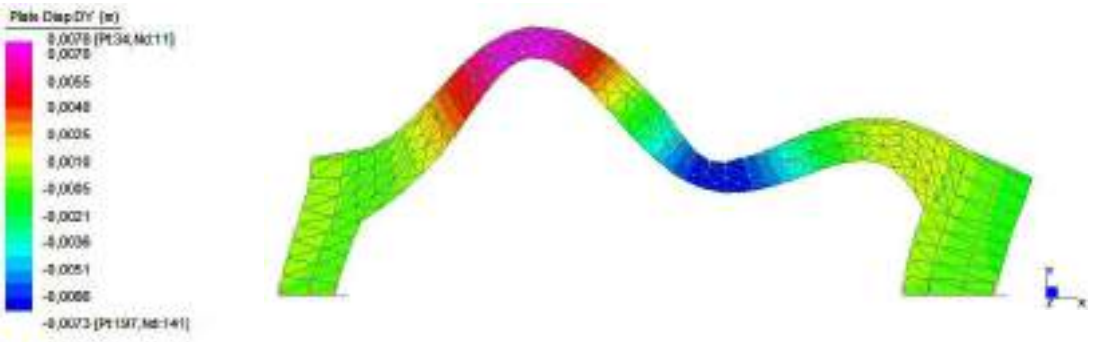

Fig. 8.34: 2-D Model 2 natural frequency analysis: Fourth modal shape.

Model 3:

Mode	Frequency	Modal mass	MP-X	MP-Y	MP-Z
	Hz	Kg	%	%	%
1	9.106E+00	9.152E+03	0.029	32.490	0.000
2	9.593E+00	1.974E+04	20.141	0.047	0.000
3	1.763E+01	1.909E+04	0.026	16.441	0.000
4	2.188E+01	2.285E+04	48.077	0.002	0.000
Total Mass Participation			68.274	48.979	0.000

Tab. 8.9: Results of natural frequency analysis of 2-D Model 3

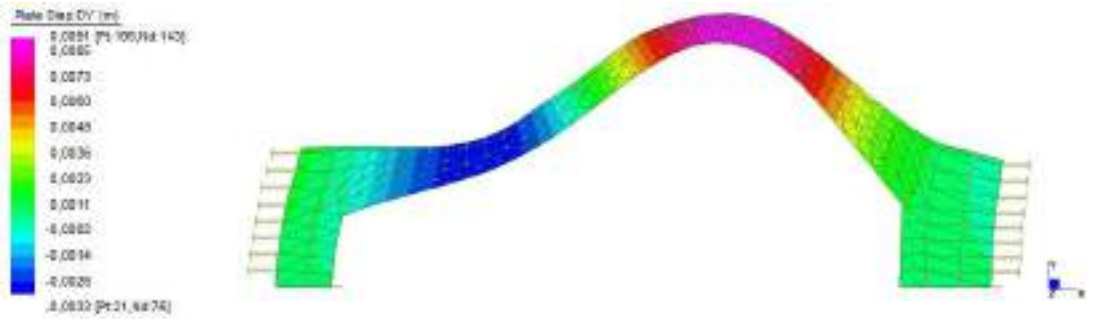

Fig. 8.35: 2-D Model 3 natural frequency analysis: First modal shape.

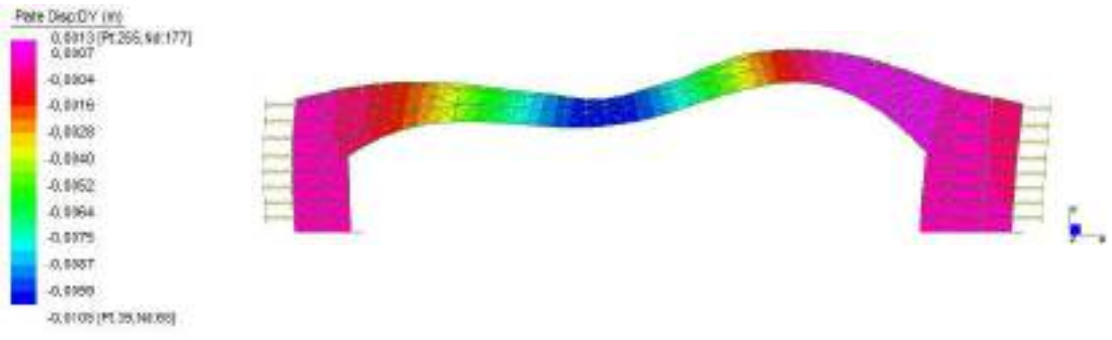

Fig. 8.36: 2-D Model 3 natural frequency analysis: Second modal shape.

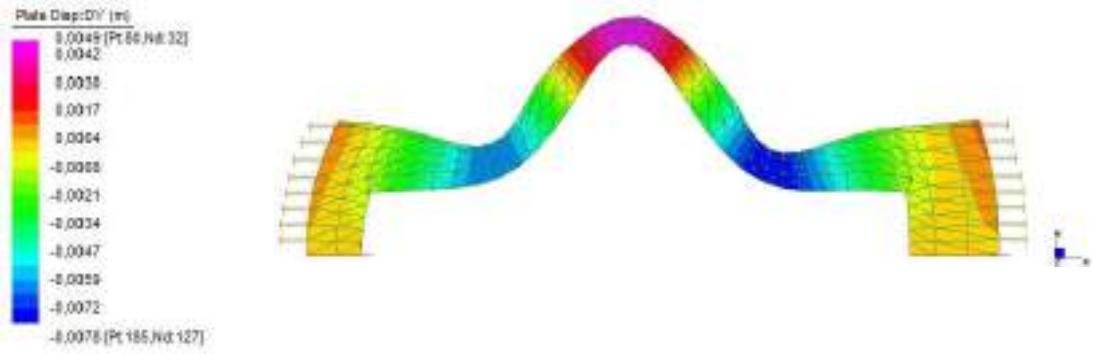

Fig. 8.37: 2-D Model 3 natural frequency analysis s: Third modal shape.

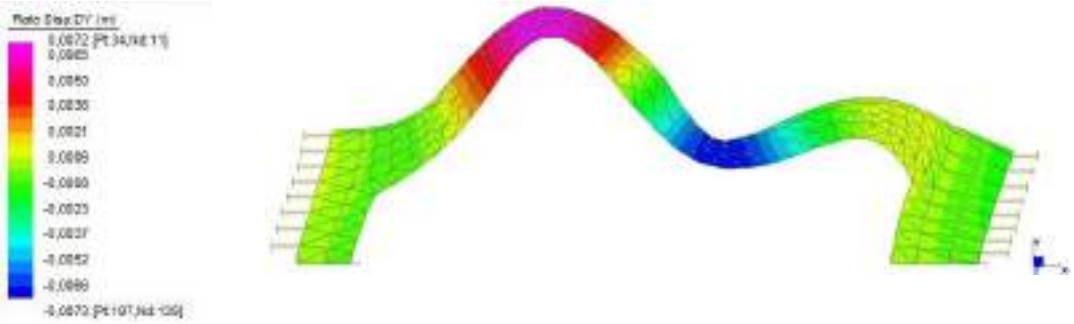

Fig. 8.38: 2-D Model 3 natural frequency analysis: Fourth modal shape.

Considering the obtained results by the natural frequencies analysis of the differently constrained models, it must be noted that the Model 3, obtained by using an intermediate condition and Model 1, modelled blocking the horizontal motions of the abutments and the vertical motions of the foundations show similar frequencies. The natural frequencies results by Model 1 are closer to the values obtained by experimental measurements.

The 2-D model is a plane one and for this reason it cannot be calibrated considering the first frequency value obtained by experimental campaign and characterized out of the plane displacement of most of the participating mass. The participating mass for the second mode and the third mode is in accordance with experimental data results, but the range of values are different because 2- D model is not able to take into consideration any out-of-plane motion. It is nonetheless useful for a first fast analysis in order to suitable bracketing a range of values, see Tab. 8.9.

The direction of participating mass of the first mode obtained by 2- D Model 3 natural frequencies analysis is in longitudinal direction according to the result acquired for the second mode in the experimental measurement campaign, see Tab. 8.3. The direction of participating mass of the second mode is longitudinal and is in accordance with third mode experimental measurements.

The model laterally constrained with springs, 2- D-model 3, produces frequency values higher than 2D-Model 1, due to the mass transversal direction of the first mode (out of plane).

8.1.5.4 3-D Modal Analysis

Mode	Frequency	Modal mass	MP-X	MP-Y	MP-Z
	Hz	Kg	%	%	%
1	6.715E+00	4.160E+04	0.033	0.209	53.781
2	9.884E+00	3.081E+04	16.013	24.056	0.000
3	1.101E+01	3.042E+04	24.744	4.117	0.000
4	1.528E+01	7.389E+04	0.440	1.842	0.404
Total Mass Participation			41.230	30.223	54.402

Tab. 8.10: Results of Natural frequency analysis of 3-D Model

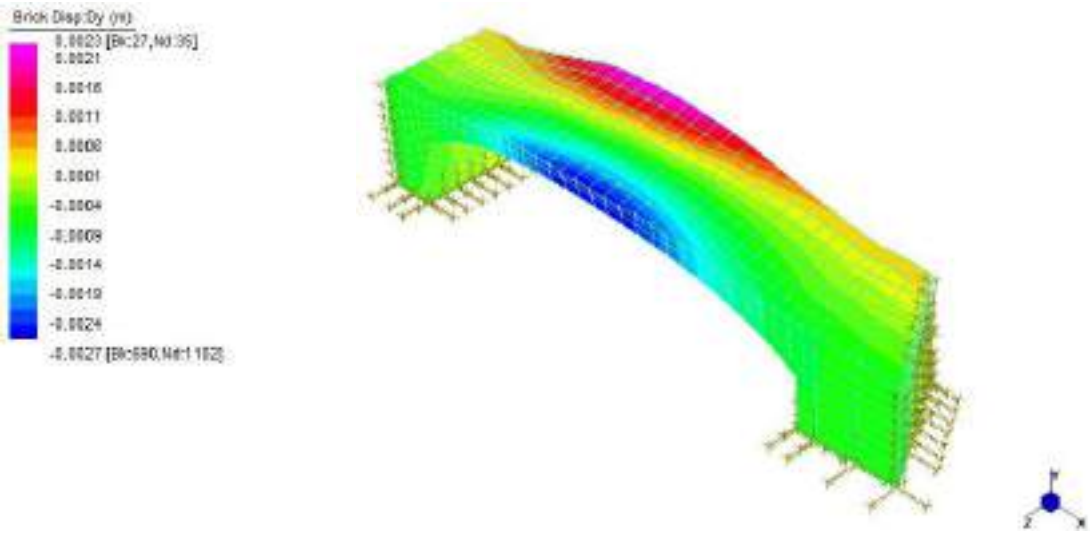

Fig. 8.39: 3-D Model natural frequency analysis: First modal shape.

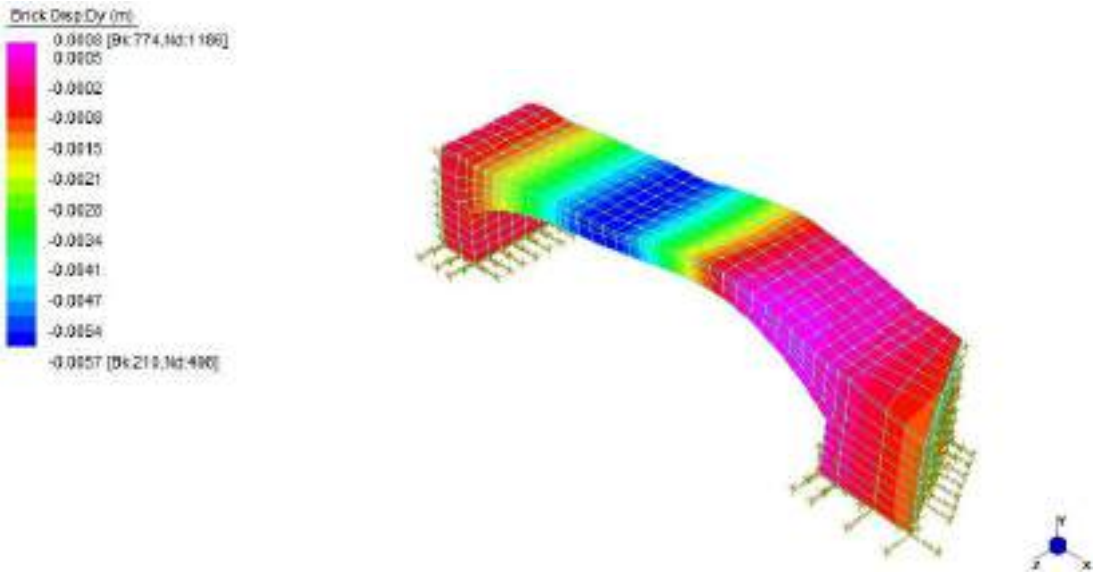

Fig. 8.40: 3-D Model natural frequency analysis: Second modal shape.

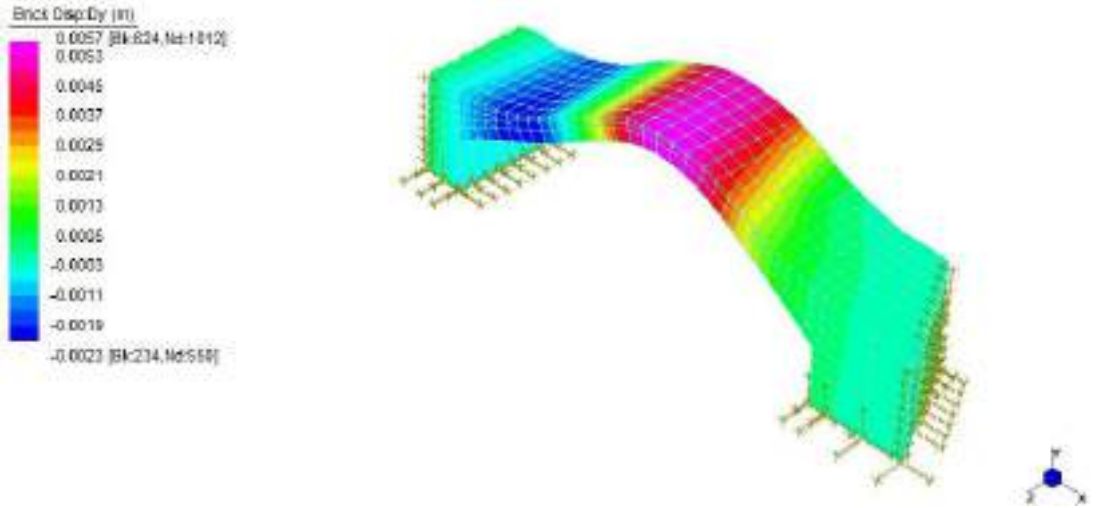

Fig. 8.41: 3-D Model natural frequency analysis**:** Third modal shape.

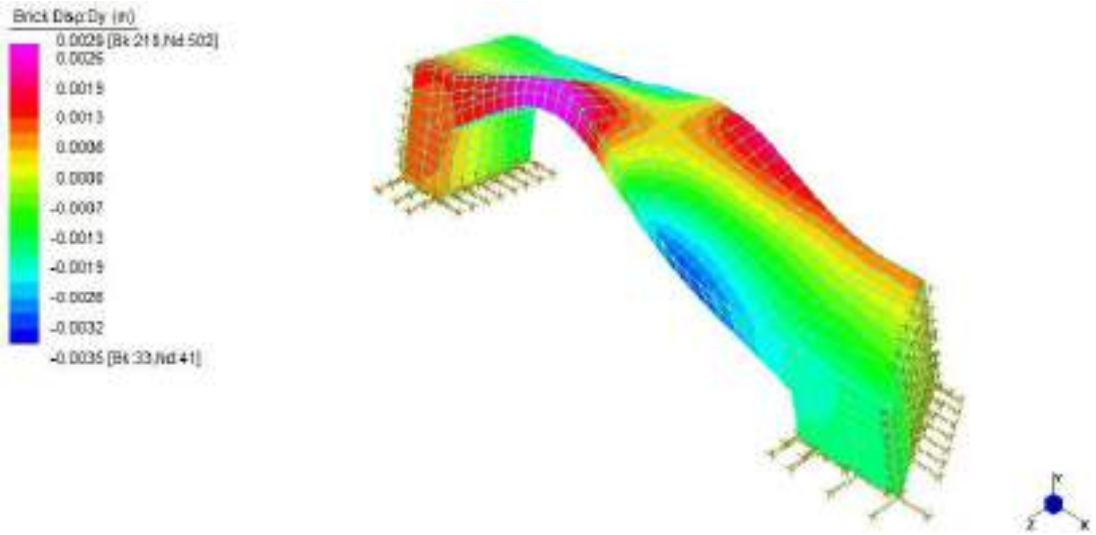

Fig. 8.42:. 3-D Model 3 natural frequency analysis: Fourth modal shape.

8.1.6 Structural and material identification

As described in section 7.6, the 2-D model was adopted to identify, in a fast way, a value range for materials characterization and correct definition of constraints. 3-D Model was calibrated with the same values used for 2-D Model calibration but it was carried out considering also transversal direction.

In data obtained by 3- D Natural Frequencies analysis, see Tab. 8.10, the first mode has a frequency value of 6.7 Hz and most of the participating mass moving in transversal direction and the difference percentage equal to 2.9%. The values obtained for second and third modal shape are respectively 9.9 Hz in vertical direction and 11 Hz in transversal direction. Second value obtained has a difference percentage equal to 6.6% while the third value is the same recoded by Tromino measurements campaign, see Tab. 8.11.

Mode	Tromino Data	FEM2-D	Difference	FEM 3-D	Difference
1°value Transversal mode	6.9 Hz	-		6.7 Hz	2.9%
2°value Vertical mode	10.6 Hz	9.1 Hz	14.1%	9.9 Hz	6.6%
3°value Longitudinal mode	11 Hz	9.6 Hz	12.7%	11 Hz	0

Tab. 8.11: Dynamic parameters and difference between Tromino experimental data and 2-D / 3-D models.

8.2 Foscarini bridge

"Foscarini bridge" is usually called "Carmini bridge" because it is located in front of "S. Maria of Carmini" church in "Sestrier Dorsoduro". It is made of masonry and Istria stone and the parapets are made also of masonry.

Fig. 8.43: "Foscarini" bridge.

8.2.1 History and description

During history, traditional fights has been made on this bridge between "Castellani" and "Nicolotti" inhabitants.

In 1752 the bridge was demolished because it was in precarious conditions and a temporary bridge made of wood was built. One year later, on 27 April 1753, the senate approved the edification of a new bridge.

Nowadays the construction presents static problems and it has been reinforced with external steel clamps.

Fig. 8.44: "Foscarini" bridge.

8.2.2 Geometric Survey

The geometrical survey was performed utilizing laser scanning as explained in Section 7.1.

Seven scans (POD files) were elaborated and the number of cloud points is 190086100.

Fig. 8.45: “Foscarini bridge” Points cloud.

Fig. 8.46: Orthophotos obtained by point cloud.

Orthophotos realized from points cloud have been imported into AutoCad and all information about geometrical dimension was obtained. In this way the span of “Foscarini” bridge is 11.68 m and the thickness in correspondence of the keystone and the crown is 0.54 m. The rise measure is 2.23 m.

8.2.3 Experimental measurements

As described in section 7.2, the experimental measurements done on this bridge took into account as a reference the results obtained from “De L’Arzere bridge” measurements

campaign. Data acquisition was performed on 21 May 2017 and was conducted with two different locations for the instruments.

Fig. 8.47: Instrument location.

8.2.4 Results analysis

Results of May 21th, 2017experimental measurement campaign are shown in the following figures (see Fig. 8.48-Fig. 8.50):

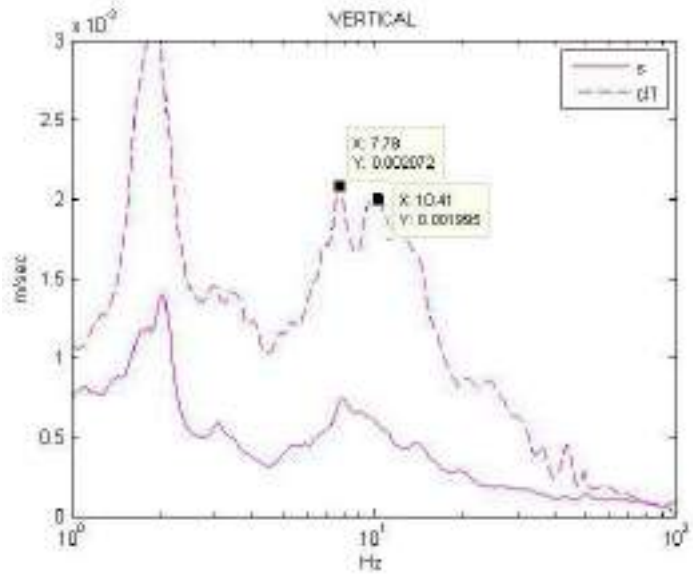

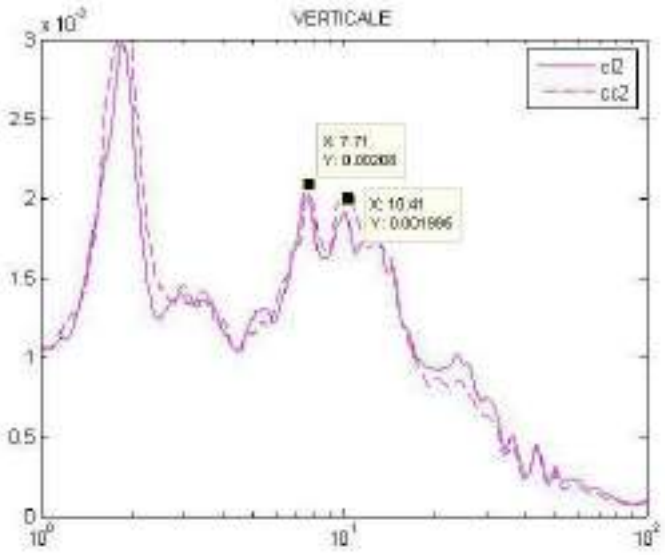

Fig. 8.48: Frequencies of Vertical-y direction.

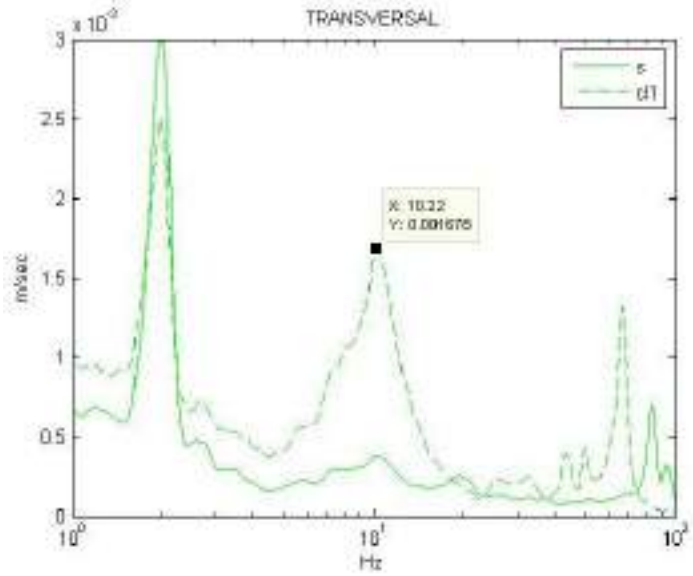

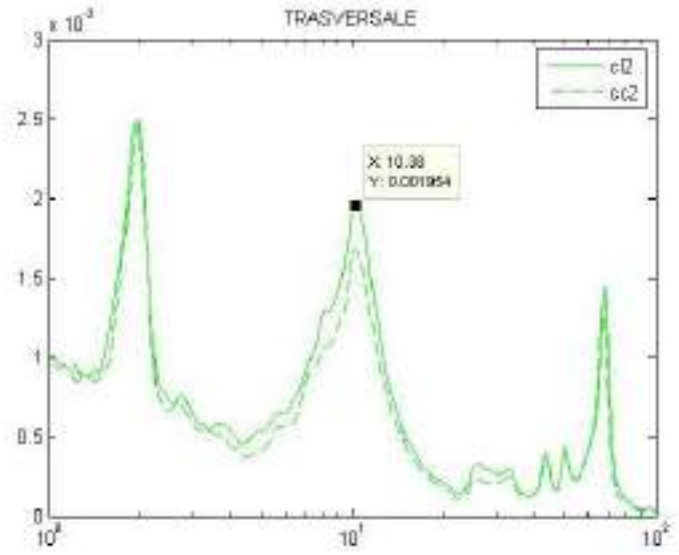

Fig. 8.49: Frequencies of Transversal-z direction.

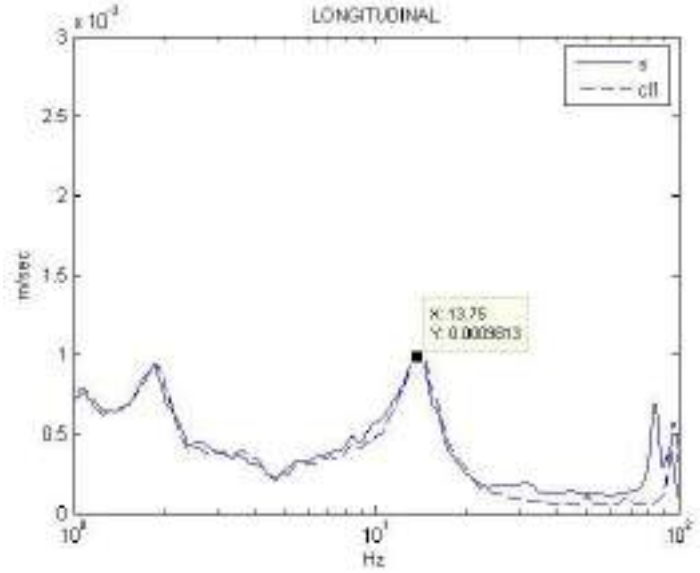

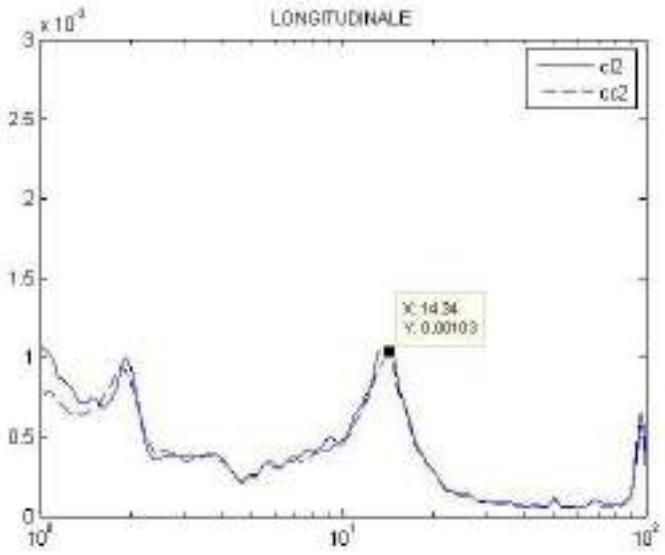

Fig. 8.50: Frequencies of Longitudinal-x direction.

Frequency	Mode shape direction
7.7 Hz	Vertical motion
10.3 Hz	Transversal motion
14 Hz	Longitudinal motion

Tab. 8.12: Experimental measurements frequency values and Mass participation direction.

The results obtained show the following frequencies:

- 7.7 Hz: First peak in the vertical-y direction
- 10.3 Hz: Second peak in the transversal-z direction
- 14 Hz: Third peak in the longitudinal-x direction

The measurements excluded a 2 Hz peak value, which was assigned to human walk noise.

8.2.5 2-D and 3-D F.E. Models description

The transversal cross-section of the bridge presents constant mechanical properties. The 2-D discretization for F.E. models consists of 672 3-node elements under plane strain assumption.

The 2-D reference system is characterized by x and y-axes, namely:

- x axis: Horizontal direction on the plane and longitudinal motion of participating mass.
- y axis: Vertical direction on the plane and vertical motion of participating mass

The materials that constituent the bridge are considered to be: masonry, fill and the pavement. The mechanical characteristics that are density (***γ***), Poisson's ratio (***v***) and Young's modulus (***E***) of adopted material are reported in Tab. 8.13.

Materials	**Model properties**		
	E (MPa)	***v***	***γ*** (Kg/m3)
Masonry	2300	0.2	2200
Fill	1000	0.2	1700
Pavement	2500	0.2	2200

Tab. 8.13: Assumed material properties for 2-D F.E. models.

2-D Model 1:

The node constraints applied to Model 1 are mentioned in Chapter 7 and are shown in Fig. 8.51.

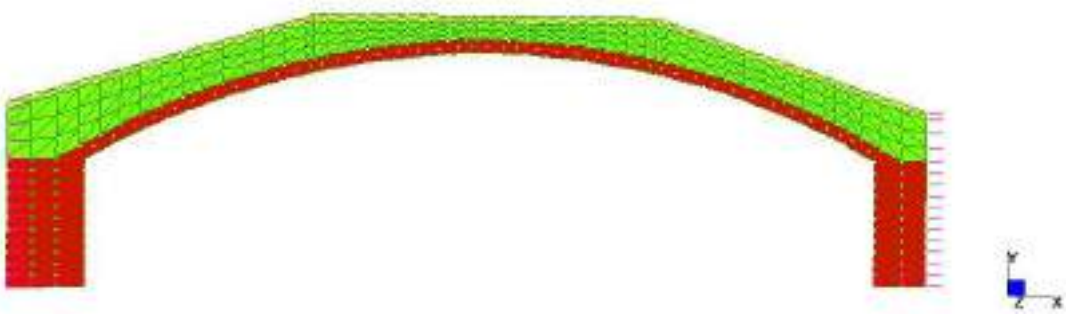

Fig. 8.51: 2-D Model of 1 "Foscarini" bridge.

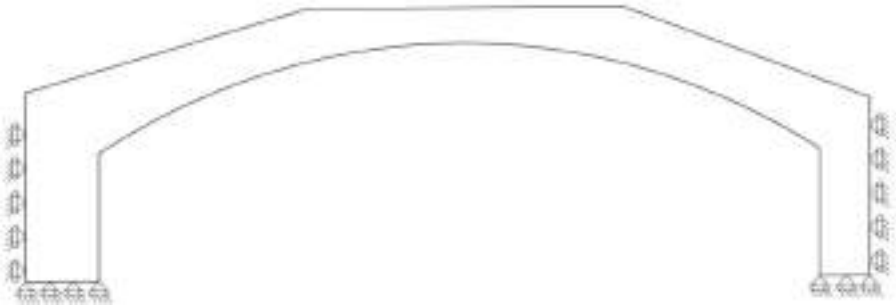

Fig. 8.52: 2- D Model 1 Diagram showing boundary conditions.

2-D Model 2:

The node constraints applied to Model 1 are mentioned in Chapter 7 and are shown in Fig. 8.53.

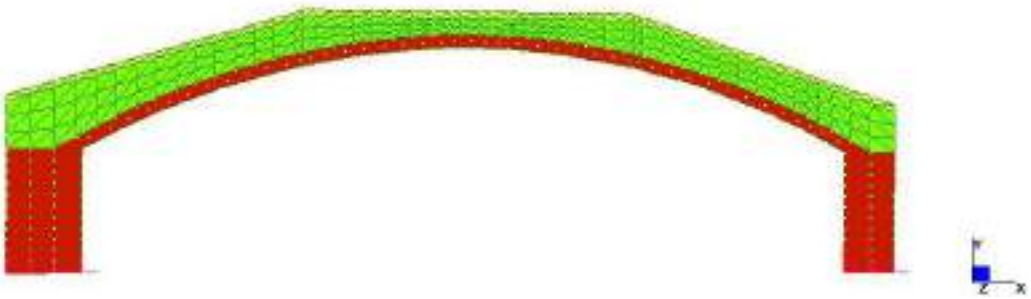

Fig. 8.53: 2-D Model of 2 “Foscarini” bridge.

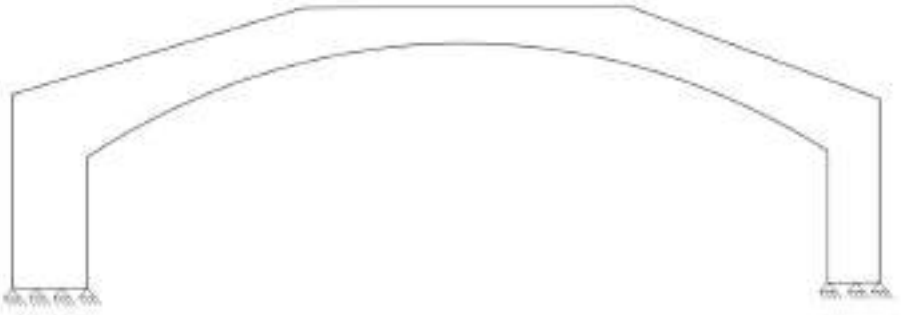

Fig. 8.54: 2- D Model 2 Diagram showing boundary conditions.

2-D Model 3:

The node constraints applied to Model 1 are mentioned in Chapter 7 and are shown in Fig. 8.55. The springs have a high stiffness value of $1 \cdot 10^7$ N/m in the horizontal direction.

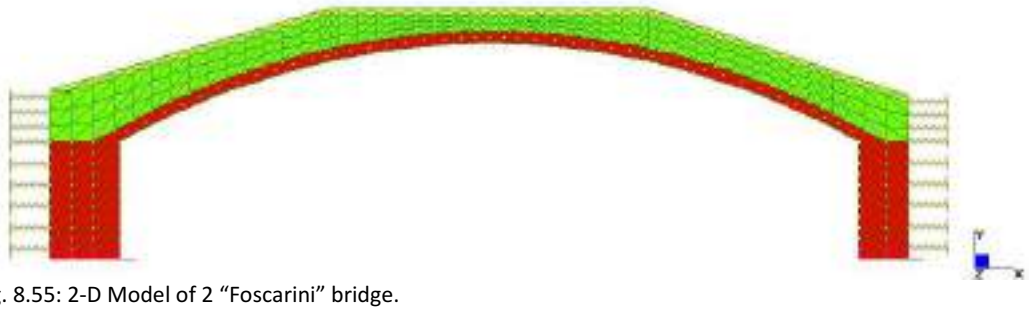

Fig. 8.55: 2-D Model of 2 “Foscarini” bridge.

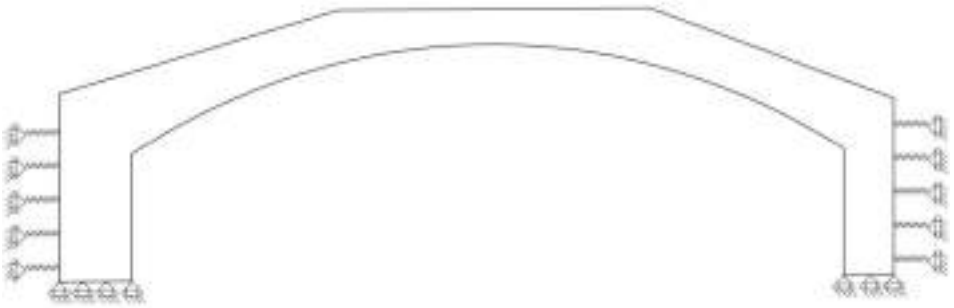

Fig. 8.56: 2- D Model 3 Diagram showing boundary conditions.

3-D Model:

3-D for F.E. model is proposed and has been realized with 2680 8-nodes elements and 20 6-nodes elements. In the foundation the springs stiffness value is $1 \cdot 10^{10}$N/m and the springs are positioned in vertical, horizontal and transversal direction. In correspondence of the abutments the springs stiffness value is $1 \cdot 10^{7}$N/m in horizontal and $1 \cdot 10^{10}$N/m transversal direction.

The 3-D reference system is characterized by the x, y, and z axes which represent:

- x axis: Horizontal direction on 3-D reference system and longitudinal motion of participating mass.
- y axis: Vertical direction on 3-D reference system and vertical motion of participating mass.
- z axis: Out of plane direction and transversal motion of participating mass.

Istria stone was also considered as a construction material.

Materials	**Model properties**		
	E (MPa)	***v***	***γ*** (Kg/m^3)
Masonry	2300	0.2	2200
Fill	1000	0.2	1700
Pavement	2500	0.2	2200
Istria stone	10000	0.2	1800

Tab. 8.14: Assumed material Properties of 3-D models.

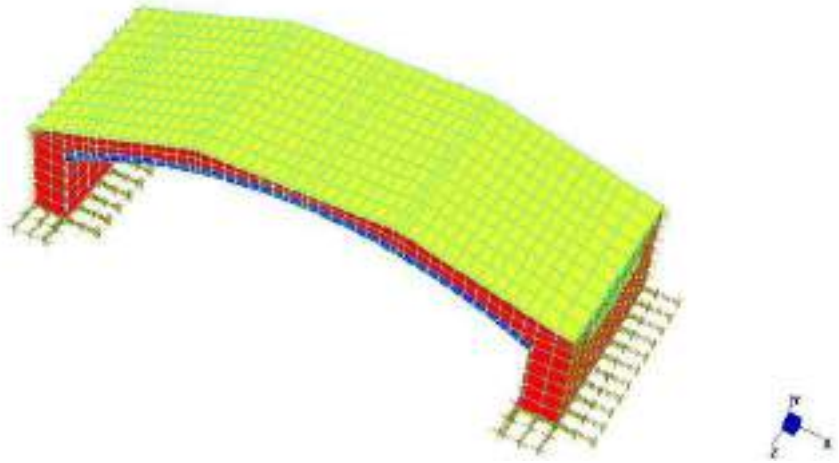

Fig. 8.57: 3-D Model “Foscarini” bridge

8.2.5.1 Analytical analysis

Also in this study case, the 2-D numerical model was validated against an analytical solution as already explained in 7.4 by making use of Eq.(7.1), calculating the value obtained by the two different methods for the maximum displacement of the middle cross-section.

$$AD_y = \frac{pl^2}{8EF} \cdot \frac{2 + \frac{25}{128} \cdot \frac{l^2}{f^2}}{1 + \frac{15}{8} \cdot \frac{i^2}{f^2}}$$

$$AD_y = 0.0036\text{m}$$

AD_y =Analytical displacement in the middle section in vertical direction

E= 3000 MPa

F= 0.23 m^2

f=1.82 m

p =150091 kN/m^2

l = 11.67 m

i =0.066 m^2

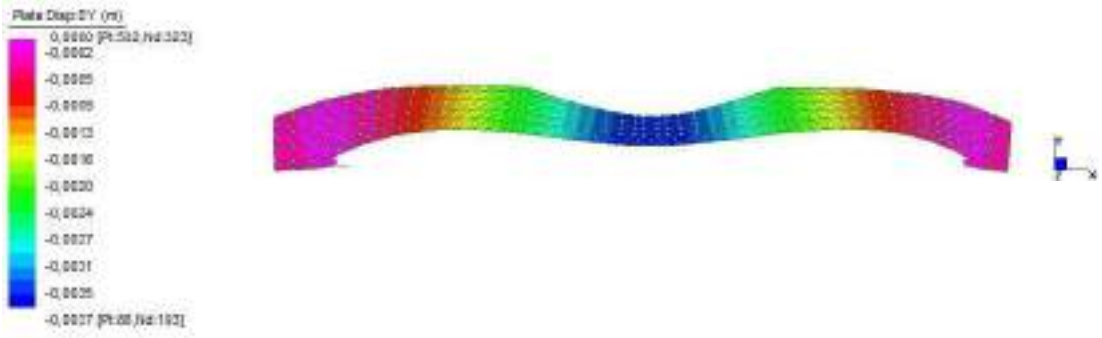

Fig. 8.58: Static Analysis. 2-D Model realized with hinges in correspondence of the foundations.

$$MDispl_y = 0.0037m$$

The percentage error ($\Delta dN_M/A_{\mathrm{M}}$) derived from the comparison between the values obtained has been calculated according to Eq. (7.2)

$$\frac{\Delta dN_M}{\mathrm{A_M}} = \frac{0.0037 - 0.0036}{0.0036} \cdot 100 = 2\%$$

8.2.5.2 Static analysis

In the case of Model 1 the maximum displacement in the middle cross-section is 0,0032 m.

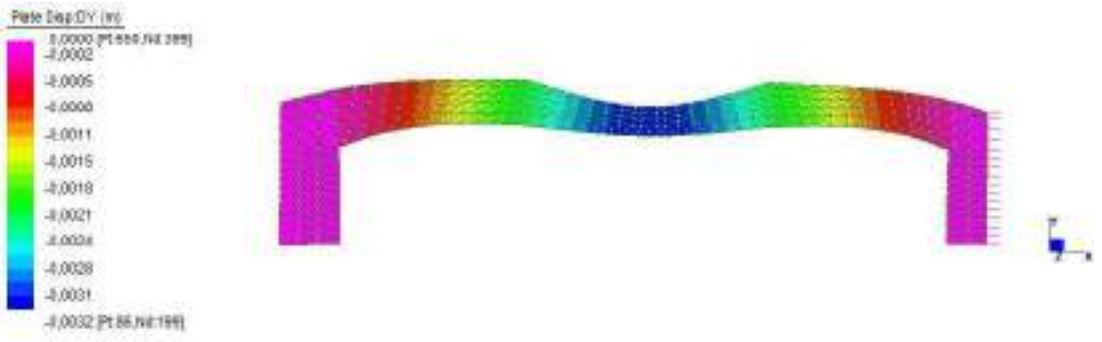

Fig. 8.59: Model 1 static analysis of “Foscarini” bridge.

In the case of Model 2 the maximum displacement in the middle cross-section is 0,0046 m.

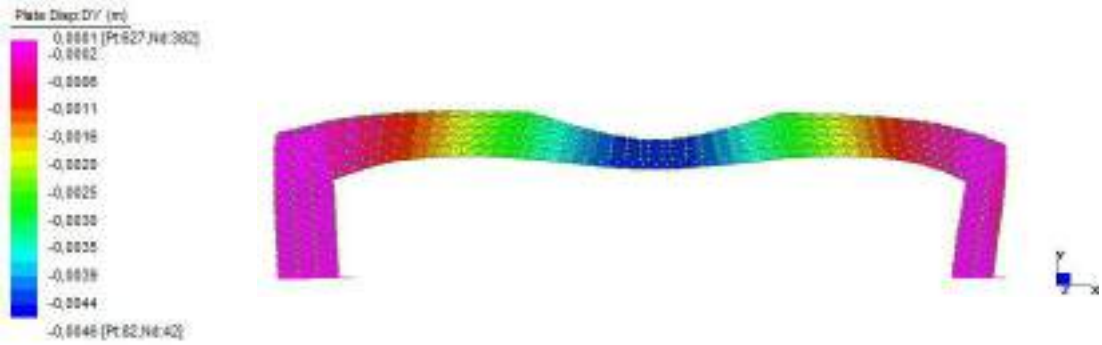

Fig. 8.60: Model 2 static analysis of “Foscarini” bridge

In the case of Model 3 the maximum displacement in the middle cross-section is 0,0044 m.

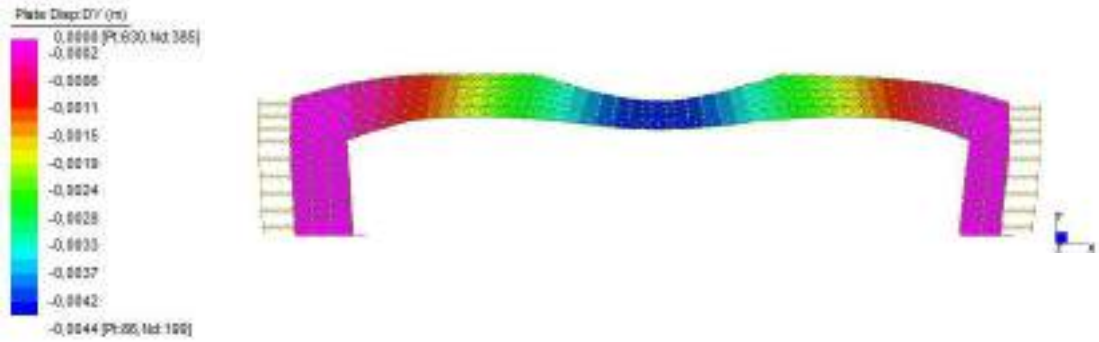

Fig. 8.61: Model 3 static analysis of “Foscarini” bridge

The percentage displacement difference between Model 1 and Model 2 (Δdiff M_2/M_1) and between Model 1 and Model 3 (Δdiff M_3/M_1) have been evaluated, according to Eq. (7.3) and Eq. (7.4).

$$\Delta diff M_2/\mathrm{M}_1 = \frac{0{,}0046\mathrm{m} - 0{,}0032\ \mathrm{m}}{0{,}0032\ \mathrm{m}} \cdot 100 = 34\%$$

$$\Delta diff M_3/\mathrm{M}_1 = \frac{0{,}0044 - 0{,}0032\ \mathrm{m}}{0{,}0032\ \mathrm{m}} \cdot 100 = 37\%$$

The constraints adopted in Model 3 produce a solution which is similar to that provided by Model 1.

8.2.5.3 2-D Modal analysis

Modal analysis, as explained in 7 was carried out.

Model 1:

Mode	Frequency	Modal mass	MP-X	MP-Y	MP-Z
	Hz	Kg	%	%	%
1	1.101E+01	5.103E+03	0.006	40.170	0.000
2	1.431E+01	9.767E+03	9.837	0.015	0.000
3	2.664E+01	8.209E+03	0.024	14.173	0.000
4	3.850E+01	9.435E+03	46.723	0.110	0.000
Total Mass Participation			56.591	54.468	0.000

Tab. 8.15: Results of natural frequency analysis of 2-D Model 1.

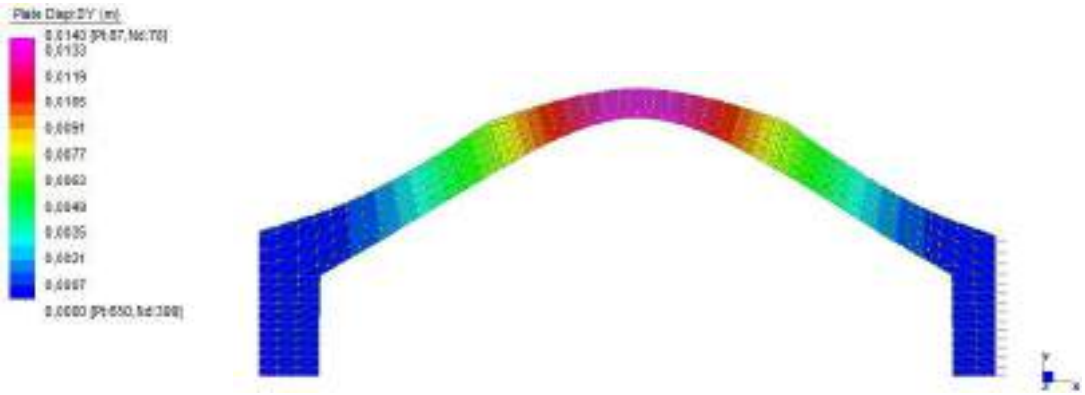

Fig. 8.62: 2-D Model 1 natural frequency analysis: First modal shape.

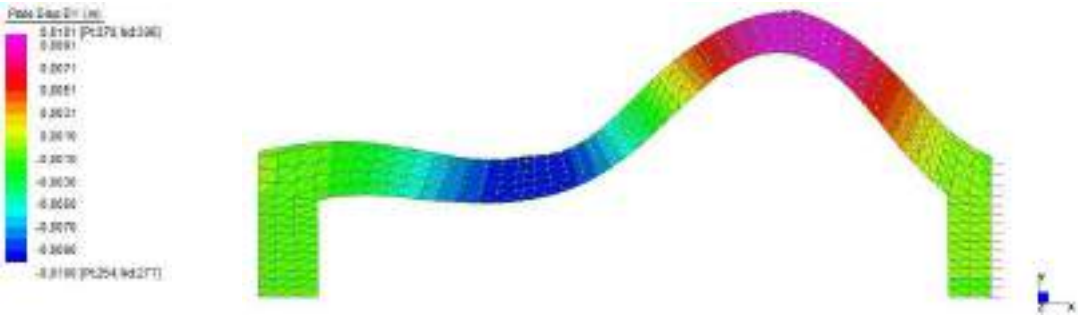

Fig. 8.63: 2-D Model 1 natural frequency analysis: Second modal shape.

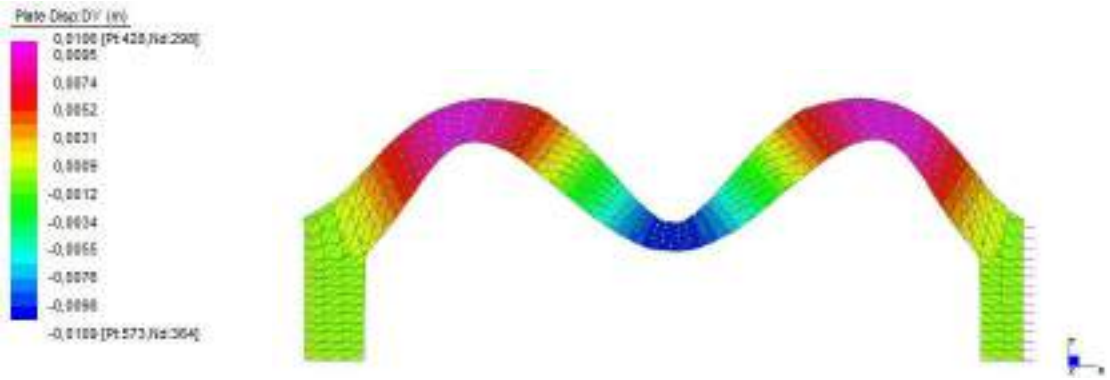

Fig. 8.64: 2-D Model 1 natural frequency analysis: Third modal shape.

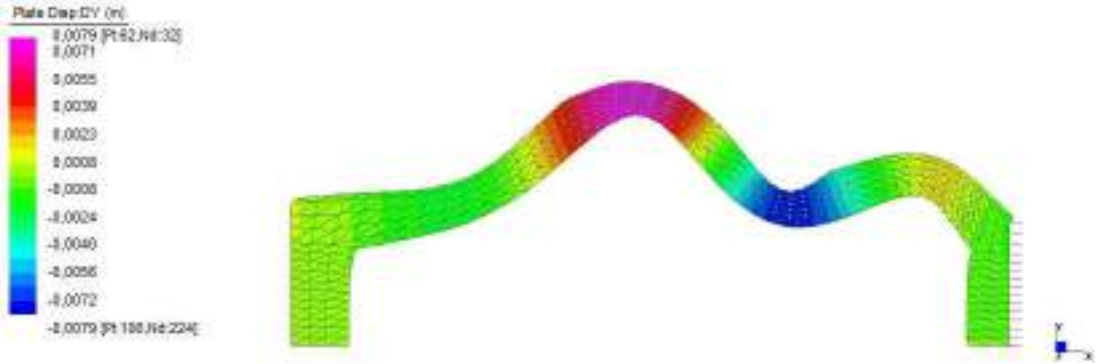

Fig. 8.65: : 2-D Model 1 natural frequency analysis: Fourth modal shape.

Model 2:

Mode	Frequency	Modal mass	MP-X	MP-Y	MP-Z
	Hz	Kg	%	%	%
1	8.097E+00	7.745E+03	24.267	20.408	0.000
2	8.820E+00	7.599E+03	24.495	16.596	0.000
3	1.867E+01	1.109E+04	33.671	0.011	0.000
4	2.222E+01	1.017E+04	0.086	17.507	0.000
Total Mass Participation			82.519	54.522	0.000

Tab. 8.16: Results of Natural frequency analysis of 2-D Model 2

Fig. 8.66: 2-D Model 2 natural frequency analysis: First modal shape.

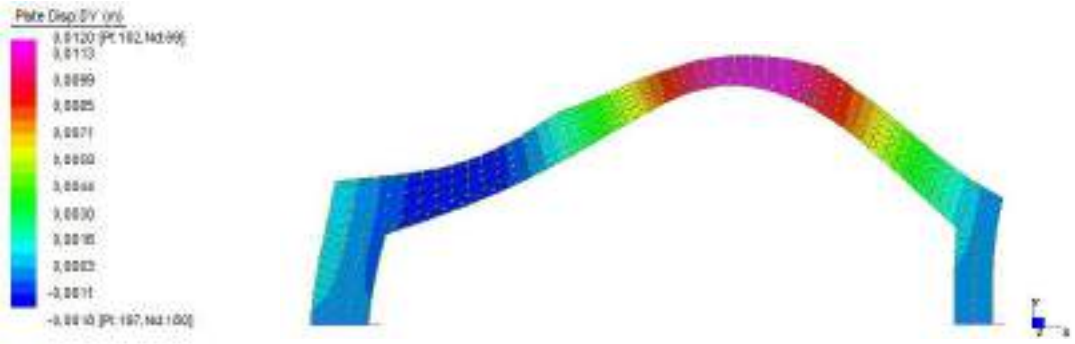

Fig. 8.67: 2-D Model 2 natural frequency analysis: Second modal shape.

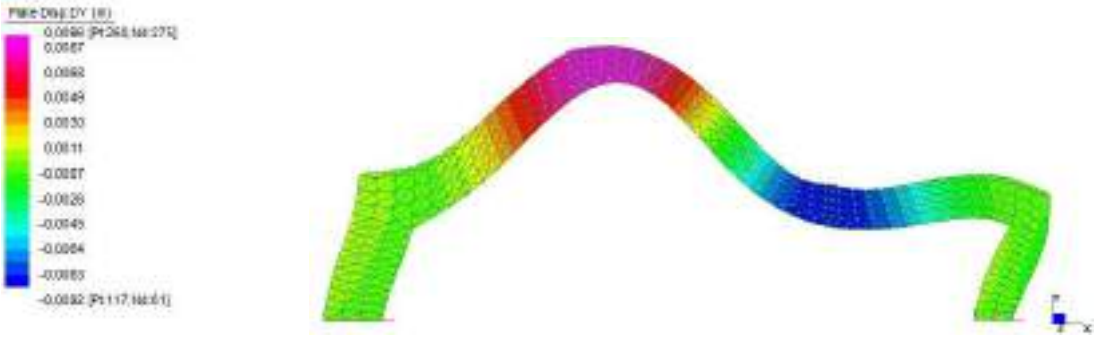

Fig. 8.68: 2-D Model 2 natural frequency analysis: Third modal shape.

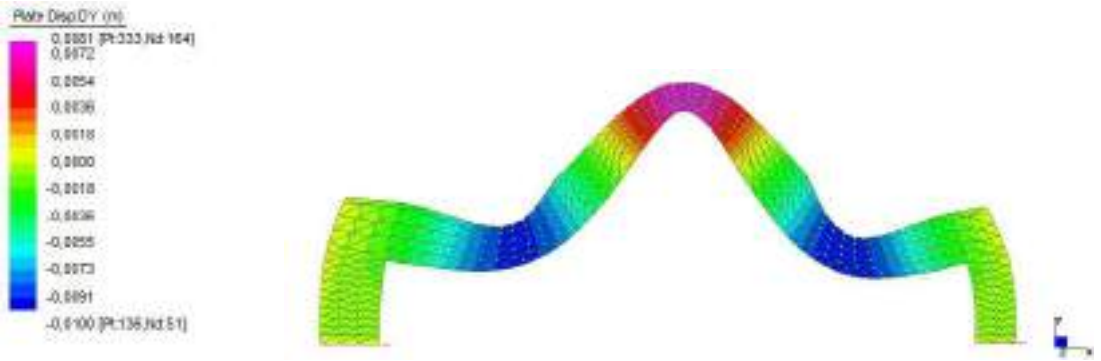

Fig. 8.69: 2-D Model 2 natural frequency analysis: Fourth modal shape.

Model 3:

Mode	Frequency	Modal mass	MP-X	MP-Y	MP-Z
	Hz	Kg	%	%	%
1	9.177E+00	5.320E+03	2.386	36.115	0.000
2	1.010E+01	1.321E+04	38.283	1.504	0.000
3	2.095E+01	1.277E+04	40.888	0.027	0.000
4	2.399E+01	1.053E+04	0.334	17.109	0.000
Total Mass Participation			81.892	54.754	0.000

Tab. 8.17: Results of natural frequency analysis of 2-D Model 3.

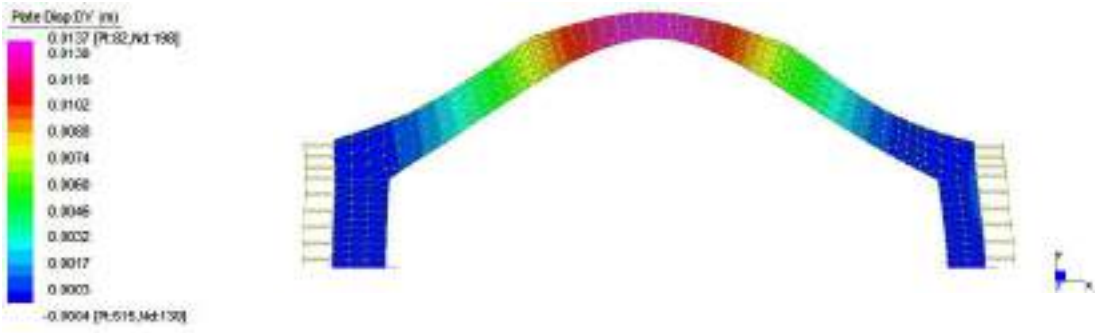

Fig. 8.70: 2-D Model 2 natural frequency analysis: First modal shape.

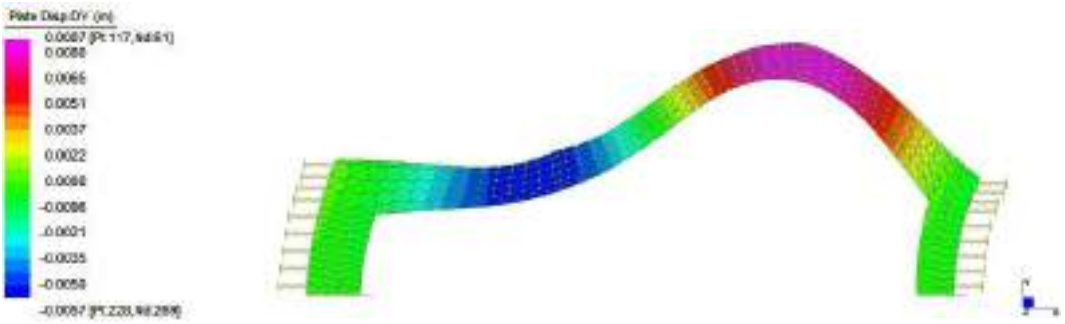

Fig. 8.71: 2-D Model 2 natural frequency analysis: Second modal shape.

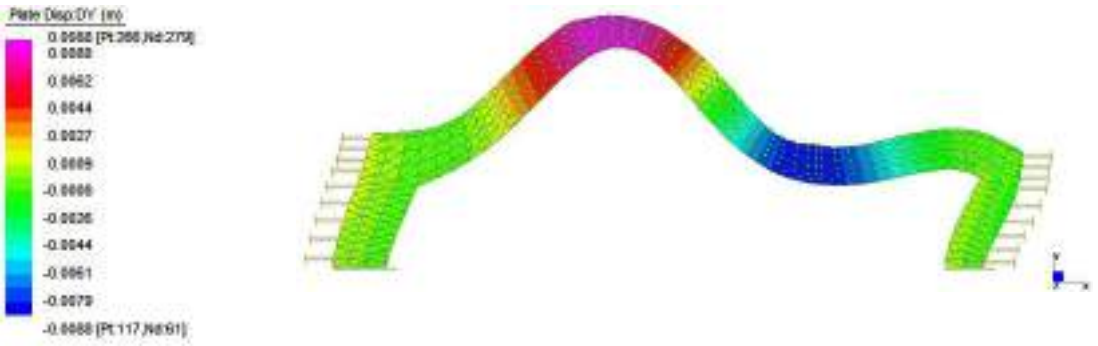

Fig. 8.72: 2-D Model 2 natural frequency analysis: Third modal shape.

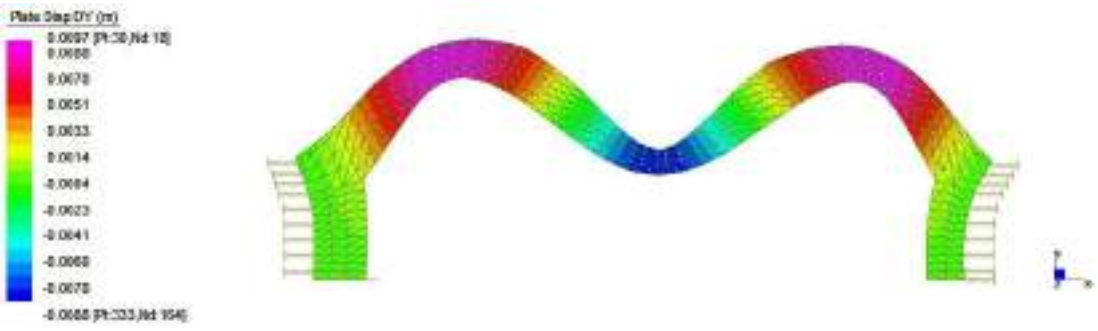

Fig. 8.73: 2-D Model 2 natural frequency analysis: Fourth modal shape.

Considering the results obtained by the natural frequencies analysis of the differently constrained models, it must be noted that the model laterally constrained with springs, Model 3, that is modelled using an intermediary condition produces frequencies for the first and second modes which are comparable with the direction of participating mass given by experimental measurements not considering transversal motion. The 2-D model is on a single plane and for this reason it cannot be calibrated considering out of plane displacement.

The direction of participating mass of the first mode obtained by 2- D natural frequencies analysis is in vertical direction according to the result recorded during experimental measurement campaign. The direction of participating mass of the second mode is longitudinal and is in accordance with third mode experimental measurements. It is useful to make a primary analysis and to identified a range of values that can be considered for 3-D model horizontal springs stiffness, see Tab. 8.17.

8.2.5.4 3-D Modal Analysis

Mode	Frequency	Modal mass	MP-X	MP-Y	MP-Z
	Hz	Kg	%	%	%
1	8.438E+00	2.896E+04	8.091	31.606	0.013
2	1.082E+01	2.142E+04	2.633	0.825	29.894
3	1.241E+01	2.131E+04	11.026	5.657	2.881
4	1.910E+01	1.835E+04	0.219	0.000	20.553
Total Mass Participation			21.969	38.08	53.341

Tab. 8.18: Results of natural frequencies analysis of 3-D Model

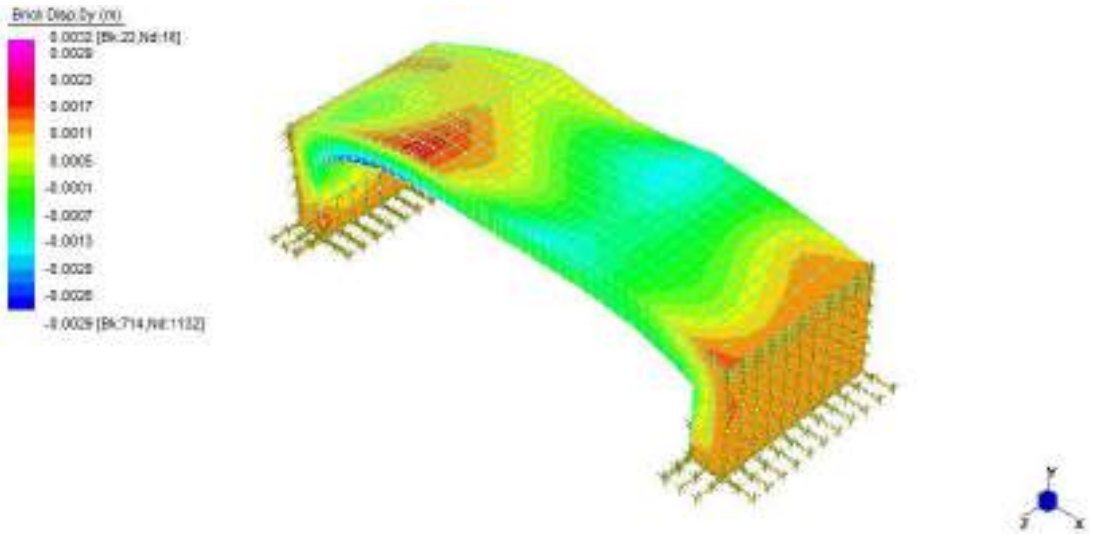

Fig. 8.74: 3-D Model natural frequency s analyses: First modal shape.

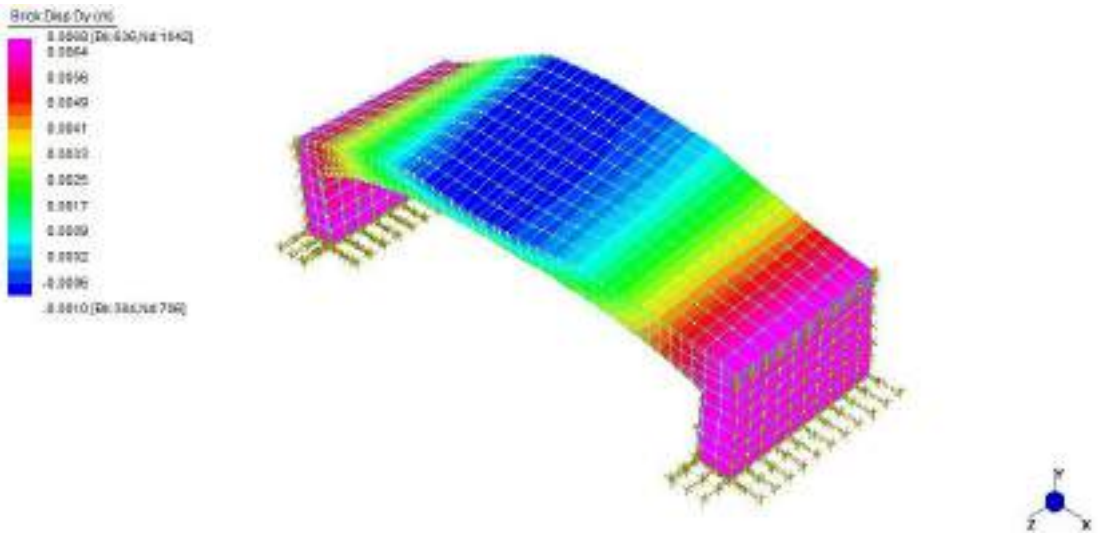

Fig. 8.75: 3-D Model natural frequency analysis: Second modal shape.

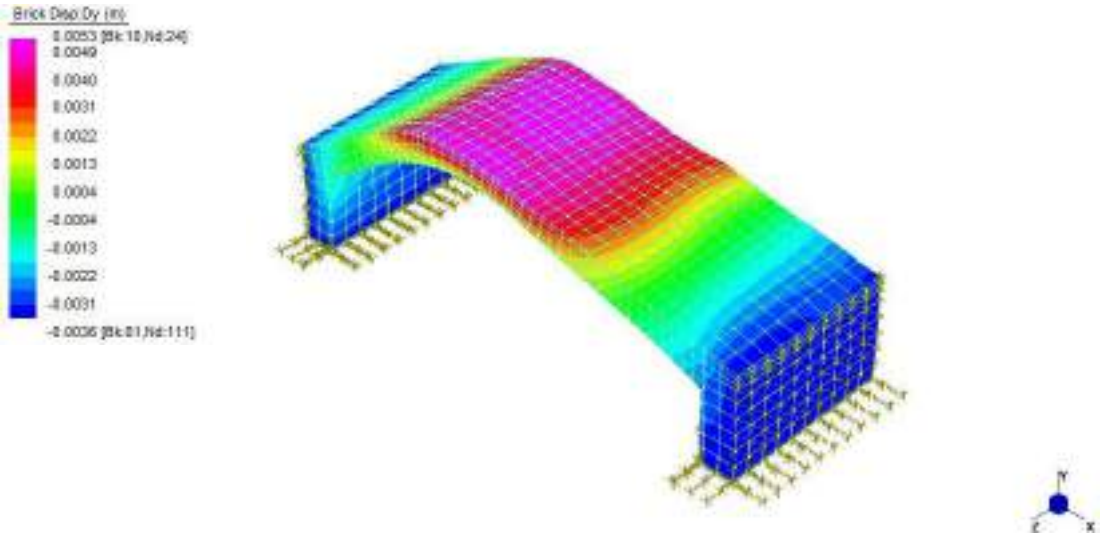

Fig. 8.76: 3-D Model natural frequency analysis:: Third modal shape.

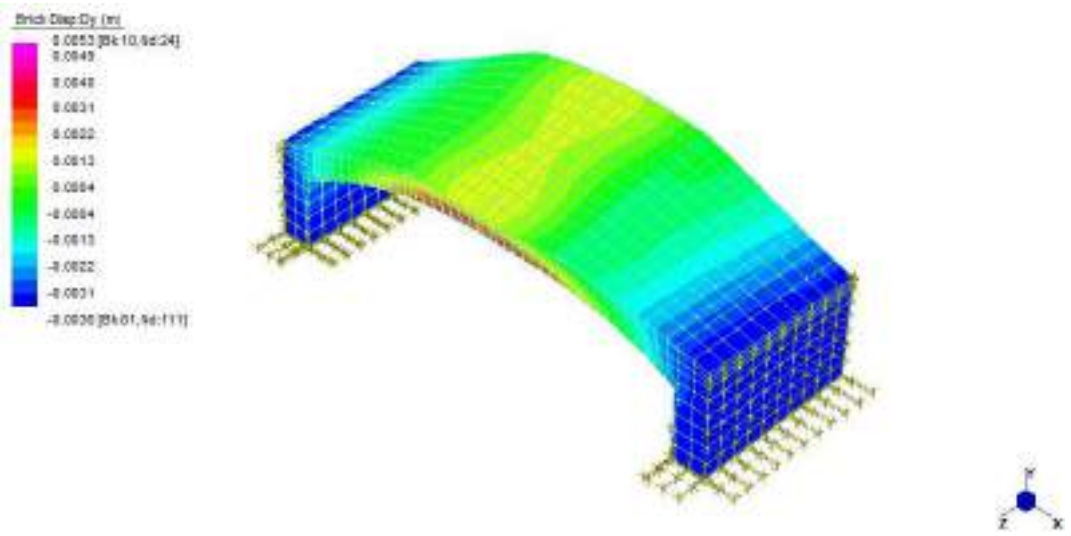

Fig. 8.77: 3-D Model natural frequencies analysis:: Fourth modal shape.

8.2.6 Structural and material identification

As already explained in section 8.2.4, the first peak in the acquired data has a value of 7.7 Hz and corresponds to a vertical motion, the second peak has a value of 10.3 Hz and involves transversal motion. The third peak has a value of 14 Hz and involves longitudinal

motion, as shown in Tab. 8.12. The 2-D Model is all on one plane and for this reason it is not possible to calibrate the model in the transversal direction as well.

Mode	Tromino Data	FEM2-D	Difference	FEM 3-D	Difference
1°value Vertical mode	7.7 Hz	9.2	19.5%	8.4 Hz	9.1%
2°value Trasversal mode	10.3 Hz	-	-	10.9Hz	5.9%
3°value Longitudinal mode	14 Hz	10.1	27%	12.4 Hz	11.4%

Tab. 8.19: Dynamic parameters and difference between Tromino experimental data and 2-D / 3-D models.

As described in section 7.6, the 2-D model has been adopted to identify, in a fast way, a value range for materials characterization and correct definition of constraints. 3-D Model has been calibrated with the same values used for 2-D Model but it has been carried out considering also transversal direction.

In data obtained by 3- D Natural Frequencies analysis, see Tab. 8.19, the first mode has a frequency value of 8.4 Hz and most of the participating mass moving in vertical direction with a difference percentage equal to 9.1%. The values obtained for second and third modal shape, respectively 10.9 Hz in transversal direction and 12.4 Hz in longitudinal direction, are close to the results obtained by the Tromino measurement campaign, see Tab. 8.12, and have a difference percentage equal to 5.9% and 11.4%, see Tab. 8.19.

8.3 S. Lorenzo bridge

“S. Lorenzo” bridge is located in “Sestrier di Castello” in front of S. Lorenzo church and it crosses the canal of “S. Lorenzo”. It is made of masonry and Istria stone, also the parapets have been realized with the same stone.

Fig. 8.78: “S. Lorenzo” bridge

8.3.1 History and description

This bridge has been represented on the famous painting by Gentile Bellini and on the iconographic Venice map drawn by Jacopo De Barberi. In 1500 it showed a three shrewd arches shape with parapets made of Istria stone.

Fig. 8.79: “Miracolo della croce” by Jacopo De Barberi.

During the course of history, this bridge was reconstructed as declared in a decree dated 1752.

8.3.2 Geometrical survey

The geometrical survey was performed using laser scanning as explained in Section 7.1.

Seven scans (POD files) have been obtained and the number of cloud points is 161978093.

Fig. 8.80: “S. Lorenzo bridge”: the point cloud.

Fig. 8.81: Orthophotos obtained by point cloud.

The geometric dimensions of “S. Lorenzo” bridge are: span is 12.72 m, the thickness in correspondence of the keystone and crown is 0.66 m and the rise is 2.34 m.

8.3.3 Experimental measurements

As described in Section 7.2, the experimental measurement campaign took the results from “De L’Arzere” Bridge as reference measurements. Data acquisition was conducted with two different instrument locations.

Fig. 8.82: Instruments location.

Two different campaigns were performed, the former on June 20, 2017 and the latter on November 21, 2017.

8.3.4 Results analysis

The results of the experimental campaign from June 20th, 2017 experimental campaign are shown in the sequel (see Fig. 8.83-Fig. 8.85):

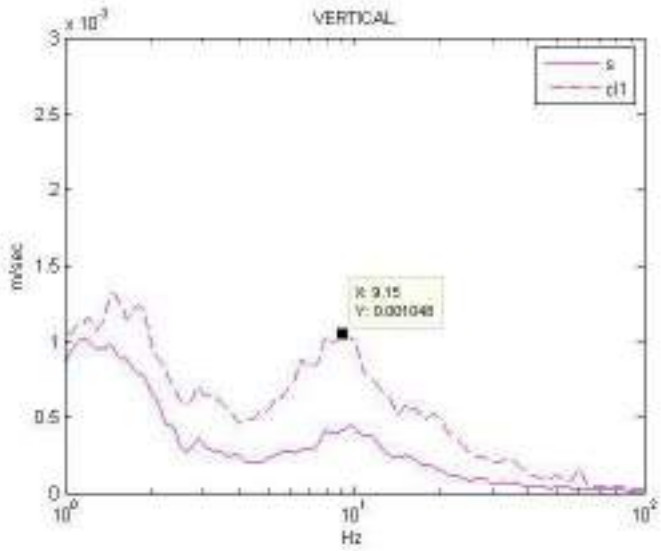

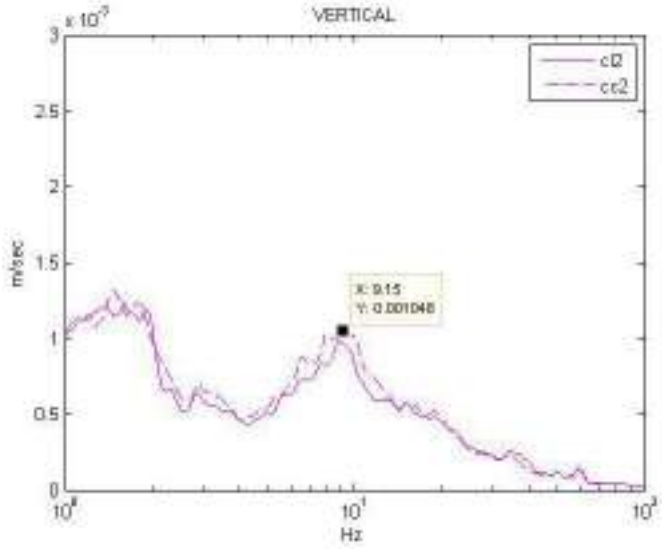

Fig. 8.83: Frequencies of Vertical-y direction.

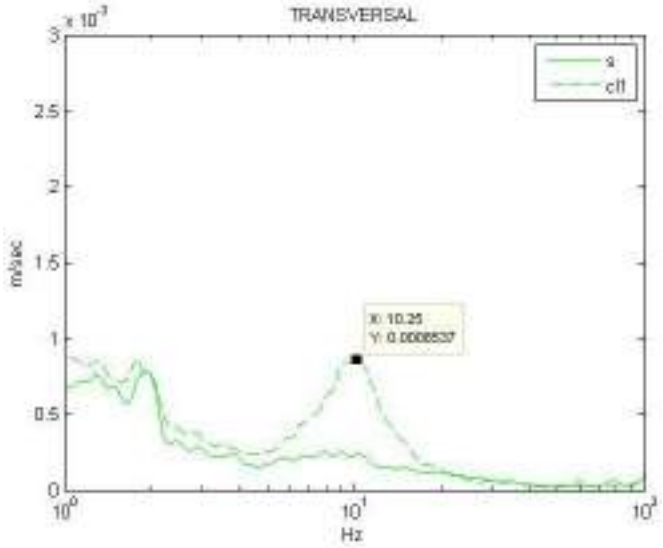

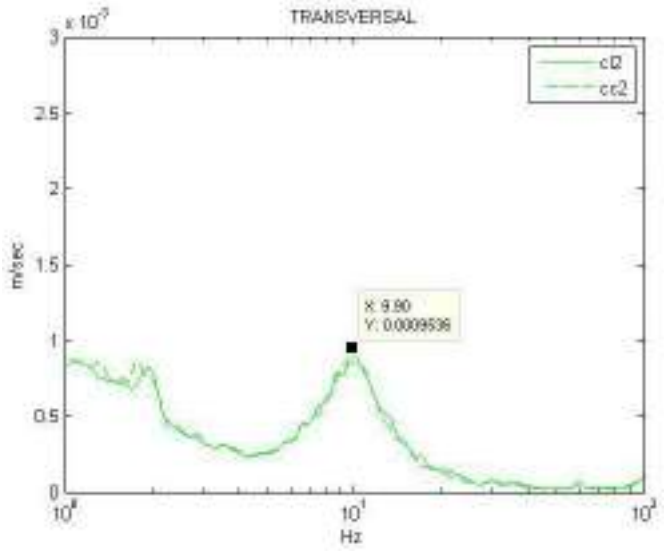

Fig. 8.84: Frequencies of Transversal-z direction.

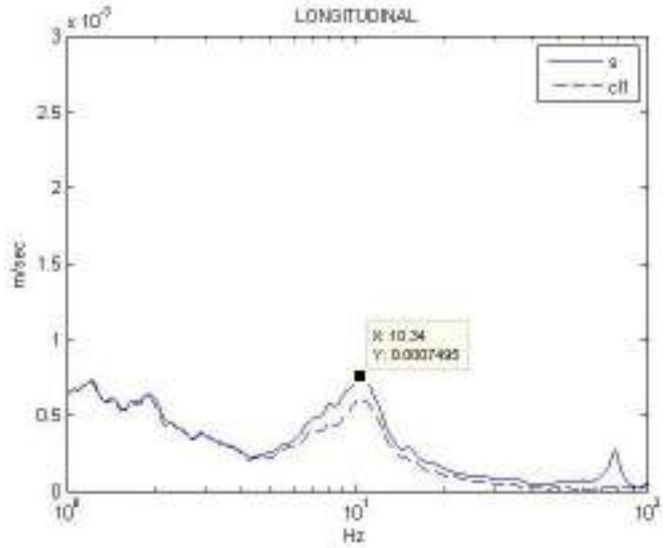

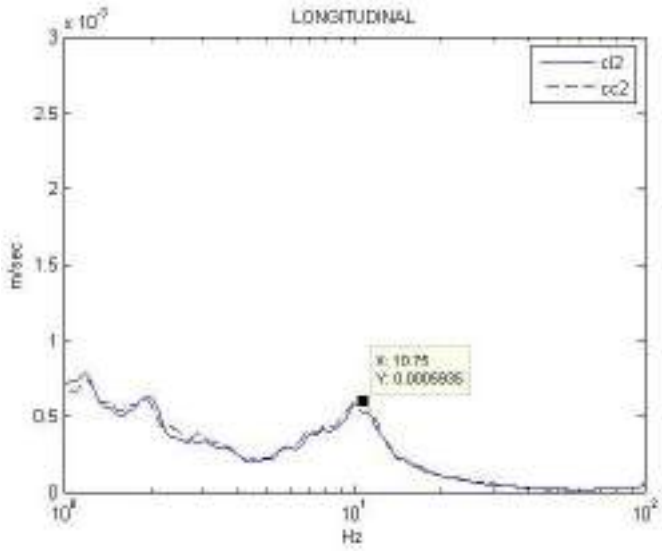

Fig. 8.85: Frequencies of Longitudinal-x direction.

Frequency	Mode shape direction
9.15 Hz	Vertical motion
10.1 Hz	Transversal direction
8.3 Hz	Longitudinal motion

Tab. 8.20. Experimental measurements values and Mass participation direction.

The two different measurement campaigns showed the same frequency results:

- 9.15 Hz: First peak for motion along the vertical-y direction
- 10.1 Hz: Second peak for motion along the transversal-z direction
- 10.5 Hz: Third peak for motion along the longitudinal-x direction

The measurements exclude a 2 Hz peak value, which can be considered due to human walk noise.

8.3.5 2-D and 3-D F.E. Models description

2-D model was constructed with 352 3-node plane elements and are considered under plain strain assumption. The transversal cross-section of the bridge presents constant mechanical characteristics.

The 2-D reference system is characterized by means of the x and y axes, these correspond to:

- x axis: Horizontal direction on the plane and longitudinal motion of participating mass.
- y axis: Vertical direction on the plane and vertical motion of participating mass

The materials constituent bridge are: masonry, fill and the pavement. The mechanical characteristics that are density (***γ***), Poisson's ratio (***ν***) and Young's modulus (***E***) of adopted material are reported in Tab. 8.21.

Materials	**Model properties**		
	E (Mpa)	***ν***	***γ*** (Kg/m^3)
Masonry	2300	0.2	2200
Fill	1000	0.2	1700
Pavement	2500	0.2	1800

Tab. 8.21: Assumed material properties of 2-D F.E. models.

2-D-Model 1:

The node constraints applied to Model 1 are mentioned in Chapter 7 and are shown in Fig. 8.86

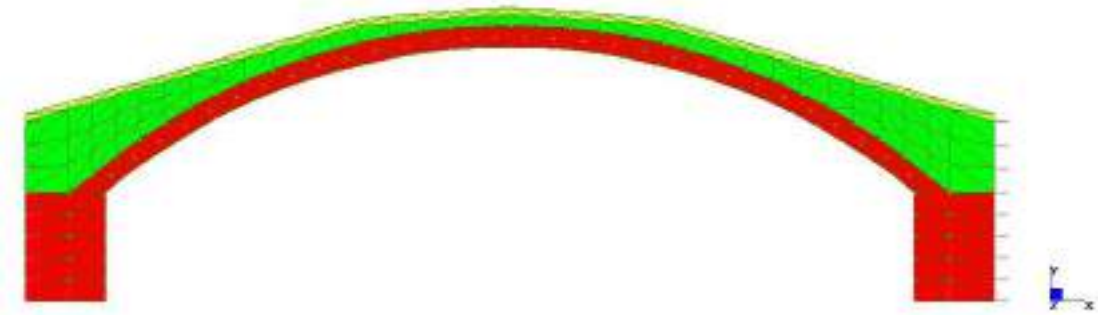

Fig. 8.86: 2-D Model 1 "S. Lorenzo" bridge.

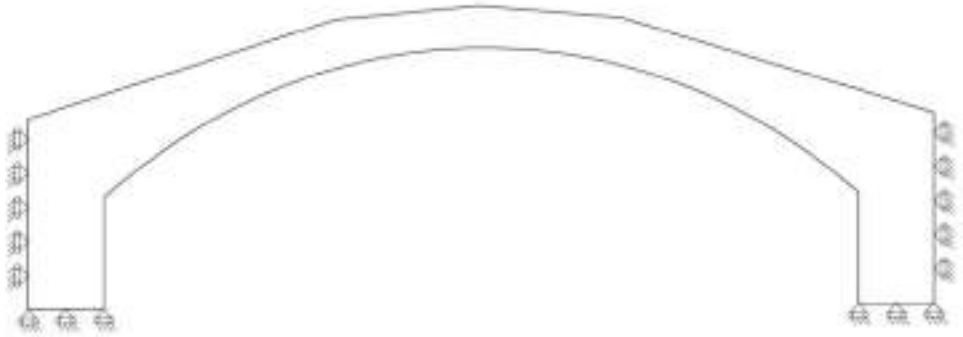

Fig. 8.87: 2- D Model 1 Diagram showing boundary condition.

2-D-Model 2:

The node constraints applied to Model 1 are mentioned in Chapter 7 and are shown in Fig. 8.55

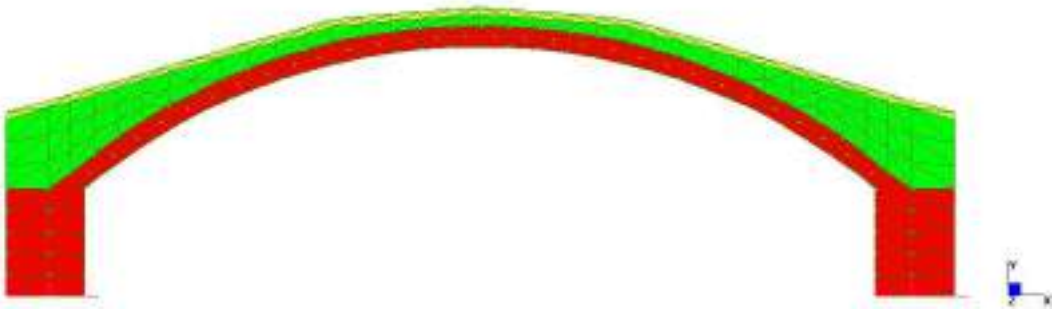

Fig. 8.88: 2-D Model 2 “S. Lorenzo” bridge.

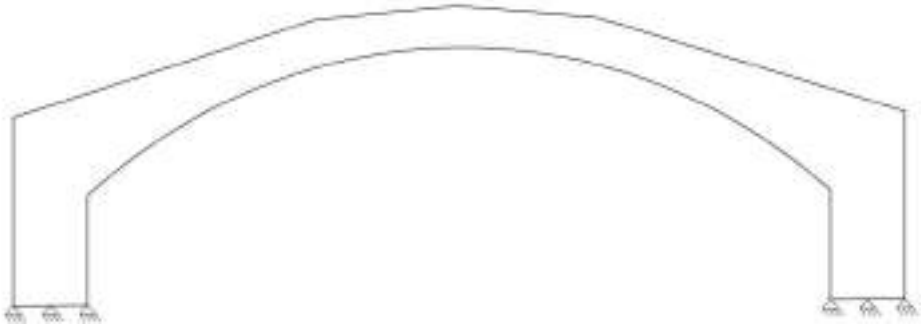

Fig. 8.89: 2- D Model 2 Diagram showing boundary condition.

2-D- Model 3:

The node constraints applied to Model 3 are mentioned in Chapter 7 and are shown in Fig. 8.90. The springs have a high stiffness value of $5.7 \cdot 10^7$ N/m in the horizontal direction.

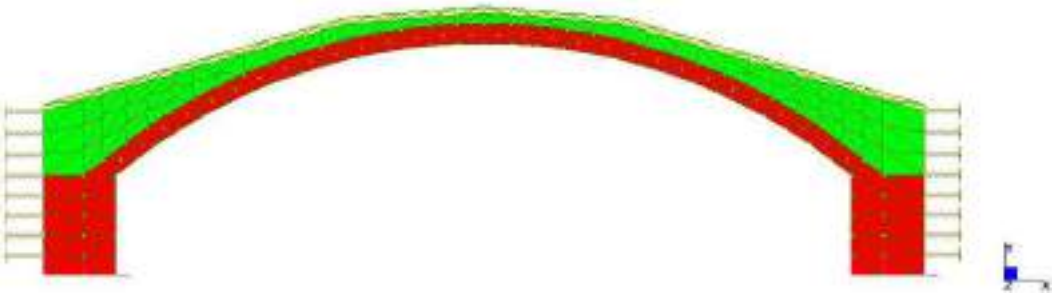

Fig. 8.90: 2-D Model 3 “S. Lorenzo” bridge.

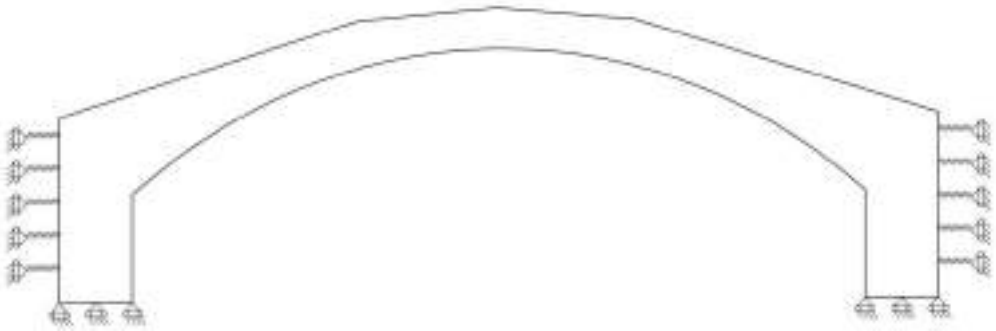

Fig. 8.91: 2- D Model 3 Diagram showing boundary condition.

3-D- Model:

A 3-D for F.E. model was realized with 2680 8-node elements and 20 6-node elements. In the foundation the springs stiffness value is $1 \cdot 10^7$ N/m and are positioned in vertical transversal and horizontal direction. In correspondence of the abutments the spring stiffness value is $5.7 \cdot 10^7$ N/m and are positioned in the longitudinal and the horizontal directions.

The 3-D reference system is characterized by the x, y, and z axes which represent:

- x axis: Horizontal direction on 3-D reference system and longitudinal motion of participating mass.
- y axis: Vertical direction on 3-D reference system and vertical motion of participating mass.
- z axis: Out of plane direction and transversal motion of participating mass.

For the 3-D model, Istria stone was also considered as a material.

Materials	**Model properties**		
	E (Mpa)	***v***	***γ*** (Kg/m^3)
Masonry	2300	0.2	2200
Fill	1000	0.2	1700
Pavement	2500	0.2	1800
Istria Stone	10000	0.2	1800

Tab. 8.22: Mechanical properties of materials for 3-D model.

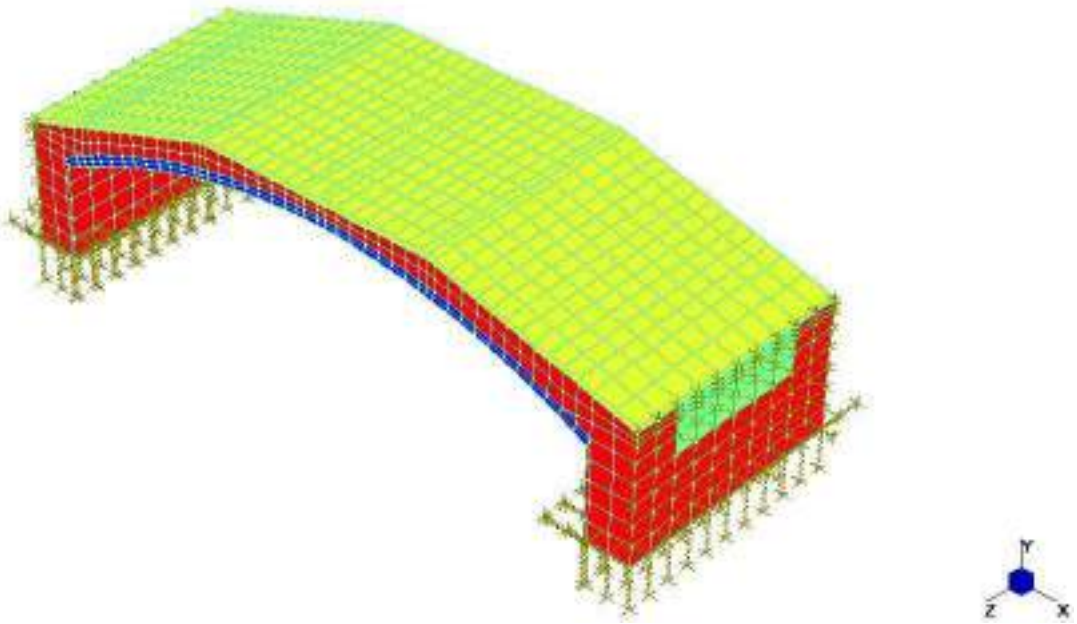

Fig. 8.92: 3-D Model of “S. Lorenzo” bridge

8.3.5.1 Analytical solution

As explain in Section 7.4, the 2-D numerical models have been validated against an analytical solution by making use of Eq (7.1) and calculating the maximum displacement of the middle cross-section.

$$AD_y = \frac{pl^2}{8EF} \cdot \frac{2 + \frac{25}{128} \cdot \frac{l^2}{f^2}}{1 + \frac{15}{8} \cdot \frac{i^2}{f^2}}$$

$$AD_y = 0.0037\text{m}$$

AD_y= Analytical displacement in the middle cross-section in vertical direction

E= 3000 MPa

F= 0.23 m^2

f =1.82 m

p=15.2003 kN/m^2

l = 11.67 m

i=0.066 m^2

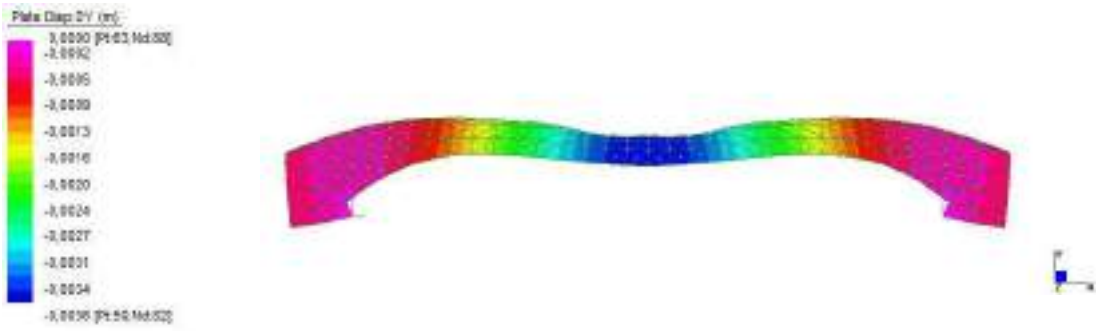

Fig. 8.93: Static Analysis. 2-D Model realized with hinges in correspondence of the foundations.

$$MD_y = 0.0037m$$

MD_y= Model displacement in the middle section in vertical direction

The percentage error ($\Delta dN_M/A_{\mathrm{M}}$) derived from the comparison between the values obtained was calculated utilizing the Eq. (7.2).

$$\frac{\Delta dN_M}{\mathrm{A_M}} = \frac{0.0036 - 0.0037}{0.0037} \cdot 100 = 2\%$$

8.3.5.2 Static analysis

In the case of Model 1 the maximum displacement in the middle section is 0,0027 m.

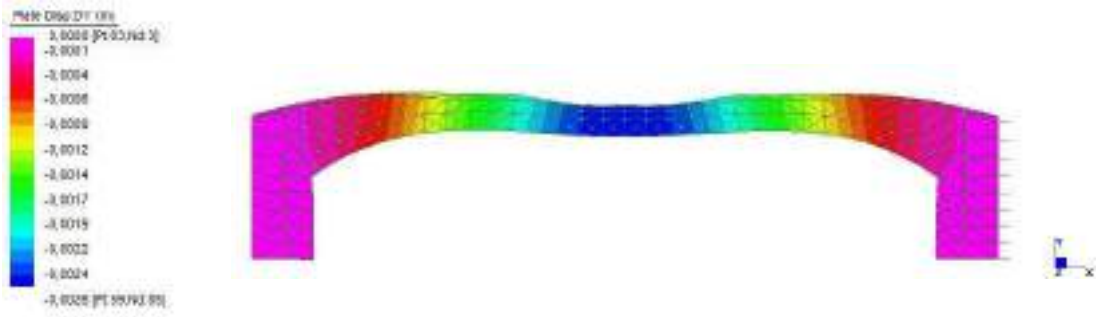

Fig. 8.94: Model 1 static analysis of “S. Lorenzo” bridge.

In the case of Model 2 the maximum displacement in the middle section is 0,0033 m.

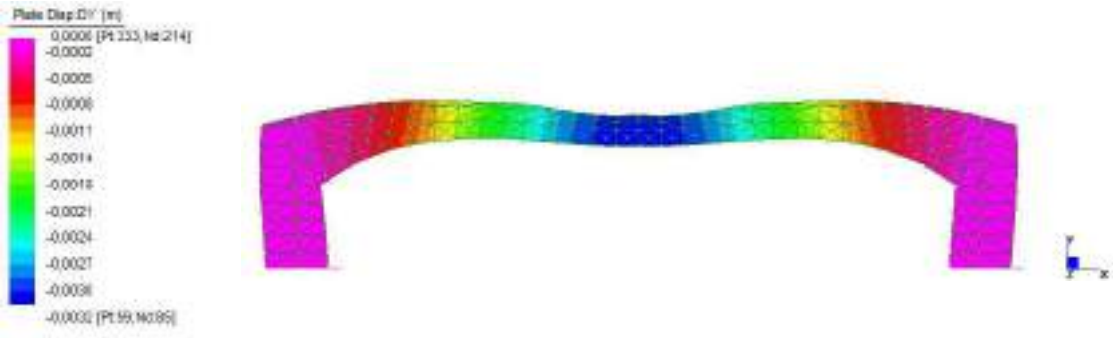

Fig. 8.95: Model 2 static analysis of “S. Lorenzo” bridge.

In the case of Model 3 the maximum displacement in the middle section is 0,0029 m.

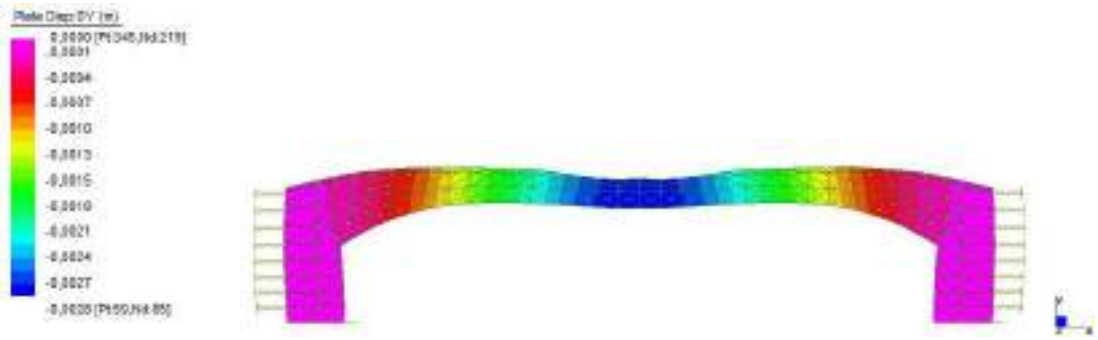

Fig. 8.96: Model 3 static analysis of “S. Lorenzo” bridge.

The percentage displacement difference between Model 1 and Model 2, Eq. (7.3) and between Model 1 and Model 3, see Eq. (7.4) was evaluated, as follows:

$$\Delta diff M_2/\mathrm{M}_1 = \frac{0{,}0033\mathrm{m} - 0{,}0027\mathrm{m}}{0{,}0027\mathrm{m}} \cdot 100 = 22\%$$

$$\Delta diff M_3/\mathrm{M}_1 = \frac{0{,}0029\mathrm{m} - 0{,}0027\mathrm{m}}{0{,}0027\mathrm{m}} \cdot 100 = 7\%$$

The obtained results underline that the constraints adopted in Model 3 provide a solution which is closer to that provided by Model 1.

8.3.5.3 2-D Modal analysis

The Modal analysis explained in Chapter 7, provided the following results:

Model 1:

Mode	Frequency	Modal mass	MP-X	MP-Y	MP-Z
	Hz	Kg	%	%	%
1	1.129E+01	6.786E+03	0.001	34.923	0.000
2	1.293E+01	1.242E+04	11.372	0.000	0.000
3	2.304E+01	1.258E+04	0.001	15.113	0.000
4	3.262E+01	1.383E+04	43.541	0.015	0.000
Total Mass Participation			54.915	50.041	0.000

Tab. 8.23 Results of natural frequency analysis of 2-D Model 1.

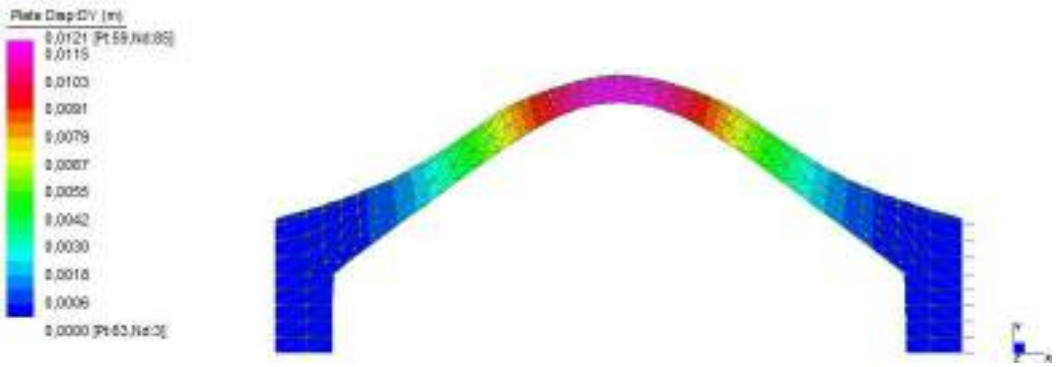

Fig. 8.972: 2-D Model 1 natural frequency analysis: First modal shape.

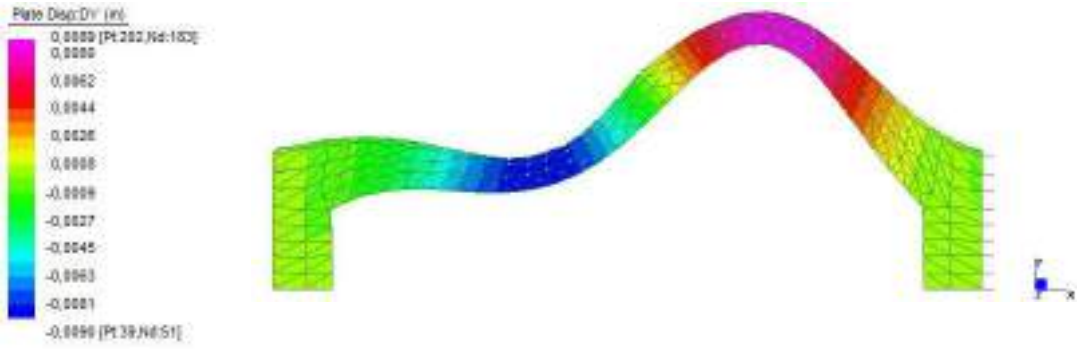

Fig. 8.98: 2-D Model 1 natural frequency analysis: Second modal shape.

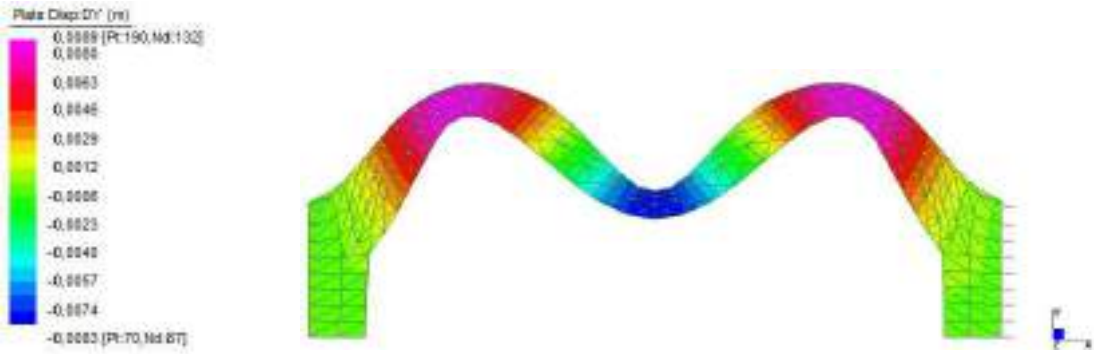

Fig. 8.99:2 -D Model 1 natural frequency analysis: Third modal shape.

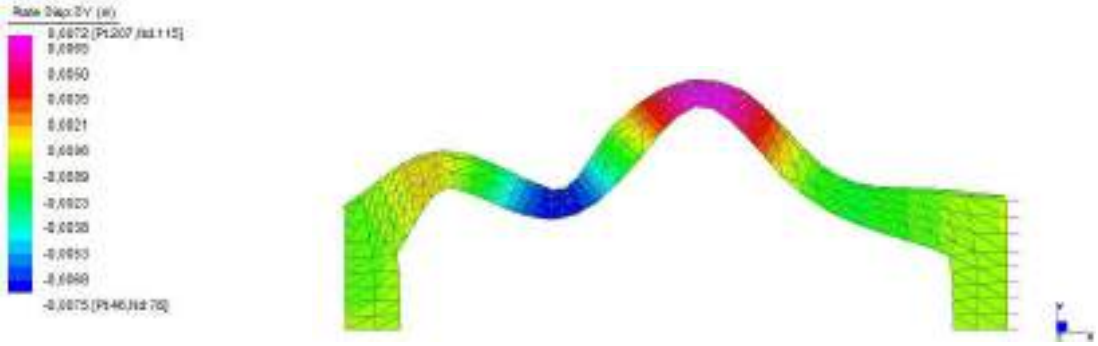

Fig. 8.100: 2-D Model 1 natural frequency analysis: Fourth modal shape.

Model 2:

Mode	Frequency	Modal mass	MP-X	MP-Y	MP-Z
	Hz	Kg	%	%	%
1	8.425E+00	2.665E+04	42.970	0.001	0.000
2	9.801E+00	6.704E+03	0.002	28.674	0.000
3	1.916E+01	1.511E+04	0.022	22.105	0.000
4	1.963E+01	1.391E+04	36.681	0.016	0.000
Total Mass Participation			79.675	50.796	0.000

Tab. 8.24: Results of Natural frequency analysis of 2-D Model 2

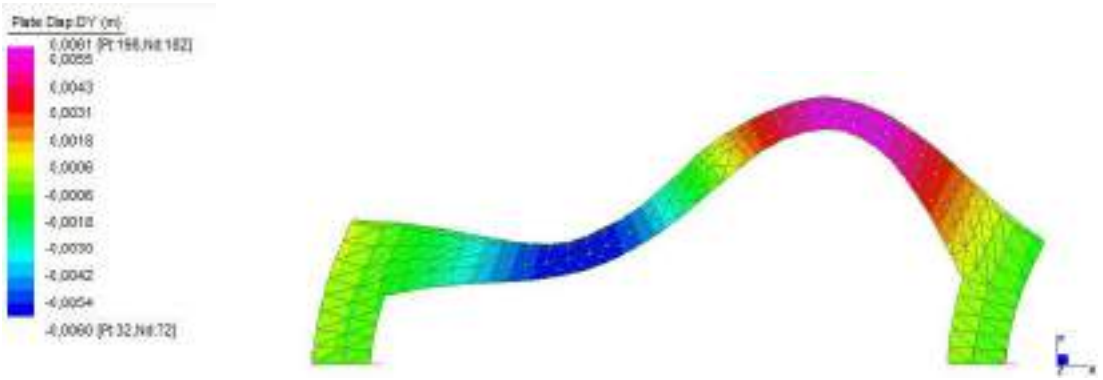

Fig. 8.101: 2-D Model 2 natural frequency analysis: First modal shape.

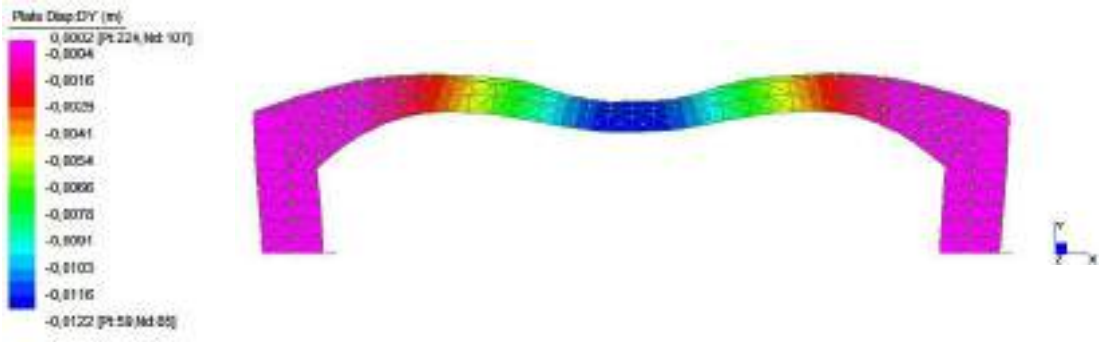

Fig. 8.102: 2-D Model 2 natural frequency analysis: Second modal shape.

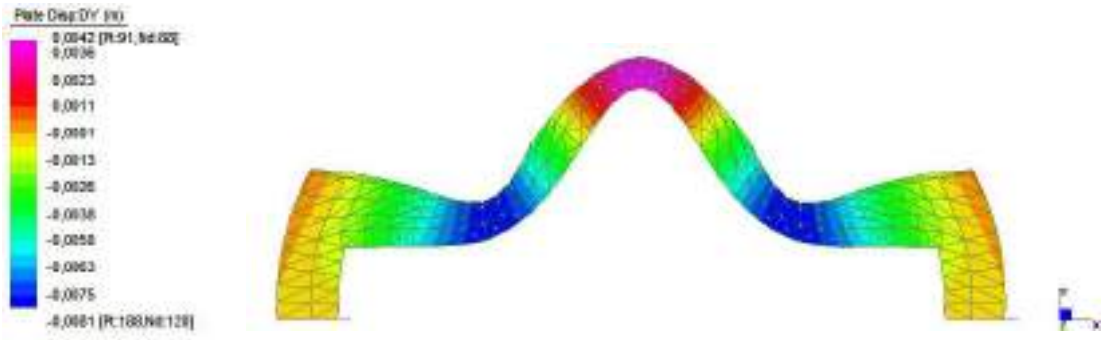

Fig. 8.103: 2-D Model 2 natural frequency analysis: Third modal shape.

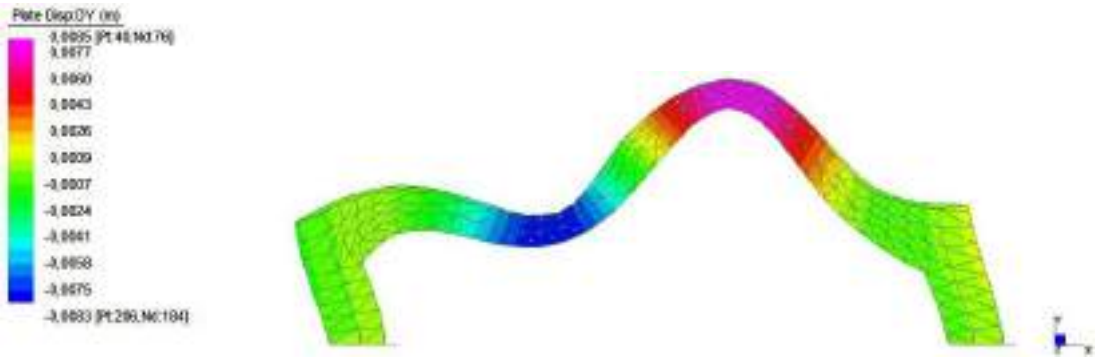

Fig. 8.104: 2-D Model 2 natural frequency analysis: Fourth modal shape.

Model 3:

Mode	Frequency	Modal mass	MP-X	MP-Y	MP-Z
	Hz	Kg	%	%	%
1	1.048E+01	6.702E+03	0.016	31.906	0.000
2	1.051E+01	1.704E+04	25.429	0.019	0.000
3	2.025E+01	1.435E+04	0.026	19.038	0.000
4	2.333E+01	1.687E+04	48.132	0.002	0.000
Total Mass Participation			73.577	50.964	0.000

Tab. 8.25: Results of natural frequency analysis of 2-D Model 3.

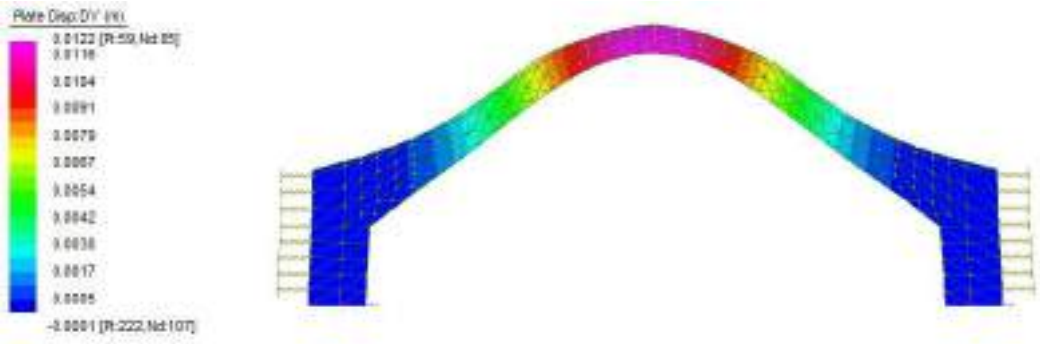

Fig. 8.105: 2-D Model 3 natural frequency analysis: First modal shape.

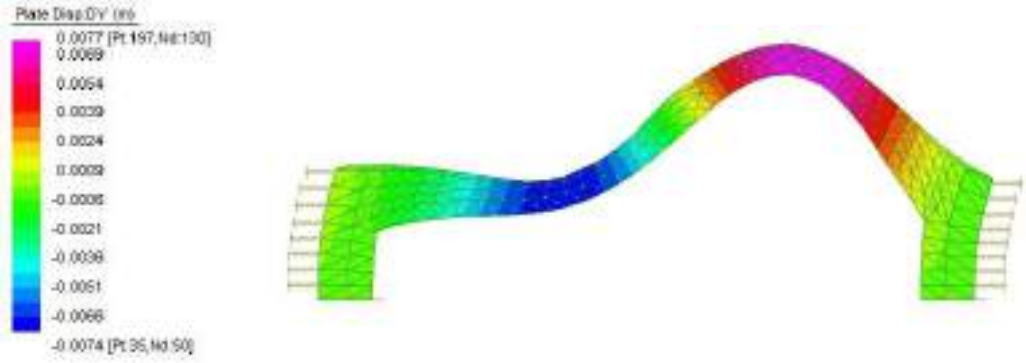

Fig. 8.106: 2-D Model 3 natural frequency analysis: Second modal shape.

: Second modal shape.

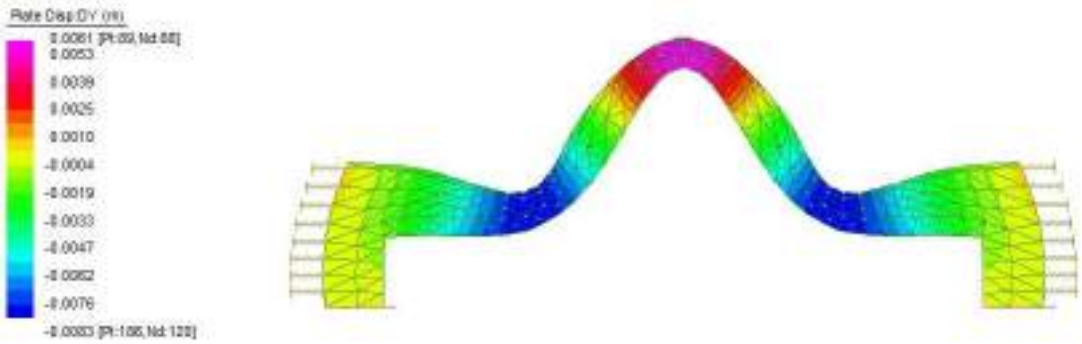

Fig. 8.107: 2-D Model 3 natural frequency analysis: Third modal shape.

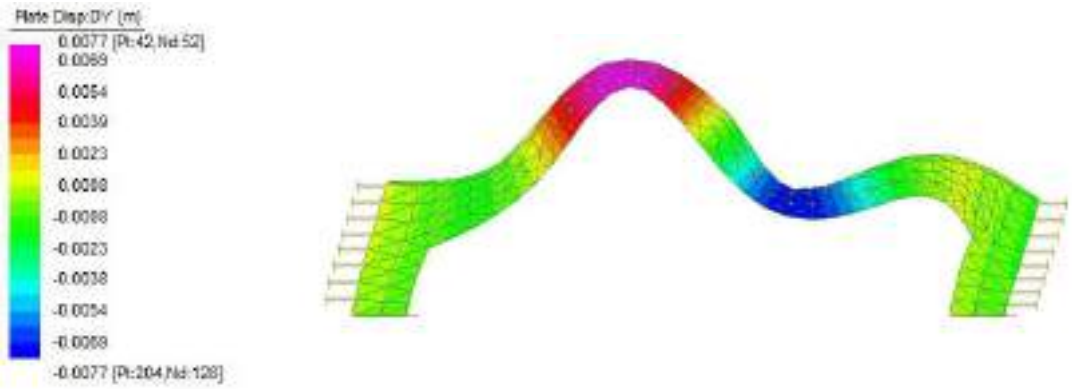

Fig. 8.108: 2-D Model 3 natural frequency analysis: Fourth modal shape.

The results obtained by experimental measurements, as explain in Section 8.3.4., have been shown the first peak at 9.15 Hz for motion along the vertical direction, the second peak at 10.1 Hz characterized by participating mass out of plane and the third peak at 10.5 Hz for motion along the transversal direction, see Tab. 8.20.

The 2-D model is all on one plane and for this reason it cannot be calibrated considering the second frequency value obtained by experimental campaign and characterized out of the plane displacement of most of the participating mass. The participating mass for the first mode obtained by 2- D natural frequency analysis is in the vertical direction and the mass direction is in accordance with First mode experimental data results. The participating mass motion of the second mode is longitudinal and is in accordance with third mode experimental measurements data. The range of values is different because 2- D Models cannot take any out-of-plane motion into consideration. It is nonetheless useful for a first fast analysis in order to obtain a preliminary range of values.

It is not possible to consider the results obtained by 2- D Model 2 because there is no correspondence with the mass movement motion obtained by experimental measurements.

8.3.5.4 3-D Modal Analysis

Mode	Frequency	Modal mass	MP-X	*MP-Y*	MP-Z
	Hz	Kg	%	%	%
1	8.848E+00	3.542E+04	0.001	74.982	0.002
2	1.075E+01	3.268E+04	0.431	0.004	32.115
3	1.114E+01	4.353E+04	4.142	0.002	0.773
4	1.663E+01	5.261E+04	6.709	14.589	0.014
Total Mass Participation			11.283	89.577	32.904

Tab. 8.26: Results of natural frequency analysis of 3-D Model.

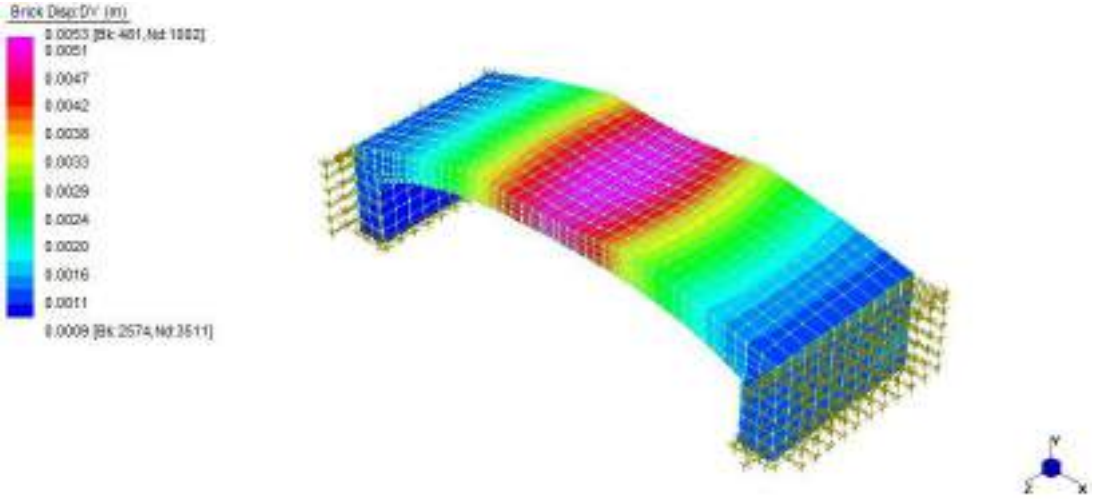

Fig. 8.109: 3-D Model natural frequency analysis: First modal shape.

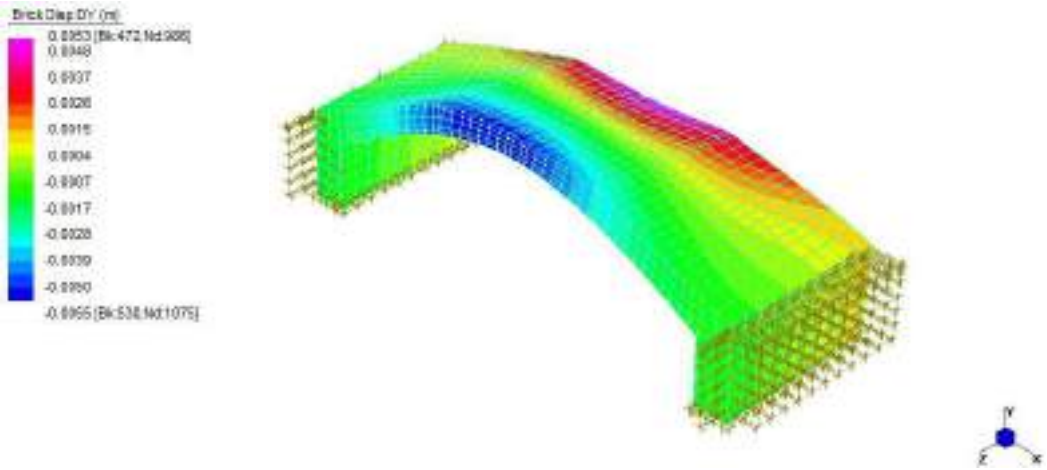

Fig. 8.110: 3-D Model natural frequency analysis: Second modal shape.

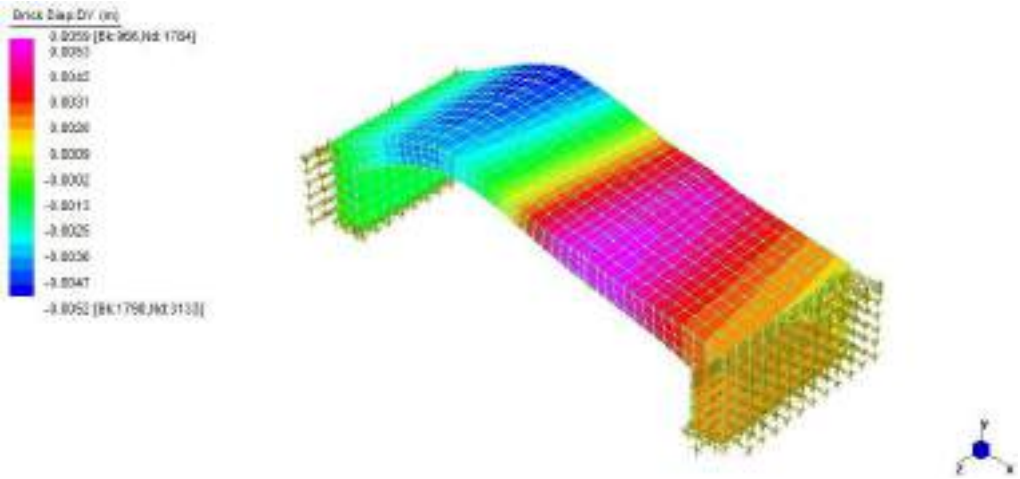

Fig. 8.111: 3-D Model natural frequency analysis: Third modal shape.

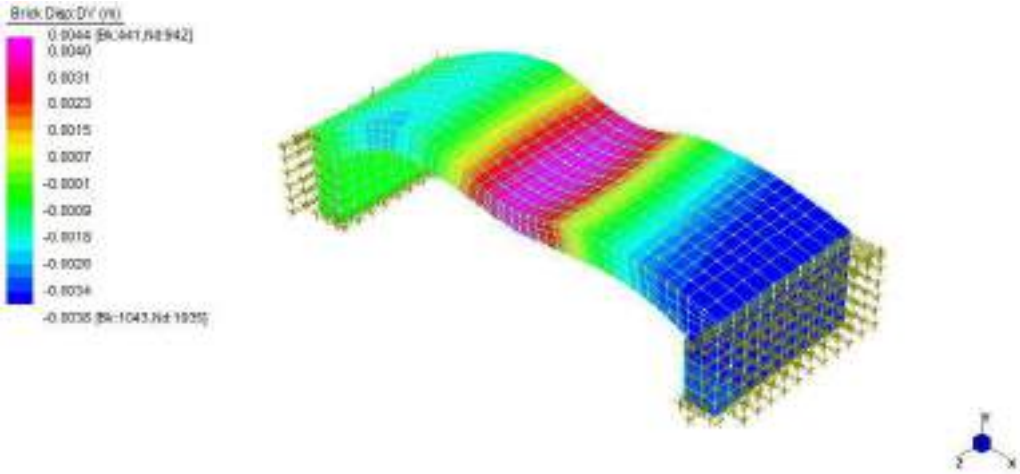

Fig. 8.112: 3-D Model natural frequency analysis: Fourth modal shape.

8.3.6 Structural and material identification

As described in section 7.6, the 2-D model has been adopted to identify, in a fast way, a value range for materials characterization and correct definition of constraints. 3-D Model was calibrated with the same values used for 2-D Model but it has been carried out considering also transversal direction.

In data obtained by 3- D Natural frequencies analysis, see Tab. 8.26, the first mode has a frequency value of 8.9 Hz and most of the participating mass moving in the vertical direction with difference percentage equal to 1.1 %. The values obtained for second and third modal shape are, respectively, 10.8 Hz in the transversal direction and 11.1 Hz in longitudinal direction and difference percentage for the second modal shape equal to 0.5 %, see Tab. 8.27. The third modal shape has the same value recorded during Tromino measurement campaign, see Tab. 8.20.

Mode	Tromino Data	FEM2-D	Difference	FEM 3-D	Difference
1° value Vertical mode	8.9 Hz	10.5 Hz	17.9%	8.8 Hz	1.1 %
2° value Transversal mode	10.8 Hz	-	-	10.75 Hz	0.5 %
3° value Longitudinal mode	11.1 Hz	10.5 Hz	5.4%	11.1 Hz	0

Tab. 8.27: Dynamic parameters and difference between Tromino experimental data and 2-D / 3-D models..

8.4 Guglie bridge

The “Guglie” bridge is one of the most important and ancient bridges of the city. The bridge is located in the “Sestiere di Cannaregio” and it crosses the “Cannareggio” before entering in the “Canal Grande”. It is made of masonry and Istria stone (compact lithographic limestone of the Tithonian age from Istria peninsula). With the same stone the parapets of the bridge and the “Guglie” were made, which give the name to the bridge can be geometrically described as four pyramids with square base posed at both ends of the bridge (Fig. 8.113), two on each side.

Fig. 8.113: Photo of “Guglie” bridge.

8.4.1 History and description

The Guglie bridge was built in wood in 1285, replacing the ferry raft that had been in use until that date.

As it can be clearly seen in the map drawn by Jacopo de Barbari (Fig. 8.114), this bridge consisted of two large ramps that were mounted on four rows of poles. In particular, in order to allow transit of boats equipped with mast, the bridge could be opened and closed in the middle.

The wooden bridge was replaced by the present arch bridge in Istria stone, completed with parapets, in 1580 on the basis of the design produced by Marchesini, as the existing inscriptions on the bridge still show. Two shields are carved on the bridge which can be connected to Doge Pasquale Da Ponte (Fig. 8.115), and numerous masks that adorn the outer arch (archivolt) of the vault (Fig. 8.116). The aim of those elements is to hide mutual sliding of the Istria stones caused by settlements.



Fig. 8.114: Particular of Venice’s map by Jacopo de Barberi,1500
Fig. 8.115: Particular of sheld
Fig. 8.116: Particular of one mask

Important restorations were made in 1641, 1760 and 1777 during the Venetian Republic. In the XIX century there were two more important interventions, both related to access stairs,

made respectively in 1823 and 1871. In 1987, when an important restoration and static consolidation was carried out, the pedestrian plan was rebuilt with the creation of a path accessible to disabled people equipped with a metal handrail. Moreover during this restoration the steps, which were previously made by asphalt, were replaced by stones .

The arcade has been realized with different materials, most of the vault is in brick, while the two head arches are made by Istria stone. The typical used brick is thick, the average size being similar to a gothic brick (27x14x6,5 cm).

8.4.2 Geometric survey

Information about the geometric survey is given by historical research and by the drawings of Marchesini's project design.

The bridge is not at at right angles with the canal. Instead, it forms a angle of approximately 79°. The span of the Guglie bridge is 19,68 m and the thickness in correspondence of the keystone and the crown is 0,38 m. The thickness in proximity of the springing is about 0,83 m and the rise is 4,45 m (Fig. 8.117).

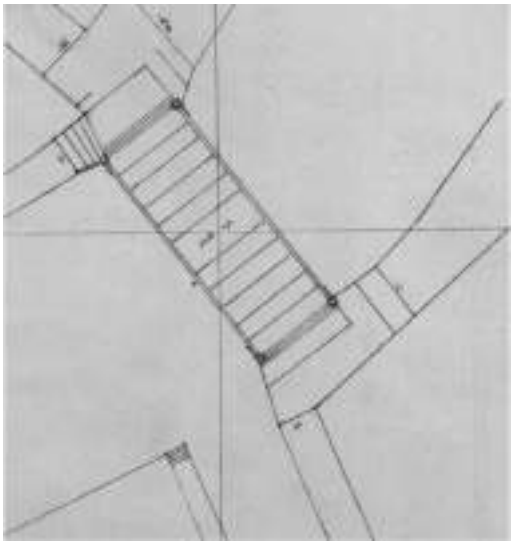

Fig. 8.117: Detail of project drawing

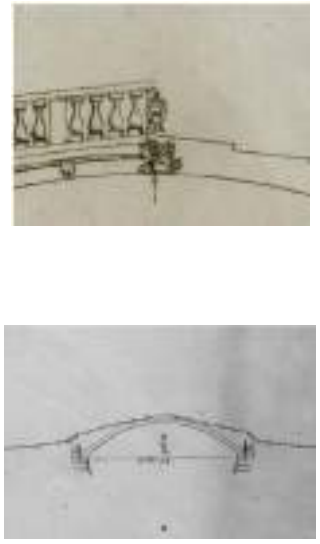

Fig. 8.118: Detail of the parapet and a section

8.4.3 Experimental measurements

As described in Chapter 7, data acquisition was carried out with two synchronized instruments location and the experimental measurement campaign have taken into

account for reference purposes the results obtained from “De L’Arzere” bridge measurements.

Fig. 8.119: Instrument location.

8.4.4 Results analysis

Results of June 27, 2011 experimental measurement campaign are shown in the following figures (see Fig. 8.120-Fig. 8.122).

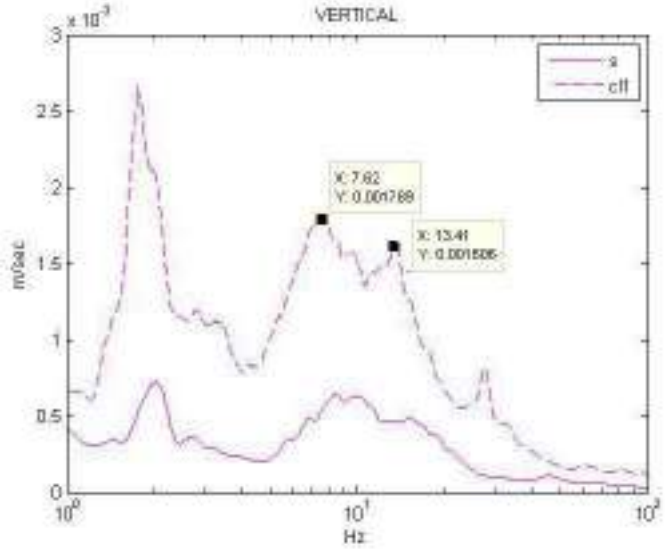

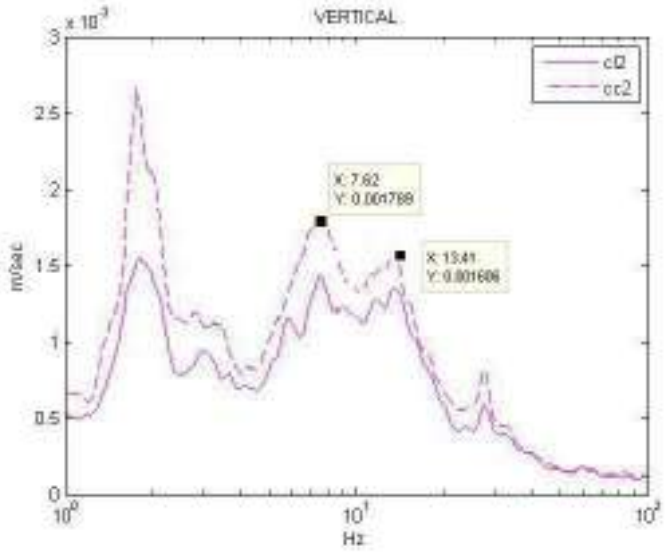

Fig. 8.120: Frequencies of Vertical-y direction.

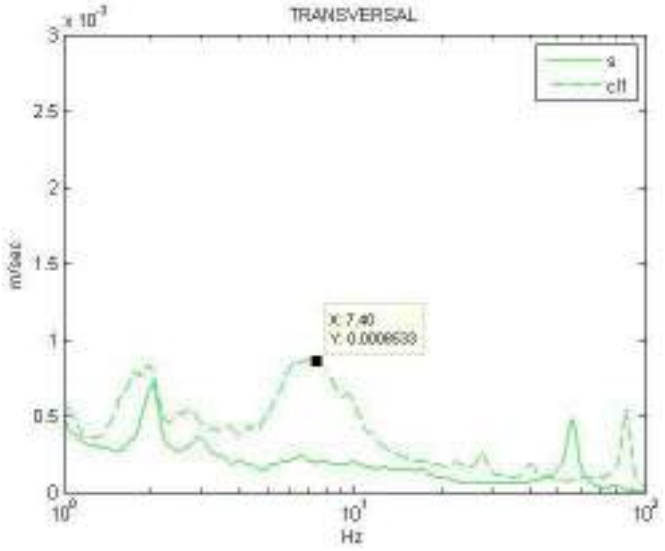

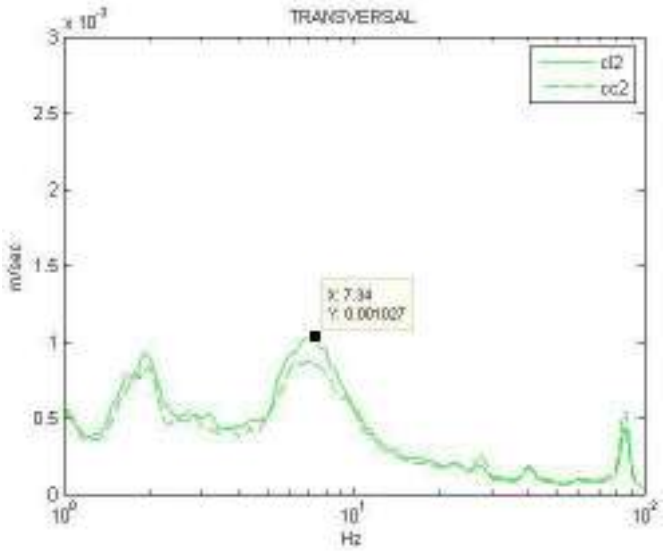

Fig. 8.121: Frequencies of Transversal-z direction.

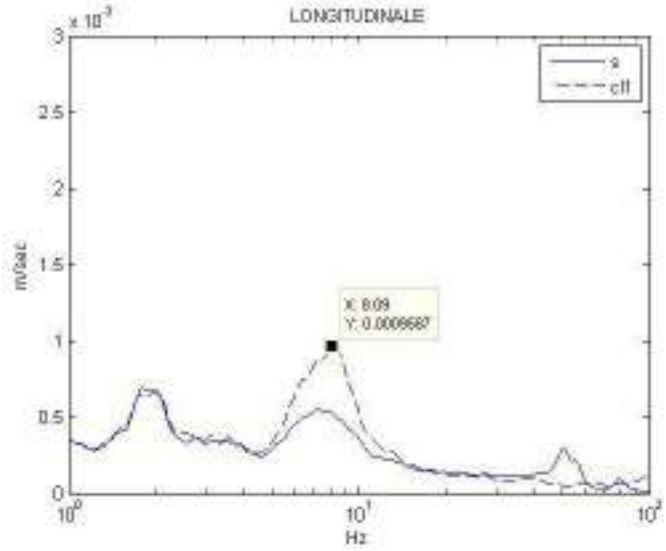

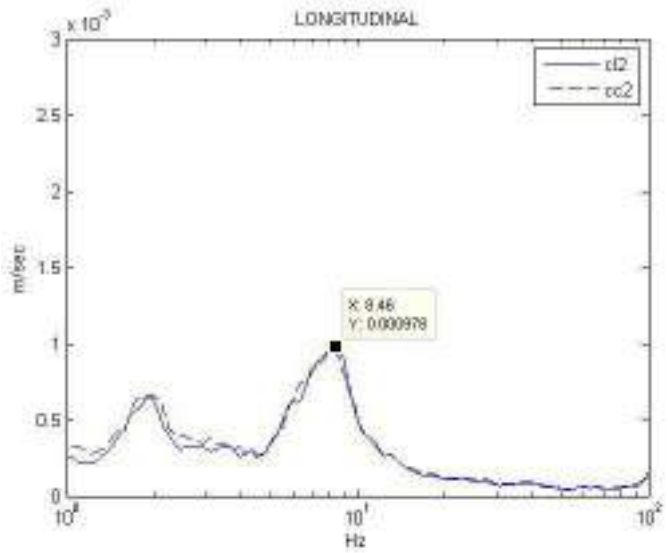

Fig. 8.122: Frequencies of Longitudinal-x direction.

Frequency	Mode shape direction
7.4 Hz	Transversal motion
7.6 Hz	Vertical motion
8.3 Hz	Longitudinal motion
13.4 Hz	Vertical motion

Tab. 8.28: Experimental measurements values and Mass participation direction.

At 7.4 Hz and at 8.3 Hz two peaks were recorded in the transversal and longitudinal directions respectively. Data are closer to the values of the first vertical frequencies acquired and have a lower signal intensity. The evident peaks that characterize first and second mode of the structure have values of 7.6 Hz and 13.4 Hz and they have vertical motion, see Tab. 8.28.

The measurements exclude a 2 Hz peak value, which is assumed to be related to human walk noise.

8.4.5 2-D and 3-D F.E. Model

For the 2-D F.E. models, the transversal cross-section of bridge presents constant mechanical properties. They are 392 3-node plane elements, under plane strain assumption.

The 2-D reference system is characterized by x and y-axes, these correspond to:

- x axis: Horizontal direction on the plane and longitudinal motion of participating mass.

- y axis: Vertical direction on the plane and vertical motion of participating mass

These constituent materials are considered for the bridge: masonry, fill and the pavement made of Istria and Basalt stone. The mechanical characteristics density (***γ***), Poisson's ratio (***v***) and Young's modulus (***E***) of adopted material are reported in Tab. 8.29.

Materials	**Model properties**		
	E (Mpa)	***v***	***γ*** (Kg/m3)
Masonry	3000	0.2	2200
Fill	1500	0.2	1700
Pavement	2500	0.2	1800

Tab. 8.29: Properties of 2-D models materials.

2-D Model 1:

The node constraints applied to Model 1 are mentioned in Chapter 7 and are shown in Fig. 8.123.

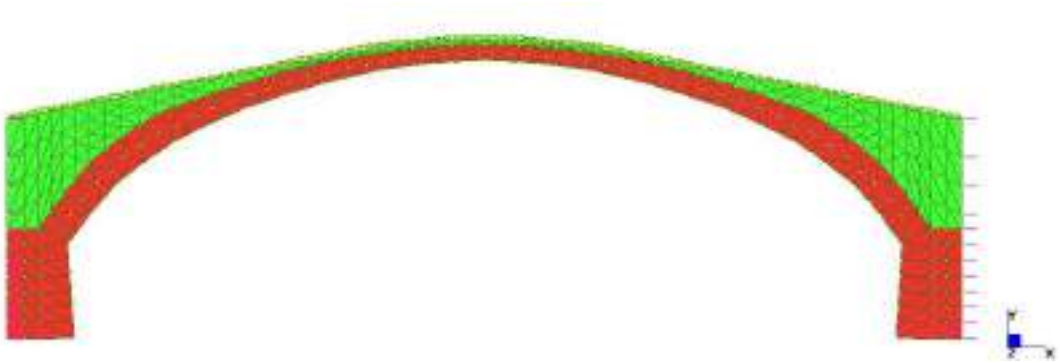

Fig. 8.123: 2-D Model 1 for " delle Guglie" bridge.

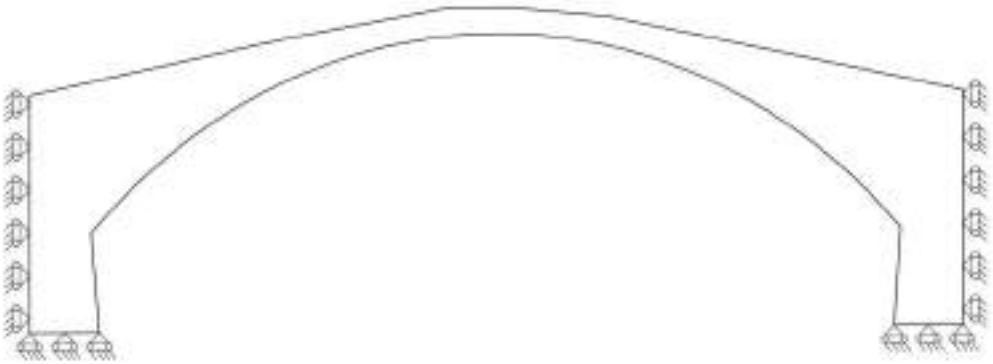

Fig. 8.124: 2- D Model 1 Diagram showing boundary conditions.

2-D Model 2:

The node constraints applied to Model 2 are mentioned in Chapter 7 and are shown in Fig. 8.125.

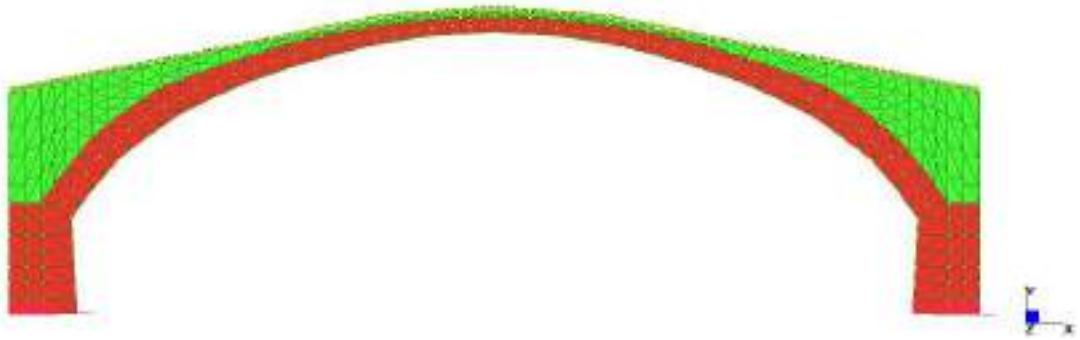

Fig. 8.125: 2-D Model 2 for " delle Guglie" bridge.

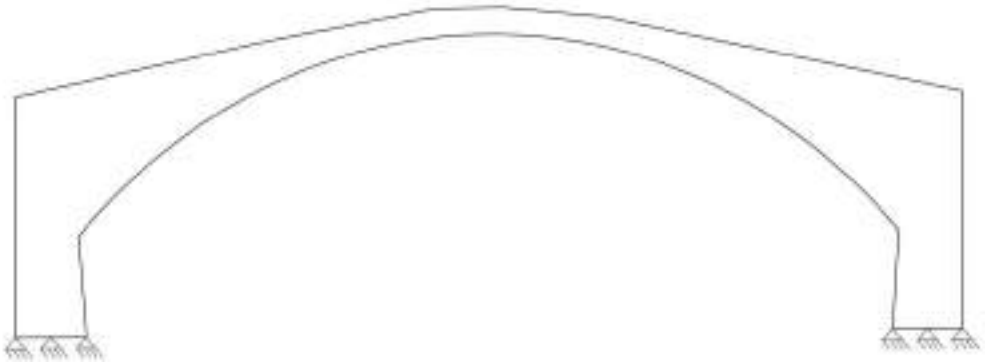

Fig. 8.126: 2- D Model 2 Diagram showing boundary conditions.

2-D Model 3:

The node constraints applied to Model 2 are mentioned in Chapter 7 and are shown in Fig. 8.127. The springs have a high stiffness value of $1 \cdot 10^{11}$N/m in horizontal direction.

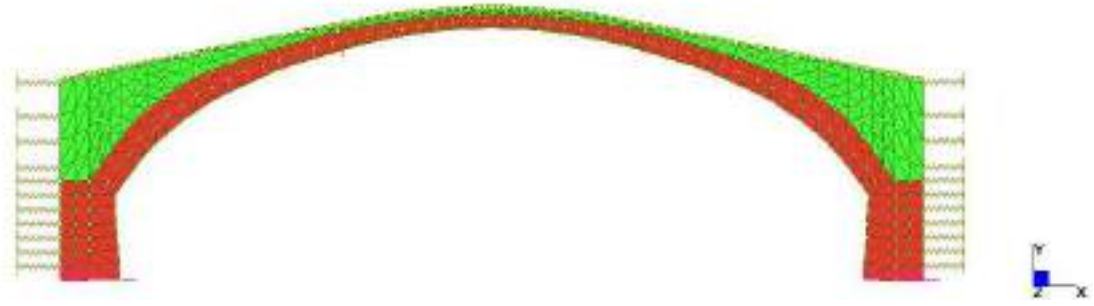

Fig. 8.127: 2-D Model 3 for " delle Guglie" bridge.

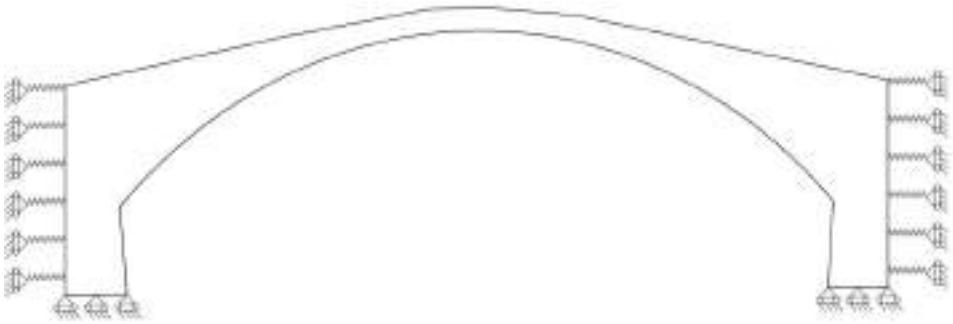

Fig. 8.128: 2- D Model 3 Diagram showing boundary conditions.

3-D Model:

A 3-D Model of "delle Guglie bridge" has been realized with 8595 8-nodes elements and 80 6-nodes elements. The spring stiffness is applied in the same value in the foundation, namely $1 \cdot 10^{11}$N/m and are located in the vertical, the horizontal and the transversal direction. The spring stiffness value in correspondence of the abutments in horizontal direction is $1 \cdot 10^{11}$N/m and in transversal direction has the value of $1 \cdot 10^{10}$N/m.

The 3-D reference system is characterized by axes x, y and z, which represent:

- x axis: Horizontal direction on 3-D reference system and longitudinal motion of participating mass.
- y axis: Vertical direction on 3-D reference system and vertical motion of participating mass.
- z axis: Out of plane direction and transversal motion of participating mass.

For the 3-D model Istria stone was considered as an additional material.

Materials	**Model properties**		
	E (Mpa)	***v***	***γ*** (Kg/m^3)
Masonry	3000	0.2	2200
Fill	1500	0.2	1700
Pavement	2500	0.2	1800
Istria Stone	10000	0.2	2300

Tab. 8.30: Material properties of materials for 3-D model.

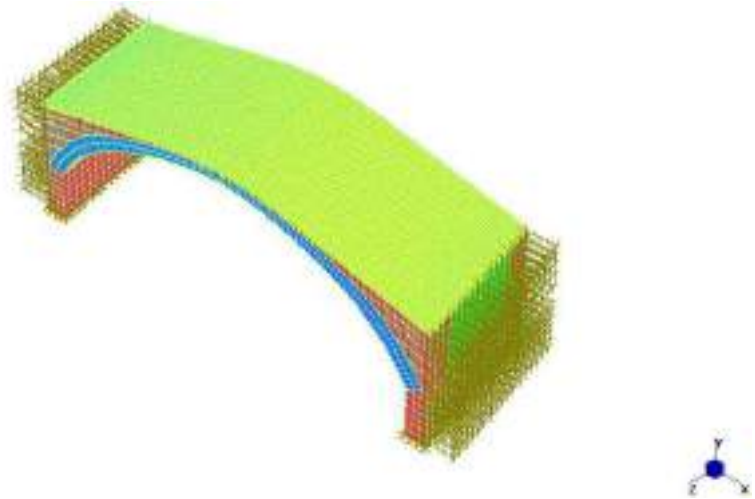

Fig. 8.129: 3-D Model of “delle Guglie” bridge.

8.4.5.1 2-D Analytical Analysis

As explained in section 7.4 utilizing the equation Eq. (7.2), the 2-D numerical model was validated by analytical analysis. The maximum displacement value in the middle section obtained by the two different analysis was calculated and by making a comparison between the value resulted.

$$AD_y = \frac{pl^2}{8EF} \cdot \frac{2 + \frac{25}{128} \cdot \frac{l^2}{f^2}}{1 + \frac{15}{8} \cdot \frac{i^2}{f^2}}$$

$$AD_y = 0.0072\text{m}$$

AD_y= Analytical displacement in the middle section in the vertical direction

E= 3000 MPa

F= 0.59 m^2

f = 4.81 m

p=47.8467 kN/m^3

l= 20 m

i=0.170 m^2

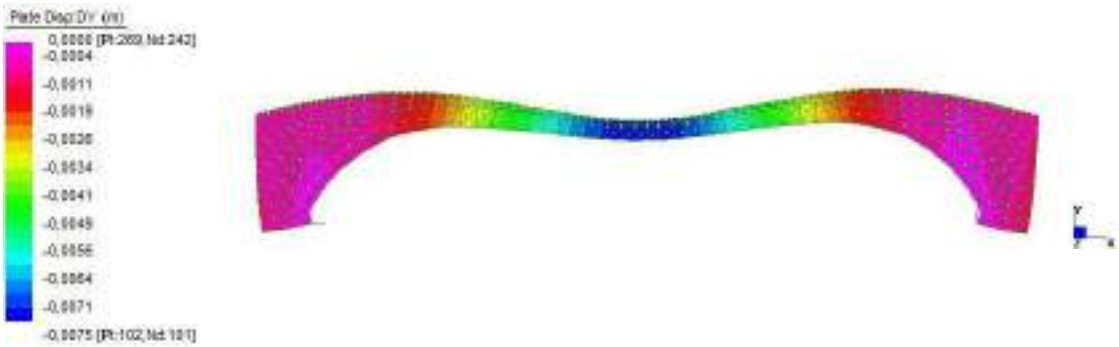

Fig. 8.130: Static Analysis. 2-D Model realized with hinges in correspondence of the foundations.

$$MD_y = 0.0075m$$

MD_y= Model displacement in the middle section in vertical direction

The percentage error ($\Delta dN_M/A_{\mathrm{M}}$) derived from the comparison between the values obtained has been calculated by making use of Eq. (7.2).

$$\frac{\Delta dN_M}{\mathrm{A_M}} = \frac{0.0075 - 0.0072}{0.0072} \cdot 100 = 4\%$$

8.4.5.2 Static Analysis

In the case of Model 1, the maximum vertical displacement in the middle cross-section is 0,0044 m.

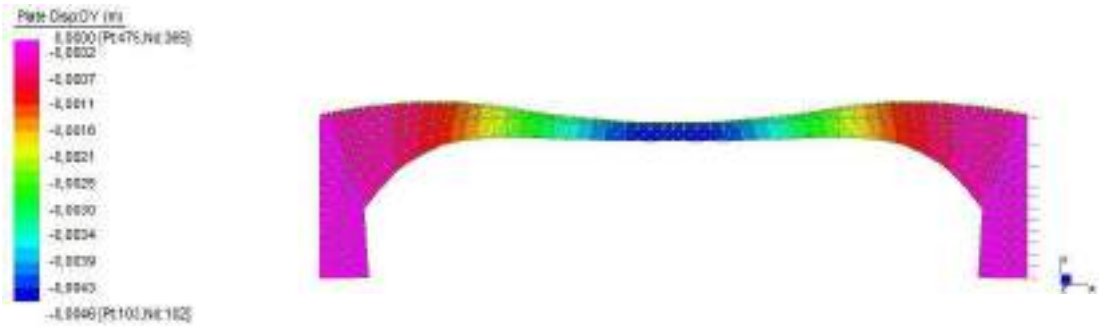

Fig. 8.131: Model 1 static analysis of “delle Guglie” bridge.

In the case of Model 2, the maximum vertical displacement in the middle cross-section is 0,0063 m.

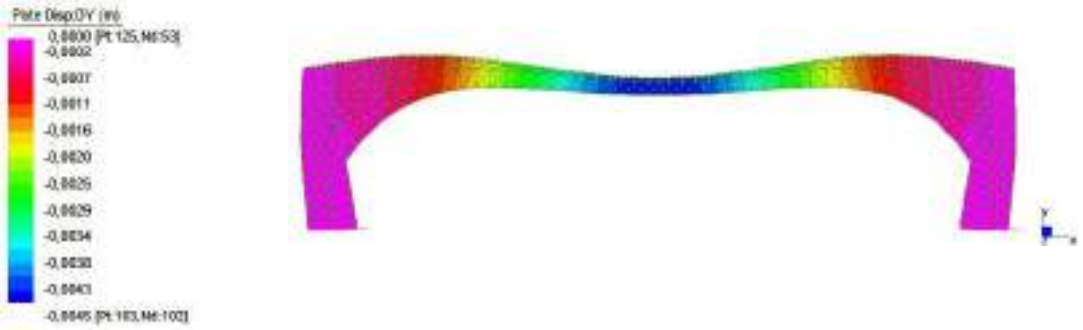

Fig. 8.132: Model 2 static analysis of “delle Guglie” bridge.

In the case of Model 3, the maximum vertical displacement in the middle cross-section is 0,0044 m.

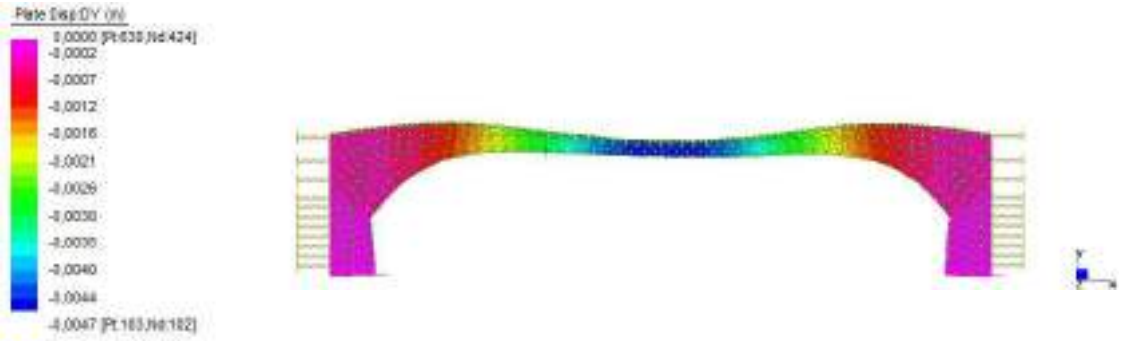

Fig. 8.133: Model 3 static analysis of “delle Guglie” bridge.

The percentage displacement difference between Model 1 and Model 2 (Δdiff M_2/M_1) and between Model 1 and Model 3 (Δdiff M_3/M_1) was evaluated, as follows:

$$\Delta diff M_2/\mathrm{M}_1 = \frac{0{,}0063\mathrm{m} - 0{,}0045\mathrm{m}}{0{,}0045\mathrm{m}} \cdot 100 = 40\%$$

$$\Delta diff M_3/\mathrm{M}_1 = \frac{0{,}0044\mathrm{m} - 0{,}0045\mathrm{m}}{0{,}0045\mathrm{m}} \cdot 100 = 2\%$$

The results obtained show that the constraints adopted in Model 3 produce similar results to Model 1, as a consequence of the high stiffness value attributed to the springs.

8.4.5.3 2-D Modal analysis

Modal analysis, as explained in section 7, has been carried out, producing the following results:

Model 1:

Mode	Frequency	Modal mass	MP-X	MP-Y	MP-Z
	Hz	Kg	%	%	%
1	7.016E+00	1.310E+04	0.192	27.512	0.000
2	8.433E+00	1.442E+04	3.454	2.002	0.000
3	1.406E+01	2.149E+04	1.172	13.916	0.000
4	1.969E+01	2.435E+04	0.254	0.651	0.000
Total Mass Participation			5.072	44.081	0.000

Tab. 8.31: Results of natural frequency analysis of 2-D Model 1.

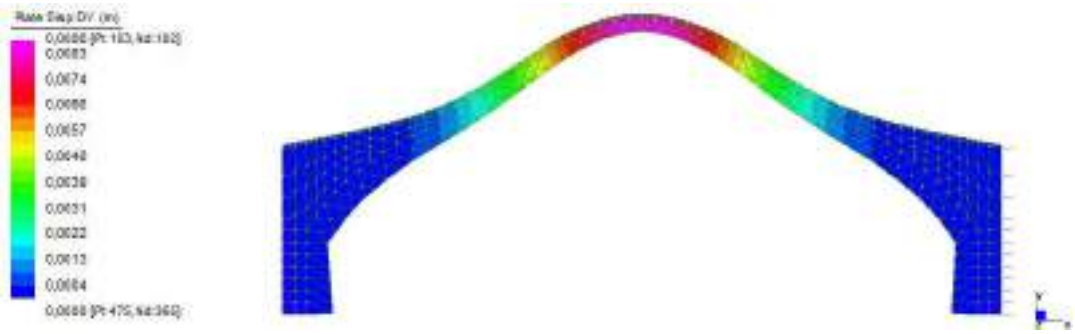

Fig. 8.134: 2-D Model 1 natural frequency analysis: First modal shape.

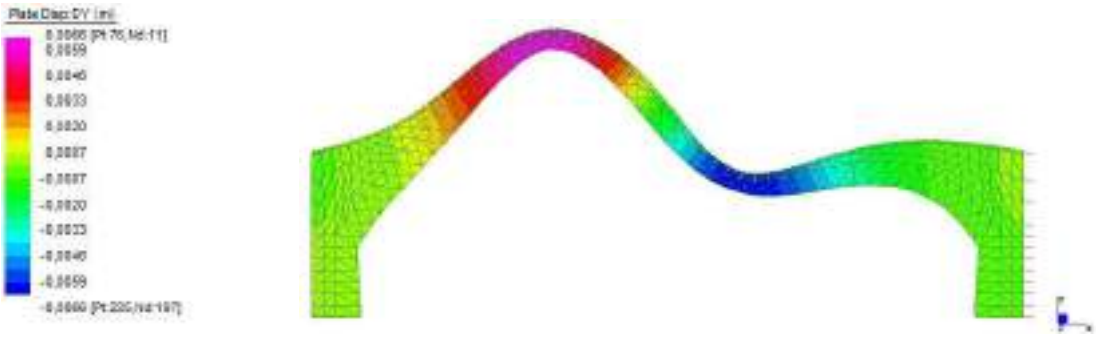

Fig. 8.135: 2-D Model 1 natural frequency analysis: Second modal shape.

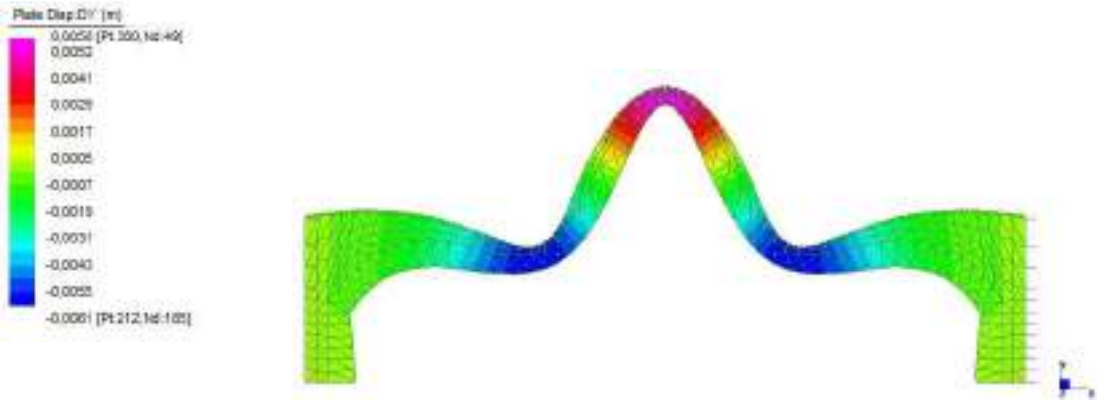

Fig. 8.136: 2-D Model 1 natural frequency analysis: Third modal shape.

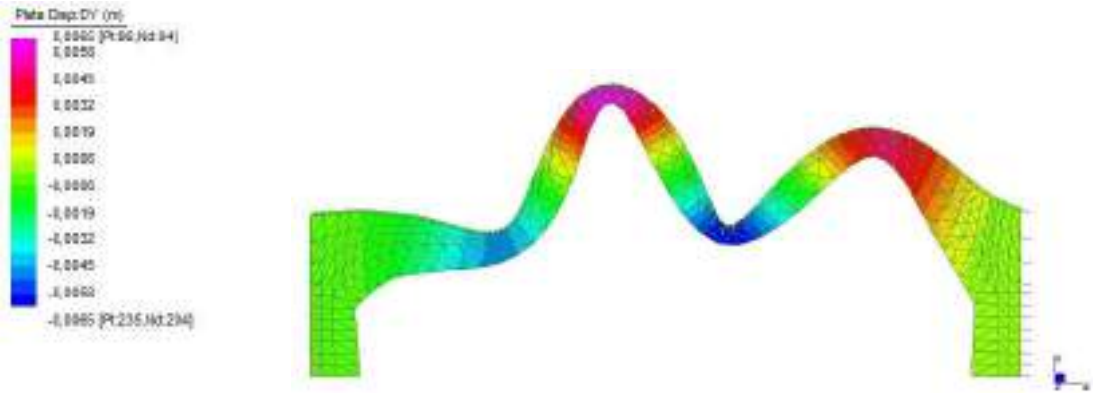

Fig. 8.137: 2-D Model 1 natural frequency analysis: Fourth modal shape.

Model 2:

Mode	Frequency	Modal mass	MP-X	MP-Y	MP-Z
	Hz	Kg	%	%	%
1	3.208E+00	7.197E+04	50.493	0.003	0.000
2	4.770E+00	1.338E+04	0.011	15.862	0.000
3	9.021E+00	2.214E+04	27.041	0.259	0.000
4	9.205E+00	2.980E+04	0.224	31.664	0.000
Total Mass Participation			77.770	47.788	0.000

Tab. 8.32: Results of natural frequency analysis of 2-D Model 2

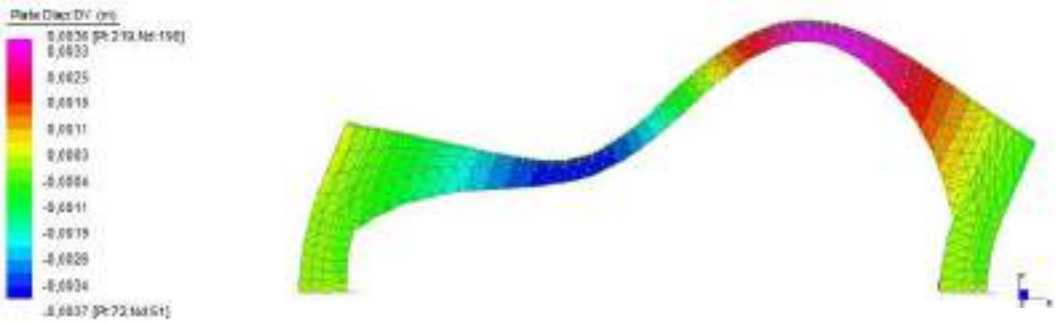

Fig. 8.138: 2-D Model 2 natural frequency analysis: First modal shape.

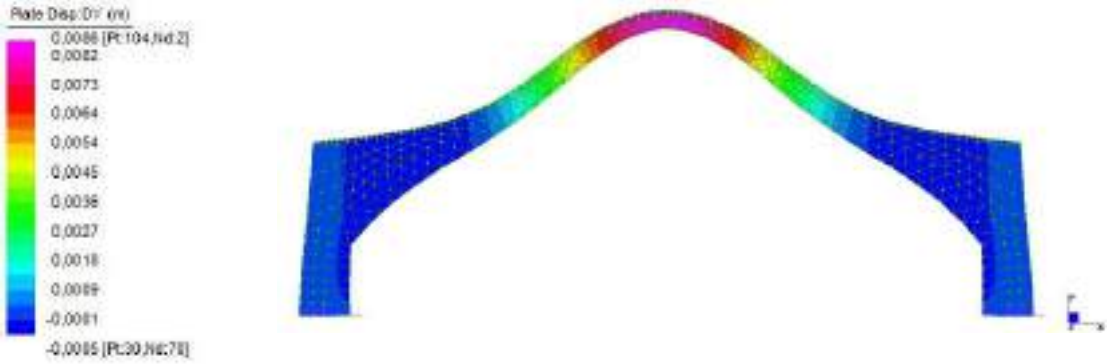

Fig. 8.139: 2-D Model 2 natural frequency analysis: Second modal shape.

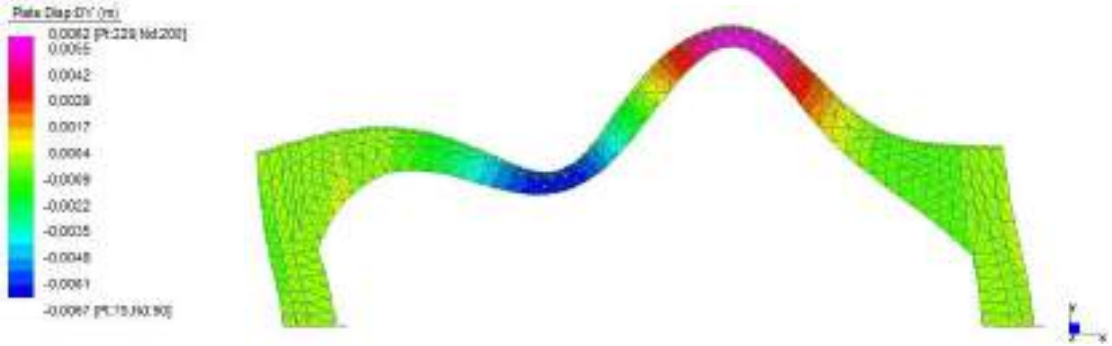

Fig. 8.140: 2-D Model 2 natural frequency analysis: Third modal shape.

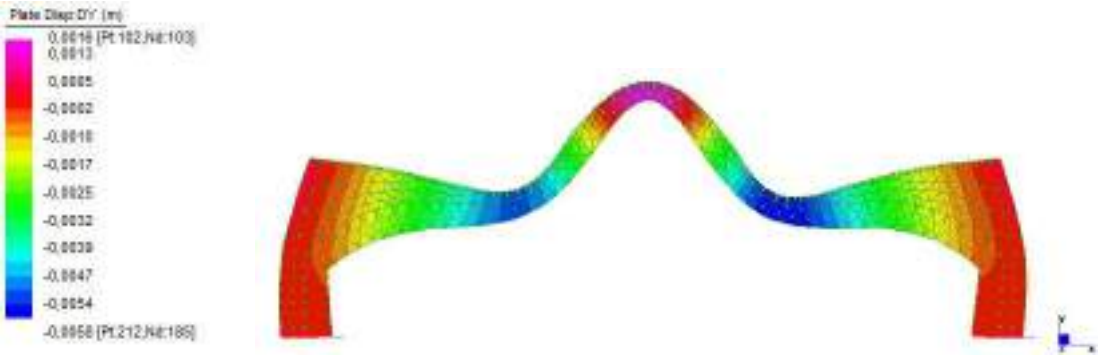

Fig. 8.141: 2-D Model 2 natural frequency analysis: Fourth modal shape.

Model 3:

Mode	Frequency	Modal mass	MP-X	MP-Y	MP-Z
	Hz	Kg	%	%	%
1	7.015E+00	1.309E+04	0. 192	27.512	0.000
2	8.431E+00	1.441E+04	3.454	3.002	0.000
3	1.406E+01	2.151E+04	1. 172	13. 916	0.000
4	1.968E+01	2.449E+04	0.254	0. 651	0.000
Total Mass Participation			5.072	45.081	0.000

Tab. 8.33: Results of natural frequency analysis of 2-D Model 3

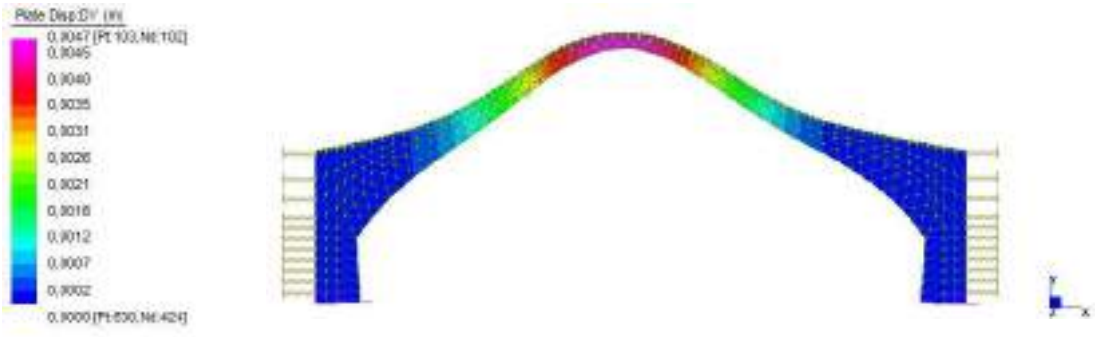

Fig. 8.142: 2-D Model 3 natural frequency analysis: First modal shape.

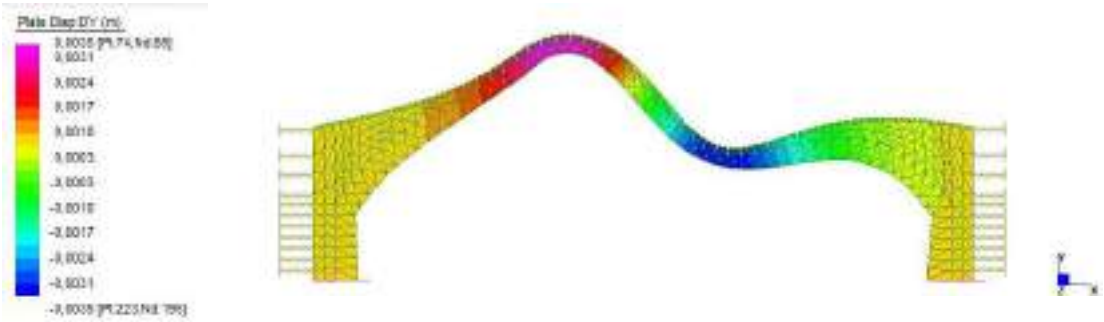

Fig. 8.143: 2-D Model 3 natural frequency analysis: Second modal shape.

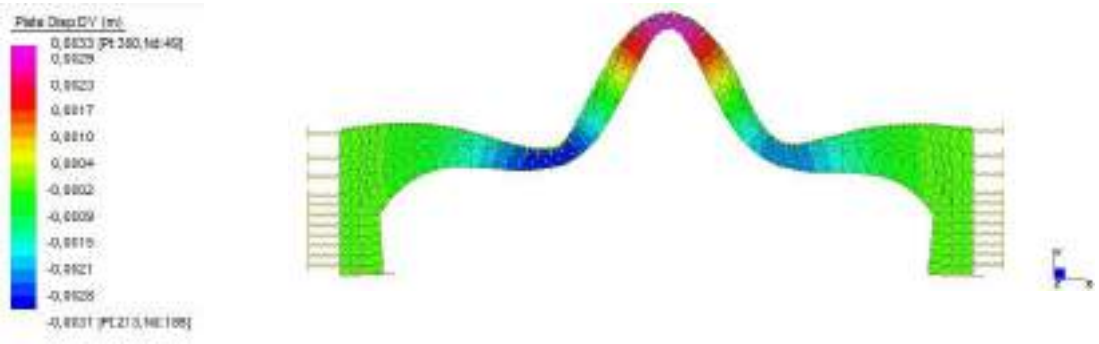

Fig. 8.144: 2-D Model 3 natural frequency analysis: Third modal shape.

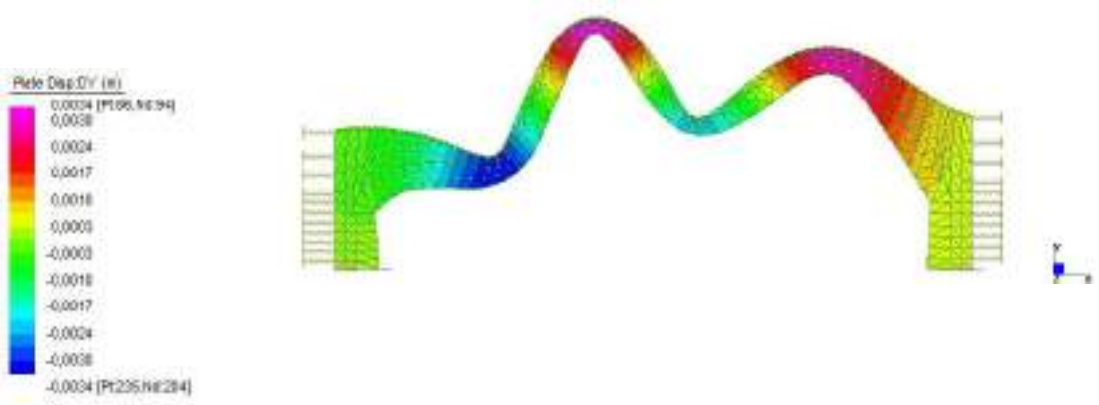

Fig. 8.145: : 2-D Model 3 natural frequencies analyses: Fourth modal shape.

Considering the results obtained from the natural frequency analysis of the differently constrained models, it must be noted that the Model 3, that is obtained using a high value for springs stiffness and the Model 1, where the horizontal motions are fixed, have similar frequencies. The natural frequency result by Model 1 and Model 3 are closer. Values obtained by experimental measurements show a first and a second peaks characterized by vertical motion at 7.6 Hz and 13.4 Hz, see Tab. 8.28.

Making a comparison between the Tromino data and 2- D model 3 results, the percentage error is 8.6% for the first vertical mode and 5.2% for the second vertical mode.

8.4.5.4 3-D Model Analysis:

Mode	Frequency	Modal mass	MP-X	MP-Y	MP-Z
	Hz	Kg	%	%	%
1	7.554E+00	8.250E+04	4.565	0.004	2.271
2	8.066E+00	5.479E+04	1.573	0.042	5.310
3	8.336E+00	6.891E+04	0.005	27.803	0.000
4	1.311E+01	1.244E+05	0.000	18.012	0.080
Total Mass Participation			6.142	45.926	7.664

Tab. 8.34: Results of natural frequency analysis of 3-D Model.

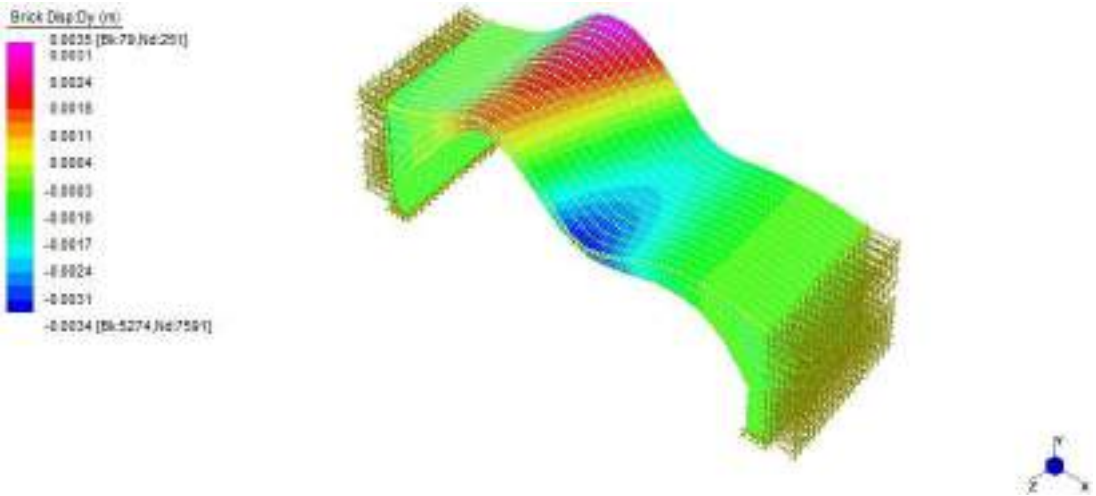

Fig. 8.146: 3-D Model natural frequency analysis: First modal shape.

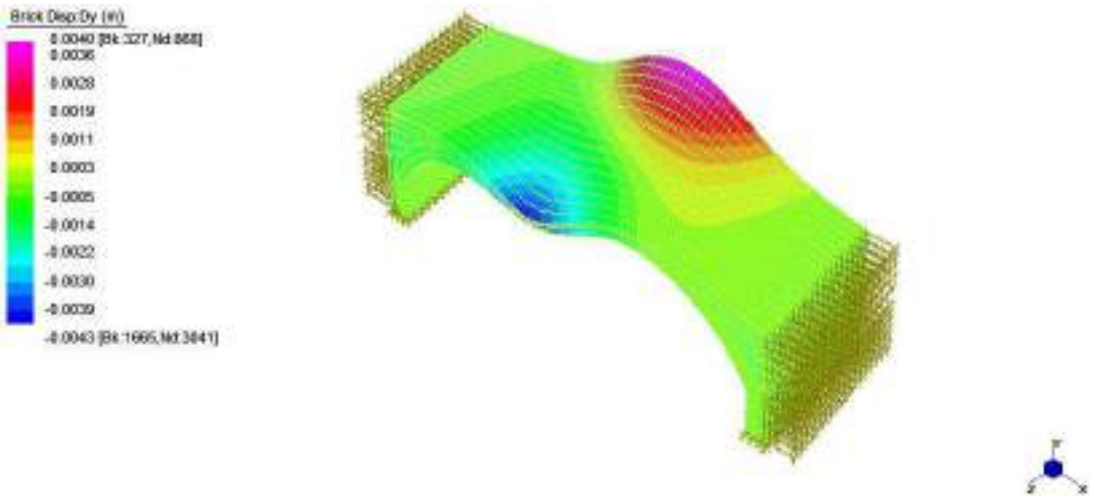

Fig. 8.147: 3-D Model natural frequency analysis: Second modal shape.

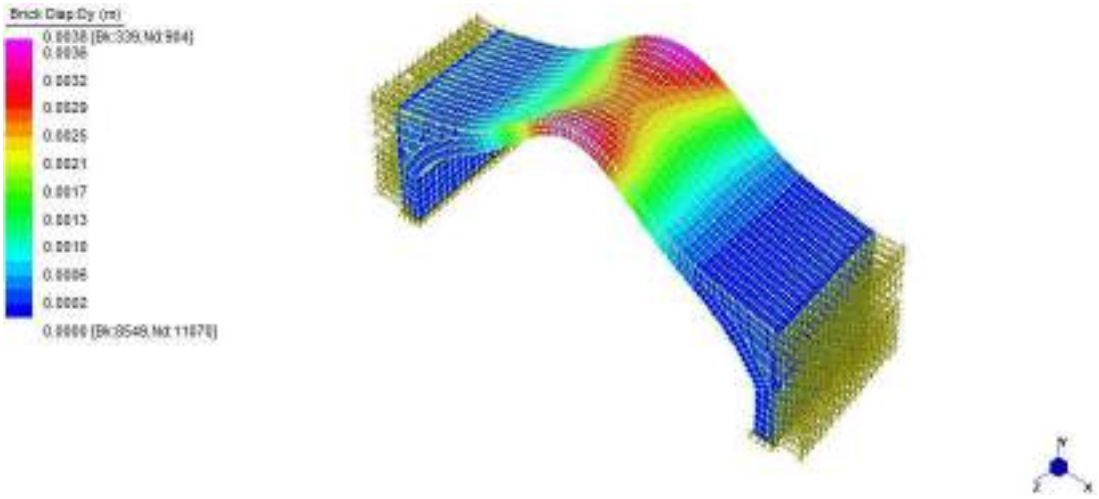

Fig. 8.148: 3-D Model natural frequency analysis: Third modal shape.

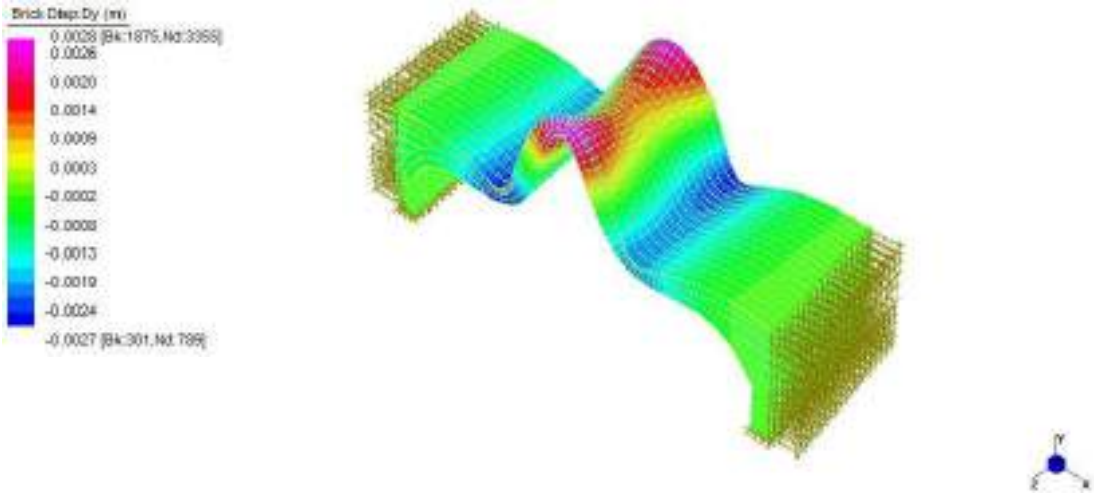

Fig. 8.149: 3-D Model natural frequency analysis: Fifth modal shape.

8.4.6 Structural and material identification

As described in section 7.6, the 2-D model were adopted to identify, in a simplified way, a value range for material characterization and reliable definition of boundary conditions. 3-D Model was calibrated using horizontal spring stiffness values that had been used for 2-D model 3.

The results obtained by experimental measurements, as explain in Section 8.4.3, show two defined peaks at 7.6 Hz and 13.4 Hz respectively, characterised by motion in vertical direction. The results obtained by 3D Model natural frequencies analysis are very close to the experimental data.

Mode	Tromino Data	FEM2-D	Difference	FEM 3-D	Difference
1°value Vertical mode	7.6 Hz	7 Hz	8.6 %	8.3 Hz	9.2 %
2°value Vertical mode	13.4 Hz	14.1 Hz	5.2 %	13.1 Hz	2.2 %

Tab. 8.35: Dynamic parameters and difference between Tromino experimental data and 2-D / 3-D models.

Two peaks have been obtained by experimental measurement at 7.4 Hz and at 8.3 Hz, see Tab. 8.28, in the transversal and in the longitudinal directions respectively. These values are closer to the values of the first vertical frequency acquired and have a lower signal intensity. This is a consequence of the bridge geometric characteristics and boundary conditions that cause lower modal shapes triggered by lower mass in horizontal directions.

This is confirmed by the results obtained by 3-D model natural frequencies analysis. The data suggests a torsional motion that involves a lower mass participation in transversal and longitudinal direction, see Tab. 8.34.

9 Conclusions

In this research project, an experimental-theoretical methodology for the study of masonry bridges has been proposed, with the specific aim of defining a procedure to effectively evaluate the structural behaviour of historical structures.

Experimental and numerical modelling were thus developed. The experiments were performed with a two-fold objective: namely, validating the proposed numerical models to simulate the behaviour of masonry bridges and calibrating the models through the use of dynamic identification procedures.

For the investigated cases studies, experimental measurements were performed by the compact digital tromograph Tromino®. This instrument was devised for the dynamic characterization of subsoils; for this reason the data obtained for the study case of De L'Arzere have been compared with another measurement campaign carried out using uniaxial piezoelectric accelerometers, which were placed in the same position as the Tromino measurement positions. Tromino records the signal as an input velocity, while accelerometers measure an acceleration signal. The difference on the results obtained for the study case of De L'Arzere is due to the different acquisition adopted for the accelerometers because the transversal direction has not been considered; on the other hand the results confirm that Tromino should be considered as a valid alternative to the instruments which are usually employed for operational modal analysis.

In a parallel manner, numerical modelling was performed adopting suitable discretization of masonry bridges. The modelling is carried out adopting 1-D, 2-D and 3-D Models.

For each study case, 1-D F.E. Model were used in order to validate the model result by comparing the maximum vertical displacement in the middle cross-section with the analytical solution.

As it is well known, 2-D plain strain elements allow models to obtain information on the mechanical behaviour of masonry arch bridges with limited computational costs.
2-D F.E. Models, under plain strain assumption, where therefore used. The material calibration and the analysis of sensitivity simulating three different boundary conditions were performed for three different 2-D models.
For all different types of models both static and dynamic modal analyses were carried out.
The limit of 2-D modelling is due to its inability of to account for out-of-plane motion.
For these reasons, starting from a 2-D model calibration, a 3-D model was constructed, using the results obtained from 2-D models, in order to consider out-of-plane movements and to give more exhaustive information.
Modal and Static were then also performed with the 3-D model.
The transversal data obtained with experimental measurements have been used for the calibration of 3-D models where all components of motion - vertical, horizontal and transversal - are taken into account.

The dynamic identification was thus obtained using non-invasive experimental measurement and numerical modelling procedure, by making use of simple and fast tools. In this way it was possible to define and propose a methodology to study this type of masonry structure which can also be easily generalized and extended to other structural typologies.

References

Abruzzese, D., Como, M., Lanni, G. (1992). On the lateral strength of multistory masonry walls with openings and horizontal reinforcing connections, Proc. of 10th World Conference on Earthquake Engineering, Rotterdam, Balkema, pp. 4525-4530.

Addessi, D., Sacco, E., Paolone, A. (2010). Cosserat model for periodic masonry deduced by non-linear homogenization, Eur. J. Mechanics A/ Solids, 29(4), pp. 724-737.

Alberti, L.B. (1450). De re aedificatoria, Firenze.

Alpa G., Monetto I. (1994). Microstructural model for dry block masonry walls with in-plane loading, J. Mechanics and Physics of solids, 47 (7), pp. 1159–1175.

Anthoine, A. (1995). Derivation of in plane elastic characteristic of masonry through homogenization theory, Int. J. Solids and Structures, 32(2), pp. 137-163.

Atkinson, R.H., Amadei, P.B., Saeb S., Sture S. (1989). Response of masonry bed joints in direct shear, J. Structural Engineering , ASCE, 115, (9) pp. 2276-2296.

Azevedo, J., Sincraian, G., Lemos, J.V. (2000). Seismic behaviour of blocky masonry structures, Earthquake Spectra, 16(2), pp. 337-365.

Bachmann, H. (1992 a). Case studies of structures with man-induced vibrations, Journal of Structural Engineering*,* ASCE*,* 118(3), pp. 631-647.

Bachmann, H. (1992 b). Dynamic forces from rhythmical human body motions. Vibration Problems in Structures: Practical Guidelines, Birkhäuser, Basel, Appendix G.

Bacigalupo, A., Gambarotta, L. (2011). Non-Local Computational Homogenization of Periodic Masonry, Int. J. Multiscale Computational Engineering, 9(5), pp. 565-578.

Backes, H.P. (1985). On the behaviour of masonry under tension in the direction of the bed joints, PhD dissertation, Aachen University of Technology, Aachen.

Baggio, C., Trovalusci, P. (2000). Collapse behaviour of three-dimensional brick-block systems using non-linear programming, Structural engineering and mechanics, 10(2), pp. 181-195.

Balletti, C., Brussa, N., Gottardi, C., Guerra, F. (2014). The documentation and reintegration of a lost past, ISPRS Annals of the Photogrammetry, Remote Sensing and Spatial Information Sciences, II-5, ISPRS Technical Commission V Symposium, June 23-25, Riva del Garda, Italy.

Baraldi, D., Brito de Carvalho Bello, C., Cecchi, A., Meroi, E., Reccia E. (2019). Nonlinear behavior of masonry walls: FE, DE, and FE/DE models, Composites: Mechanics, Computations, Applications: An International Journal, 10(3), pp. 253-272.

Bard, P. Y. (2008). The H/V technique: capabilities and limitations based on the results of the SESAME project , Bulletin of Earthquake Engineering,6, pp. 75-108.

Bićanić, N., Stirling, C., Pearce, C.J. (2003). Discontinuous modelling of masonry bridges, Computational Mechanics, 31, pp 60–68.

Binda, L., Tiraboschi, C., Mirabella Roberti, G., Baronio, G., Cardani, G. (1995) Measuring masonry material properties: detailed results from an extensive experimental research, Experimental and Numerical Investigation on a brick Masonry Building Prototype, Report 5.0 - G.N.D.T.

Boothby, T.E., Domalik, D.E., Dalad V.A. (1998). Service load response of masonry, J. Structural Engineering 124(1), pp 79-86.

Braga, F., Dolce, M. (1982). Un metodo per l'analisi di edifici multipiano in muratura antisismici, Proc. 6th I.B.Ma.C., Roma.

Braga, F., Liberatore, D. (1990). A finite element for the analysis of the response of masonry buildings, Proceedings of the 5th North American Masonry Conference, University of Illinois at Urbana-Champaign.

Brasile, S., Casciaro, R., Formica, G. (2007). Multilevel approach for brick masonry walls part II: On the use of equivalent continua, Computer Methods in applied Mechanics and engineering, 196 (49-52), pp. 4801-4810.

Brencich, A., Lagomarsino, S. (1998). A macro-element dynamic model for masonry shear walls, Proc. of the Int. Symp, Computer methods in structural masonry - 4, E&FN Spon, London, pp. 67-75.

Breymann, G.A. (1903). Allgemeine Baukonstruktionslehre, 2, die konstruktionen in Holz, Verlag J.M., Gebhardt, Leipzig, Nachdruckt 1982, Hannover J.M., Verlag Th. Schafer.

Bridle, R.J., Hughes, T.G. (1990). An energy method for arch bridges analysis, Proceedings of the Institution of Civil Engineers, 89(3), pp. 375-378

Brookes, C., Collings, M. (2003). ARCHTEC – Verification of Structural Analysis. Gifford and Partners Document No: B1660A/V10/R03.

Calderini, C., Lagomarsino, S. (2008). A continuum model for in-plane anisotropic inelastic behaviour of masonry, J. Structural Engineering , ASCE, 134(2), pp. 209-220.

Calderoni, B., Cordasco, E.A., Lenza, P. (2007). Analisi teorico sperimentale del comportamento della fascia di piano delle pareti murarie per azioni sismiche, Atti XII Convegno Nazionale ANIDIS, 10-14 June, Pisa.

Casapulla, C., D'Ayala, D. (2006). In-plane collapse behaviour of masonry walls with frictional resistance and openings, Proc. of V Int. Conference Structural Analysis of Historical Constructions, New Delhi, pp. 1059-1066.

Casolo, S. (2006). Macroscopic modelling of structured materials: Relationship between orthotropic Cosserat continuum and rigid elements, Int. J. Solids and Structures, 438(3-4), pp. 475-496.

Cavalieri San Bertolo, N. (1845). Istituzioni di architettura, statica e idraulica, Mantova,F.lli Negretti.

Cecchi, A., Sab, K. (2002a). A multi-parameter homogenization study for modelling elastic masonry, Eur. J. Mechanics A/ Solids, 218(2), pp. 249-268.

Cecchi A., Sab K. (2002b). Out of plane model for heterogeneous periodic materials: the case of masonry, Eur. J. Mechanics A/ Solids, 21(5), pp. 715-746.

Cecchi, A., Milani, G., Tralli, A. (2005). Validation of analytical multiparameter homogenisation models for out-of-plane loaded masonry walls by means of finite element method, J. Structural Engineering , ASCE, 131(2), pp. 185-198.

Cecchi, A., Milani, G., Tralli, A. (2007). A Reissner-Mindlin limit analysis model for out-of-plane loaded running bond masonry walls, Int. J. Solids and Structures, 44(5), pp. 1438-1460.

Cecchi, A., Milani, G. (2008). A kinematic limit analysis model for thick English bond masonry walls, Int. J. Solids and Structures, 45(5), pp. 1302-1311.

Cecchi, A., Sab, K. (2009). Discrete and continuous models for in plane loaded random elastic brickwork, Eur. J. Mechanics A/ Solids, 28(3), pp. 610-625.

Choo, B.S., Coutie, M.G., Gong, N.G. (1991). Finite-element analysis of masonry arch bridges using tapered elements, Proceedings of the Institution of Civil Engineers, 91(4), pp 755–770.

Cluni, F., Gusella, V. (2004). Homogenization of non-periodic masonry structures, Int. J. Solids and Structures, 41 (7), 1911–1923.

Collignon, M.E. (1869). Course de mécanique appliquée aux construction, Paris, Dunod.

Colombo, G. (1877). Manuale dell'Ingegnere, Milano, Hoepli.

Commission of the European Union Communities. (1996). 6: Design of Masonry Structures, ENV

COST-345 (2004). Procedures Required for the Assessment of Highway Structures: Numerical Techniques for Safety and Serviceability Assessment, Report of Working Groups 4 and 5, European Commission Directorate General Transport and Energy: COST 345.

Corigliano, A., Maier, G. (1995). Dynamic shakedown analysis and bounds for elastoplastic structures with non associative, internal variable constitutive laws, Int. J. Solids and Structures, 32 (21), pp. 3145-3166.

Crisfield, M.A. (1984). A finite element computer program for the analysis of masonry arches, Transport and Road Research Laboratory, Dept of Transport, Report LR1115, TRRL, Crowthorne, London.

Crisfield, M.A. (1985). Finite Element and Mechanism Methods for the Analysis of Masonry and Brickwork Arches, TRRL Report RR 19, Transport and Road Research Laboratory, Chrowthorne, London.

Cundall, P.A. (1976). Explicit finite difference methods in geo mechanics, in: Numerical Methods in Engineering , Blacksburg, Virginia, 1, pp. 132-150.

Curioni, G. (1864-1884). L'arte di fabbricare, ossia corso completo di istituzioni teorico pratiche per gli Ingegneri, per Periti in Costruzione e per periti Misuratori, Torino, Augusto Federico Negro.

Curti, E., Lemme, A., Podestà, S., Resemin, S. (2006). Criteri di verifica per la progettazione di interventi di miglioramento sismico di edifici monumentali, Ingegneria Sismica, XXIII(1), pp. 56-71.

D'Asdia, P., Viskovic, A. (1994). L'analisi sismica degli edifici in muratura, Ingegneria Sismica, XI(1), pp. 32-42.

D'Ayala, D., Speranza, E. (2003). Definition of collapse mechanisms and seismic vulnerability of historic masonry buildings, Earthquake Spectra, 19 (3), pp. 479-509.

De Buhan, P., De Felice, G. (1997). A homogenisation approach to the ultimate strength of brick masonry, J. Mechanics and Physics of Solids, 45(7), pp. 1085-1104.

De Felice, G., Giannini, R. (2001). Out-of-plane seismic resistance of masonry walls, J. Earthquake Engineering , 5(2), pp. 253-271.

Dhanasekar, M., Kleeman, P.W., Page, A.W. (1985). Biaxial stress-strain relations for brick masonry, J. Structural Engineering , ASCE, 111(5), 1085-1100.

Di Pasquale, S. (1977). Costruzioni, Firenze, Le Monnier.

Donghi, D. (1905), Manuale dell'Architetto, Torino, UTET.

Drucker, D.C., Prager, W., Greenberg, H.J. (1952). Extended limit design theorems for continuous media, Quarterly of Applied Mathematics, 9, pp. 381–389.

Drucker, D.C. (1953). Coulombs friction, plasticity and limit loads, Transactions of the American Society of Mechanical Engineers, 21, pp. 71 – 74.

El-Kafafy, M., Guillaume, P., Peeters, B., Marra, F., Coppotelli, G. (2012). Advanced Frequency-Domain Modal Analysis for Dealing with Measurement Noise and Parameter Uncertainty, Topics in Modal Analysis I, 5, pp. 179-199.

Ewins, DJ., Elnashai, AS., Broderick, BM. (1996). Seismic response of composite frames-II. Calculation of behaviour factors. Engineering Structures, 18(9), pp. 707-723.

Falconer, R.E. (1994). Assessment of multi-span arch bridge, Proc. 3rd Int. Conf. on Inspection, Appraisal, Repair and Maintenance of Building and Structures, Bangkok, pp 79-88.

Ford, T.E., Augarde, C.E., Tuxford, S.S. (2003). Modelling masonry arch bridges using commercial finite element software, 9th International Conference on Civil and Structural Engineering Computing, Egmond aan Zee, 2–4 September 2003, Netherlands.

Forest, S., Pradel, F., Sab, K. (2001). Asymptotic analysis of heterogeneous Cosserat media, Int. J. Solids and Structures, 385(26-27), pp. 4585-4608.

Ferraioli, M., Mandara, A., Abruzzese, D., Miccoli, L. (2011). Dynamic identification and Seismic safety of masonry bell towers, Proceedings of the 14th Conference of Associazione Nazionale Italiana di Ingegneria Sismica (ANIDIS), September 18-22, Bari, Italy.

Ferris, M., Tin-Loi, F. (2001). Limit analysis of frictional block assemblies as a mathematical program with complementarily constraints, Int. j. Mechanical and Sciences, 43(1), pp. 209-224.

Gabba, A., (1876), Corso di costruzioni civili e militari, Torino, Stamperia dell'unione tipografico.

Gambarotta, L., Lagomarsino, S. (1997). Damage models for the seismic response of brick masonry shear walls. Part I: The mortar joint model and its applications; Part II: the continuum model and its applications, Earthquake Engineering & Structural Dynamics, 26(4), pp. 423-439.

Gauthey, E. M. (1809-1813). Traitè de la construction des pontes, 1-2, Firmin Didot., Paris.

Gilbert, M., Melbourne, C. (1994). Rigid block analysis of masonry structures, Structural Engineer, 72(21), pp. 356-361.

Gilbert, M. (2007). Limit analysis applied to masonry arch bridges: state-of-the-art and recent developments, Proceedings of the Arch`07 – 5th International Conference on Arch Bridges. Lourenço, PB., Oliveira, DV., Portela, A. (Eds), 12–14 September 2007, Madeira, pp. 13–28.

Giuffrè, A. (1991). Letture sulla meccanica delle murature storiche, Roma, Kappa.

Gocht, R. (1978). Untersuchungen zum Tragverhalten rekonstruierter Eisenbahngewonlbebrücken, Dissertation Hochschule für Verkehrswesen, Dresden, Friedrich List.

Guidi, C. (1928). Lezioni di Scienza delle Costruzioni, Torino, Bona Vincenzo.

Guillaume, P.; Van der Auweraer H.; Verboven P.; Vanlanduit S., Peeters B. (2003). A poly-reference implementation of the least-squares complex frequency domain-estimator, in Proceedings of the 21th International Modal Analysis Conference, 3-6 Febbraio, Kissimmee , Florida.

Haghshenas, E.Y., Bard, P., Theodulidis, N. (2008). Empirical evaluation of microtremor H/V spectral ratio, Bulletin of Earthquake Engineering, 6(1), pp. 75-108.

Hannawald, F. (2006). Zur physikalisch nichtlinearen Analyse von VerbundStabtragwerken unter quasi-statischer Langzeitbeanspruchung, Dissertation, Technische Universität Dresden, Institut für Stahl- und Holzbau.

Heyman, J. (1966).The stone skeleton, Int. J. Solids Structures, 2, p. 249-279.

Heyman, J. (1969). The safety of masonry arches, International Journal of Mechanical Sciences, 11(4), pp. 363-385.

Heyman, J. (1982). The masonry arch, Chichester, Hellis Horwood.

Heymann, J. (1995). The stone skeleton, Cambridge, Cambridge University Press.

Hendry, A.W. (1981). Structural Brickwork, New York, Wiley.

Hendry, A.W., Sihna B.P. and Davies S.R. (2004). Design of masonry structures, London, Taylor and Francis.

Hilsdorf, H.K. (1969). Investigation into the failure of brick masonry loaded in axial compression, Designing, Engineering, and constructing with masonry products, University of Texas, Gulf Publishing Company, Houston, pp. 34-41.

Iliceto, V., Boaga, J. (2006). Il rumore sismico in ambiente lagunare, risposta sismica locale del sottosuolo ed edifici storici, Atti del Convegno Geologia Urbana di Venezia, 24 Novembre, in Supplemento 3/2008, Periodico della SIGEA Società Italiana di Geologia Ambientale.

Limit State Ltd (2020). Computer software manual RING, Sheffild.

Jackson, P. (2004). Highways Agency BD on New Masonry Arch Bridges, 27th February 2004, University of Salford, Manchester.

Karaesmen, E., Oktar, O., Karaesman, E. (1996). A comparative study of historic aqueducts and viaducts in seismic zones, Proc. of 11th World Conf. on Earthquake Engineering, paper n° 1813, Acapulco, Messico.

Kooharian, A. (1953). Limit analysis of voussoir (segmental) and concrete arches, Journal Proceedings, 49(12), pp. 317 – 328.

Kurrer, K.E. (2008). The history of the theories of structures. From arch analyses to computational mechanics, Berlin, Erst and Son.

Lemos, J.V. (1995). Assessment of the ultimate load of a masonry arch using discrete elements, Computer Methods in Structural Masonry, GN Pande & J Middleton, Svansea, Books Journals International, pp 294–302.

Lemos, J.V. (2007). Discrete element modelling of masonry structures, Int. J. Arch. Heritage, 1(2), pp. 190 213.

Lionello A., (2011). Tecniche costruttive, dissesti e consolidamenti dei campanili di Venezia, Ministero per i beni e le attività culturali, Sopraintendenza per i beni architettonici e paesaggistici di Venezia e Laguna, Venezia, Corbo e Fiore Editori.

Livesley, R.K. (1978). Limit analysis of structures formed for rigid blocks, Int. j. Numerical methods in Engineering., 1(12), pp. 1853-1871.

Obvis Ltd. (2007). Computer software manual Archie-M, masonry arch bridge and viaduct assessment software, Gairloch.

Lofti, H.R., Benson Shing, P. (1994). Interface model applied to fracture of masonry structures, J. Structural Engineering, ASCE,, 120(1), pp. 63-80.

Loo, Y.C., Yang, Y. (1991). Cracking and failure analysis of masonry arch bridges, ASCE Journal of Structural Engineering, 117(6), pp 1641-1659.

Lourenço, P.B., Rots, J.G. (1993). Discrete models for jointed block masonry walls, in Sixth North American Masonry Conference, Philadelphia, pp. 939-959.

Lourenço, P.B., Rots, J.G. (1997). On the use of homogenisation techniques for the analysis of masonry structures, Masonry International, 11(1), pp. 26-32.

Lourenco, P.B., Rots ,J.G., Blaauwendraad, J. (1998). Continuum model for masonry: parameter estimation and validation, J. Structural Engineering , ASCE, 124(6), pp. 642-652.

Lourenço, P.B. (2002). Computations on historic masonry structures, Progress in structure engineering materials, 4(3), pp 301–319.

Luciano, R., Sacco, E. (1997). Homogenization technique and damage model for old masonry material, Int. J. Solids and Structures, 34(24), pp. 3191-3208.

Magenes, G., Della Fontana, A. (1998). Simplified Non-linear Seismic Analysis of Masonry Buildings, Proc. of the British Masonry Society, 8, pp. 190-195.

Magenes, G., Bolognini, D., Braggio, C. (2000). Metodi semplificati per l'analisi sismica non lineare di edifici in muratura, CNR- Gruppo Nazionale per la Difesa dai Terremoti, Roma.

Markov, K.Z. (1999). Elementary micromechanics of heterogeneous solids, in: Heterogeneous media: micromechanics modelling methods and simulations, K.Z. Markov and L. Preziosi Eds, Boston: Birkhauser, pp. 1-162.

Masciari Genoese, F. (1915). Costruzioni Antisismiche, Milano, Hoepli.

Masiani, R., Rizzi, N., Trovalusci, P. (1995). Masonry as structured continuum, Meccanica, 30(6), pp. 673-683.

Masonry Standards Joint Committee. (1992). Building Code Requirements for Masonry Structures (ACI 530-92/ ASCE 5-92/TMS 402-92), Specifications for Masonry Structures (ACI 530.1-92/ ASCE 6-92/TMS 602-92), Commentary on Building Code Requirements for Masonry Structures (ACI 530-92/ ASCE 5-92/TMS 402-92), Commentary on Specifications for Masonry Structures (ACI 530.1-92/ ASCE 6-92/TMS 602-92), American Society of Civil Engineers, New York.

Massart, T.J., Peerlings, R.H.J., Geers, M.G.D. (2004). Mesoscopic modelling of failure and damage-induced anisotropy in brick masonry, Eur. J. Mechanics A/ Solids, 23(5), pp. 719-735.

Maunder, E.A.W. (1993) Limit analysis of masonry structures based on discrete elements, Structural Repair and Maintenance of Historical Building III (STREMAH), Computational Mechanics Publication, CA Brebbia & RJB Frewer , Glasgow, pp. 367–374.

McNary, S.W., Abrams, D.P. (1985). Mechanics of masonry in compression, J. Structural Engineering , ASCE,, 111(4), pp. 857-870.

McKibbins, L.; Melbourne, C.; Sawar, N.; Sicilia, C. (2006). Masonry arch bridges: condition appraisal and remedial treatment, Ciria, C656, London.

Melbourne, C., Hodgson, J.A. (1996). The behaviour of skewed brickwork arch bridges, proceeding of the First International Conference on arch bridges, Melbourne, London.

Mesqui, J. (1986). Le pont en France avant le temps des ingénieurs, Grands Manuels Picard, Parigi.

Micromed (2010). Guida all'uso di Tromino, Micromed, Venezia.

Micromed (2013) Grilla ver. 6.4, spectral and HVSR analysis. Micromed, Treviso.

Milani, G., Lourenço, P.B., Tralli A. (2006). Homogenised limit analysis of masonry walls Part I: Failure surfaces; Computers and Structures, 84(3-4), pp. 166-180.

Ministero delle Infrastrutture e dei trasposti (2018). Aggiornamento delle Norme tecniche per le costruzioni, 42, supplemento ordinario 8, Gazzetta Ufficiale.

Model, P.(1977) Beitrag zur Berücksichtigung der Gewölbehintermauerung, der Rissbildunghüt und der elastischen Stützung durch den Baugrund und die Dammsctung bei der statischen Berechnung einfeldriger Gewölbebrücken, Dissertation Hochschule für Verkehrswesen "Friedrich List",Dresden.

Molins, C., Roca, P. (1998a). Capacity of masonry arches and spatial structures, J. Structural Engineering , ASCE, 124(6), pp 653–663.

Molins, C., Roca, P. (1998b). Load capacity of multi-arch masonry bridges. The behaviour of masonry arch bridges, Proc. II Int. Arch Bridge Conf., Sinopoli A., Balkema, Rotterdam, pp 213-222.

Mucciarelli, M. (2010). Ambient noise measurements on soil and buildings, Bulletin of Earthquake Engineering, 8, pp. 481-482.

Munjiza, A. (2004). The Finite/Discrete Element Method, Chichester: John Wiley and Sons.

Navarro, P.C., Balboa A. (1994).Puentes de España, Fomento de Construcciones y Contratas, Barcellona.

Navier, C.L. (1838). Résumé des leçons données à l'École des ponts et et des chaussées sur l'application de la Mécanique à l'établissement des constructions et des machines, Chez Carilian, Paris.

Obvis Ltd. (2007). Computer software manual Archie-M, masonry arch bridge and viaduct assessment software, Gairloch.

Oliveira, C.S., Martins, A., Sameiro, Lopes M. (1995). Seismic studies for the Aguas Livres aqueduct in Lisbon, Proc. of the 10th European Conference on Earthquake Engineering , Vienna.

Onat, E.T., Prager, W. (1953). Limit Analysis of Arches, J. Mechanics and Physics of solids, 1(2), pp. 77 – 89.

Orduna, A., Lourenço, P.B. (2005). Three-dimensional limit analysis of rigid blocks assemblages. Part I: Torsion failure on frictional interfaces and limit analysis formulation; Part II: load-path following solution procedure and validation, Int. J. Solids and Structures, 42(18-19), pp. 5140-5180.

Owen, D.R., Peric, D., Petric, N., Brookes, C.L., James P.J. (1998). Finite/discrete element models for assessment and repair of masonry structures, Arch Bridges: History, Analysis, Assessment, Maintenance and Repair. Proceedings of the Second International Arch Bridge Conference, A Sinopoli (Ed), Venice 6.–9. October 1998, Balkema Rotterdam, pp 173–180.

Ozaeta, R.G., Martín-Caro, J.A. (2006). Catalogue of Damages for Masonry Arch Bridges, UIC Report.

Page, A.W. (1978). Finite element model for masonry, J. Structural Engineering , ASCE, 104(8), pp. 1267-1285.

Page, A.W. (1981). The biaxial compressive strength of brick masonry, Proceeding of the institution of. Civil Engineers, Part 2, 71(3), pp. 893-906.

Page, A.W. (1983). The strength of brick masonry under biaxial tensioncompression, Int. J. Masonry Constructions, 3, pp. 26–31.

Palladio, A. (1750). I quattro libri dell'architettura, Edizione riprodotta, Hoepli, Milano, 1945.

Pegon, P., Anthoine, A. (1997). Numerical Strategies for Solving Continuum Damage Problems with Softening: Application to the Homogenization of Masonry, Computer and Structures, 64(1-4), pp. 623-642.

Pippard, A.J.S., Ashby, E.R.J. (1939). An experimental study of the voissour arch, J. Institution of civil engineers,10(3), pp. 383-403.

Pippard, A.J.S. (1948). The approximate estimation of safe loads on masonry bridges, Civil engineer in war: Institution of Civil Engineers, London, Thomas Telford.

Podestà, S. (2001). Risposta sismica di antichi edifici religiosi in muratura, Tesi di Dottorato, Università degli studi di Pavia.

Prager, W. (1959). An Introduction to Plasticity London, Addison-Wesley Publishing Company.

Proske, D., Van Gelder P. (2009). Safety of historical stone arch bridge, Berlino, Springer.

Pietruszczak, S., Ushaksaraei, R. (2003). Description of inelastic behaviour of structural masonry, Int. J. Solids and Structures., 40(15), pp. 4003-4019.

Re, L.(1996). Architettura e conservazione dei ponti piemontesi, Torino, Celid.

Re, L.(1999). I ponti piemontesi. Progetti e cantieri, Torino, Celid.

Rennie, G., (1818). Account of Experiments Made on the Strength of Materials, Phylosophical Transaction of the Royal Society of London, 108, p. 118-136.

Resini, D. (2011). Venezia I ponti, 1-2, Milano, Hoepli.

Roberti, M.G., Calvetti, F. (1998). Distinct element analysis of stone arches, Arch Bridges: History, Analysis, Assessment, Maintenance and Repair. Proceedings of the Second International Arch Bridge Conference, A. Sinopoli , Venice 6-9 October, Balkema Rotterdam, pp. 181-186..

Rondelet, J. B. (1831). Traité théorique et pratique de l'art de bâtir, Firmin Didot fréres, Paris.

Rosson, B.T., Søyland, K., Boothby, T.E. (1998). Inelastic behaviour of sand-lime mortar joint masonry arches, Engineering Structures, 20(1-2), pp 14-24.

Rouxinol, G.A.F., Providencia, P., Lemos, J.V. (2007). Bridgemill bridge bearing capacity assessment by a discrete element method, Proceedings of the Arch`07 – 5th International Conference on Arch Bridges. PB Lourenco, DV Oliveira & A Portela, 12–14 September 2007, Madeira, pp. 669–676

Russo, S., Boscato, G., Sciarretta, F. (2008). Behaviour of a Historic Masonry Structure Subjected to Fire, J.British masonry society, 21(1), pp. 1-48.

Sab, K. (2003). Yield design of thin periodic plates by a homogenisation technique and an application to masonry walls, Comptes Rendus Mechanique, 331(9), pp. 641-646.

Sacco, E. (2009). A nonlinear homogenization procedure for periodic masonry, Eur. J. Mechanics A/ Solids, 28(2),pp. 209-222.

Salvatore W., Benneti S., Maggiora M.D. (2003). On the collapse of masonry tower subjected to Earthquake loadings, Proceedings of the 8th International Conference on Structural Studies, Repairs and Mainteinence of heritage Architecture, May 7-9, Halkidiki, Greece

Schlegel, R. (2004). Numerische Berechnung von Mauerwerksstrukuren in homogenen und diskreten Modellierungsstrategien, Dissertation, Bauhaus Universität, Weimar.

Schubert,P., Wesche, K. (1984). Verformung and Rissesicherheit von Mauerwerk, Deformations and cracking behaviour of masonry, MauerwerkKalender, Berlin, Ernst & Sohn, pp. 85-98.

Séjourné, P. (1913 –1916). Grandes Voûtes, Imprimerie Vve Tardy-Pigelet et Fils, Bourges.

Stefanou, I., Sulem, J., Vardoulakis, I. (2008). Three-dimensional Cosserat homogenization of masonry structures: elasticity, Acta Geotecnica, 3 (1), pp. 71-83.

Sulem, J., Mühlhaus, H.B. (1997). A continuum model for periodic two-dimensional block structures, Mechanics of Cohesive-frictional materials, 2(1), pp. 31-46.

Sutcliffe, D.J., Yu, H.S., Page, A.W. (2001). Lower bound limit analysis of unreinforced masonry shear walls, Computers and Structures, 79814), pp. 1295-1312.

Tassios, T. P. (1988). Meccanica delle murature, Napoli, Liguori.

Thavalingam, A., Bicanic, N., Robinson, J.I., Ponniah, D.A. (2001). Computational framework for discontinuous modelling of masonry arch bridges, Computers and Structures, 79(19), pp. 1821–1830.

Teza, G., Pesci, A., Trevisani, S. (2015). Multisensor surveys of tall historical buildings in high seismic hazard areas before and during a seismic sequence, J. Cultural Heritage, 16(3), pp. 255-266.

Tomazevic, M. (1978). The Computer Program POR, Report ZRMK, Lubiana, Slovenia.

Tomazevic, M., Weiss P. (1990). A rational experimentally based method for the verification of earthquake resistance of masonry buildings, Proc. of the 4th U.S. National Conference on Earthquake Engineering , Palm Springs, 2, pp. 349-359.

Torre, C. (2003). Ponti in muratura, dizionario storico-tecnologico, Firenze, Alinea.

Towler, K.D.S. (1985). Applications of non-linear finite element codes to masonry arches, Proceedings of the 2nd International Conference on Civil and Structural Engineering Computing, 3-5 December 1985, London.

Troyano, C.F. (2006). Terra sull'acqua. Atlante universale dei ponti, Palermo, Dario Flaccovio.

Trovalusci, P., Masiani, R. (2003). Non-linear micropolar and classical continua for anisotropic discontinuous materials, Int. J. Solids and structures, 40(5), pp. 1281-1297.

Tyrell, H.G. (1911). A treatise on the design and construction of mill buildings and other industrial plants,, Myron C. Clark, New York.

Van der Pluijm, R. (1992). Material properties of masonry and its component under tension and shear, Proc. 6th Canadian Masonry Symposium, Saskatoon, Canada, pp.675-686.

Van der Pluijm, R. (1993) "Shear behaviour of bed joints", Proc. 6th North American Masonry Conference, Abrams D.P., Philadelfia, 6-9 June, pp.125-136.

Verband Deutscher Architekten., Ingenieur- Vereine. (1884). Baukunde des Architekten, Berlin, E. Toeche.

Vicat L., (1833), C.f. Barbisan, Il labirinto di Dedalo, Milano 2000, p. 141

Voigtländer, J. (1971). Beitrag zur Ermittlung der Schnittkraftumlagerung in Gewonlbebrücken infolge Rissbildung, Dissertation Hochschule für Verkehrswesen, Friedrich List, Dresden.

Young, T. (1807). A course of lectures on Natural Philosophy and Mechanical Arts, London, J. Johnson.

Zago, F., Riva, G. (1981). Proprietà fisico-meccaniche dei mattoni e comportamento della muratura del centro storico di Venezia. Parte Prima: Il mattone, Atti dell'Istituto di Scienza delle Costruzioni, Istituto Universitario di Architettura di Venezia,43-45, Scuola Tipografica Emiliana Artigianelli, pp. 1-27.

Zago, F., Riva, G. (1982). Proprietà fisico-meccaniche dei mattoni e comportamento della muratura del centro storico di Venezia. Parte Seconda: La muratura, Atti dell'Istituto di Scienza delle Costruzioni, Istituto Universitario di Architettura di Venezia,43-45, Scuola Tipografica Emiliana Artigianelli, Venezia. 1-23.

Zucchetta, G. (1992). Venezia ponte per ponte, Venezia, Stamperia di Venezia.